Performance Analysis of Two Early NACA High Speed Propellers With Application to Civil Tiltrotor Configurations

Franklin D. Harris

National Aeronautics and
Space Administration

Performance Analysis of Two Early NACA High Speed Propellers With Application to Civil Tiltrotor Configurations

Franklin D. Harris

University of Maryland
Dept. of Aerospace Engineering
College Park, MD 20742

TABLE OF CONTENTS

iii

Performance Analysis of Two Early NACA High Speed Propellers With Application to Civil Tiltrotor Configurations

Summary

The helicopter industry is vigorously pursuing development of civil tiltrotors. One key to efficient high speed performance of this rotorcraft is prop-rotor performance. Of equal, if not greater, importance is assurance that the flight envelope is free of aeroelastic instabilities well beyond currently envisioned cruise speeds. This latter condition requires study at helical tip Mach numbers well in excess of 1.0. Two 1940s "supersonic" propeller experiments conducted by NACA have provided an immensely valuable data bank with which to study prop-rotor behavior at transonic and supersonic helical tip Mach numbers. Very accurate "blades alone" data were obtained by using nearly an infinite hub. Tabulated data were recreated from the many thrust and power figures and are included in two Appendices to this report. This data set is exceptionally well suited to reevaluating classical blade element theories as well as evolving computational fluid dynamic (CFD) analyses. A limited comparison of one propeller's experimental results to a modern rotorcraft CFD code is made. This code, referred to as TURNS, gives very encouraging results.

Detailed analysis of the performance data from both propellers is provided in Appendix A. This appendix quantifies the minimum power required to produce usable prop-rotor thrust. The dependence of minimum profile power on Reynolds number is quantified. First order compressibility power losses are quantified as well and a first approximation to design airfoil thickness ratio to avoid compressibility losses is provided.

Appendix A's results are applied to study high speed civil tiltrotor cruise performance. Predicted tiltrotor performance is compared to two turboprop commercial transports. The comparison shows that there is no fundamental aerodynamic reason why the rotorcraft industry could not develop civil tiltrotor aircraft which have competitive cruise performance with today's regional, turboprop airliners. Recommendations for future study that will insure efficient prop-rotor performance to well beyond 400 knots are given.

Symbols

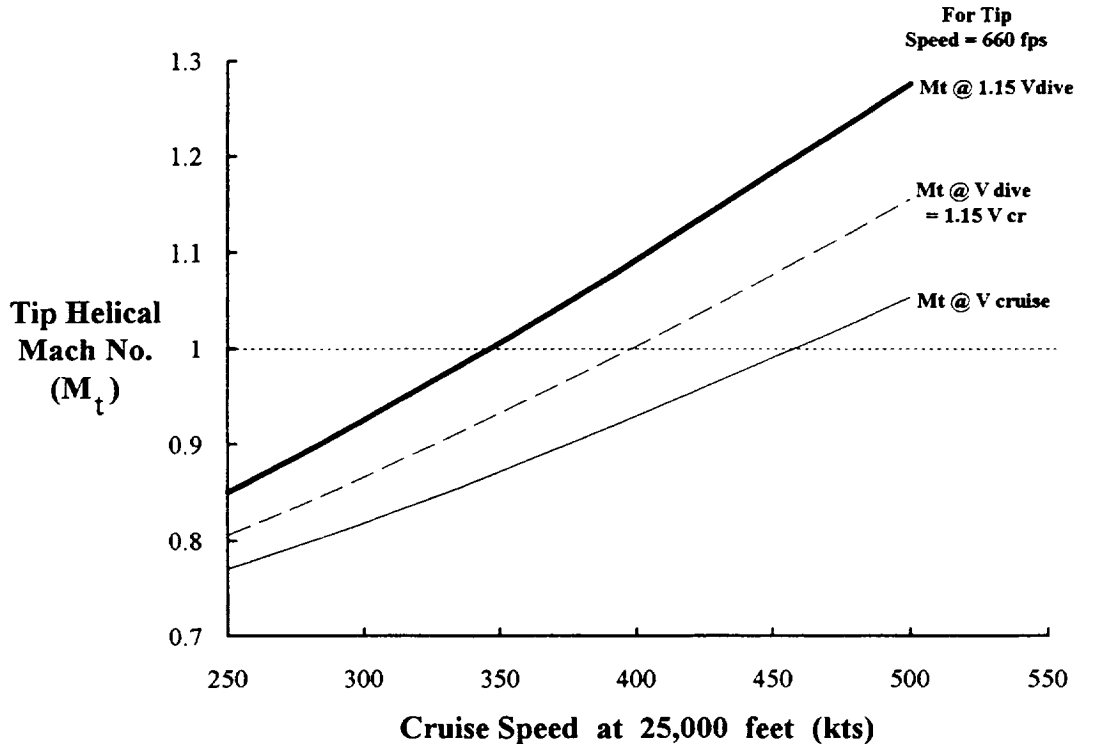|	
A	prop-rotor swept disc area, πR^2
a_s	speed of sound
B	number of blades
b	chord or blade number
c	chord
$\overline{C}_L$	average lift coefficient, see page A-29
$\overline{C}_D$	average drag coefficient, see page A-29
C_P	power coefficient, see page 9
C_T	thrust coefficient, see page 9
D	diameter
h	blade section maximum thickness
J	propeller advance ratio, V / nD
M	free stream Mach number, V / a_s
M_x	blade element helical Mach number
n	shaft rotational speed
Q	torque
P	power
q	dynamic pressure
R	radius
r	radius station
T	thrust
t	airfoil thickness
V	forward speed
V_t	tip speed
v_i	induced velocity
x	blade element radius
α_s	shaft angle of attack
α_{tpp}	tip path plane angle of attack
β	blade pitch angle
$\beta_{0.75R}$	blade pitch angle at ¾ radius
λ_o	rotor inflow ratio due to speed, $V \sin \alpha_{tpp} / V_t$
λ_i	rotor induced inflow ratio, v_i / V_t
μ	rotor advance ratio, $V \cos \alpha_{tpp} / V_t$
θ	blade pitch angle
$\theta_{0.75R}$	blade pitch angle at ¾ radius
ρ	air density
η_P	propulsive efficiency, TV / P_{actual}
Ω	shaft rotational speed
Subscripts	
i	induced
o	profile
p	propulsion

Introduction

The helicopter industry is developing the tiltrotor configuration as a new rotorcraft product. This aircraft is well suited to both commercial passenger and freight carrying use and can be competitive with current turboprop airliners. The commercial success of this configuration depends, in part, on its prop-rotors. These prop-rotors are relatively large diameter propellers that are lightly loaded. They must (1) provide both efficient hovering and cruise performance and (2) be free of aeroelastic instabilities at least to speeds on the order of 1.15 times dive speed. While cruise flight is not likely to incur supersonic helical tip Mach numbers, clearing the flight envelope to $1.15\,V_{dive}$ most certainly will.

The helicopter industry has a nearly 60 year background in hovering rotor technology. This industry is, however, relatively unfamiliar with axial flight behavior of propellers of any size. Furthermore, supersonic helical tip speeds within the flight envelope have been purposely and carefully avoided by the rotorcraft industry. The fixed wing industry, on the other hand, has a long and successful history of providing heavily loaded, relatively small diameter propellers that frequently encounter transonic to supersonic helical tip Mach numbers. Furthermore, the diameter of typical fixed wing propellers has been constrained by ground clearance. This historical constraint is removed with the tilt rotor configuration. It appears then that neither the helicopter nor fixed wing industries are well prepared to maximize large diameter prop-rotor performance in high speed and solve the structural dynamic problems that are likely to arise.

Future civil tiltrotor configurations are currently not expected to cruise at supersonic helical tip Mach numbers. However, prudent design criteria (and indeed FAA regulations) require that the aircraft have a considerable aeroelastic stability margin of safety at 1.15 times the dive speed, V_{dive}. The dive speed itself can easily be 1.15 times the cruise speed. Taken together the need to analyze prop-rotors at helical tip Mach numbers above 1.0 is quite clear as the figure below shows.

A common starting point for both helicopter and fixed wing prop-rotor performance and aeroelastic study does exist. This point lies not in the most recent 1980's propfan efforts summarized by Reference 1, but in 1940s and 1950s efforts to understand and develop propeller technology for airplanes that were expected to cruise above Mach 0.80. This early propeller work was curtailed when the turbojet airplane proved its passenger appeal and profitability to the airline industry.

For Tip
Speed = 660 fps

Mt @ 1.15 Vdive

Mt @ V dive
= 1.15 V cr

Mt @ V cruise

Tip Helical
Mach No.
(M_t)

Cruise Speed at 25,000 feet (kts)

MT_VDIVE.xls

**Prop-rotors For Advanced Tiltrotor Aircraft Must Consider Cases
Of Supersonic Helical Tip Mach Numbers.**

Two NACA experiments have been examined to provide (to both helicopter rotor and fixed wing propeller aeronautical engineers) a comprehensive performance data base. This data bank has been put back into tabulated form by digitizing the graphical results given in two NACA reports. This immensely valuable data bank offers a number of correlation opportunities. The two propellers, tested beyond axial Mach number's of 0.9, provide data for helical tip Mach numbers above 1.4. In addition, the earlier propeller was tested over a complete range in blade pitch angle. This propeller's maximum aerodynamic thrust coefficient was found at several wind tunnel Mach number and blade angle combinations. These data offer computational fluid dynamic analysts a chance to explore transonic to supersonic flow regimes at both low angle of attack and above stall. Conventional blade element analyses may also be validated using two-dimensional airfoil properties extended well beyond currently tabulated data sets in use by the rotorcraft industry.

The thrust and power trends exhibited by these two early propellers provides an opportunity to re-examine prop-rotor performance fundamentals. These fundamentals suggest realistic design goals for future high speed civil tiltrotor designs.

4

Description of Propeller Experiments

The first propeller, having two blades and a 4 foot diameter, was tested up to a wind tunnel Mach number of 0.925 in the late 1940s. The combination of forward speed and tip speed provides performance data at helical tip Mach numbers from about 0.3 to over 1.4. The results (Reference 2) were reported in NACA Research Memorandum L9G06 by James B. Delano and Melvin M. Carmel. This World War II document was declassified in 1954. The second propeller, having three blades and a 9.75 foot diameter, was tested to Mach 0.96. The helical tip Mach number ranged from 0.735 to 1.443. These results were initially published as NACA Research Memorandum L53F01 by Albert J. Evans and George Liner in 1953. This RM was deemed so significant that it was formally reported in the NACA bound volume for 1958 as Technical Report 1375 (Reference 3).

These two experiments are of particular value not only because of the operating range, but because of the test setup itself. As Figures 1 and 2 show, the propeller installation nearly removed all hub and spinner complications from the performance data leaving "a blades alone" data bank of unique value. (The only thing more that could be asked is that the authors had included the test results in tabulated as well as graphical form. However, reading the nearly 1,200 data points from the many figures back into tables has now been done with reasonable engineering accuracy. The tables are provided as Appendix B and C in this report.)

Propellers One and Two

These two early propellers, unlike the 1980s propfan experiments of Reference 1, had few blades and relatively low solidity (helicopter definition) or Activity Factor (airplane nomenclature). The first propeller, the 4-foot diameter NACA 4-(5)(08)-03, had a nominal solidity of 0.0721 with tailored blade geometry typical of the era. The second propeller, the full scale 9.75-foot diameter, had a nominal solidity of 0.2292. The blades were constant chord and the airfoil was symmetrical. Only the airfoil thickness ratio and twist varied along the radius. (This second propeller may well require the least amount of CFD grid generation work of any propeller that one can find in the literature.)

The long cylinder housing the drive system as shown in Figures 1 and 2 acts as nearly an infinite hub. For both propellers, this "hub" diameter coincidentally had virtually the same proportion to propeller diameter. The root station of each propeller was at blade radius station $r_{root} = 0.27\,R$.

Before describing each propeller's blade geometry, some familiarity with and translation between propeller and rotor nomenclature should be helpful. For example,

Parameter	Helicopter Rotor	Airplane Propeller
Prop-rotor Diameter	D	D
Blade Radius	R	R
Blade Chord	c	b
Blade Number	b	N or B
Airfoil Thickness	t	h
Blade Width Ratio	Rarely used alone	b/D
Airfoil Thickness Ratio	t/c	h/b
Blade Pitch Angle	θ	β
Planform Area	Rarely used	Rarely used
Radial Station	r or x	r or x

In addition, the propeller designer frequently refers to a propeller's geometry by its Activity Factor, a measure of the integrated capacity of the blade elements to absorb power. As discussed, for example in Reference 4, a propeller's AF is generally calculated as

$$\text{Activity Factor} = AF = \text{Blade No.} \times \frac{100,000}{16} \times \int_{root}^{tip} (r/R)^3 (b/D) \ d(r/R) \qquad (1)$$

The helicopter designer, using Reference 5, will recognize this Activity Factor as a form of power weighted solidity because of the $(r/R)^3$ term multiplying the chord to diameter ratio (b/D) before integration. A power weighted chord in the helicopter world is generally calculated as

$$\text{Power Weighted Chord} = c_e = \frac{\int_0^1 c \ x^3 dx}{\int_0^1 x^3 dx} = 4 \int_0^1 c \ x^3 dx \qquad (2)$$

These two views of prop-rotor geometry are related simply as

$$\text{Rotor Power Weighted Solidity} \equiv \sigma_e = \frac{b \ c_e}{\pi \ R} = \frac{128 \ AF}{100,000 \ \pi} \qquad (3)$$

Both power weighted solidity and Activity Factor are definitions that, strictly speaking, apply only to the hover or static thrusting regime. This is because the chord is weighted only by the cube of local velocity due to rotation. At the other extreme, when the prop-rotor is in forward flight but not rotating, the actual blade area would be numerically correct. This would be the case, for example, in calculating the drag of a feathered propeller during engine out flight.

The blade geometry of PROP 1 [i.e., the low solidity, 2-bladed configuration designated as NACA 4-(5)(08)-03] and of PROP 2 (i.e., the high solidity, 3-bladed, constant chord configuration) are compared in Figures 3a, b, c, and d. These geometric parameters are tabulated in Appendix B for PROP 1 and in Appendix C for PROP 2.

6

The blade twist distributions which are compared in Figure 3a have been referenced to zero degrees at the 0.75 R radius station although both References 2 and 3 show the design twist in absolute terms as tabulated in the Appendices. All test data were obtained with reference to values of blade pitch angle at the three-quarter radius station (i.e., $\beta_{.75}$). It is not clear for PROP 1 (which has cambered NACA 16 series airfoils) whether the absolute design blade angle is referenced to the airfoil chord line or to the angle of zero lift. PROP 2 has symmetrical NACA 16 airfoils.

The distribution of blade chord (divided by radius) for both propellers is shown in Figure 3b. PROP 2 was untapered and had a constant chord of 0.24 R. The tip of PROP 2 appears to be completely squared off. PROP 1 was linearly tapered from the root, 0.27 R, to about the 0.93 R radius. This chord distribution was found to be (in feet) approximately $c_{(x)} = 0.4512 - 0.2680$ (r/R) . The variation outboard of the 0.93 R radius station appears to have some conic shape perhaps in the parabolic family.

The airfoil thickness ratio distributions, shown in Figure 3c, illustrate, at least for PROP 2, just how thin propellers could (and can) be made. However, Reference 3 includes a flutter boundary encountered with PROP 2 which had solid, 6415 steel blades. Reference 3 states that PROP 2 "was designed to operate at a rotational speed of 2,600 RPM at a forward Mach number of 0.95 at 35,000 feet altitude, corresponding to an advance ratio [J] of 2.2." This would be 550 knots with a tip speed of 1,327 feet per second.

Finally, the contrast in airfoil design lift coefficient distribution is provided by Figure 3d. Both PROP 1 and PROP 2 used the NACA 16 series airfoil. PROP 2 was uncambered so its airfoil design lift coefficient is zero. Additional background about an earlier test with PROP 1 as part of an airfoil camber investigation is given in Ref. 6 and particularly in Ref. 7. The details, including airfoil coordinates, of the NACA 16 series airfoils that supported these early "supersonic propeller" experiments are clearly explained in Ref. 8 and also available in Ref. 9.

The contrast between the symmetrical NACA 16-012 airfoil familiar to the fixed wing propeller engineer and the NACA 0012 airfoil historically used by rotorcraft engineers is illustrated by the following figure. The NACA 16-012 is referred to as one of the NACA 1-series wing sections in Reference 9. This series was the first family to strive for low-drag and high critical Mach number. The maximum thickness of the NACA 1-series occurs at the 50 % chord station and the leading edge radius is defined (Ref. 8) as 0.386 $(t/c)^2$ /0.0081 $\approx$ 0.4889 $(t/c)^2$. The NACA 0012, a member of the four digit airfoil family, has maximum thickness at the 25 % chord station and a larger nose radius defined by 1.1019 $(t/c)^2$.

7
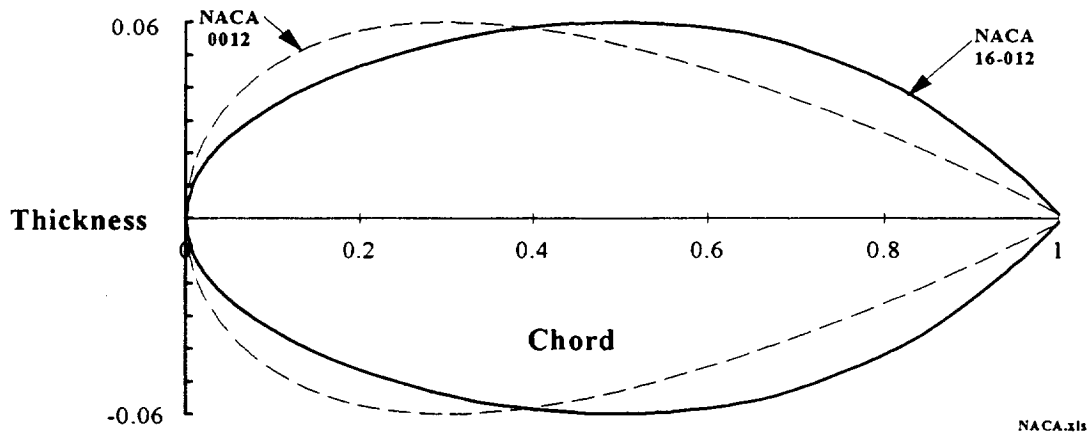
Note: (1) Airfoils not shown to scale.
(2) Co-ordinates referenced to unity chord.

The Contrast Between Propeller And Rotor Airfoils Is Significant.

Wind Tunnel Interference

The 4 foot diameter, low solidity PROP 1 was tested in the Langley 8 foot diameter high speed tunnel with a closed test section. The later experiment with the 9.75 foot, high solidity PROP 2 was conducted in the Langley 16-foot transonic tunnel with slotted test section. In both experiments, considerable study was made of velocity distributions within the tunnels to confirm that the test setup provided nearly uniform Mach number profiles in the propeller plane. Tunnel wall interference correction factors were carefully discussed for both experiments. For PROP 1 in the solid test section, this correction was established and applied to the correction of propeller advance ratio (J) *but not to the "tunnel-datum Mach number"* or to the final plotted data (or to the tabulated data of Appendix B). The correction from the nominal speed used in the calculation of propeller advance ratio and associated with the tunnel datum Mach number was given by figure 9 in Ref. 2. This correction, given here as a curve fit equation, is

$$\frac{V_{free\ air}}{V_{tunnel}} \approx 1 - \frac{0.10345\tilde{T}}{\sqrt{1 + 6.6\tilde{T}}} \quad \text{where} \quad \tilde{T} = \frac{T/qD^2}{\sqrt{1-M^2}} \tag{4}$$

Both dynamic pressure (q) and Mach number (M) are based on the wind tunnel datum velocity and atmosphere. Rigorous analysis would require correction of the tunnel-datum Mach number at each test point of Appendix B. The larger corrections, found at the lowest dynamic pressure, lowest wind tunnel datum Mach number and higher thrusts, were on the order of $V_{free\ air} = 0.95\ V_{tunnel}$.

Since PROP 2 was operated in a slotted wind tunnel, the wall interference corrections were considered small so no correction was made to the plotted data (or to the tabulated data of Appendix C).

8

Discussion of Test Results

Both PROP 1 testing (the 4 foot diameter, 2 bladed, low solidity prop experiment) and the later PROP 2 testing (the 9.75 foot diameter, 3 bladed, high solidity prop experiment) gathered thrust and power performance data over a very wide range of $\beta_{.75}$ and tunnel Mach number. This data was obtained by varying propeller RPM while holding $\beta_{.75}$ and tunnel Mach number constant. A low RPM generally gave near zero thrust because the resultant of forward speed and rotational speed was nearly aligned with the average blade element pitch angle. By increasing RPM, the average blade element angle of attack was increased and thrust began to increase. The RPM was continually increased until the propeller reached maximum thrust or the power supply limit was reached. In the case of PROP 2, flutter and other limits kept the test from establishing maximum thrust for this thin bladed configuration.

Nomenclature

The test results are presented in both References 2 and 3 in propeller nomenclature. However, in this present report, the results are examined in helicopter terms. Therefore, an understanding of and translation between both helicopter and airplane definitions is quite helpful. For example,

Parameter	Helicopter Rotor	Airplane Propeller
Prop-rotor Diameter (ft)	D	D
Blade Radius (ft)	R	R
Shaft Rotational Speed	Ω (radians / sec)	n (revolutions / sec)
Tip Speed (ft / sec)	$V_t = \Omega R$	$V_t = \pi n D$
Disc Area (sq. ft)	$A = \pi R^2$	$A = \pi D^2 / 4$
Air Density (slug / ft^3)	ρ	ρ
Flight Speed (ft / sec)	V	V
Thrust (lb)	T	T
Thrust Coefficient	$C_T = T / \rho A V_t^2$	$C_T = T / \rho n^2 D^4$
Power (ft-lb / sec)	P	P
Power Coefficient	$C_P = P / \rho A V_t^3$	$C_P = P / \rho n^3 D^5$
Tip Path Plane Angle Of Attack (radian)	α_{tpp} measured from rotor disc parallel to wind	α measured from shaft horizontal
Advance Ratio	$\mu = V \cos \alpha_{tpp} / V_t$	$J = V / nD$
Inflow Ratio	$\lambda_o = V \sin \alpha_{tpp} / V_t$	See Advance Ratio
Induced velocity (ft / sec)	v_i	u or w
Induced Inflow Ratio	$\lambda_i = v_i / V_t$	Rarely used
Propulsive Efficiency	$\eta_P = C_T \lambda_o$ /Measured C_P	$\eta_P = C_T J$ /Measured C_P

Since performance of the two propellers is discussed and presented in this report in helicopter rotor nomenclature, the following conversions should be noted.

1. The propeller represents a rotor in axial flight. Therefore, a reference to "advance ratio" means J for a propeller but λ_o for a rotor. For the rotor, the tip

path plane is perpendicular to the free stream velocity and therefore $\alpha_{tpp} = +90$ degrees. Thus, for the rotor, $\mu = 0$ and,

$$\lambda_o = J / \pi \qquad (5)$$

2. Thrust refers to the axial force in the shaft. However, the thrust coefficients are related as

$$\text{Rotor } C_T = (4/\pi^3) \times \text{Propeller } C_T \qquad (6)$$

3. Power implies torque times shaft rotational speed for both rotor and propeller. The power coefficients are related as

$$\text{Rotor } C_P = (4/\pi^4) \times \text{Propeller } C_P \qquad (7)$$

Given that it is clearly understood that the data of References 2 and 3 have been translated from propeller nomenclature to helicopter rotor nomenclature for the majority of this report, a discussion of the these two experiments can continue.

Typical Results From PROP 1

Propeller 1 was tested at 13 tunnel-datum Mach numbers beginning at 0.175 and reaching 0.925. At each Mach number, data were acquired at no less than four blade angle settings ranging between $\beta_{.75} = 20$ to 45 degrees at low speed and 55 to 70 degrees at the three highest Mach numbers tested. In nearly one third of the RPM sweeps with fixed $\beta_{.75}$ and tunnel Mach number, a condition of aerodynamically limited maximum thrust was established. In virtually all test sweeps, the operating point for maximum propulsive efficiency was established.

A representative example of PROP 1's performance occurs at the axial Mach of 0.70. This Mach number corresponds to roughly 421 knots at 25,000 feet on a standard day. The thrust behavior during an RPM sweep with fixed $\beta_{.75}$ is given by Figure 4a in rotor coefficient form. Considering that the nominal power weighted solidity of PROP 1 is 0.0721, this propeller is demonstrating a thrust coefficient to solidity ratio (i.e., the familiar helicopter parameter of C_T / σ) of at least 0.2 for $\beta_{.75}$ from 55 to 70 degrees. This high level of blade loading is achieved at the transonic and supersonic *helical* tip Mach numbers noted at each maximum C_T. There is little evidence, in the corresponding rotor power coefficient shown in Figure 4b, of unexpected behavior. Power required to produce thrust is first dependent on thrust times flight velocity (i.e., Rotor $C_T \times \lambda_o$) which Figure 4b illustrates. The lowest power point on each $\beta_{.75}$ line on Figure 4b corresponds to zero thrust. This power is excessive at $\beta_{.75}$ of 65 and 70 degrees in part because the blade root is now near 90 degrees and producing negative thrust. PROP 1 achieves a propulsive efficiency well above 0.80 over a wide range in rotor inflow ratio as Figure 4c clearly shows. To achieve this propulsive performance level,

10

PROP 1 must be fairly heavily loaded with rotor thrust coefficients in the range of 0.008 to 0.01.

These typical results from PROP 1 can become more meaningful when applied to a representative prop-rotor as used, for example, on the Bell / Boeing V-22. This tiltrotor is being produced to U. S. Marine specifications. The V-22 prop-rotor diameter is 38 feet and in cruise flight it operates at a tip speed of 660 ft/sec (which is reduced from the hover tip speed of 790 ft/sec). The gross weight of the V-22 is roughly 50,000 pounds. Assume a civil tiltrotor version using the V-22's prop-rotor diameter but be otherwise a scaled up version of PROP 1. Since this civil tiltrotor might easily cruise at an aircraft lift to drag ratio of 10 at 25,000 feet (density of 0.001065 slug/ft^3 and speed of sound of 1015.5 ft/sec) and Mach number of 0.70 (i.e., 421 knots or 711 ft/sec), then each prop-rotor would need to produce 2,500 pounds of thrust. This sets the inflow ratio at $\lambda_o = 711/660 = 1.077$, the helical tip Mach number at 0.955 and the rotor thrust coefficient at $C_T = 0.00475$. Note that this thrust condition leads to a rather lightly loaded propeller when compared to the C_T level (i.e., 0.008 to 0.010) at which PROP 1 obtains maximum propulsive efficiency. Interpolating on Figure 4a estimates $\beta_{.75}$ at just under 55 degrees. Then, from Figure 4b, rotor power coefficient is estimated by interpolation as $C_P = 0.00652$. The rotor horsepower required therefore amounts to about 4,120 hp of which 3235 hp is used to produce 2,500 pounds of thrust at 421 knots and 885 hp goes to overcoming the blade drag and induced power. The ideal induced power calculated by momentum theory amounts to only 7 hp. The propulsive efficiency, η_P, is 0.785 at this very lightly loaded condition associated with tilt rotor configurations.

From hover and transition points of view, it is somewhat doubtful that PROP 1 would be adequately sized. PROP 1 has a power weighted solidity of 0.0721. The V-22 prop-rotor power weighted solidity is nominally 0.102. This difference suggests that PROP 1 would have considerably less stall margin in hover and low speed flight. Unfortunately, no static thrust and power performance of PROP 1 appears to have been published.

Typical Results From PROP 2

Propeller 2 was tested first at a constant 1,600 RPM. At each $\beta_{.75}$ (ranging from 20.2 to 50.8 degrees) the wind tunnel speed was varied to develop a thrust variation with inflow ratio. This data set gave performance over a tunnel Mach number range from 0.10 to just below M = 0.67. Testing also established a flutter boundary shown on figure 6 of Reference 3. Additional testing was then conducted holding $\beta_{.75}$ constant and tunnel Mach number constant while varying propeller RPM. PROP 2 performance was obtained at 8 wind tunnel Mach numbers ranging from 0.6 to 0.96.

A representative example of PROP 2's performance occurs at the axial Mach of 0.70. Again, this Mach number corresponds to roughly 421 knots at 25,000 feet on a standard day. The thrust behavior during an RPM sweep with fixed $\beta_{.75}$ is given by Figure 5a in rotor coefficient form. Considering that the nominal power weighted solidity of PROP 2 is 0.229, this propeller is demonstrating a thrust coefficient to solidity ratio (C_T/σ) of at least 0.1 at a helical tip Mach number of 1.05. There is little evidence in the corresponding rotor power coefficient shown in Figure 5b of unexpected behavior. The dashed line on Figure 5b corresponds to zero thrust. Unlike PROP 1, PROP 2 was not tested at excessive values of $\beta_{.75}$. PROP 2 achieves a propulsive efficiency well above 0.80 over a wide range in rotor inflow ratio as Figure 5c clearly shows. To achieve this propulsive performance level, PROP 2, with its higher solidity, must be fairly heavily loaded with rotor thrust coefficients in the range of 0.015.

The thrust and power coefficient data of Figures 5a and 5b can also be used to obtain a power required for the civil tiltrotor discussed above with respect to PROP 1. Again the flight condition of $\lambda_o = 711/660 = 1.077$ and a rotor thrust coefficient of $C_T = 0.00475$ is the example point. Interpolating on Figure 5a estimates $\beta_{.75}$ at just over 54.7 degrees. Then, from Figure 5b, rotor power coefficient is estimated by interpolation as $C_P = 0.006393$. Experimentally then, PROP 2 produces 2,500 pounds of thrust with about 4,040 hp. Of this total, 3235 hp is used to produce usable thrust at 421 knots and 805 hp goes to overcoming the blade drag and induced power. The ideal induced power calculated by momentum theory amounts to only 7 horsepower. The propulsive efficiency is 0.80 at this very lightly loaded condition for such a high solidity prop-rotor.

While PROP 2 has a power weighted solidity more than twice the V-22, its thin airfoil geometry may create an unacceptably low stall margin in hover and low speed flight. As was the case with PROP 1, no static thrust and power performance of PROP 2 appears to have been published.

Computational Fluid Dynamics Theory Versus Test

A comparison of theory to test results is referred to in both of these early NACA propeller reports. Reference 2 notes in the summary that PROP 1's performance trends with Mach number and advance ratio "are in good agreement with theory." The theory provided in the report examines PROP 1 from an average airfoil section point of view. In the summary to PROP 2's performance report, the authors state that "A comparison of the experimental results with calculated results showed that maximum propeller efficiency can be calculated with good accuracy by using ordinary subsonic strip theory when the blade-section speeds are supersonic." Later in Reference 3, the authors state that "Airfoil data, which were cross-plotted and extrapolated for use with the blade-thickness ratios of the test propeller, were

12

obtained for the [strip theory] calculations from" Curtiss-Wright Corp. Report Number C-2000 which is dated December 2, 1948. Strip theory, as noted in these two propeller reports, has served both fixed and rotary wing industries surprisingly well since the early 1900's.

The use of strip theory will, of course, continue to offer considerable value in the design of prop-rotors for tiltrotor aircraft. However, the sheer volume of tables to look up airfoil aerodynamic lift, drag and moment coefficients for the increased number of flight conditions can be a non-trivial task. Furthermore, "cross-plotting and extrapolating" a small sample of experimental airfoil data leaves much to be desired in today's world. Airfoil calculations using computational fluid dynamics (CFD) may well offer the only practical way to obtain the required airfoil data at correct Reynolds and Mach numbers. Fortunately, progress has been made in using CFD to compute the helicopter's complete rotor performance in hover and low speed.

Recently, pioneering progress has been made in using one CFD method to predict prop-rotor performance in high speed cruise flight. This ground breaking work was completed by Lt. James R. Watkins in September of 1995. He reported his work in Reference 10. (His full thesis is currently restricted to DoD distribution because it contains MV-22 aircraft specification data.) Lt. Watkins used the CFD code called TURNS (Transonic Unsteady Rotor Navier-Stokes-Reference 11) to first demonstrate theory correlation with PROP 2 experimental data. Four experimental data points (referred to as target points) were selected from the 16 points from the test data set obtained at a wind tunnel Mach number of 0.60 and $\beta_{.75} = 50.4$ degrees. The computational results were obtained in about two weeks elapsed time—including grid generation. A CFD data point was obtained in about one day using the Naval Postgraduate School's Cray Y-MP EL 98 computer (on a low priority basis). Lt. Watkins' reported his summary correlation as figure 6-4 which is reproduced here below. This initial effort was very encouraging considering the general problem's complexity.

Additional examination of Lt. Watkins' TURNS code results is quite informative. For example, the trend of PROP 2's rotor thrust coefficient with rotor inflow ratio, λ_o, is shown in Figure 6. The corresponding prediction of rotor power coefficient is provided with Figure 7. The prop-rotor thrust is, in this case, under predicted using the experimental $\beta_{.75}$ as Figure 6 shows. The inability to "match thrust given the experimental blade angle and operating condition" is a rather common occurrence in theory-test correlation. Experience has shown that (1) experimental blade angle is rarely accurate to better than 1/4 degree and (2) performance theories generally do not include blade elastic deflection, particularly in torsion. Because thrust is under predicted at a given speed, it follows that power will be under predicted which Figure 7 bears out. The corollary to the detailed prediction of C_T and C_P versus λ_o is to either adjust the $\beta_{.75}$ used in the theory
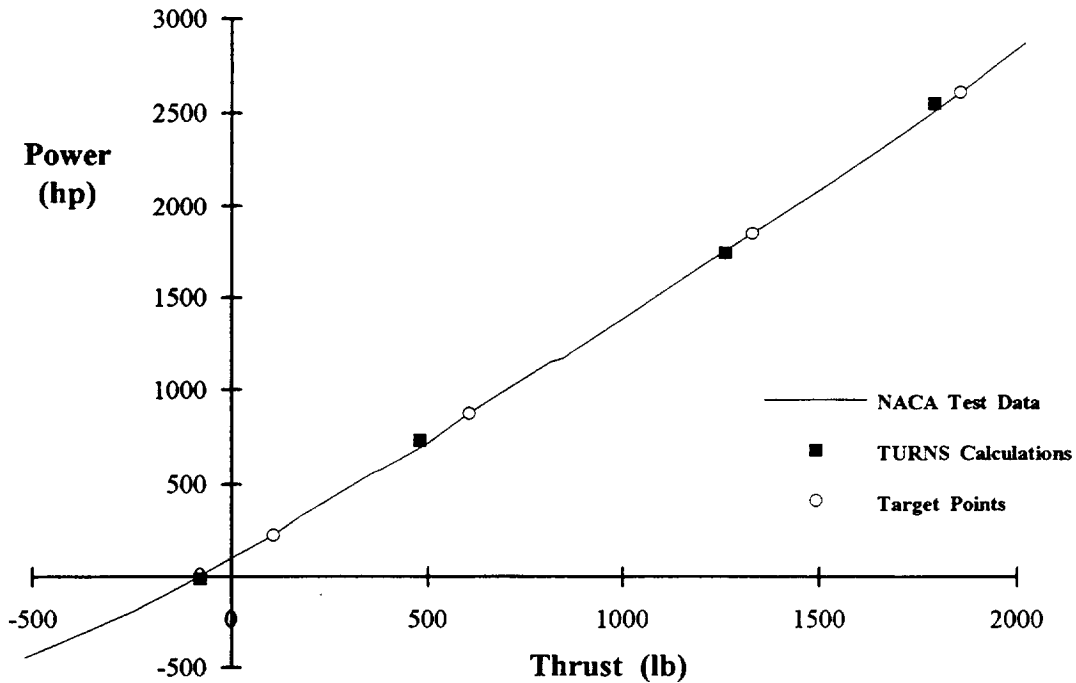
Ref. 10, Figure 6-4. Comparison of TURNS Results to [PROP 2] Test Results.

or, as Lt. Watkins' did, plot horsepower or C_P versus thrust or C_T. The difference between targeted and theoretical points can then be noted.

Prop-rotor performance viewed in terms of propulsive efficiency is shown in Figure 8. The TURNS solution to the Navier-Stokes equations gives results quite comparable to PROP 2's test data. The definition of efficiency as used here is ideal power divided by actual power; that is

$$\eta_P = \frac{C_T \lambda_o}{\text{Measured } C_P} \qquad (8)$$

This traditional efficiency definition suggests another way of viewing theory versus test which is described more fully in Appendix A, Prop-rotor Performance Fundamentals. The suggestion is that measured (or calculated) power can be graphed versus ideal power, (i.e., $C_T \lambda_o$). This useful view of the TURNS results in comparison to PROP 2 test data is shown in Figure 9. If the efficiency were 100 per cent, then the test and theory data would fall along the dashed line shown on Figure 9. Since the propulsive efficiency is less than 100 per cent, the actual power is greater than the ideal power.

14

The line of actual power lies above the 100 per cent efficiency dashed line on Figure 9. The increment in power over ideal is attributed primarily to profile power which is discussed in Appendix A. That is, power can be defined as

$$\text{Power} = TV + Tv_i + P_o \qquad (9)$$

or in rotor coefficient nomenclature

$$C_P = C_T \lambda_o + C_T \lambda_i + C_{Po} \qquad (10)$$

The first term in these equation, TV or $C_T \lambda_o$, defines the power required to produce usable thrust. This is the minimum or propulsive power. The second term, Tv_i or $C_T \lambda_i$, accounts for the induced power required to add momentum to the air flowing through the prop-rotor. From Reference 5, the lowest or ideal induced power comes when

$$v_i = \sqrt{\left(\frac{V}{2}\right)^2 + \frac{T}{2\rho A}} - \frac{V}{2} \quad \text{where} \quad v_i \approx \frac{T}{2\rho AV} \text{ for high speed} \qquad (11)$$

or

$$\lambda_i = \frac{v_i}{V_t} = \frac{1}{2}\sqrt{\lambda_o^2 + 2C_T} - \frac{1}{2}\lambda_o \quad \text{where} \quad \lambda_i \approx \frac{C_T}{2\lambda_o} \text{ for high speed} \qquad (12)$$

The third term, P_o or C_{Po}, is referred to as profile power in the helicopter world. It accounts for the product of airfoil drag and local resultant velocity of each airfoil element along the blade. The sum along the blade (or integral from the blade root to tip) of each blade element's drag times velocity leads to the profile power of one blade. The sum of each blade's profile power gives the prop-rotor's total profile power.

The above power required equations can be used to "back out of the test data" an approximate non-ideal power. That is, a "Test" profile power can be defined as

$$\text{"Test" } C_{Po} = (\text{Measured } C_P) - (C_T \lambda_o + C_T \lambda_i) \qquad (13)$$

This "Test" profile power illuminates the difference between ideal and actual power. In Figure 10 the "Test" profile power as derived from TURNS calculations is compared to the "Test" profile power derived from the measured power. The agreement between test and this TURNS CFD correlation analysis initiated by Lt. Watkins is very encouraging.

Application to Civil Tiltrotor Aircraft

Accurate preliminary design of prop-rotors to achieve efficient cruise performance is of great importance to future civil tiltrotor aircraft. The preceding discussions, the tabulated data provided in Appendices B and C and the analysis of this data included in Appendix A can be applied to prop-rotor preliminary design. The key issues are (1) maximum propulsive efficiency, (2) minimizing cruise power required, (3) raising tiltrotor aircraft lift to drag ratio and (4) satisfying hover performance and low speed design requirements.

Maximum Propulsive Efficiency

Maximum propulsive efficiency of airplane propellers has been studied for nearly a century. Because propellers tend to be heavily loaded, this decades long study has concentrated first on minimizing induced power to maximize propulsive efficiency. That is, given that propulsive efficiency is written as

$$\eta_P = \frac{C_T \lambda_o}{\text{Actual } C_P} = \frac{C_T \lambda_o}{C_T \lambda_o + C_{P_i} + C_{P_o}} \tag{14}$$

the effort to first minimize induced power, C_{P_i}, and then minimize profile power, C_{P_o}, appears as the traditional way to address propeller performance. The so called ideal propulsive efficiency is an immediate byproduct of this classical approach. This ideal propulsive efficiency is defined by setting profile power, C_{P_o}, to zero and assuming that induced power, C_{P_i}, is equal to $C_T \lambda_i$. These assumptions lead to an ideal propulsive efficiency at high speed on the order of

$$\text{Classical Ideal } \eta_P = \frac{C_T \lambda_o}{C_T \lambda_o + C_{P_i}} = \frac{C_T \lambda_o}{C_T \lambda_o + C_T \lambda_i} = \frac{1}{1 + \lambda_i / \lambda_o} \cong \frac{1}{1 + C_T / 2\lambda_o^2} \tag{15}$$

When applied to a civil tiltrotor where $C_T \approx 0.005$ and $\lambda_o \approx 1$ (from the earlier examples), Equation (15) suggests that the classical ideal propulsive efficiency is on the order of 0.997. This is clearly an unrealistic goal reflecting the lightly loaded prop-rotor characteristic of $C_T \approx 0.005$. The low induced power levels inherent to the civil tiltrotor aircraft significantly alter the approach to setting realistic goals for prop-rotor propulsive efficiency. *It is the profile power – not the induced power – that must first be minimized for lightly loaded prop-rotors.*

Given these introductory comments, questions arise as to (1) what is a realistic minimum profile power of a prop-rotor and then (2) what is the associated propulsive efficiency? The study included in Appendix A provides an answer to both these questions. To begin with, profile power depends on airfoil drag and airfoil drag depends on Reynolds number. Appendix A suggests (from

16

Equations A-33 and A-34 on page A-18) that these fundamental airfoil considerations lead to a minimum profile power magnitude of about

$$C_{P_{o\ min.}} = 1.25 \times 0.074 \frac{(bc/\pi R)}{(V_t c/\nu)^{1/5}}\left[\frac{5}{18}T_{(\lambda,x_c)}\right] = \frac{0.0257\ \sigma\ T_{(\lambda,x_c)}}{RN_{tip}^{1/5}} \qquad (16a)$$

where $T_{(\lambda,x_c)}$ (see Equations A-34 and A-35) is closely approximated by

$$\begin{aligned}T_{(\lambda,x_c)} \cong &\left[\left(1+\lambda^2\right)^{13/10} - x_c\left(x_c^2+\lambda^2\right)^{13/10}\right] + \frac{9}{5}\lambda^2\left[\left(1+\lambda^2\right)^{3/10} - x_c\left(x_c^2+\lambda^2\right)^{3/10}\right]\\ &+\frac{18}{25}\lambda^4\left\{\ln\left[\frac{1+\left(1+\lambda^2\right)^{3/10}}{x_c+\left(x_c^2+\lambda^2\right)^{3/10}}\right]\right\} \quad \text{for } \lambda \text{ less than } 1.3\end{aligned} \qquad (16b)$$

The primary assumptions behind Equation 16 are that

   a. the blades are rectangular,

   b. every blade element is aligned with its local helical flow,

   c. airfoil skin friction drag coefficient variation with Reynolds is that of a flat plate with completely turbulent, incompressible flow as described by Prandtl's $C_f = 0.074/RN^{1/5}$ semi-empirical suggestion and

   d. airfoil form drag and other prop-rotor incompressible flow affects are accounted for by empirically increasing the total result by 25 percent.

As suggested earlier, the propulsive efficiency more applicable to a prop-rotor assumes the induced power is zero and that the airfoil drag is a minimum. Therefore, it follows from Equations 14 and 16 that

$$\eta_P = \frac{C_T \lambda_o}{C_P} \cong \frac{C_T \lambda_o}{C_T \lambda_o + C_{P_{o\ min}}} = \frac{C_T \lambda_o}{C_T \lambda_o + \dfrac{0.0257\ \sigma\ T_{(\lambda,x_c)}}{RN_{tip}^{1/5}}} \qquad (17a)$$

Factoring the propulsive power, $C_T \lambda_o$, illuminates prop-rotor propulsive efficiency in the useful form of

$$\eta_P \cong \frac{1}{1 + \dfrac{0.0257\ T_{(\lambda,x_c)}/\lambda_o}{\left(RN_{tip}^{1/5}\right)\left(C_T/\sigma\right)_{FF}}} \qquad (17b)$$

Equation 17b shows quite clearly that the upper bound to prop-rotor propulsive efficiency is dependent on (1) inflow ratio, λ, or λ_o for small λ_i, (2) tip Reynolds number (based on tip speed, not helical tip speed) and (3) the classical rotorcraft blade loading parameter C_T/σ (evaluated in forward flight not in hover).

Representative values for Equation 17b's parameters can be defined by following the earlier civil tiltrotor example. For instance, at 25,000 feet the kinematic viscosity is 0.0003 ft^2/sec. With a forward flight tip speed of 660 ft/sec and a representative blade chord of 2 feet, the tip Reynolds number is 4.4 million. The solidity is 0.1 (with three, 2 foot chord, 19 foot long blades per rotor) so that the forward flight C_T is 0.005. The forward flight blade loading is $(C_T/\sigma)_{FF}$ = 0.05. Conveniently in this example, the product of $RN^{1/5}$ and $(C_T/\sigma)_{FF}$ is on the order of 1.0. At 421 knots the inflow ratio is 1.077 and $T_{(\lambda, x_c)}$ is calculated from Equation 16a as 5.46 assuming a root cutout, x_c, of 0.15. Therefore, the propulsive efficiency is very unlikely to be greater than 0.89.

Figure 11 illustrates the propulsive efficiency trend with inflow ratio, λ_o. The design variable is the product of $RN^{1/5}$ and forward flight $(C_T/\sigma)_{FF}$. This product ranges from perhaps as low as 0.2 to somewhat over 1.2. Since the induced inflow ratio is assumed small for prop-rotors, $T_{(\lambda, x_c)}$ is calculated assuming $\lambda = \lambda_o + \lambda_i \approx \lambda_o$. The trends shown with Figure 11 do not include losses due to compressibility, induced power or profile power due to prop-rotor thrust. Therefore, it seems safe to state that Figure 11 presents a reasonable upper bound to prop-rotor propulsive efficiency–at least for rectangular blades.

Forward Flight Blade Loading $(C_T/\sigma)_{FF}$

A first order estimate of forward flight blade loading $(C_T/\sigma)_{FF}$ for a civil tiltrotor can be determined rather easily. This key design parameter depends on the hover blade load loading, the aircraft lift to drag ratio, and the hover and cruise altitude and tip speed. Fifty years of rotorcraft industry experience has shown that near maximum hovering and low speed performance is achieved with low disc loading, $W/(2\pi R^2)$, when the hover blade loading $(C_T/\sigma)_H$ is near 0.1. That is, for a twin prop-rotor civil tiltrotor configuration

$$\text{Design} \left(\frac{C_T}{\sigma}\right)_H \cong \frac{W}{\left[\rho(2\pi R^2)V_t^2\right]_H} = \frac{W/(2\pi R^2)}{\left[\rho V_t^2\right]_H} \approx 0.1 \tag{18}$$

Now in forward flight, the twin prop-rotor's thrust is equal to aircraft drag. However, the aircraft drag is simply $D \approx W (D/L)_{A/C}$ so it follows that

$$\left(\frac{C_T}{\sigma}\right)_{FF} \cong \frac{D}{\left[\rho(2\pi R^2)V_t^2\right]_{FF}} \approx \frac{W}{(L/D)_{A/C}\left[\rho(2\pi R^2)V_t^2\right]_{FF}} = \frac{W/(2\pi R^2)}{(L/D)_{A/C}\left[\rho V_t^2\right]_{FF}} \tag{19}$$

Therefore the forward flight blade loading (assuming constant diameter between hover and forward flight) is related to the hover design condition by removing

disc loading, $W/(2\pi R^2)$, from Equations 18 and 19. This gives the forward flight blade loading as

$$\left(\frac{C_T}{\sigma}\right)_{FF} \cong \frac{\left[\rho V_t^2\right]_H}{(L/D)_{A/C}\left[\rho V_t^2\right]_{FF}}\left\{\text{Design}\ \left(\frac{C_T}{\sigma}\right)_H\right\} \approx \frac{\left[\rho V_t^2\right]_H}{\left[\rho V_t^2\right]_{FF}}\frac{0.1}{(L/D)_{A/C}} \quad (20)$$

Equation 20 shows immediately the difficulty tiltrotor designers face in matching hover to cruise blade loading. Even if cruise altitude and tip speed remained constant at, say, the hover design point, the primary aerodynamic effort to maximize aircraft lift to drag ratio at cruise will drive the prop-rotor to very low blade loading and, therefore, to less than optimum propulsive efficiency (for a given tip Reynolds number and inflow ratio). To illustrate these points, consider the example tiltrotor taking off at 5,000 feet density altitude with a 790 feet per second tip speed, but cruising at 25,000 feet density altitude and 660 feet per second tip speed. Then

$$\frac{\left[\rho V_t^2\right]_H}{\left[\rho V_t^2\right]_{FF}} = \frac{0.002049\left(790^2\right)}{0.001065\left(660^2\right)} \approx 2.7565$$

The direction suggested here is to take the hover dictated prop-rotor blade area to high altitude cruise and slow the tip speed down. However, even with a relatively poor fixed wing aircraft L/D of, say, 10, the forward flight blade loading $(C_T/\sigma)_{FF}$ is still only a modest 0.0276. This light blade loading will, of course, be even lower as aircraft L/D is improved to achieve optimum cruise at minimum power required.

Maximizing Cruise Performance

The aerodynamic performance objective is not, of course, to maximize prop-rotor propulsive efficiency. Rather the objective is to minimize cruise power required per pound of gross weight. Therefore, while forward flight blade loading $(C_T/\sigma)_{FF}$ and propulsive efficiency may suffer by increasing aircraft L/D, total cruise power can be reduced. A continuation of the example illustrates the design fundamentals. Consider first that at a given cruise speed the gross weight per horsepower required can be written in terms of propulsive efficiency and aircraft L/D [assuming $D = W\ (D/L)_{A/C}$] simply as

$$\frac{W}{HP} = \frac{550\,\eta_P(L/D)_{A/C}}{1.69 V_{kts}} \quad (21)$$

Equation 21 shows that it is the product of propulsive efficiency and aircraft lift to drag ratio that must be maximized to obtain competitive cruise performance.

Now suppose, for simplicity's sake, that the tip Reynolds number is on the order of 4.4 million and the cruise inflow ratio is 1.077 (which corresponds to 421 knots at 25,000 feet density altitude, 660 feet per second tip speed and 2 foot chord). Then the forward flight blade loading will vary as

$$\left(\frac{C_T}{\sigma}\right)_{FF} \cong \frac{\left[\rho V_t^2\right]_H}{\left[\rho V_t^2\right]_{FF}} \frac{0.1}{(L/D)_{A/C}} = \frac{0.276}{(L/D)_{A/C}} \qquad (22)$$

This variation can adversely affect the propulsive efficiency as Figure 11 suggests. However, it is the greatest product, η_P times $(L/D)_{A/C}$, that is sought.

The weight to horsepower ratio for this example at 412 knots varies with aircraft L/D as shown by Figure 12. The propulsive efficiency, following Equations 20 and 17b and Figure 11, unfortunately drops significantly as the aircraft L/D is improve (in comparison to more heavily loaded, fixed wing propellers). Figure 12 also includes the results had a lower cruise speed of 350 knots been chosen (i.e., $\lambda_o = 1.69 \times 350/660$) but holding all other parameters constant. Figure 12 shows that with an aircraft L/D in the 10 to 15 range, competitive high cruise speeds can be achieved with power loadings at cruise altitude on the order of 6 to 8 pounds per horsepower.

Two fixed wing turboprop points are provided on Figure 12 for comparison. The first point is for a modern regional twin turboprop, the 50 to 58 passenger Saab 2000, which has a gross weight of slightly over 50,000 pounds. At this weight, its maximum cruising speed at 25,000 feet is 366 knots. It cruises at this maximum continuous speed and density altitude on about 2,850 shp from each engine*. The Saab 2000 therefore has a power loading of GW/HP $\approx$ 8.8 lbs/shp. Guessing that the Saab 2000 propellers have a propulsive efficiency of about 0.85 leads to an aircraft L/D on the order of 11.6. The second point refers to the Lockheed Electra of the post World War II era. This 80 passenger, 116,000 pound takeoff gross weight airplane used four 3,750 eshp Allison Model 501 (military designation T-56) turboprop engines. These engines each gave 2,060 shp for cruising at 20,000 feet on a standard day. At 85,500 pound mid-mission gross weight, the Electra cruise speed was slightly over 350 knots. Thus the Electra, at these cruise conditions, had a GW/HP $\approx$ 10.4 lbs/shp. With a propulsive efficiency again guessed at 0.85, the Electra aircraft lift to drag ratio was probably about 13.1.

---

* The Saab 2000 engines are Allison AE 2100A which are a commercial version of the V-22's power plant (military designation T406-AD-400). Each Saab 2000 turboprop engine is flat rated (i.e., continuous transmission limit) at 4,125 shp up to a reasonable altitude. For the turboshaft version used in the V-22, the takeoff rating at sea level standard is 6,150 shaft horsepower. At 25,000 feet altitude and 350 knots, both civil turboprop and military turboshaft versions have a maximum continuous horsepower capability of roughly 3,200 shp per engine.

From the analysis to this point as summarized by Figure 12, it should be clear that civil tiltrotor cruise performance competitive with an equivalent modern turboprop aircraft is an achievable objective.

Analysis of civil tiltrotor forward flight power required using propulsive efficiency can be, in fact, an indirect and awkward approach. A more direct way to study twin prop-rotor tiltrotor performance is to see the power required in dimensional form. Using Equations 11 and 16 the *practical* minimum power required at forward flight speed takes the form

$$550 \, HP = DV + D \frac{D}{2\rho(2\pi R^2)V} + \rho(2\pi R^2)V_{tip}^3 \left\{ \frac{0.0257 \, \sigma \, T_{(\lambda,x_c)}}{RN_{tip}^{1/5}} \right\} \tag{23}$$

The first term in Equation 23 is the power to over come aircraft drag. Estimating aircraft drag at a given weight using $D = W \, (D/L)_{A/C}$ is quite direct because an aircraft's best lift to drag ratio is such a fundamental aerodynamic parameter. For commercial passenger aircraft, a conceptual design level of maximum $(L/D)_{A/C}$ is frequently approximated in terms of wing span, body diameter and a frontal area drag coefficient, $C_{D\pi}$, simply as

$$\text{Max.} \, (L/D)_{A/C} = \frac{1}{\sqrt{C_{D_x}}} \times \frac{\text{wing span}}{\text{body diameter}} \approx 1.0 \text{ to } 1.5 \text{ times } \frac{b_w}{d_f} \tag{24}$$

where $C_{D\pi}$ is empirically on the order of 0.5 to 1.0 for many commercial passenger carrying airplanes.* Aircraft designers will, quite naturally, go to almost any lengths to maximize aircraft L/D. The second term in Equation 23 is the prop-rotor induced power required to produce the thrust that overcomes aircraft drag. The induced power is nearly negligible in the tiltrotor case. Equation 23's third term is the minimum profile power required by the pair of prop-rotors.

Equation 23 can take another useful form better suited to studying power required at a given weight and design speed. This form is obtained using the substitutions of $\lambda_o = V/V_{tip}$, $\pi R^2 \sigma = bcR$ and $D = W/ (L/D)_{A/C}$. With these substitutions, the power required can be estimated from

$$550 \, HP = \frac{W \, V}{(L/D)_{A/C}} + \frac{W^2}{2\rho(2\pi R^2)V(L/D)_{A/C}^2} + 0.0257\rho(2bcR)V^3 \left\{ \frac{T_{(\lambda,x_c)}/\lambda_o^3}{RN_{tip}^{1/5}} \right\} \tag{25}$$

To minimize horsepower required for a given weight, altitude and at a given speed, *the major effort must first be placed on achieving the maximum aircraft lift to drag ratio.* This is in contrast to the rotorcraft industry's emphasis over the

---

* Equation 24 is derived by rewriting the classical $C_D = C_{Do} + C_L^2/\pi AR$ drag versus lift equation in dimensional form as $D = q(\frac{\pi}{4}d_f^2)C_{D_x} + L^2/\pi q \, b_w^2$ and then solving for max. L/D.

21

last 50 years. The secondary effort is placed on reducing prop-rotor minimum profile power (i.e., the third term in Equation 25). Since, for the rotary wing engineer, hover requirements dictate most of the parameters in the profile power term, only the behavior of $T_{(\lambda, x_c)} / \lambda^3_o = f(\lambda_o)$ warrants additional discussion. This function, graphical shown on Figure 14, approaches about 3 in the limiting case of infinite λ_o. This limit corresponds to a stopped and feathered prop-rotor.

One last point about maximizing cruise performance is in order. The rotorcraft industry has not emphasized maximum aircraft lift to drag ratio as their helicopters have repeatedly shown. However, without this primary aerodynamic emphasis, future civil tiltrotor aircraft will fall short of industry hopes. It is frequently suggested, for example, that the V-22 wing and propulsion system would, with a commercial fuselage, make a satisfactory configuration. While this might reduce development costs and make some short term business sense, the resulting aircraft suggests a poor future.

The reason for this concluding statement is two fold. The first fact is illustrated by the planform comparison shown in the following sketch. If the V-22 wing and prop-rotor system were adapted to the Saab 2000 it would degrade aircraft maximum $(L/D)_{A/C}$ by at least 30 percent because of inadequate wing span. The Saab 2000 wing span is 81.19 feet and its fuselage maximum diameter is 7.58 feet. From Equation 24, the Saab 2000 $(L/D)_{A/C}$ of about 11.6 means that $C_{D\pi}$ is roughly 0.8. With the V-22 wing span, including tip mounted nacelles, of 50.92 feet (and constant frontal area drag coefficient), the maximum $(L/D)_{A/C}$ drops to 7.2. While the V-22 wing area is sufficient for a reasonable flight envelope at 50,000 pound gross weight, its aspect ratio is quite low when compared to all successful commercial transports.

The second reason a wing patterned after the V-22 is a poor design direction deals with the wing airfoil. To insure freedom from aeroelastic instabilities throughout the design envelope, the V-22 design solution uses a constant wing airfoil having a thickness to chord ratio of 0.23. This thickness ratio was required to obtain high wing torsional stiffness. In stark contrast the Saab 2000 wing thickness ratio varies from root to tip and is, on average, nearly 1/2 of the V-22 wing airfoil thickness ratio. This thinner wing has considerably less drag.

Not withstanding these two measures of current tiltrotor technology, the author firmly believes, based on Figure 12, that future civil tiltrotor turboshaft aircraft can be designed that are cruise speed competitive with current regional turboprop aircraft. The foundation to this author's belief is that rotary wing engineers can design high lift to drag ratio airplanes.
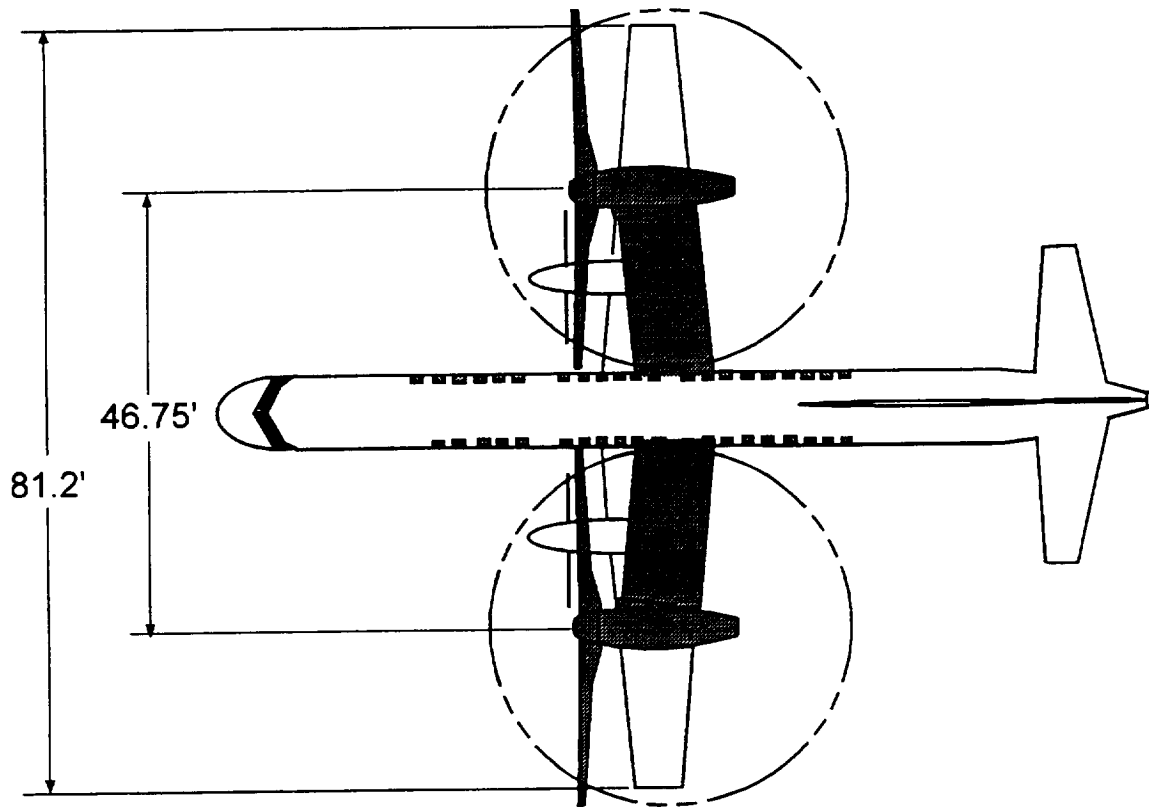
**A V-22 Wing And Prop-rotor System Mounted On The Saab 2000
Body Leads To An Aircraft With A Comparatively Poor Lift To Drag
Ratio In Cruise Flight Because The Wing Span Is Too Short.**

Vertical Takeoff Performance

Given that current regional turboprop aircraft cruise performance can be matched at equal power loading by a comparably well designed civil tiltrotor, the question of vertical takeoff power required still remains to be answered.

The rotorcraft industry, with its considerable knowledge of the low speed regime, continually emphasizes efficient hover performance by maximizing the ratio of rotorcraft weight to horsepower. Their helicopter experience can be summed up with a simple empirical equation and the flight test results from over 50 designs. When the hover thrust is taken as aircraft weight in pounds, this simple empirical equation becomes

$$\frac{\text{Weight}}{\text{Horsepower}} = \frac{37.93}{\sqrt{W/\sigma' A}}(\text{Figure of Merit}) \tag{26}$$

23

In Equation 26, the horsepower required to lift a given weight depends first on the total rotor swept disc area. For the tiltrotor with twin prop-rotors, this area amounts to $2(\pi R^2)$. The horsepower requirement increases with density altitude which is reflected by density ratio, $\sigma' = \rho/\rho_o$. Figure of Merit (FM) is a measure of hovering efficiency relative to ideal*. Figure 14 shows that the rotorcraft industry appears to have reached an upper bound to Figure of Merit. The median FM performance (shown by the solid line on Figure 14) is described by

$$FM = \frac{1}{\dfrac{0.0085 \times \text{Solidity}}{4\sqrt{2} \times (\text{Weight Coeff.})^{3/2}} + 1.5} \tag{27}$$

In general the rotorcraft industry's helicopters achieve higher Figure of Merit when the ratio of $C_W^{3/2}$ to solidity is above 0.01 and the weight coefficient to solidity ratio is on the order of 0.1. In general, the industry has tried to use the lowest solidity rotor that technology and design specifications will allow.

An estimate of hover power loading can be made for the 50,000 pound, civil tiltrotor example. For instances, at a 5,000 foot density altitude for takeoff, the weight coefficient is 0.01724 based on twin, 38 foot diameter prop-rotors and 790 feet per second tip speed. The solidity for each prop-rotor is 0.1 so this example tiltrotor should have a Figure of Merit on the order of 0.64 by following Equation 27. The disc loading, accounting for density ratio, is 25.6 pounds per square foot. Therefore, using Equation 26, the power loading at takeoff would be on the order of 4.8 pounds per horsepower. Thus, this 50,000 pound civil tiltrotor would need two turboshaft engines takeoff rated at roughly 5,200 horsepower at 5,000 feet. The Allison turboshaft engine used for the V-22 (rated at 6,150 shp for takeoff and 5,920 shp maximum continuous at sea level) will easily produce 5,200 shp at 5,000 feet for takeoff.

---

* Discussion of Figure of Merit can be found in any number of rotorcraft technical books. The ideal Figure of Merit is 1.0. A value of 0.5 says that the rotorcraft will required two times ideal power to hover.

Conclusions

The primary objective of this effort has been to re-discover, re-evaluate and report performance data from two early NACA propeller experiments. This objective has been accomplished with tabulated data contained in Appendices B and C and the analysis provided by Appendix A. The analysis shows that PROP 2 data is more applicable to future, high speed, civil tiltrotor aircraft because of its Reynolds and Mach number test range. For PROP 2, thrust variations with collective pitch and inflow ratio appear, with minor zero shifting, to be consistent with simple blade element theory. The power versus thrust and inflow ratio behavior is also consistent with simple energy theory. PROP 1 data, while also consistent with simple blade element theory, was obtained in the airfoil laminar to turbulent boundary layer transition Reynolds number range. The effects of compressibility in this PROP 1 Reynolds number range offers a more difficult challenge to theory–test correlation. PROP 1 data does not appear directly applicable to future tiltrotor needs.

Appendix A's results have been used to establish prop-rotor propulsive efficiency goals. These goals are very dependent on Reynolds number and blade loading. A conservative design criteria for compressibility loss avoidance is derived. Predicted tiltrotor performance goals at 350 and 420 knots have been established. These aircraft performance goals account for both propulsive efficiency and aircraft lift to drag ratio. It is noted that tiltrotor aircraft developed to date have shortened wing span when compared to equivalently powered turboprop airliners. This relatively low aspect approach has been required to meet military design requirements. However, undersizing wing span penalizes the cruise lift to drag ratio of currently flying tiltrotor aircraft at least 30 percent in comparison to modern airliners. A comparison to two turboprop commercial aircraft shows that future civil tiltrotor aircraft can have competitive cruise speed performance.

There appears to be no fundamental aerodynamic reason why the rotorcraft industry can not develop civil tiltrotor aircraft which are competitive with today's regional, turboprop airliners. In addition to comparable forward flight performance, these future tiltrotor aircraft will provide vertical takeoff and landing capability. With both VTOL and comparable cruise performance, it is quite plausible to suggest that traditional, propeller driven turboprop airliners can be rendered obsolete by future rotorcraft industry efforts.

Recommendations

To exploit the full potential offered by tiltrotor aircraft, the following tasks must be included in the overall research and development program:

1. The PROP 2 performance data set should be compared to CFD computations to obtain a validated design theory.

2. Prop-rotor configurations suited to several cruise speeds up to at least 425 knots must be established to assure that future tiltrotor aircraft (beyond first generation XV-15 and MV-22 civil derivatives) have competitive cruise performance with modern, regional turboprop airliners.

3. The rotorcraft industry must learn how to design a performance efficient airplane. This learning would begin by thinking of the tiltrotor as a turboprop aircraft. This would include recognizing the much larger position in the transportation field this unique aircraft can have. This learning would also include:

   a. Thoroughly understanding the capabilities of past, current and future propeller driven aircraft.

   b. Removing military design requirements and associated solutions when developing civil aircraft. For example, both wing span and area differ markedly from military aircraft when maximum aircraft lift to drag ratio is a design objective. A second example is compressibility losses. These losses, currently incurred by flying tiltrotor aircraft, must be virtually eliminated to achieve efficient performance above 400 kn.

   c. Understanding how to better match VTOL takeoff and cruise power requirements for the unique tiltrotor aircraft.

   d. Introducing large prop-rotor diameter, civil turboprop aircraft having these VTOL and cruise performance features without incurring the excessive price and operating costs associated with helicopters.

Acknowledgments

References

1. Hager, Roy D. and Vrabel, Deborah, "Advanced Turboprop Project," NASA SP-495, Prepared at NASA Lewis Research Center, 1988.

2. Delano, James B. and Carmel, Melvin M., "Investigation of the NACA 4-(5)(08)-03 Two-Bladed Propeller at Forward Mach Numbers to 0.925," NACA Research Memorandum L9G06a, September 15, 1949.

3. Evans Albert J. and Liner, George, "A Wind Tunnel Investigation of the Aerodynamic Characteristics of a Full-Scale Supersonic-Type Three-Bladed Propeller at Mach Numbers to 0.96," NACA Technical Report 1375, 1958.

4. Perkins, Courtland D. and Hage Robert E., *Airplane Performance, Stability and Control*, John Wiley & Sons, Inc., New York, 1949.

5. Gessow, Alfred and Myers, Garry C., Jr., *Aerodynamics of the Helicopter*, Frederick Ungar Publishing Co., New York, Third Printing, 1967.

6. Delano, James B., "Investigation of the NACA 4-(5)(08)-03 and NACA 4-(10)(08)-03 Two-bladed Propellers at Forward Mach Numbers to 0.725 to Determine the Effects of Camber and Compressibility on Performance," NACA Technical Report 1012, 1951.

7. Carmel, Melvin M. and Robinson, Harold L. "Further Investigation of NACA 4-(5)(08)-03 Two-blade Propeller at High Forward Speed," NACA RM No. L7E12, May 26, 1947.

8. Stack, John, "Tests of Airfoils Designed to Delay the Compressibility Burble," NACA Technical Report 763, 1943.

9. Abbott, Ira H. and Von Doenhoff, Albert E., *Theory of Wing Sections*, Dover Publications, Inc. New York, New York, 1959.

10. Watkins, Lt. James R., "Redesign of Tiltrotor Blades for 400 Knot Flight Using Computational Fluid Dynamics," Thesis for Naval Postgraduate School, Monterey, California, Sept. 1995. (Available via the Defense Technical Information Center, Cameron Station, Alexandria VA, 22304-6145 and referring to Code 043, Naval Postgraduate School, Monterey, CA, 93943-5000.)

11a. Srinivasan, G. R., Baeder, J. D., Obayashi, S., and McCroskey, W. J., "Flowfield of a Lifting Rotor in Hover," AIAA Journal, Vol. 30, No. 10, pg. 2371-2378, October 1992.

11b. Strawn, R. C. and Biswas, R., "Computation of Helicopter Rotor Acoustics in Forward Flight," Presented at the 19th Army Science Conference, Orlando, FL, 20-24 June 1994.

12. Thwaites, Bryan, *Incompressible Aerodynamics*, Dover Publications, Inc. New York, 1987.

13. Schairer, George S., "Looking Ahead in V/STOL," Presented at IAS-RAeS 8 th Anglo-American Aeronautical Conference, London, England, September 1961.

14. Schairer, George S., "Some Opportunities for Progress in Aircraft Performance," 27 th Wright Brothers' Lecture, Presented at AIAA Meeting, January 20, 1964, New York, New York. (Also Boeing Document No. D1-80-0019.)

15. Johnson, Wayne, *Helicopter Theory*, Princeton University Press, Princeton, New Jersey, 1980.

16. Hoerner, Sighard F., *Fluid-Dynamic Drag*, Hoerner Fluid Dynamics, Brick Town, New Jersey, 1965.

17. von Karman, Theodore, "The Similarity Law of Transonic Flow," Journal of Mathematics and Physics, Volume XXVI, No. 3, October 1947, pg. 182-190.

18. Spreiter, J. R., "Similarity Laws for Transonic Flow About Wings of Finite Span," NACA TN 2273, January 1951.

19. McCroskey, William James, Baeder, James D. and Bridgeman, John O., "Calculation of Helicopter Airfoil Characteristics for High Tip-Speed Applications," Presented at the 41 st Annual Forum of the American Helicopter Society, Ft. Worth, Texas, May 1985.

20. Becker, John V., *The High-Speed Frontier, Case Histories of Four NACA Programs, 1920-1950.*, NASA SP-445, 1980.
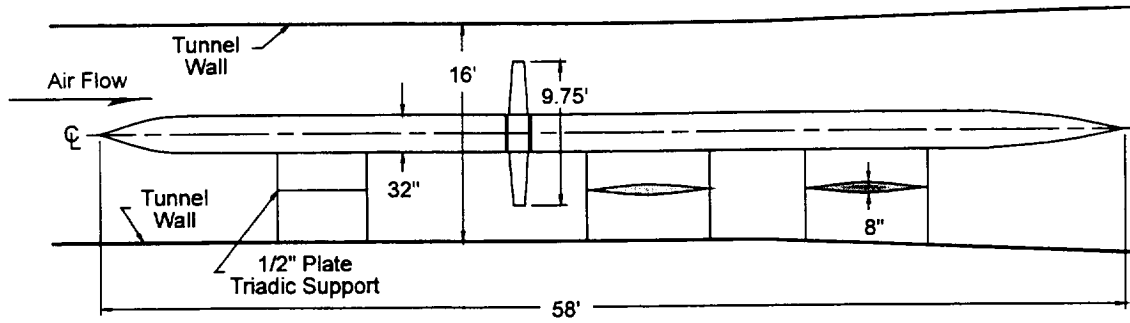
Figure 1. Installation of the 9.75 Foot Diameter, 3-Bladed Propeller in the Langley 16-foot High Speed Wind Tunnel. (Ref. 3)
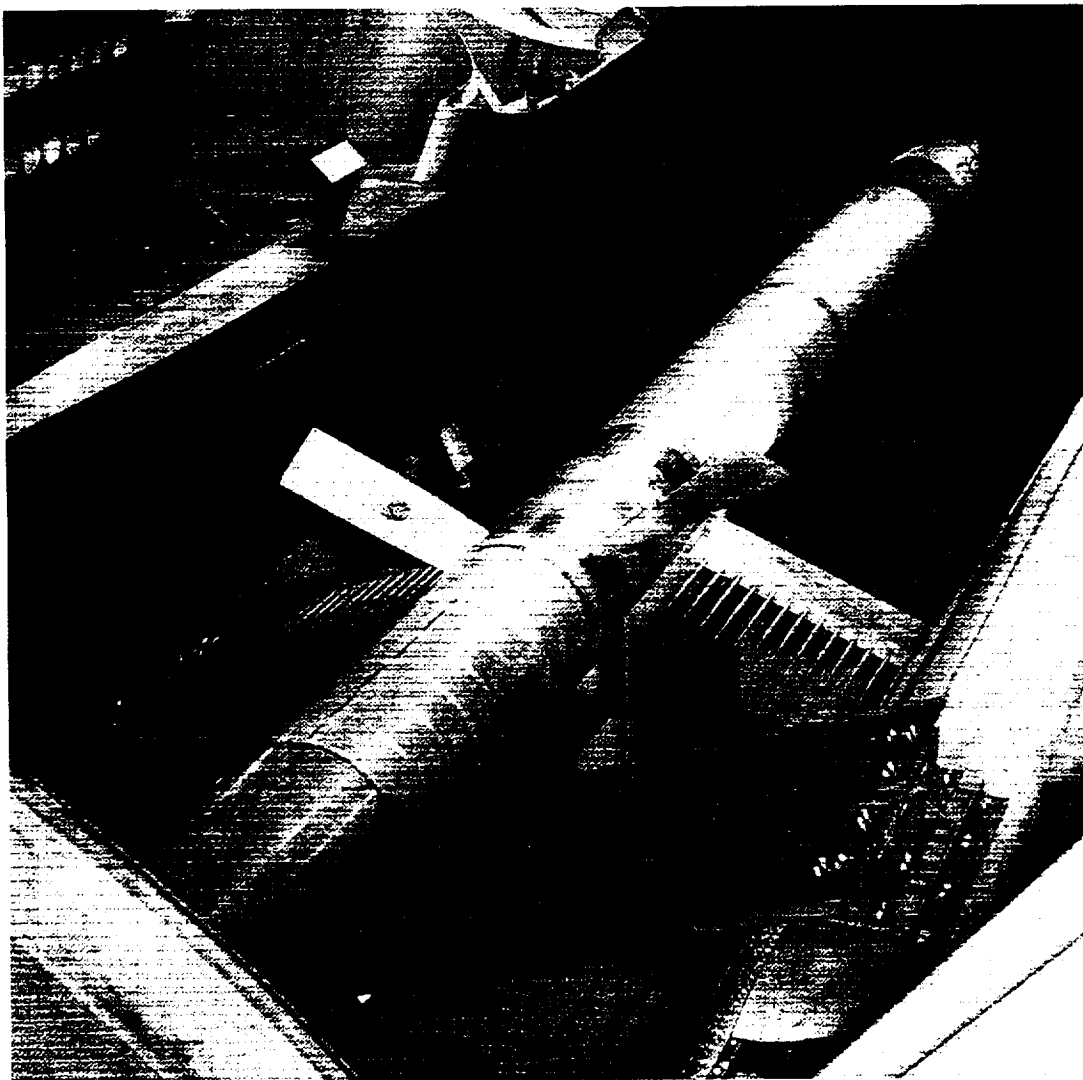
Figure 2. The 9.75 Ft, 3-Bladed, Propeller Mounted on the 6,000 Horsepower Dynamometer in the Langley 16-foot Transonic Wind Tunnel. (Ref. 3)
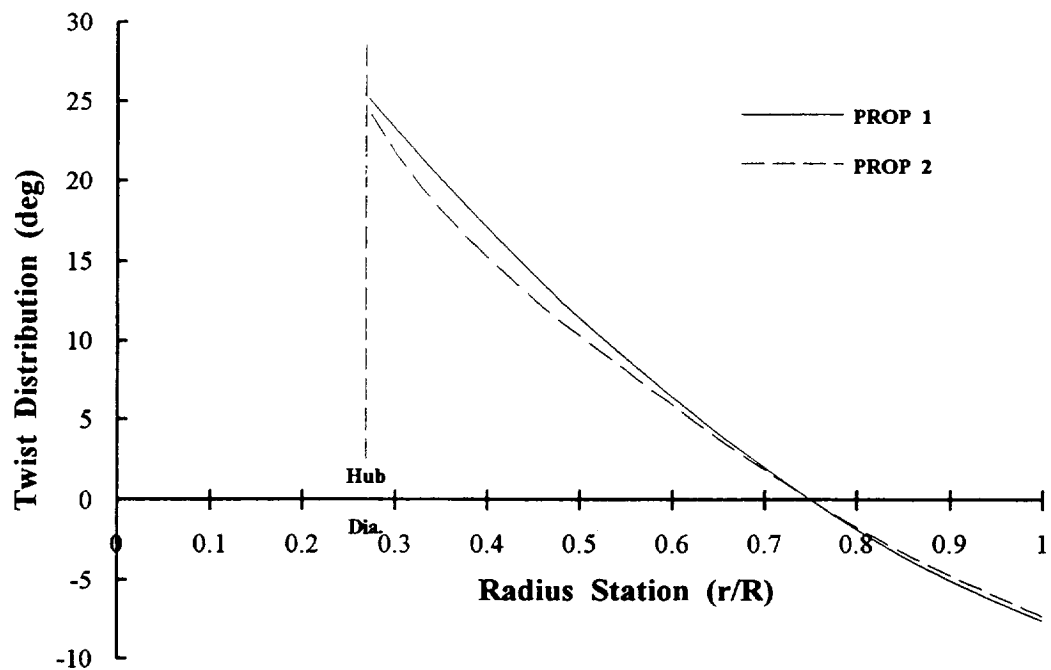
Figure 3a. PROP's 1 & 2 Had Quite Similar Twist Distributions.
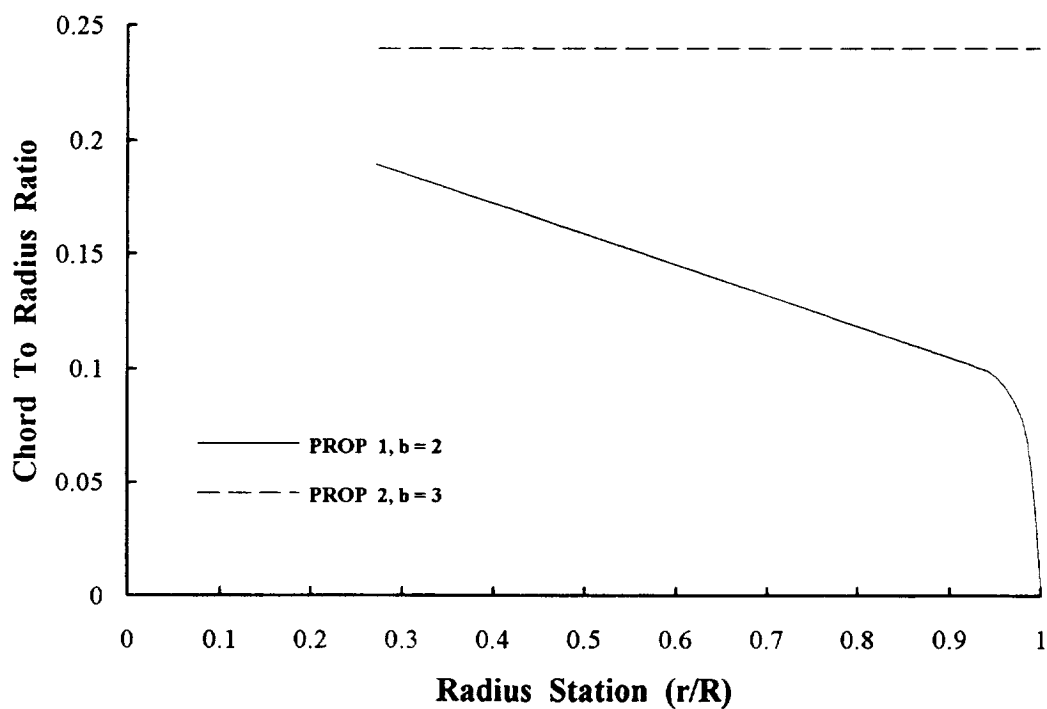
Figure 3b. PROP 1 Solidity = 0.0721; PROP 2 Solidity = 0.2292.

Prop_Geo.xls
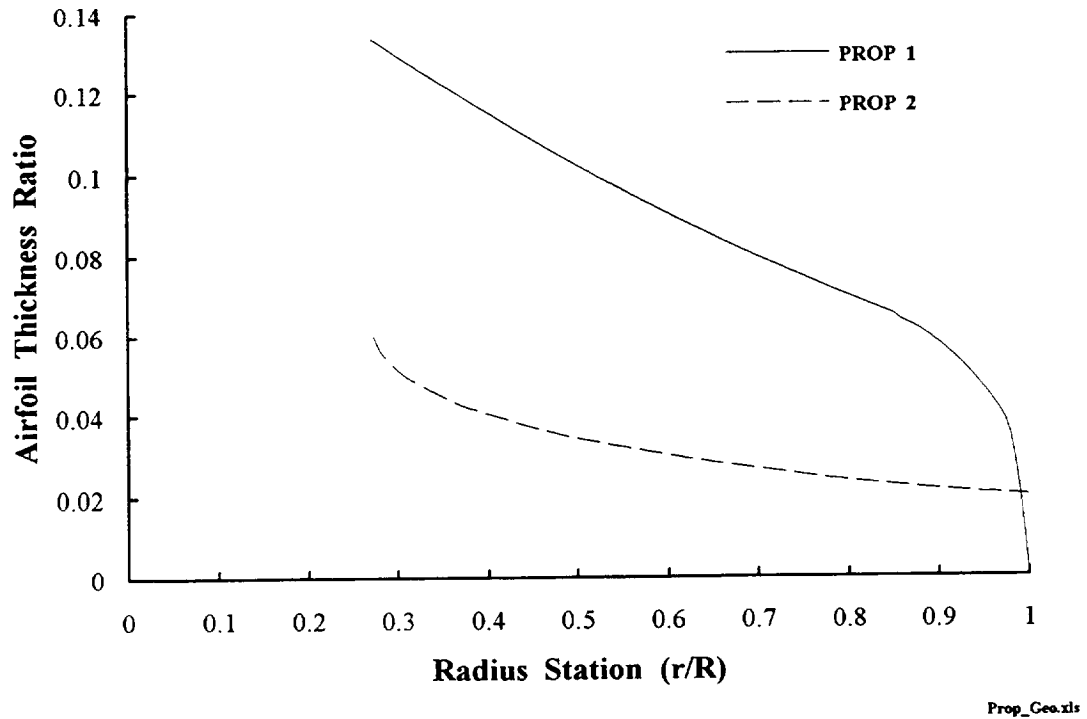
Figure 3c. PROP 2 Had Very Thin Airfoils.

Note: PROP 2 is symmetrical
and design Cl is zero.

Prop_Geo.xls
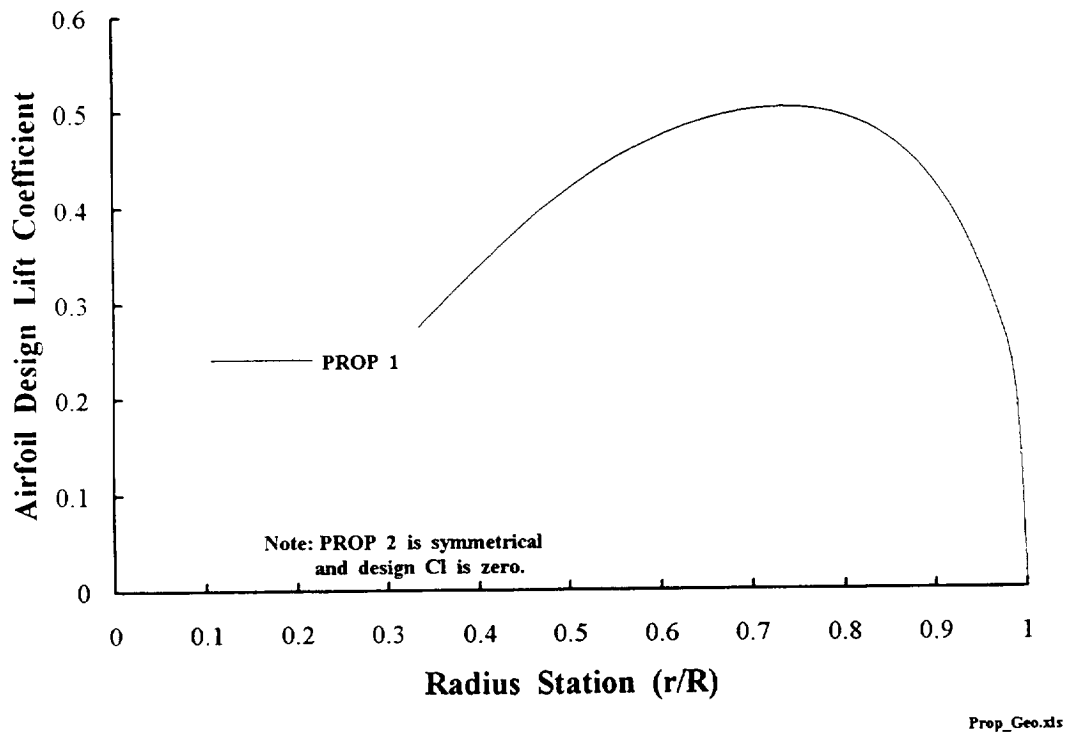
Figure 3d. NACA 16-xxx Series Airfoils Were Used For Both PROP s.
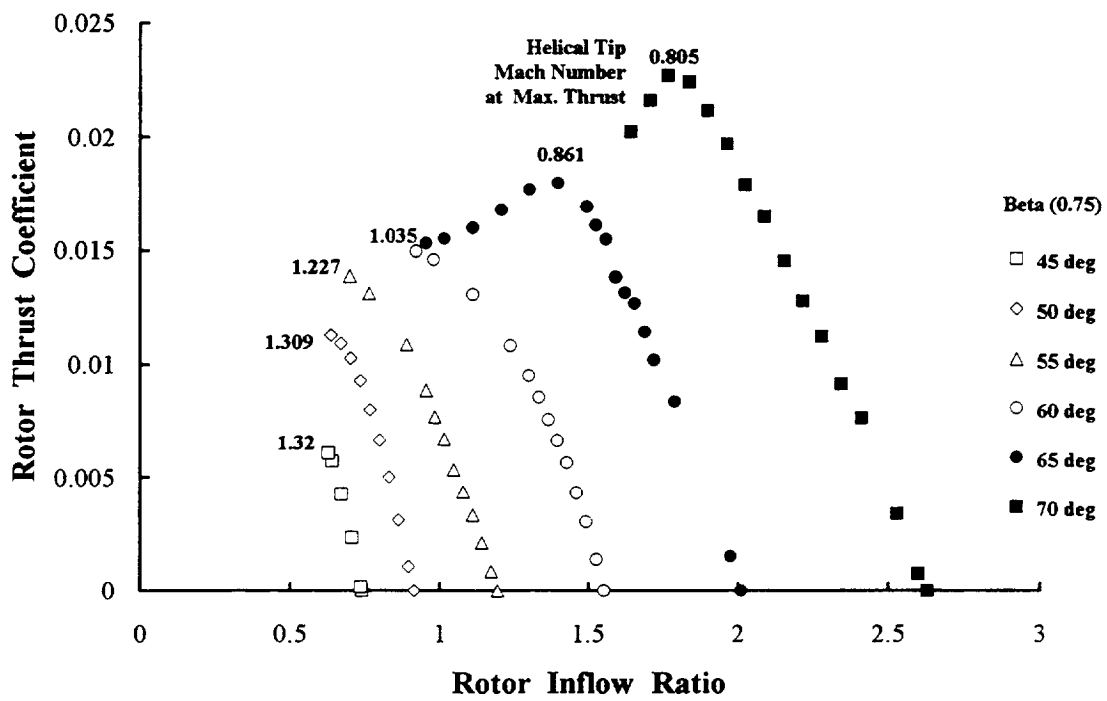
Figure 4a. PROP 1 Thrust Coefficient at Wind Tunnel Mach Number of 0.70.
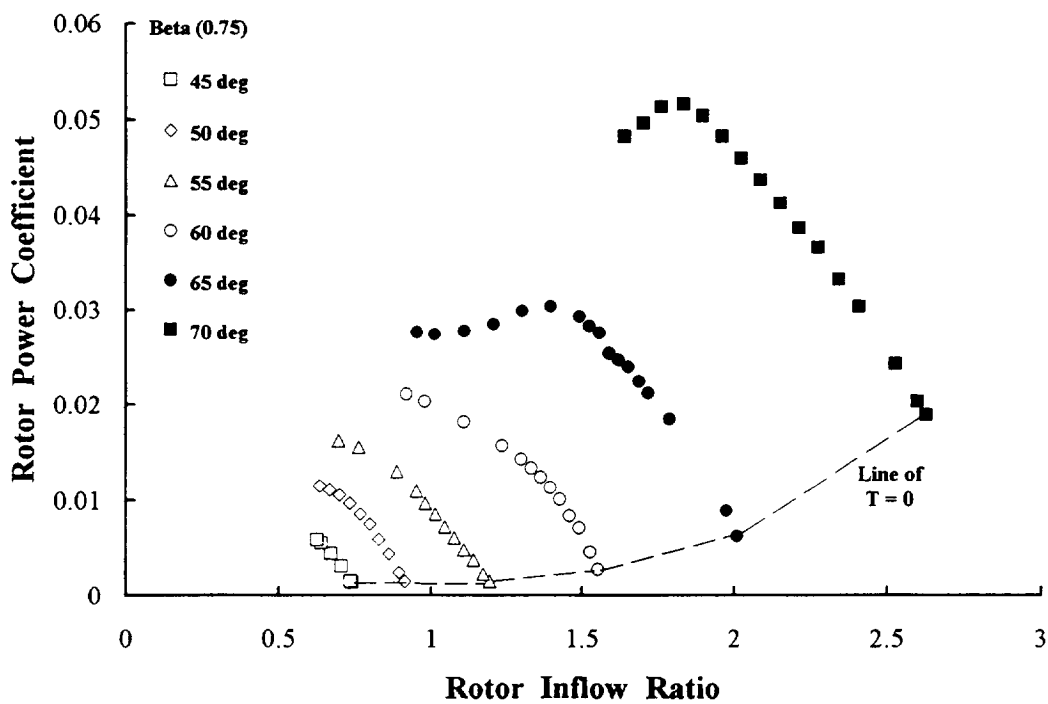
Figure 4b. PROP 1 Power Coefficient at Wind Tunnel Mach Number of 0.70.

32
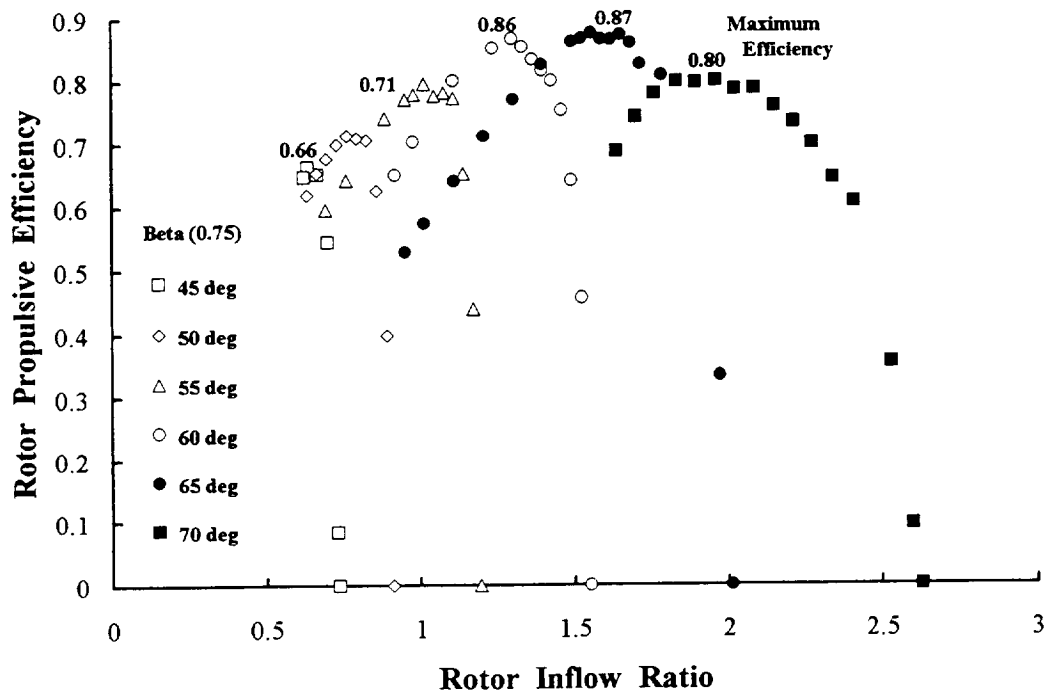
Figure 4c. PROP 1 Propulsive Efficiency at Tunnel Mach Number of 0.70.
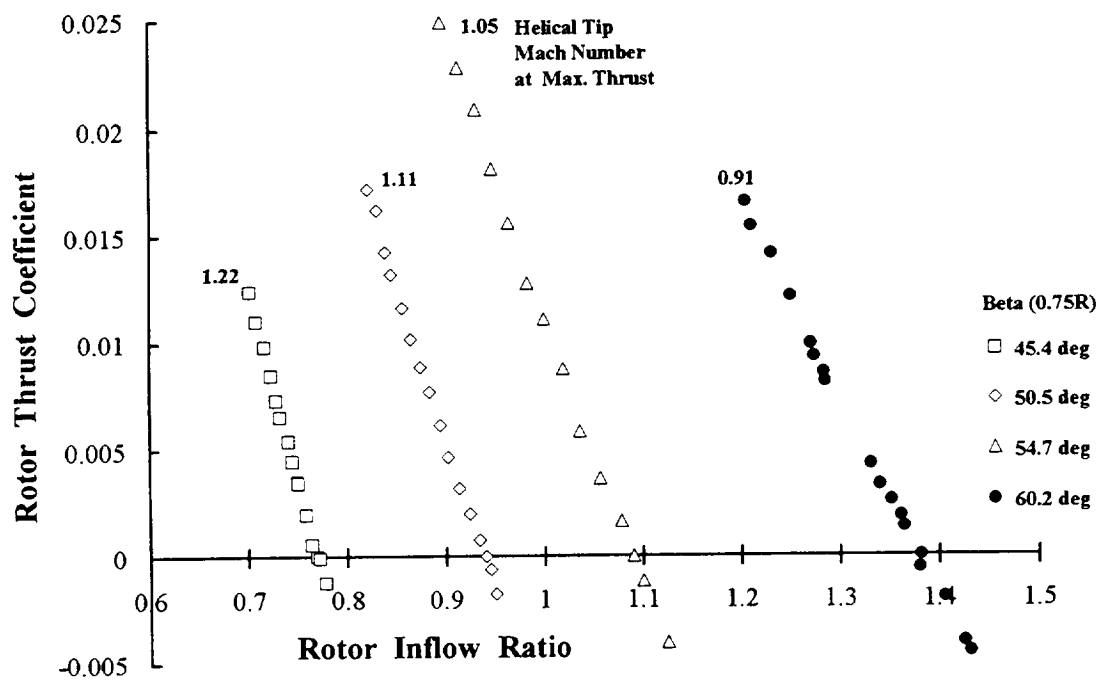
Figure 5a. PROP 2 Thrust Coefficient at Wind Tunnel Mach Number of 0.70.

33
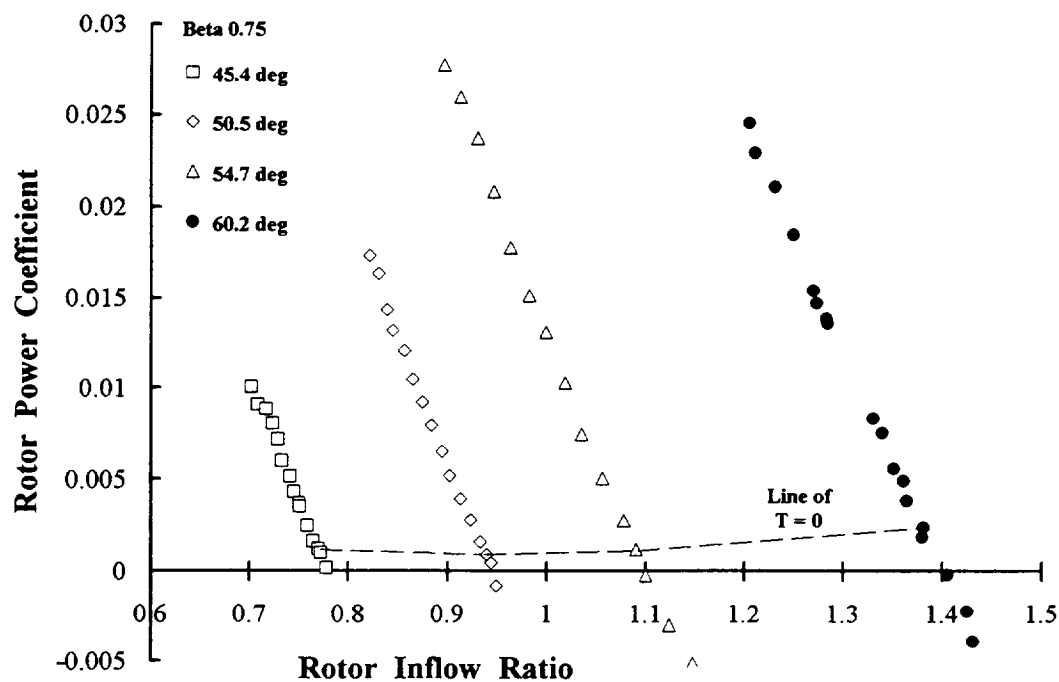
Figure 5b. PROP 2 Power Coefficient at Wind Tunnel Mach Number of 0.70.
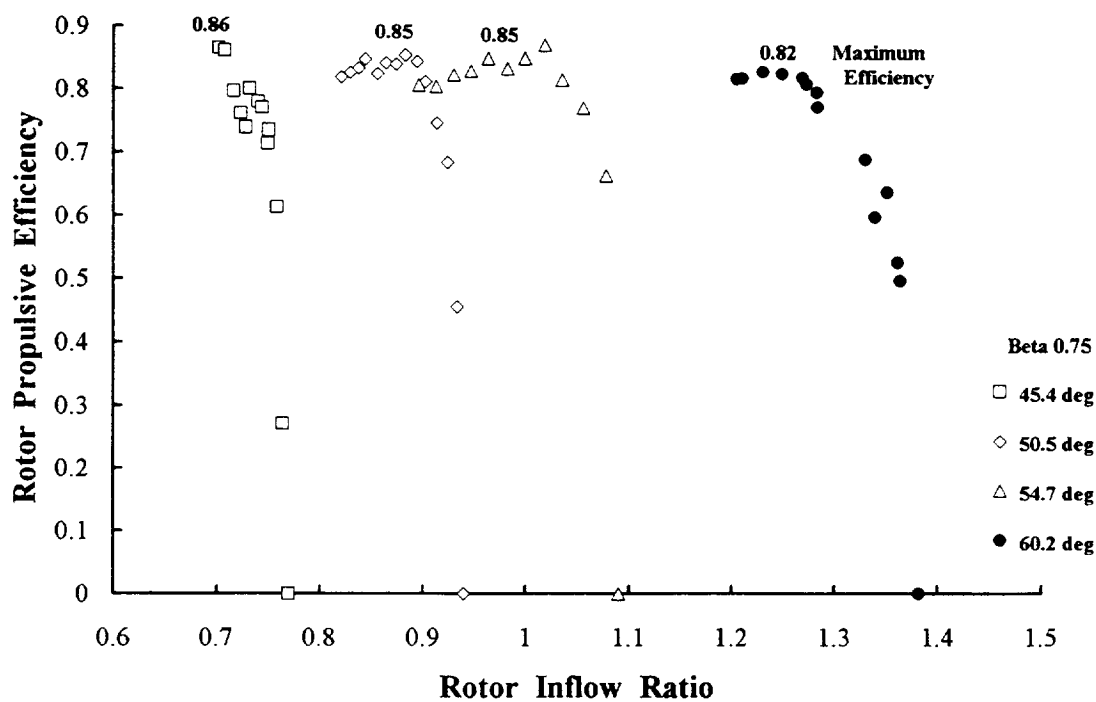
Figure 5c. PROP 2 Propulsive Efficiency at Tunnel Mach Number of 0.70.

34
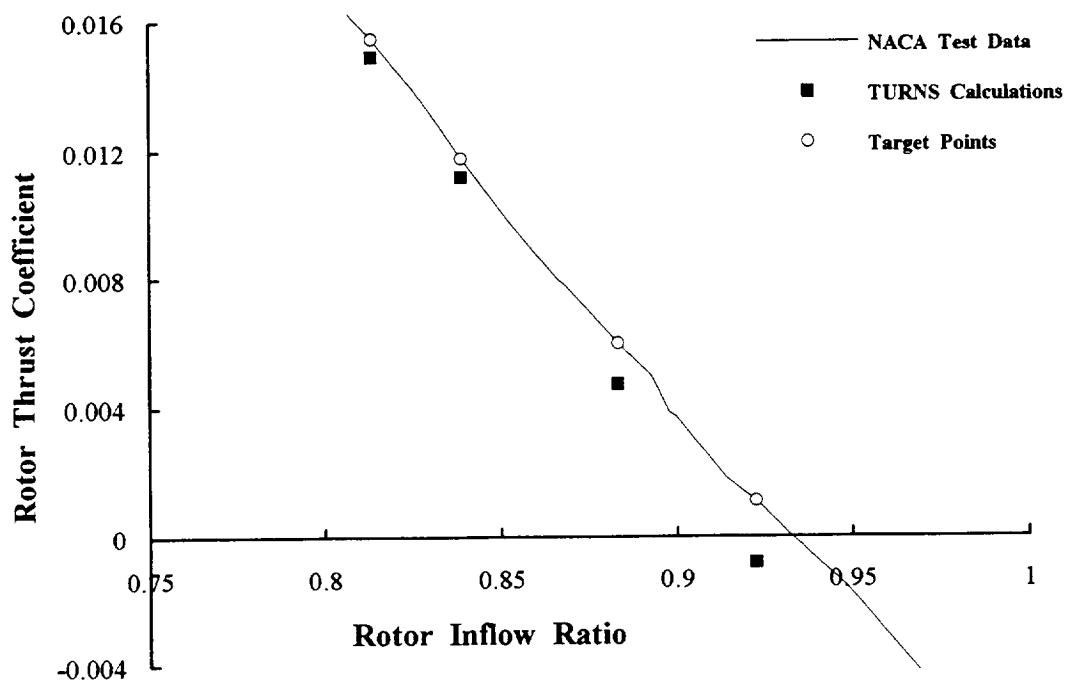
CFDJamey.xls

Figure 6. TURNS CFD Code Under Predicts Thrust (β.75 = 50.4 °, M = 0.60)
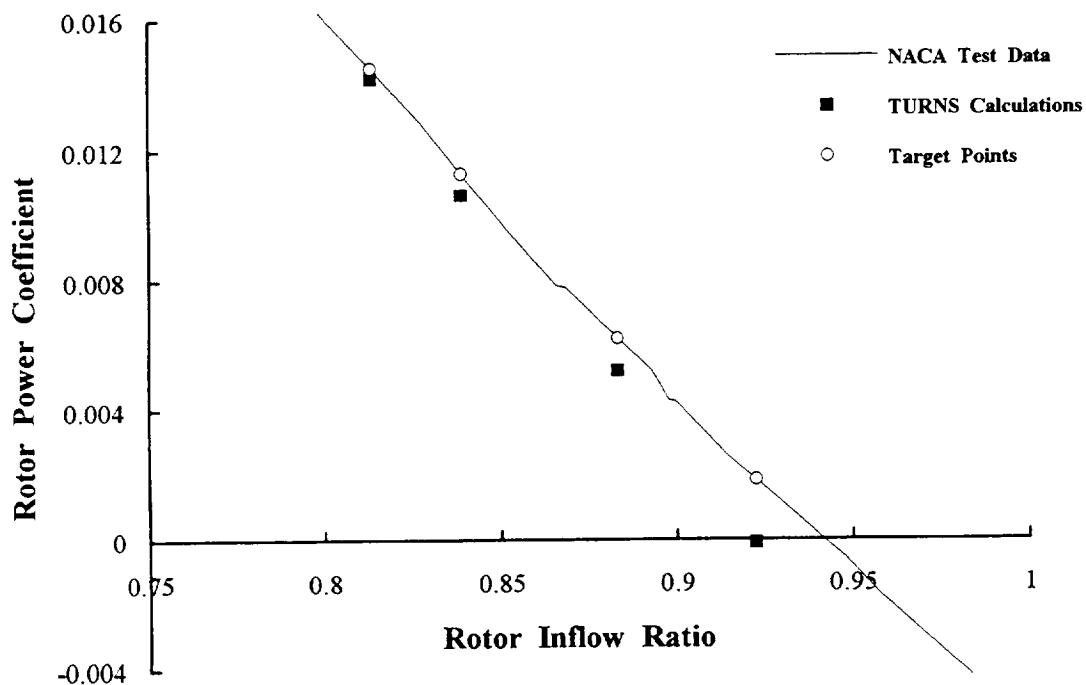
CFDJamey.xls

Figure 7. TURNS CFD Code Under Predicts Power (β.75 = 50.4 °, M = 0.60)

35
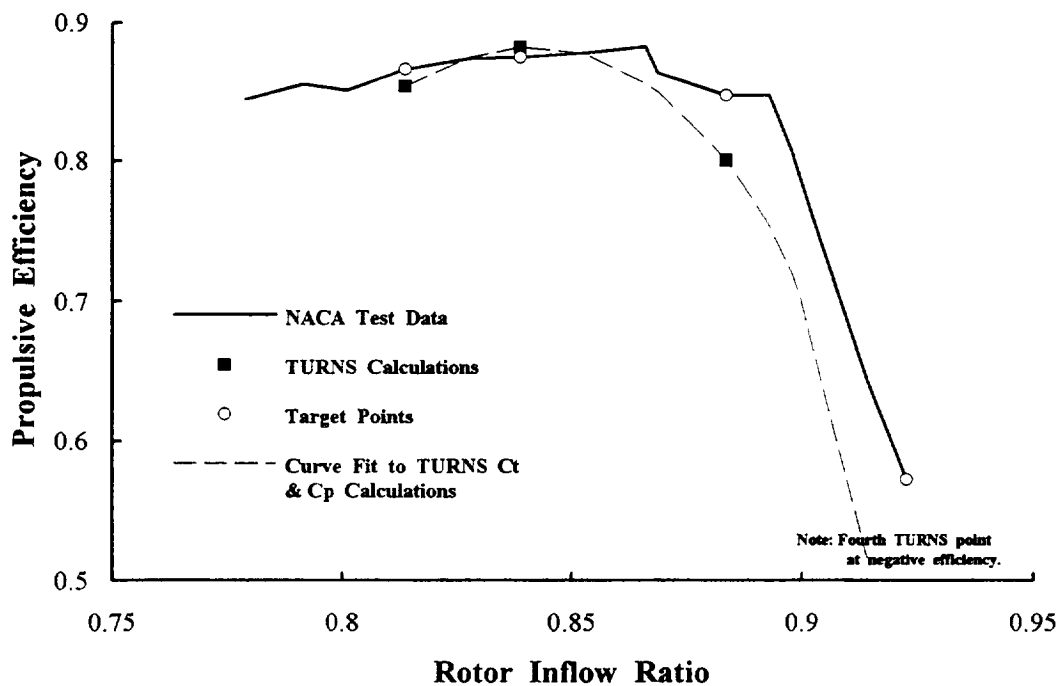
Figure 8. TURNS CFD Code Accurately Predicts Max. Propulsive Efficiency
($\beta.75 = 50.4$ °, M = 0.60)
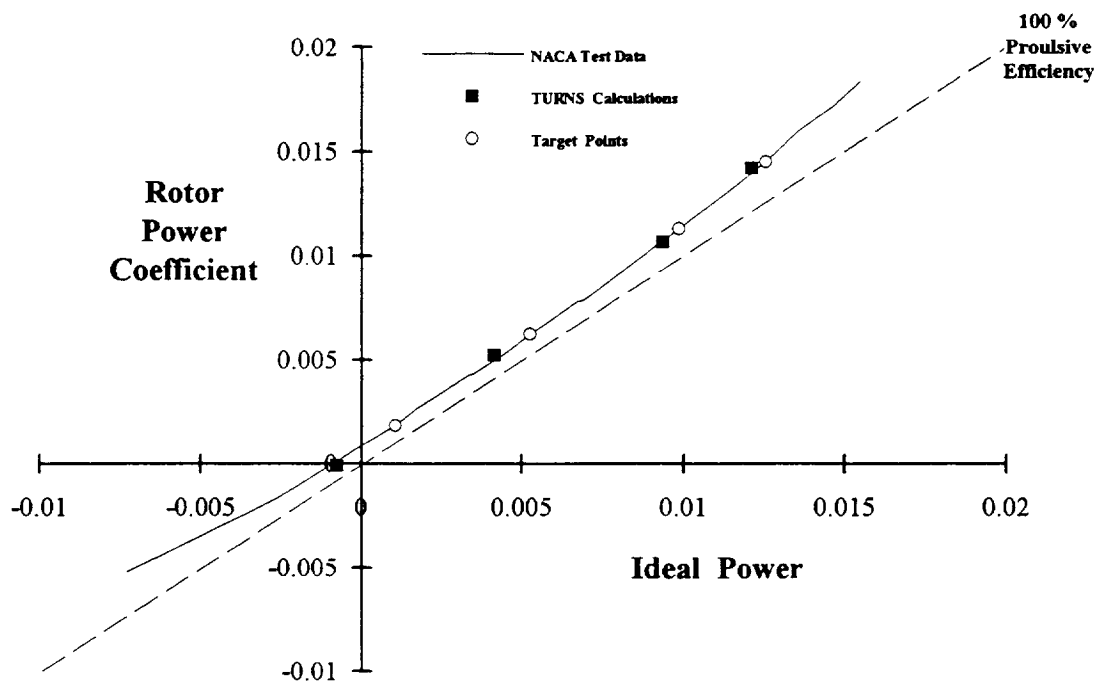
Figure 9. TURNS Should Accurately Predict Power When Thrust Is Matched.

"Test"
Profile
Power
Coeff.

NACA Test Data

TURNS Calculations

Target Points

Curve Fit to TURNS Ct & Cp Calculations

Ideal Power
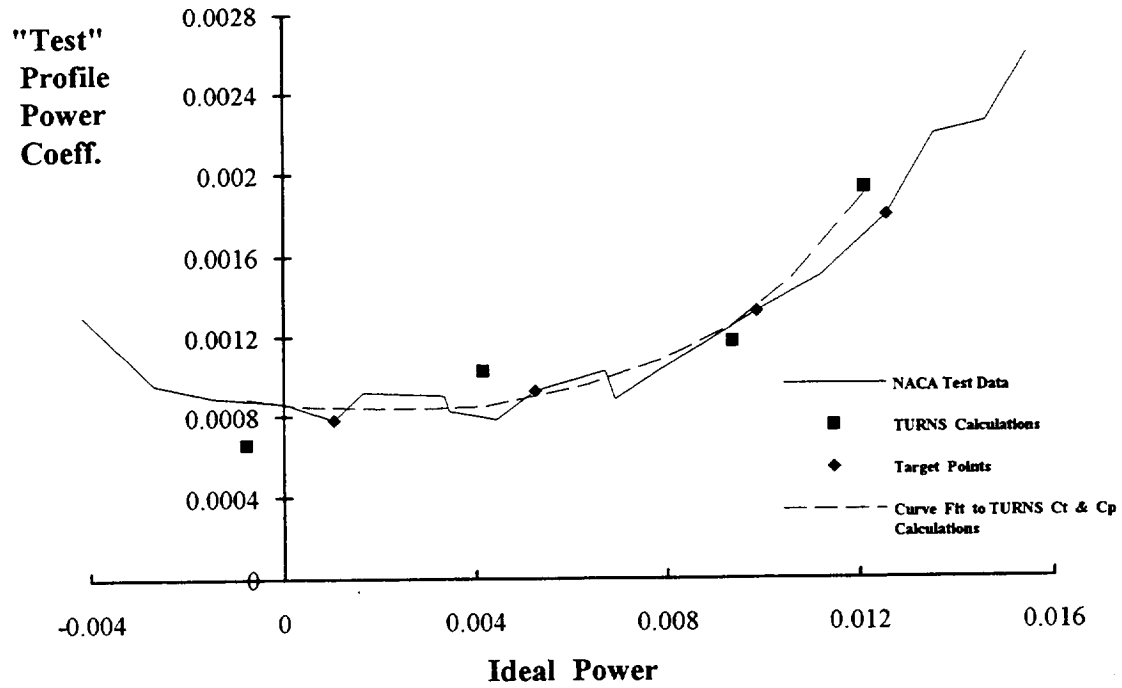
CFDJamey.xls

Figure 10. TURNS And Experiment Are In Agreement About Profile Power.

$(RN_{tip}^{1/5})(C_T/\sigma)_{FF}$

1.2
1.0
0.8
0.6

0.4

0.2

Propulsive Efficiency
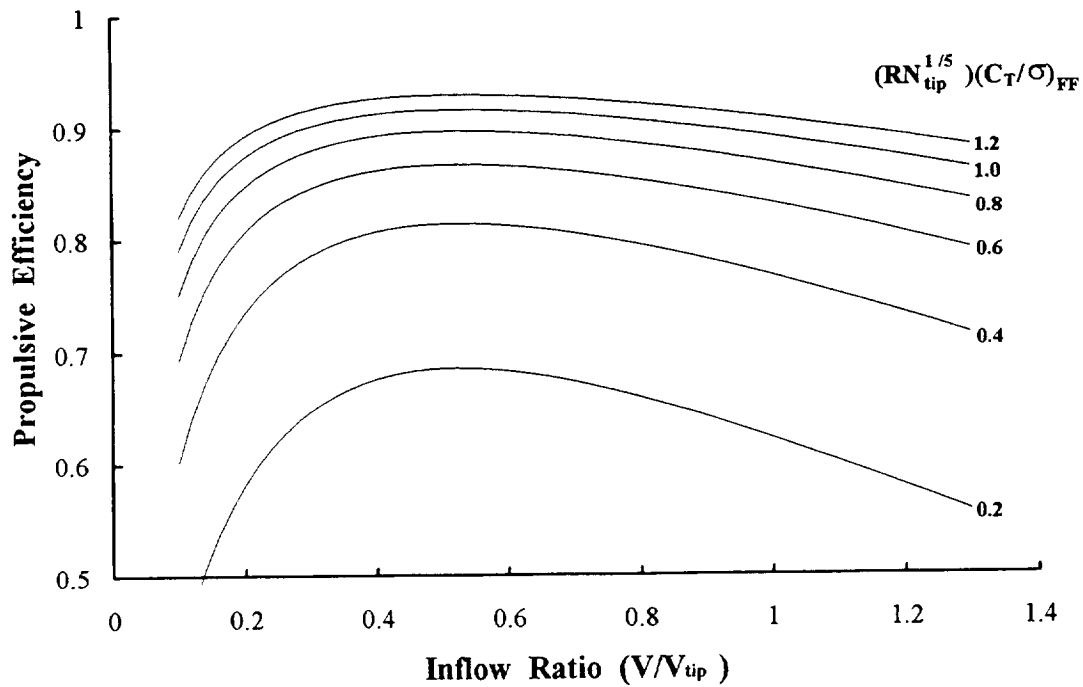
Inflow Ratio (V/V_{tip})

IdealEff.xls

Figure 11. Prop-rotor Propulsive Efficiency Goal.
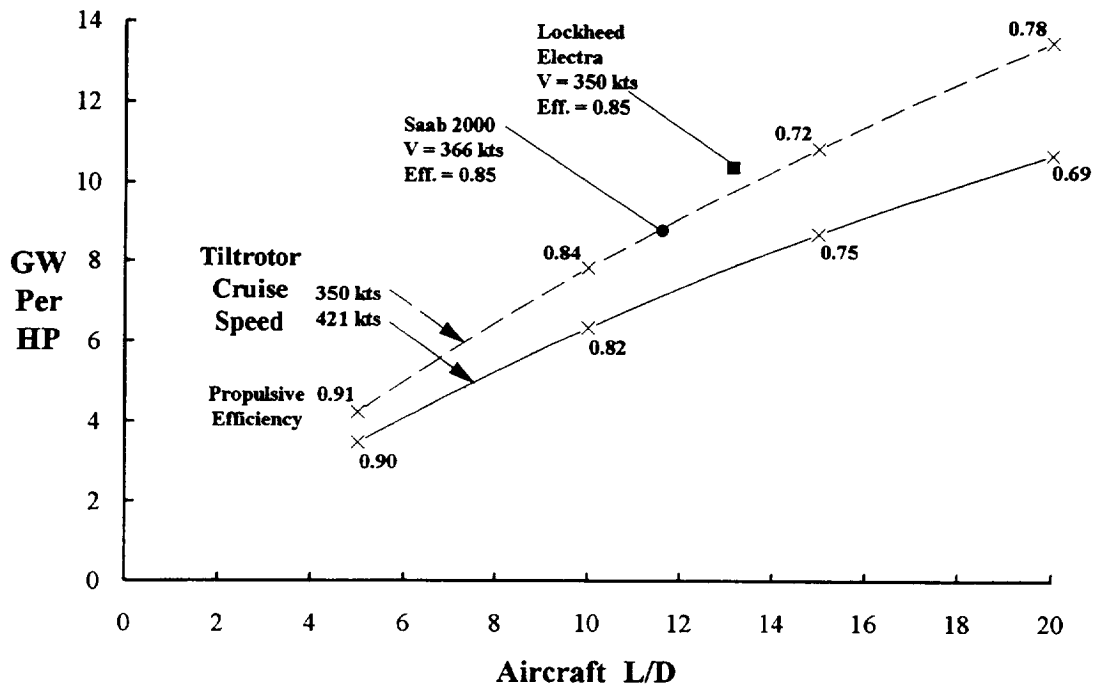
Figure 12. Civil Tiltrotor Power Loading Goal In Cruise At 25,000 Ft.
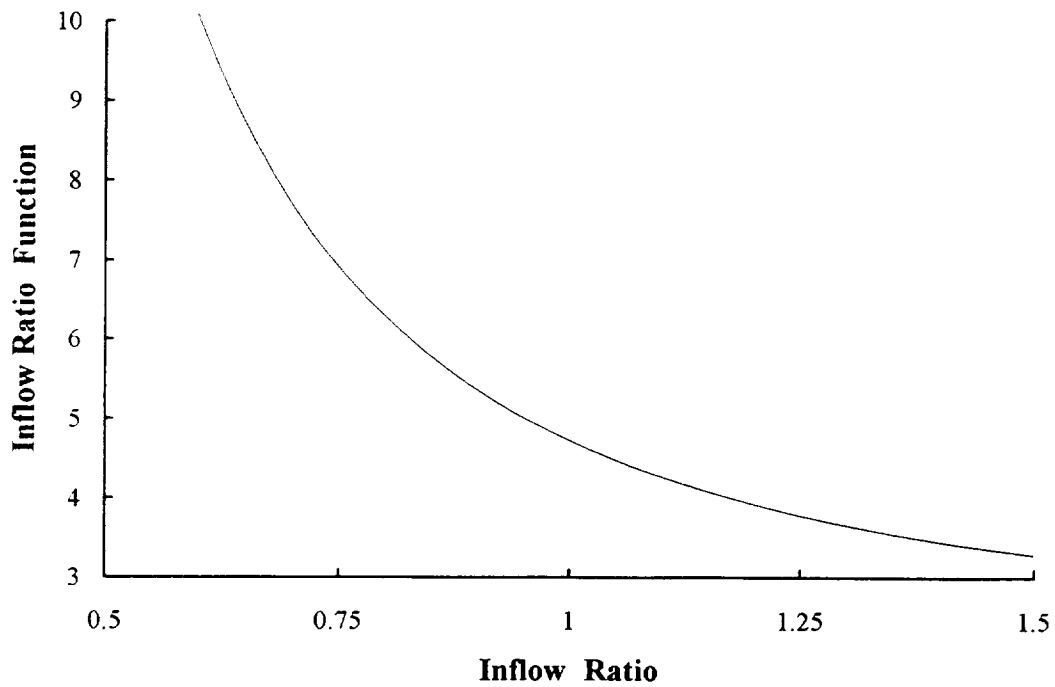
Figure 13. Profile Power Inflow Ratio Function, $f(\lambda_o) = T_{(\lambda, x_c)} / \lambda^3_o$
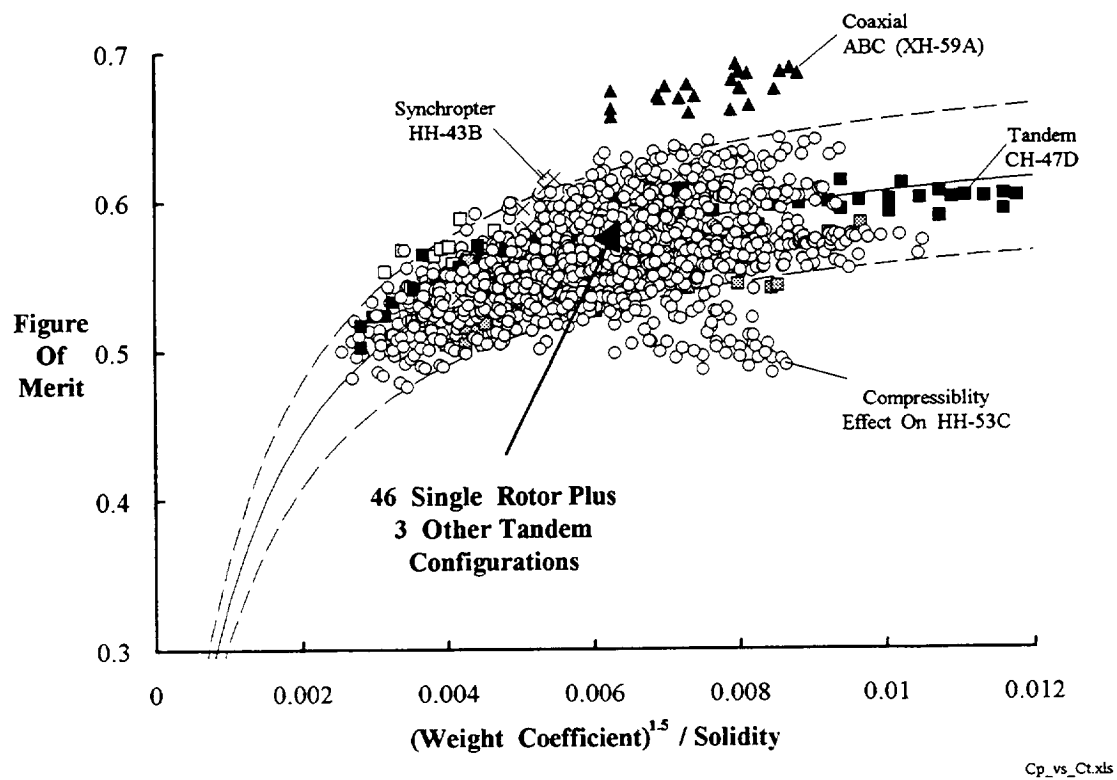
Figure 14. The Rotorcraft Industry, Over the Last 50 Years, Has Established Figure Of Merit Performance Boundarys For Its Helicopters.

This page intentionally left blank

APPENDIX A

Prop-rotor Performance Fundamentals

This page intentionally left blank

Appendix A

Prop-rotor Performance Fundamentals

A basic understanding of prop-rotor performance fundamentals is of considerable value for at least three reasons:

1. Aeronautical engineers have, since World War II, received little background about this propulsive device prior to entering the aerospace industry.

2. Understanding and confirming basic trends computed with very elaborate theory is always helpful.

3. Critical decisions can often be made during conceptual and even preliminary design based solely on fundamental physics.

Understanding the key fundamentals of lightly loaded propeller performance is relatively easy given the exceptional experimental data provided by the two early NACA tests reports. Furthermore, the estimation of power required to produce thrust using a force times velocity approach is by far the easiest path to this understanding. Figure A, below, shows an organization chart of the three major elements that contribute to total power required to produce useful thrust. A discussion of these elements including simple methodology to understand each and its magnitude is given shortly.

```
          ┌─────────────────────────┐
          │  Total Prop-rotor Power │
          │   Required To Produce   │
          │     A Given Thrust      │
          └─────────────────────────┘
         ╱            │              ╲
┌──────────────┐ ┌──────────────┐ ┌──────────────┐
│Propulsive Power│ │ Induced Power│ │Profile Power │
│(Thrust Times │ │(Thrust Times │ │(Airfoil Drag │
│Forward Velocity)│ │Induced Velocity)│ │Times Velocity)│
└──────────────┘ └──────────────┘ └──────────────┘
```

Minimum Incompressible Drag
a. Skin Friction Drag
b. Form Drag

Minimum Compressible Drag
Increment Due To
a. Pressure or Wave Drag

Incremental Drag Due To Lift
a. Incompressible
b. Compressible

Figure A. There Are Three Major Contributors To The Power Required To Produce Usable Propulsive Force (i.e. Forward Thrust).

A-1

The basic equation that states Figure A and calculates power required is

$$P = TV + Tv_i + P_o \qquad \text{(A-1)}$$

The first term in this equation, T V, defines the power required to produce thrust. This is the minimum or ideal power. The second term, $T v_i$, accounts for the induced power required to add momentum to the air flowing through the prop-rotor. From Reference 5, the lowest or ideal induced power comes when

$$v_i = \sqrt{\left(\frac{V}{2}\right)^2 + \frac{T}{2\rho A}} - \frac{V}{2} \quad \text{where } v_i \approx \frac{T}{2\rho A V} \text{ for high speed} \qquad \text{(A-2)}$$

The third term, P_o, in this energy form of the power required equation is referred to as profile power in the helicopter world. It accounts for the product of airfoil drag and local resultant velocity of each airfoil element along the blade. The sum along the blade (or integral from the blade root to tip) of each blade element's drag times velocity leads to the profile power of one blade. The sum of each blade's profile power gives the prop-rotor's total profile power.

A representative distribution of propulsive, induced and profile power elements is shown in Figure B below using PROP 1's experimental data at a tunnel Mach number of 0.70 and $\beta_{.75} = 65$ degrees from Figure 4b. At this operating condition, PROP 1 started at zero thrust with a rotor inflow ratio just over 2.0. The measured power at zero thrust was $C_P = 0.00616$. Since $C_T = 0$, both induced and propulsive power are, for practical engineering purposes, also zero. It follows then from Equation A-1 that the profile power at $C_T = 0$ is on the order of $C_{Po} \approx C_P = 0.00616$. Typically, induced power is very small as Figure B indicates. The propulsive power is, of course, the dominate power component. Figure B shows the total of induced plus propulsive power as a somewhat jagged line because the experimental thrust at each inflow ratio is used. Figure 4a shows that the experimental thrust variation with inflow ratio is not a smooth data set. Note that as rotor inflow is reduced and thrust increases to high levels, the profile power element becomes a very large percentage of the total power.

There are, in turn, three sub-components making up the profile power increment shown on Figure B. These three sub-categories were suggested on the organizational chart, Figure A. Emphasis is first placed on profile power created by minimum airfoil drag. This drag is a minimum, for example, when a symmetrical airfoil is operating at zero lift in the subsonic speed range. Classically, this minimum, incompressible drag is dominated by skin friction and a small amount of form drag. The skin friction drag is a minimum when the boundary layer is completely laminar over the complete airfoil. The magnitude of this lowest possible drag is obtained with a flat plate (i.e., an airfoil of zero thickness operating at zero lift) and is classically defined from Blasius's solution which is
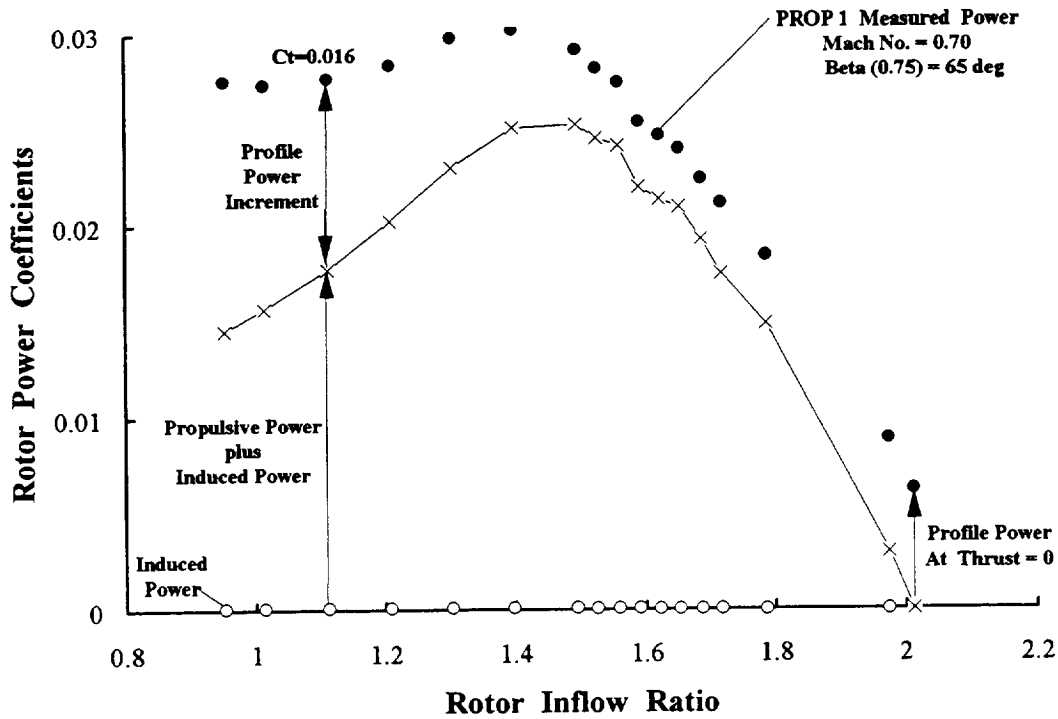
Figure B. Power Required Is Dominated By Propulsive and Profile Elements.

$$C_{d\,min.} = \frac{2.656}{\sqrt{RN}} \quad \text{for laminar flow and Reynolds number} \equiv RN = \frac{Vc}{v} \qquad (A-3)$$

When the boundary layer is fully turbulent over the complete airfoil, this minimum, incompressible drag (for a flat plate) increases. Prandtl and von Kármán suggested that

$$C_{d\,min.} = \frac{0.144 \text{ to } 0.148}{RN^{1/5}} \quad \text{for turbulent flow and } RN = \frac{Vc}{v} \qquad (A-4)$$

Form drag arises because of the pressure distribution about a finite thickness airfoil. Twaites, in Reference 12, page 183, summarizes typical variations of form drag with airfoil thickness ratio. He suggests that form drag has the approximate magnitude

$$C_{d\,form} \approx \frac{t/c}{1-t/c} C_{d\,min.} \qquad (A-5)$$

In addition to this minimum, incompressible drag, the outline on Figure A refers to an *increment* in drag that is due to compressibility. This increment is primarily a form or pressure distribution created drag. At supersonic speeds this incremental drag is frequently referred to as wave drag. The magnitude of this

A-3

increment can be obtained from transonic similarity theory as will be subsequently discussed.

Lastly, the outline places drag (either incompressible or compressible) due to lift as the third contributor to profile power. The affect of this drag increment is very dependent on airfoil geometry and Mach number as will be discussed.

The three airfoil drag categories shown on the preceding outline chart each contribute to a profile power calculation that accounts for all blades and requires an integration having the general form

$$P_o = b \int_{root}^{tip} V_{resultant} \, dD \tag{A-6}$$

Therefore, discussion of performance fundamentals addresses prop-rotor profile power in total and its three elements of

$$\text{Minimum Incompressible } P_o \equiv P_{o\,min} = b \int_{root}^{tip} V_{resultant} \, dD_{min} \tag{A-7a}$$

$$\text{Minimum Compressible Increment } P_o \equiv \Delta P_{o\,comp} = b \int_{root}^{tip} V_{resultant} \, dD_{comp} \tag{A-7b}$$

$$\text{Incremental } P_o \text{ Due To Thrust} \equiv \Delta P_{o\,thrust} = b \int_{root}^{tip} V_{resultant} \, dD_{lift} \tag{A-7c}$$

Regardless of the "bookkeeping" of airfoil drag elements, profile power is an undesirable power loss in producing usable thrust.

Finally, both induced and profile power represent real fluid losses that an engine must overcome with extra power. This inefficiency causes total power to be greater than the ideal power to produce usable thrust. These power losses lead to a definition of propulsive efficiency of the form

$$\eta_P = \frac{\text{Ideal Power}}{\text{Actual Power}} = \frac{T V}{T V + T v_i + P_o} \tag{A-8}$$

Examples of propulsive efficiency for PROP's 1 and 2 are shown in Figures 4c and 5c respectively. These data suggest that even at a flight Mach number of 0.70, efficiency well over 0.80 should be expected from any practical propeller provided it is properly loaded (i.e. operating near its best C_T for a design rotor inflow ratio).

Several performance fundamentals will now be discussed using PROP 1 and PROP 2 experimental data to confirm key points. The topics to be discussed are:

1. Converting from a torque times shaft rotational speed power calculation to computing power as a force times velocity.

2. Different ways of looking at prop-rotor performance trends.

3. Profile power and its three elements due to airfoil

    a. minimum, incompressible drag,

    b. minimum, compressible drag increment and

    c. incremental drag due to lift.

4. Thrust versus blade pitch angle, $\beta_{.75}$.

5. Summary of the fundamentals and the key equations.

Converting Power From
Torque × Ω to Force × V

The lightly loaded propeller is a relatively uncomplicated device to picture as the following two sketches, Figures C and D, suggest. A representative blade element at some radius station, r , will have an airfoil shaped cross-section as shown in Figure C. This blade element is acted upon by two axial velocities. The prime velocity is flight speed, V. The secondary velocity is the axial component of the induced velocity, v_i. The inplane velocity is dominated by shaft rotational speed times the radius station, Ω r. The inplane component of the induced velocity is frequently called the swirl velocity. This swirl velocity is not shown in the sketches. For the lightly loaded propeller, the induced velocity is considered very much smaller than either V or Ω r.

These simple schematics can first be used to derive the power equation introduced at the beginning of this Appendix. To begin with, the thrust acts parallel to the shaft. The inplane force times the radius station gives a torque about the shaft. Power is torque times shaft rotational speed denoted as Ω. However, power can also be calculated as a force times a velocity. Three basic equations are immediately apparent from the blade element diagram. That is

$$dT = dL\cos\phi - dD\sin\phi$$
$$dQ = r(dL\sin\phi + dD\cos\phi)$$
$$dP = \Omega dQ = \Omega r(dL\sin\phi + dD\cos\phi)$$

(A-9)

The transfer from calculating power as $Q\,\Omega$ to a force times velocity proceeds as follows:

a. First solve for dL from dT and substitute the result into the dP equation.

$$dL = \frac{dT + dD \sin \phi}{\cos \phi}$$

$$dP = \Omega r \left[\left(\frac{dT + dD \sin \phi}{\cos \phi} \right) \sin \phi + dD \cos \phi \right]$$

b. Next, expand the dP expression collecting the primary forces dT and dD

$$dP = \Omega r \frac{\sin \phi}{\cos \phi} dT + \Omega r \left[\frac{\sin^2 \phi}{\cos \phi} + \cos \phi \right] dD$$

$$dP = \Omega r \frac{\sin \phi}{\cos \phi} dT + \Omega r \left[\frac{1}{\cos \phi} \right] dD$$

c. Then, recognize that the velocity vector diagram defines Ωr in two ways. Thus,

$$\Omega r = V_r \cos \phi \quad \text{and} \quad V + v_i = V_r \sin \phi \quad \text{or} \quad V_r = \frac{V + v_i}{\sin \phi}$$

But then a second definition of Ωr comes by eliminating V_r

$$\Omega r = \frac{V + v_i}{\sin \phi} \cos \phi \quad \text{or} \quad \Omega r \frac{\sin \phi}{\cos \phi} = V + v_i$$

as well as $\dfrac{\Omega r}{\cos \phi} = V_r$

d. Now, substitute the two ways of expressing Ωr into the power equation to get

$$dP = (V + v_i) dT + V_r dD$$

e. Finally, integrate the elemental dP over the blade span. If the induced velocity is assumed uniform, it follows that the total power accounting for all blades is

$$P = TV + Tv_i + b \int_{root}^{tip} V_r \, dD$$

or, as stated by Equation A-1,

$$P = TV + Tv_i + P_o$$

The preceding logic reduces the performance problem to calculating the profile power, P_o, while conceding that the error in induced power will be small. It is not always easy to accurately estimate profile power, particularly when the resultant velocity at a blade element is transonic or supersonic or when there are large areas of separated flow. However, profile power can be closely approximated rather simply in many more cases than one might expect.
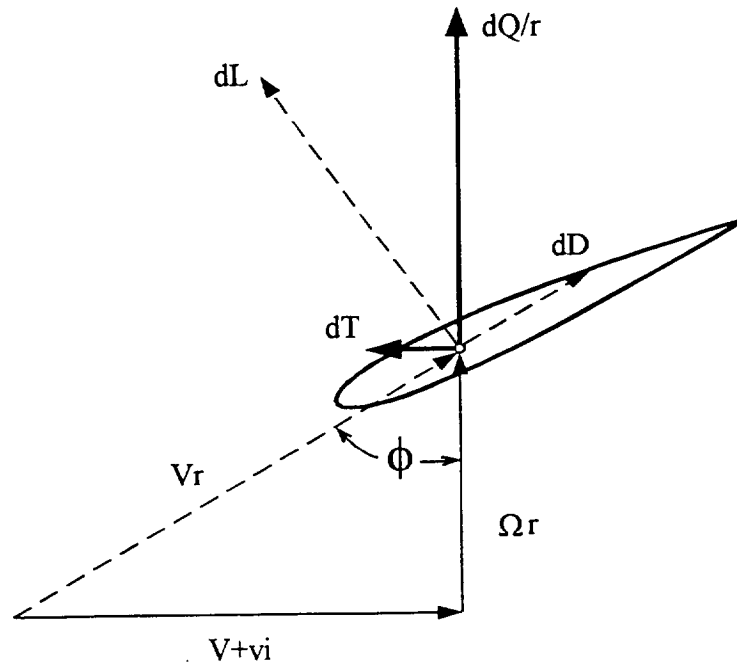
Figure C. Blade Element Aerodynamics
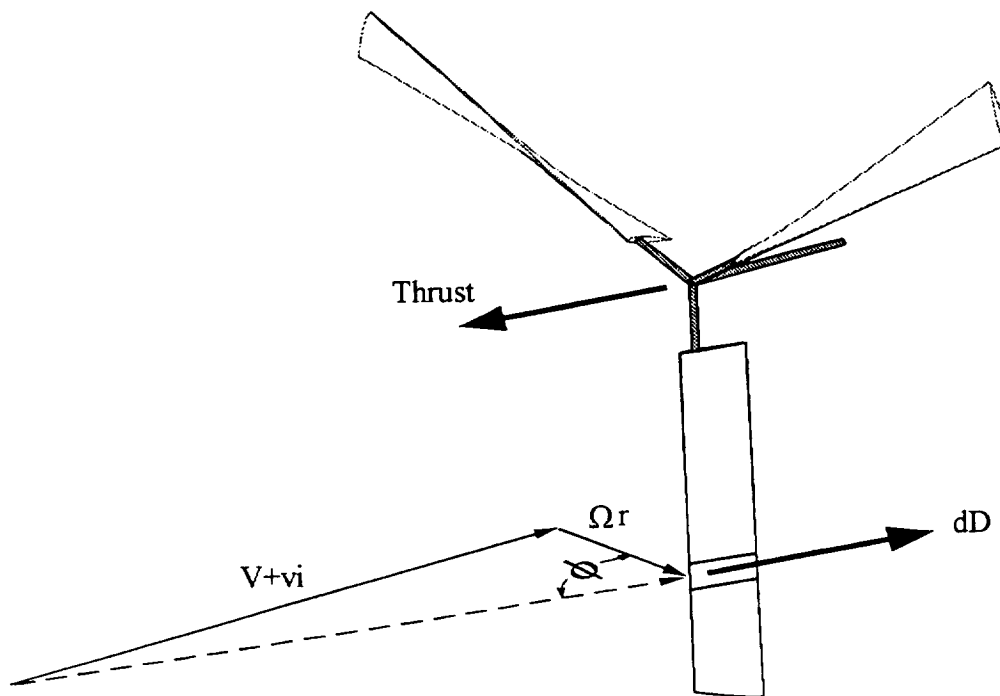
Figure D. Prop-rotor Aerodynamics

Different Ways To Look At
Propeller Performance

Figures 4 and 5 present prop-rotor performance in the classical form found in the literature. However, there are (at least) two other, rarely seen, ways to examine experimental prop-rotor data. The first way was used to good advantage by George Schairer of the Boeing Company. Two examples of his work are described in References 13 and 14. The second way is discussed by Wayne Johnson in his well known helicopter theory book, Reference 15.

In George Schairer's approach, total power (either from experiment or theory) is plotted versus T V. In the ideal world, a graph of P = T V is simply a straight line. Any difference between this straight line [that begins at (T V) = 0, P = 0 and has a one-for-one slope] and the experimental data is simply the real fluid dynamics creating losses such as induced power and profile power. This different way of looking at propeller or prop-rotor performance can be viewed in two different non-dimensional forms.

The first view showing George Schairer's approach non-dimensionalizes the three terms in the power equation by the rotor aerodynamic parameters of

$$\rho A V_t^3$$

This gives the power equation stated by Equation A-1 in rotor nomenclature as

$$C_P = C_T \lambda_o + C_T \lambda_i + C_{Po} \tag{A-10}$$

and the ideal induced velocity becomes

$$\lambda_i = \frac{v_i}{V_t} = \frac{1}{2}\sqrt{\lambda_o^2 + 2 C_T} - \frac{1}{2}\lambda_o \quad \text{where } \lambda_i \approx \frac{C_T}{2\lambda_o} \text{ for high speed} \tag{A-11}$$

The experimental power in coefficient form can be plotted versus the ideal power in rotor coefficient form (i.e., actual C_P versus $C_T \lambda_o$). Using PROP 1 data from Figure 4 changes the classical view to the presentation shown in Figure A-1 while PROP 2 changes from Figure 5's classical view to that given by Figure A-2.

In the views presented by Figures A-1 and A-2, the experimental data forms an envelope that is nearly a straight line. At first glance, this "straight line" appears to be nothing more than the 100 % propulsive efficiency line moved up so that the power loss at zero thrust--where ideal power is by definition also zero--is seen as a Y-axis intercept. This "first glance" is indicated by the dashed line on both Figures A-1 and A-2. While this impression is not too accurate, it does emphasizes the point that a minimum profile power at zero thrust exists.

The second view showing George Schairer's approach non-dimensionalizes the three terms in the power equation by the aerodynamic product

$$q V D^2$$

The division of power by velocity gives an equivalent drag; that is, $P / V = $ Drag. Dividing this equivalent drag by dynamic pressure, q, gives an "equivalent drag area." Then dividing this D / q by prop-rotor diameter squared gives a non-dimensional coefficient. Using this approach, the power equation transforms into

$$\overline{P} \equiv \frac{P}{q V D^2} = \overline{T} + \overline{T}\left(\frac{v_i}{V}\right) + \overline{P}_o \quad \text{where} \quad \overline{T} \equiv \frac{T}{q D^2} \qquad \text{(A-12)}$$

and the ideal induced velocity becomes

$$\frac{v_i}{V} = \frac{1}{2}\sqrt{1 + \frac{4}{\pi}\overline{T}} \ - \frac{1}{2} \qquad \text{(A-13)}$$

One very useful feature of this non-dimensional form is that the curve of ideal power (i.e. 100 % propulsive efficiency) is defined by $\overline{P} = \overline{T}$ which is quite simple. There is another feature that dividing by $q V D^2$ accomplishes which becomes apparent for the lightly loaded propeller or for a conventional prop-rotor. The propeller at reasonable forward speed is lightly loaded when

$$\overline{T} = \frac{T}{q D^2} \text{ is considerably smaller than } \frac{\pi}{4}$$

In this low thrust region of practical prop-rotors designed for high speed tiltrotor aircraft, the induced velocity can be closely approximated by

$$\frac{v_i}{V} \approx \frac{\overline{T}}{\pi} \qquad \text{(A-14)}$$

This approximation reduces the fundamental power equation introduced by Equation A-1 to the very simple form of

$$\overline{P} \approx \overline{T} + \frac{\overline{T}^2}{\pi} + \overline{P}_o \qquad \text{(A-15)}$$

The experimental power in this aerodynamic coefficient form can then be plotted versus the ideal power (i.e., actual $\overline{P}$ versus $\overline{T}$). PROP 1 data now takes the view shown in Figure A-3 while PROP 2's results are seen in Figure A-4. In the views presented by Figures A-3 and A-4, the experimental data again forms nearly a straight line in the low thrust region as it did in Figures A-1 and A-2. At first glance, this "straight line" appears again to be nothing more than the 100 percent propulsive efficiency line moved up so that the power loss at zero thrust is seen as a Y-axis intercept.

With increasing thrust, the envelope to the experimental data as viewed in Figures A-3 and A-4 shows power increasing more as thrust squared. This trend is not due to induced power. A simple calculation shows that

$$\text{for } \overline{T} = 0.05 \quad \overline{P}_{induced} = \frac{\overline{T}^2}{\pi} = \frac{(0.05)^2}{\pi} = 0.0008$$

which amounts to 1.6 percent of the ideal power of 0.05. Therefore, the power at zero thrust and the parabolic increase in test power with thrust seen in Figs. A-1 through A-4 must be due, primarily, to profile power losses.

A second way to look at prop-rotor performance was suggested by Wayne Johnson in Reference 15, page 35. His approach bridges the gap between rotorcraft and airplane concepts of efficiency. The rotorcraft world uses a Figure of Merit to quickly convey efficiency primarily in hovering flight. This parameter is classically defined as

$$FM \equiv \frac{\text{Ideal Power}}{\text{Actual Power}} = \frac{T v_i}{\text{Actual P}} \quad \text{where} \quad FM = \frac{C_T^{3/2}/\sqrt{2}}{\text{Actual } C_P} \quad \text{for hover} \quad (A\text{-}16)$$

This rotorcraft definition is of relatively little value in forward flight because induced velocity approaches zero as speed increases. In contrast, the airplane propeller world uses a propulsive efficiency defined as

$$\eta_P \equiv \frac{\text{Ideal Power}}{\text{Actual Power}} = \frac{TV}{\text{Actual P}} = \frac{C_T \lambda_o}{\text{Actual } C_P} \quad \text{for forward flight} \quad (A\text{-}17)$$

but at zero speed this definition becomes meaningless. Johnson suggests the logical combination of the two definitions as a useful way of viewing prop-rotor efficiency over the complete speed range. That is, he suggests defining figure of merit as

$$FM_J \equiv \frac{\text{Ideal Power}}{\text{Actual Power}} = \frac{T(V + v_i)}{\text{Actual P}} = \frac{C_T(\lambda_0 + \lambda_i)}{\text{Actual } C_P} = \frac{C_T \lambda}{\text{Actual } C_P} \quad (A\text{-}18)$$

All of the experimental data obtained with PROP's 1 and 2 can easily be viewed using Johnson's suggested Figure of Merit as defined with Equation A-18. This view is given for PROP 1 with Figure A-5 and, for PROP 2, with A-6. The Johnson suggested Figure of Merit is plotted against rotor inflow ratio due only to forward speed (i.e. $\lambda_o = J / \pi$). Note that PROP 1 provides data over a much greater rotor inflow ratio range than does PROP 2. A clear envelope to FM_J versus λ_o is apparent for both propellers. Because no experimental data has yet been found for the static or hover, zero speed condition, there is a data gap in the zero to low inflow ratio range. An extrapolation of the forward speed data to zero inflow ratio is of questionable value because static performance is such a

special case. Finally, PROP 1 appears to enjoy a Johnson Figure of Merit advantage over PROP 2. Both prop-rotors reach maximum FM_J at the lower values of T/qD^2.

Examining the experimental data in these two additional ways (i.e., Schairer's P versus TV and Johnson's FM_J) leads to the third topic in this discussion of performance fundamentals. This topic deals with profile power and its three elements.

Profile Power

Understanding profile power in general and its three elements in particular is helped by first extracting a representative value from the experimental data. In this report, profile power is established by using Equation A-1 to "back out" approximate "test" values. That is

$$\text{Backed Out "Test" } P_o = (\text{Experimental Power}) - (TV + Tv_i) \qquad (A\text{-}19)$$

In rotor coefficient nomenclature this first order estimate of non-ideal power becomes

$$\text{"Test" } C_{P_o} = (\text{Test } C_P) - C_T \lambda_o - C_T \lambda_i \qquad (A\text{-}20)$$

A typical magnitude of profile power in relation to the total power was seen earlier in Figure B on page A-3. Using that figure's PROP 1 data leads to the trend of "Test" C_{P_o} provided by Figure E below.

Many of the broad characteristics of a prop-rotor's profile power are seen on Figure E. Two key points can be made. First, in this illustration with PROP 1 data, the test procedure creates changes in all key parameters that affect profile power. As inflow ratio is decreased by increasing RPM at constant tunnel-datum Mach number and fixed $\beta_{.75}$, the (1) helical tip Mach number, (2) tip Reynolds number, (3) thrust and, of course, (4) inflow ratio are all changing. Each of these four parameters has an individual influence on profile power. These four key parameters, all varying together, makes it considerably more difficult to allocate reasons for the profile power trend shown in Figure E. Second, maximum propulsive efficiency does generally occur as close to maximum thrust as possible-- when there is not a large profile power increase from the minimum C_{P_o} "bucket."

Fortunately, both PROP 1 and PROP 2 experimental data provide enough, well defined, trends in profile power to explore individual parameter influences on this most important power category. Given the introduction with Figure E, consider first the 0.70 tunnel Mach number data for both prop-rotors that has been presented in several forms earlier. The behavior of PROP 1's "Test" C_{P_o} is shown in Figure A-7 and PROP 2's in Figure A-8.

Derived From
PROP 1 Measured Power
Mach No. = 0.70
Beta (0.75) = 65 deg

Max. Ct = 0.01791
Eff. = 0.827
Mt = 0.863
RNt = 1.13 million

Max. Eff. = 0.877
Ct = 0.01546
Mt = 0.833
RNt = 1.09 million

× Ct = 0.0
Mt = 0.782
RNt = 1.02 million

"Test" Profile Power Coefficient

Rotor Inflow Ratio
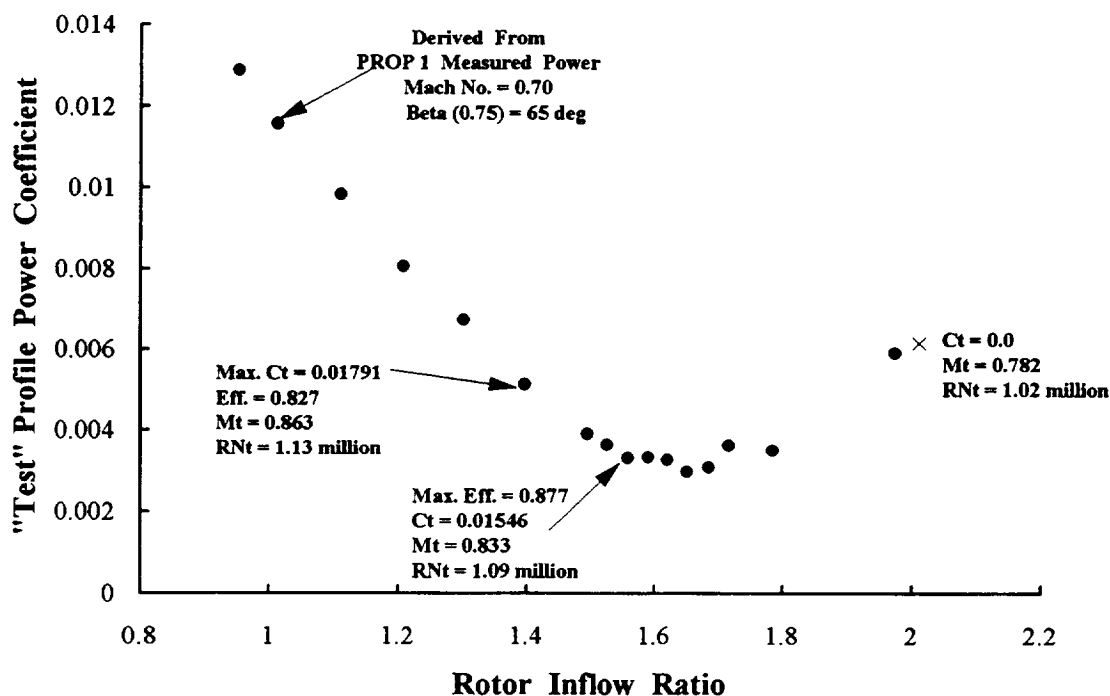
P_1949A.xls

Figure E. Profile Power Is The Dominated Cause Of Prop-rotor Inefficiency In Producing Usable Thrust.

In Figures A-7 and A-8, the several sets of data reflect test sweeps at fixed $\beta_{.75}$ values. The first point to note on each figure is that as $\beta_{.75}$ increases, the minimum C_{P_0} "bucket" increases in value and occurs at higher total rotor inflow ratio (i.e. $\lambda = \lambda_0 + \lambda_i$). This trend says that C_{P_0} is strongly influenced by λ regardless of thrust level. The second point to note is that the highest blade angle data tested with each prop-rotor created the lowest helical tip Mach and Reynolds numbers. Conversely, at low $\beta_{.75}$, both PROP 1 and PROP 2 incurred the highest helical tip Mach and Reynolds numbers. The third point to note is that the three lowest blade angles reached virtually the same minimum C_{P_0} despite successively lower total inflow ratios. This says that while reduced inflow ratio is lowering profile power, compressibility is increasing profile power. The net effect appears, for PROP 1 at this wind tunnel Mach number of 0.70, to be a "floor" to minimum profile power of $C_{P_0} \approx 0.0022$ to 0.0022. For PROP 2, this "minimum of the minimums" gives $C_{P_0} \approx 0.0011$ to 0.0011. The last point to note is that the zero thrust point, shown by the symbol ×, is at or very near the minimum C_{P_0} "bucket" for the practical values of $\beta_{.75}$ tested with both prop-rotors.

The key message from Figures A-7 and A-8 is that profile power starts with a minimum value that is very dependent on total inflow ratio. This fundamental parameter's influence on C_{P_0} forms a base on which to add

A-12

compressibility and thrust affects. As a step in capturing this major influence of λ on C_{Po}, consider the solid line shown on Figures A-7 and A-8.

Both Figures A-7 and A-8 include the simplest theoretical trend in profile power with total inflow ratio. This theoretical trend is shown as a solid line on each figure. The simple theory behind these C_{Po} versus λ trends is based upon assuming a constant, average airfoil drag coefficient at each blade element along the span when calculating profile power. That is, assume that

$$dD = \left(\tfrac{1}{2}\rho V_r^2\right)\left(c\ dr\right)C_{d\ ave.}$$ (A-21)

Then the profile power, accounting for all blades, becomes

$$P_o = b\int_{root}^{tip} V_r dD = b\ C_{d\ ave.}\int_{root}^{tip} V_r\left\{\left(\tfrac{1}{2}\rho V_r^2\right)\left(c\ dr\right)\right\}$$ (A-22)

This integral is somewhat simplified by using the non-dimensional parameters of

$$x = \frac{r}{R}\quad \text{so that}\quad dr = R\,dx\quad \text{and}\quad root = x_c\ ,\ tip = 1.0$$

$$V_r = \sqrt{\left(\Omega r\right)^2 + \left(V + v_i\right)^2} = V_t\sqrt{x^2 + \lambda^2}$$

On this basis, the profile power integral becomes

$$P_o = b\left(\tfrac{1}{2}\rho V_t^3\ R\right)C_{d\ ave.}\left[\int_{x_c}^1 (c_x)\left(x^2 + \lambda^2\right)^{3/2}dx\right]$$ (A-23)

which reduces to the rotor coefficient form of

$$C_{Po} = \frac{bC_{d\ ave.}}{2\pi}\left[\int_{x_c}^1 (c_x/R)\left(x^2 + \lambda^2\right)^{3/2}dx\right]$$ (A-24)

If the blades are constant chord (as in PROP 2's case), the integral which Equation A-24 requires is readily obtained from many math handbooks to give

$$C_{Po} \equiv \frac{P_o}{\rho\ \pi R^2 V_t^3} = \frac{\left(bc/\pi R\right)}{8}\times C_{d\ ave.}\times F(\lambda, x_c)$$ (A-25a)

where

$$F(\lambda, x_c) = \left[\left(1 + \lambda^2\right)^{3/2} - x_c\left(x_c^2 + \lambda^2\right)^{3/2}\right] + \tfrac{3}{2}\lambda^2\left[\left(1 + \lambda^2\right)^{1/2} - x_c\left(x_c^2 + \lambda^2\right)^{1/2}\right]$$

$$+ \tfrac{3}{2}\lambda^4\left\{\ln\left[\frac{1 + \sqrt{1 + \lambda^2}}{x_c + \sqrt{x_c^2 + \lambda^2}}\right]\right\}$$ (A-25b)

A-13

In Figure A-7 for PROP 1, Equation A-24 is used with $C_{d\,ave.} = 0.016$ to trace out the solid line envelope to minimum profile power. For PROP 2 with its constant chord shown in Figure A-8, Equation A-25 with $C_{d\,ave.} = 0.0065$ appears to be an "adequate guess" of the trend in minimum profile power.

To conclude this discussion of total profile power, the key message from Figures A-7 and A-8 is that profile power starts with a minimum value that is very dependent on total inflow ratio. The factor of two difference in $C_{d\,ave.}$ values between PROP 1 and PROP 2 indicates, however, that other factors not captured by a semi-empirical simple theory are involved. Questions about Reynolds number, differences in airfoil thickness ratio affecting compressibility losses, etc. are immediately raised. Still, the primary and most fundamental question remains:

What is the minimum, incompressible profile power loss of a prop-rotor?

Minimum Incompressible Profile Power

The calculation of minimum incompressible profile power with a blade element theory depends upon the airfoil drag coefficient used at each blade radius. In the case of PROP's 1 and 2, some experimental airfoil data was available for their initial design. This airfoil data is of value in understanding both incompressible and compressible contributions to minimum profile power.

The earliest, comprehensive, experimental set of aerodynamic lift and drag coefficient data for the NACA 16-xxx airfoils was obtained by John Stack. These results, published in NACA Technical Report 763 in 1943 after ten years of research (Reference 8), were obtained with a 5 inch chord by 30 inch span duralumin model. The test Reynolds number range was from approximately 700,000 to slightly over 2,000,000. For nominal sea level atmospheric conditions, this gives a Reynolds number in terms of Mach number on the order of $RN = 3 \times 10^6\ M$. Unfortunately, this Reynolds number and Mach number range is only partially suited to PROP 1 and wholly inadequate for PROP 2 as Figures A-9 and A-10 show.

The two figures that follow summarize representative NACA 16-xxx two dimensional airfoil experimental data from figures 23 and 24 of Reference 8. Both Figures F and G include data for the NACA 16-106 which was the lowest drag airfoil tested by John Stack. Figure F confirms the increasing drag with airfoil thickness ratio increases. The increase is, however, considerably larger than Twaites's suggested trend given by Equation A-5. Figure G shows the trend in minimum drag coefficient as design lift coefficient is increased. The symmetrical NACA 16-009, according to Reference 8, apparently had surface imperfections that kept it from being the lowest drag airfoil in the 9 % thickness ratio family.
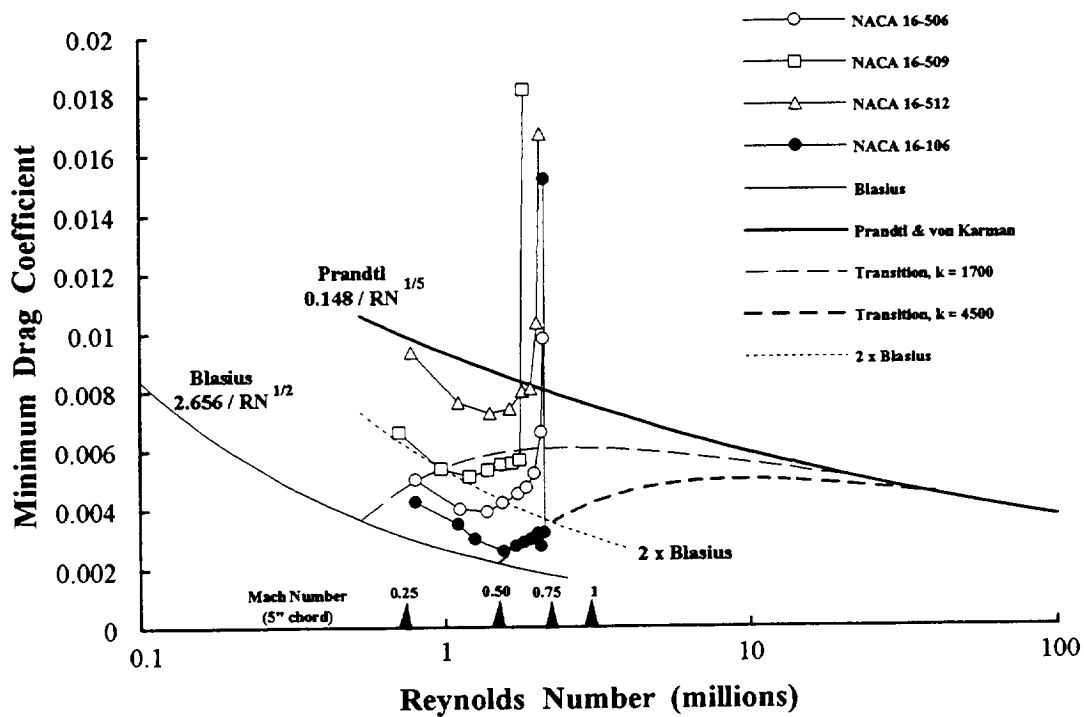
NACA_16.xls

Figure F. Thickness Ratio Variation At Constant Design Lift Coefficient.
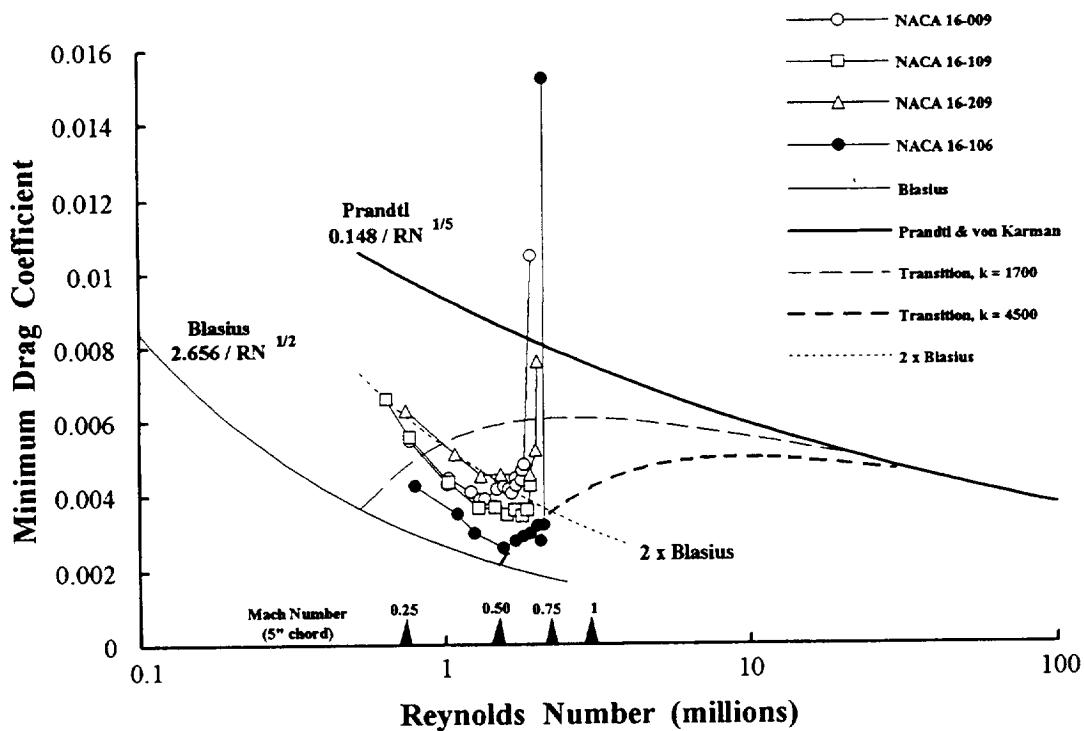
NACA_16.xls

Figure G. Camber Variation at Constant Thickness Ratio.

A-15

The airfoil minimum drag coefficient is, fortunately, bounded. A comparison to classical laminar and turbulent flat plate drag coefficients (as discussed by Hoerner in Reference 16, pages 2-6, 7) is shown on both Figures F and G. These two classical drag coefficient trends with Reynolds number form lower and upper bounds to thin airfoil minimum drag. The transition from laminar to turbulent boundary layer along the flat plate raises drag in the empirical manner shown by the dashed lines on each figure. Laminar to turbulent boundary layer transition is also discussed by Hoerner in Ref. 16. The NACA 16-xxx airfoil data provided by John Stack in Ref. 8 are for a 5 inch chord airfoil which leads to potential shock wave formation mixed within the boundary layer transition Reynolds number range.

The two summary sets of airfoil data shown on Figures F and G are directly applicable to PROP 1 but are of considerably less value to PROP 2. In PROP 1's case, the primary airfoil can be taken as the NACA 16-509. This is the airfoil used in the region of the 3/4 radius station as can be seen from Figures 3c and 3d. Outboard of the 3/4 radius station, PROP 1 has a tailored reduction in thickness ratio and design lift coefficient until a NACA 16-106 or -206 could be considered more representative. Inboard of the 3/4 radius station, thickness ratio increases to 12 to 14 percent range while design lift coefficient decreases to about 0.2. Taken in total, it appears that PROP 1's airfoil distribution follows a laminar boundary layer trend. Broadly speaking, the minimum, incompressible, airfoil drag coefficients appear bracketed approximately as

$$1.5 \times \frac{2.656}{RN^{1/2}} \le C_{d \, min.} \le 2.0 \times \frac{2.656}{RN^{1/2}} \quad \text{Probable for PROP 1} \tag{A-26}$$

In PROP 2's case of very thin airfoils shown by Figure 3c and much higher Reynolds number as seen from Figure A-10, the airfoil data obtained by Stack appears to be of little direct use. It seems most likely that PROP 2's blade would be dominated by a fully turbulent boundary layer. Therefore, for PROP 2, the minimum airfoil drag coefficient is more likely to behave as

$$1.0 \times \frac{0.148}{RN^{1/5}} \le C_{d \, min.} \le 1.5 \times \frac{0.148}{RN^{1/5}} \quad \text{Probable for PROP 2} \tag{A-27}$$

The Reynolds number range where the boundary layer transitions from laminar to turbulent is frequently described empirically as

$$C_{d \, min.} = \frac{0.148}{RN^{1/5}} - \frac{2k}{RN} \tag{A-28}$$

This description of flat plate drag variation in the transition region is shown as light and heavy dashed lines on both Figures F and G. Two values of $k = 1,700$ and $k = 4,500$ are shown.

This brief summary of an airfoil's minimum drag coefficient is sufficient to make two calculations of minimum incompressible profile power. The most optimistic is to assume every blade element is operating with the laminar boundary layer of a flat plate. The more practical estimate is to assume each blade element has a fully turbulent boundary layer. Both assumptions can be compared to PROP 1 and PROP 2 test results as the following discussion conveys.

The profile power integral from Equation A-7a is performed first assuming that every blade element airfoil (1) is a flat plate operating at zero lift in a subsonic flow, (2) has a *completely laminar boundary layer* on both sides of the airfoil and (3) has the drag coefficient variation with Reynolds number found by Blasius and repeated in this report as Equation A-3. With these assumptions, the blade element drag, dD, then becomes

$$dD_{min} = \left(\tfrac{1}{2}\rho V_r^2\right)(c\ dr)C_{d\ min} = \left(\tfrac{1}{2}\rho V_r^2\right)(c\ dr)\left[\frac{2.656}{\sqrt{V_r c/\nu}}\right] \tag{A-29}$$

The profile power accounting for all blades and, to repeat, assuming a *laminar* boundary layer is

$$P_{o\ min} = b\int_{root}^{tip} V_r dD_{min} = b\int_{root}^{tip} V_r\left\{\left(\tfrac{1}{2}\rho V_r^2\right)(c\ dr)\left[\frac{2.656}{\sqrt{V_r c/\nu}}\right]\right\} \tag{A-30}$$

Again, this integral is somewhat simplified by using the non-dimensional parameters

$$x = \frac{r}{R} \quad \text{so that} \quad dr = R\ dx \quad \text{and} \quad root = x_c\ , \ tip = 1.0$$

$$V_r = \sqrt{(\Omega r)^2 + (V + v_i)^2} = V_t \sqrt{x^2 + \lambda^2}$$

On this basis, the profile power integral assuming *laminar flow* becomes

$$P_{o\ min} = 2.656\frac{b\left(\tfrac{1}{2}\rho V_t^3\ R\right)}{\sqrt{V_t/\nu}}\left[\int_{x_c}^{1} (c_x)^{1/2}\left(x^2 + \lambda^2\right)^{5/4} dx\right] \tag{A-31a}$$

which reduces to the rotor coefficient form of

$$C_{Po\ min} = \frac{1.328\ b}{\pi\sqrt{V_t R/\nu}}\left[\int_{x_c}^{1} (c_x/R)^{1/2}\left(x^2 + \lambda^2\right)^{5/4} dx\right] \tag{A-31b}$$

Note that in the Equation A-31b, non-dimensional form, the Reynolds number is now based on prop-rotor radius. This basis for Reynolds number is somewhat unusual. However, it becomes meaningful because the chord distribution is scaled by radius and the integral is performed on a planform configuration.

In PROP 2's case where the chord is constant, this minimum, incompressible profile power expression assuming a *laminar* boundary layer can be written more conventionally and informatively as

$$C_{Po\ min.} = 1.328\frac{(bc/\pi R)}{\sqrt{V_t c/\nu}}\left[\int_{x_c}^{1}\left(x^2 + \lambda^2\right)^{5/4}dx\right] = 1.328\frac{(bc/\pi R)}{\sqrt{V_t c/\nu}}\left[\frac{2}{7}\times L(\lambda,x_c)\right] \quad (A\text{-}31c)$$

The integral required by Equation A-31c falls in the elliptical integral family. However, for engineering purposes, a handier evaluation of $L(\lambda,x_c)$ is with

$$L(\lambda,x_c) = \left[\left(1+\lambda^2\right)^{5/4} - x_c\left(x_c^2 + \lambda^2\right)^{5/4}\right] + \tfrac{28}{15}\lambda^2\left[\left(1+\lambda^2\right)^{1/4} - x_c\left(x_c^2+\lambda^2\right)^{1/4}\right]$$
$$+ \tfrac{21}{40}\lambda^4\left\{\ln\left[\frac{1+\left(1+\lambda^2\right)^{1/4}}{x_c + \left(x_c^2+\lambda^2\right)^{1/4}}\right]\right\} \quad \text{for } \lambda \text{ less than 1.3} \quad (A\text{-}32)$$

Now consider the profile power integral assuming that every blade element airfoil (1) is a flat plate operating at zero lift in a subsonic flow, (2) has a completely *turbulent* boundary layer and (3) has the drag coefficient variation with Reynolds number offered by Prandtl and von Kármán. The blade element drag, dD , then becomes

$$dD_{min.} = \left(\tfrac{1}{2}\rho V_r^2\right)(c\ dr)C_{d\ min.} = \left(\tfrac{1}{2}\rho V_r^2\right)(c\ dr)\left[\frac{0.148}{\left(V_r c/\nu\right)^{1/5}}\right] \quad (A\text{-}33)$$

The profile power for all blades and assuming a *turbulent* boundary layer is

$$P_{o\ min.} = 0.148\frac{b\left(\tfrac{1}{2}\rho V_t^3\ R\right)}{\left(V_t/\nu\right)^{1/5}}\left[\int_{x_c}^{1}(c_x)^{4/5}\left(x^2 + \lambda^2\right)^{13/10}dx\right] \quad (A\text{-}34a)$$

which reduces to the rotor coefficient form of

$$C_{Po\ min.} = \frac{0.074\ b}{\pi\left(V_t R/\nu\right)^{1/5}}\left[\int_{x_c}^{1}(c_x/R)^{4/5}\left(x^2 + \lambda^2\right)^{13/10}dx\right] \quad (A\text{-}34b)$$

For the constant chord case, this minimum, incompressible profile power expression assuming a fully *turbulent* boundary layer over the entire blade becomes

$$C_{Po\ min.} = 0.074\frac{(bc/\pi R)}{\left(V_t c/\nu\right)^{1/5}}\left[\int_{x_c}^{1}\left(x^2 + \lambda^2\right)^{13/10}dx\right] = 0.074\frac{(bc/\pi R)}{\left(V_t c/\nu\right)^{1/5}}\left[\frac{5}{18}T(\lambda,x_c)\right] \quad (A\text{-}34c)$$

Note again that when the chord distribution is (1) non-dimensionalized by radius and (2) included within the integral as is done with Equation A-34b, then Reynolds

number becomes based on radius--not chord. This is another reminder of how carefully the scaling of data from one configuration to another must be done. It also suggests a more meaningful basis for scaling model data to full scale.

The integral required by Equation A-34c falls in the elliptical integral family. However, for engineering purposes, a handier evaluation of $T(\lambda, x_c)$ is with

$$T(\lambda, x_c) = \left[\left(1+\lambda^2\right)^{13/10} - x_c\left(x_c^2 + \lambda^2\right)^{13/10}\right] + \frac{9}{5}\lambda^2\left[\left(1+\lambda^2\right)^{3/10} - x_c\left(x_c^2 + \lambda^2\right)^{3/10}\right]$$
$$+ \frac{18}{25}\lambda^4\left\{\ln\left[\frac{1+\left(1+\lambda^2\right)^{3/10}}{x_c + \left(x_c^2 + \lambda^2\right)^{3/10}}\right]\right\} \qquad \text{for } \lambda \text{ less than } 1.3 \qquad \text{(A-35)}$$

To conclude this theoretical discussion, Equations A-31 and A-34 form, respectively, lower and upper bounds to the minimum, incompressible, profile power of a prop-rotor.

There is an abundance of prop-rotor experimental data with which to compare the above theoretical solutions. However, test results obtained with PROP 2 at constant 1600 RPM are of particular value. By holding rotational speed constant with this constant chord prop-rotor, the Reynolds number parameter becomes constant at $V_t c / v = 9.93 \times 10^6$ or $V_t R / v = 4.14 \times 10^7$ and $bc/\pi R = 0.2292$. For this special case, the lower and upper bounds are defined by Equations A-31c and A-34c respectively. Substitution of PROP 2 constants reduces the minimum, incompressible, profile power for this prop-rotor to lying between two boundaries which are:

$$C_{Po\ min} = 0.000096587\left[\int_{x_c}^1 \left(x^2 + \lambda^2\right)^{5/4} dx\right] \qquad \text{for PROP 2 if Laminar} \qquad \text{(A-36)}$$

$$C_{Po\ min} = 0.000676128\left[\int_{x_c}^1 \left(x^2 + \lambda^2\right)^{13/10} dx\right] \qquad \text{for PROP 2 if Turbulent} \qquad \text{(A-37)}$$

The two figures that follow compare the PROP 2, 1600 RPM "Test" rotor profile power coefficient to both laminar and turbulent boundary layer solutions. In Figure H, the complete range in PROP 2 experimental data from zero thrust to the highest thrust obtained is shown. In Figure I, only the data capturing the minimum profile power is shown to provide an expanded view. The general trend shows PROP 2 profile power decreasing from excessive values at high thrust down to minimum values on the order of the turbulent boundary layer solution of Equation A-34c or A-37. The minimum profile power appears to occur at slightly positive prop-rotor thrust coefficients on the order of $C_T \approx 0.005$.

Figure I associates helical tip Mach number values (and $\beta_{.75}$ values) with each zero thrust point. This particular PROP 2 data suggests that operating the

prop-rotor near or at sonic helical tip Mach numbers is beneficial. This would be a hasty conclusion as will be seen when the complete set of PROP 2 experimental data is examined. A valid conclusion from Figure H or I is that PROP 2 does appear dominated by turbulent boundary layer flow because of "better correlation."

The preceding examination of a special case where the prop-rotor has constant chord and is operated at constant RPM provides a brief introduction to minimum, incompressible profile power. A much broader survey is presented in Figures A-11 through A-14. The questions answered by these several figures are

What boundary layer flow assumption best fits the "Test" minimum

profile power for PROP 1? What about for PROP 2?

To answer these questions, consider first a correlation of measured PROP 1 profile power data assuming a laminar boundary layer theoretical solution as given by Equation A-31b. Let the "Test" profile power values near zero thrust be considered as the representative minimum.

A broader comparison of PROP's 1 and 2 "Test" minimum profile power data with laminar and turbulent theories is made in Figures A-11 through A-14. From Figures A-11a and A-11b it appears that PROP 1 follows laminar theory empirically increased by a factor of 2.0 as long as the tip helical Mach number is clearly in the incompressible range. This would be consistent with the two-dimensional airfoil (prior to compressibility onset) as shown by Figures F and G on page A-15. The ratio of PROP 1 "Test" minimum profile power to either laminar or turbulent theories is shown versus helical tip Mach number on Figure A-12. The influence of compressibility becomes apparent as early as $M_t = 0.65$.

In contrast to PROP 1, PROP 2 "Test" minimum profile power data correlates "extremely well" with a fully turbulent boundary layer assumption as Figures A-13a and A-13b show. The onset of compressibility losses appears delayed to at least $M_t = 1.0$ with PROP 2's thin airfoil geometry as shown by Figure A-14.

To conclude this discussion of minimum incompressible profile power, it appears that small diameter prop-rotors designed using laminar flow airfoils may well demonstrate excellent performance when tested in a laboratory environment. PROP 1's correlation of "Test" minimum profile power data with roughly two times Blasius's laminar theory for a flat plate supports this conclusion. It is, however, doubtful that PROP 1 would sustain this performance in field use. The performance of the virtually full scale propeller exhibited by PROP 2 shows that practical, full scale prop-rotor blades suited to advanced civil tiltrotor aircraft are likely to be dominated by a turbulent boundary layer with very little laminar flow except, perhaps, at the blade inboard region and then at high altitude. As such, an assumption that
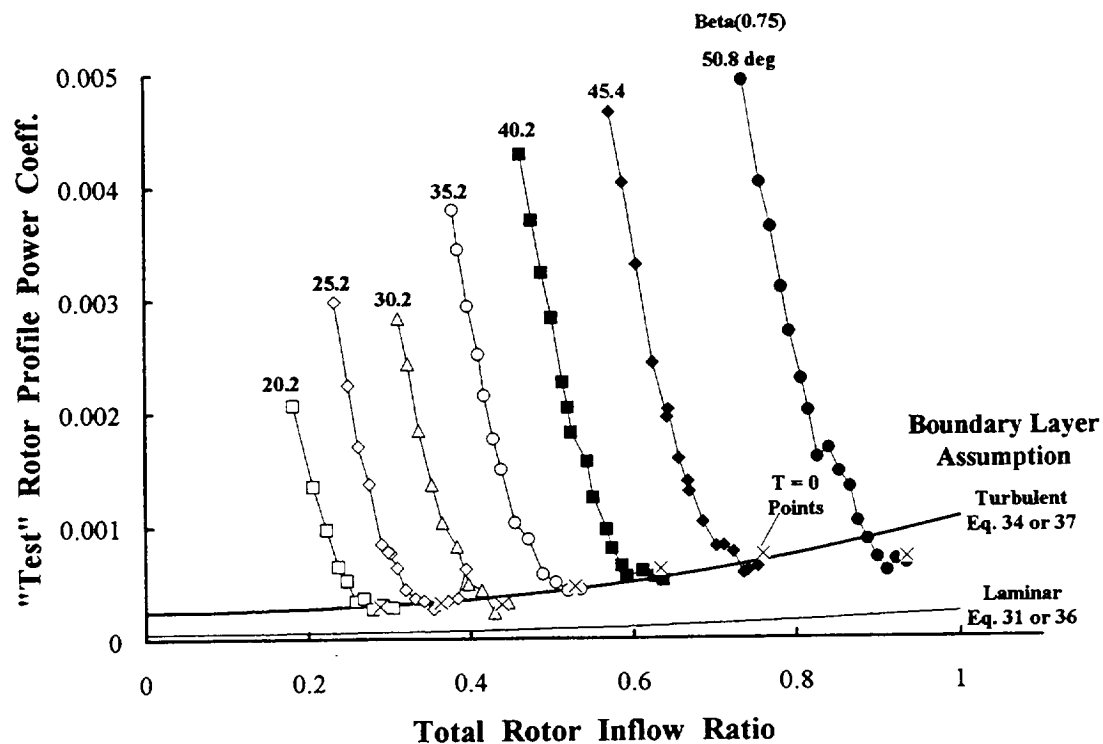
Figure H. Profile Power Trends With Inflow Ratio And $\beta_{.75}$ (PROP 2 at 1600 RPM)
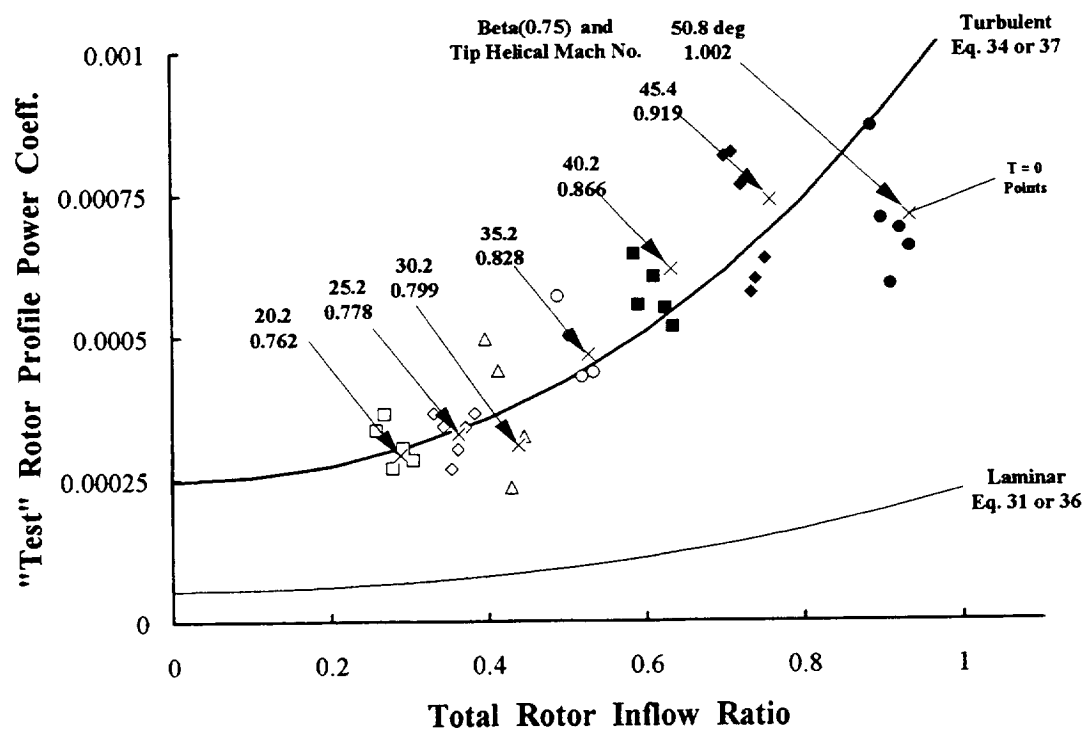
Figure I. Minimum Profile Power Rises Rapidly With Inflow Ratio.

$$C_{d \, min.} \approx 1.25 \times \frac{0.148}{(Vc/v)^{1/5}} = \frac{0.185}{(Vc/v)^{1/5}} \quad \text{for full scale prop-rotors} \quad \text{(A-38)}$$

must be recommended for blade element analysis as the basis for minimum profile power in the incompressible Mach number range.

There is, of course, a reasonable chance that smaller prop-rotors may be studied. In that instance the combination of PROP 1 and 2 data suggest that

$$C_{d \, min.} \approx 2 \times \frac{2.656}{(Vc/v)^{1/2}} = \frac{5.312}{(Vc/v)^{1/2}} \quad \text{for } Vc/v \text{ up to } 1.75 \times 10^6 \quad \text{(A-39)}$$

and then, with a boundary layer transition at higher Reynolds number, assuming that above $Vc/v = 1.75 \times 10^6$ reasonable airfoils will be used so that

$$C_{d \, min.} \approx 1.25 \left[\frac{0.148}{(Vc/v)^{1/5}} - \frac{2 \times 4500}{Vc/v} \right] = \frac{0.185}{(Vc/v)^{1/5}} - \frac{11,250}{Vc/v} \quad \text{(A-40)}$$

Equation A-40 recommends using an empirical factor of 1.25 to increase the Prandtl and von Kármán drag (of a flat plate with fully turbulent boundary layer) up to practical drag coefficient levels. This increase accounts for form drag to some extent. The factor of 1.25 does not account for airfoil drag rise due to compressibility.

It is apparent from Figures A-11, A-12, A-13 and A-14 that minimum profile power is increased by a factor of 5 or more as the tip helical Mach number enters the supersonic range. Therefore, an additional increment of minimum profile power due to compressibility must be obtained. This compressibility increment, when added to the base minimum incompressible profile power, defines the maximum achievable performance of any given prop-rotor. The minimum, compressibility increment to base profile power is the subject of this Appendix's next section.

Minimum Compressible Profile Power

The minimum, *incompressible* profile power can be minimized (relative to total power required to produce usable thrust) by operating at high inflow ratio. However, in the practical case, high inflow ratio tends to introduce high Mach numbers, both axial and helical. Compressibility drag losses can then very easily create excessive profile power that overshadows all other power components. This is an immediate conclusion drawn from Figures A-11 through A-14. An order of magnitude estimate of this compressibility impact on performance is fundamental to understanding prop-rotor design.

A relatively simple theory to calculate a minimum profile power *increment* due to compressibility is available. This incremental profile power is obtained from the *increment* in airfoil drag coefficient *at zero lift* due to compressibility. That is,

$$\text{incremental} \quad dD_{comp.} = \left(\tfrac{1}{2}\rho V_r^2\right)\left(c\ dr\right)\left(\Delta C_{d\ compressibility}\right) \tag{A-41}$$

The incremental profile power due to compressibility, accounting for all blades, is then obtained from the integral

$$\Delta P_{o\ comp.} = b\int_{root}^{tip} V_r\left[\left(\tfrac{1}{2}\rho V_r^2\right)\left(c\ dr\right)\left(\Delta C_{d\ compressibility}\right)\right] \tag{A-42}$$

The difficulty in Equation A-42 is, of course, estimating $\Delta C_{d\ compressibility}$ accurately.

One method of estimating the incremental drag coefficient due to compressibility was developed in the late 1940's and early 1950's by von Kármán and others as presented, for example, in References 17 and 18. These aerodynamists used small perturbation theory around $M = 1.0$ plus other assumptions to solve the Navier-Stokes equations. Their solutions led to a transonic similarity theory. They found transonic similarity parameters for two dimensional airfoils took the form

$$\tilde{C}_d = \frac{\Delta C_{d\ comp.}M^{2/3}(\gamma+1)^{1/3}}{(t/c)^{5/3}} \qquad \tilde{M} = \frac{M^2-1}{M^{4/3}(t/c)^{2/3}(\gamma+1)^{2/3}} \tag{A-43}$$

where $\gamma = 1.4$ is the specific heat constant for air. These parameters allow the incremental compressibility drag coefficient for a given airfoil family to be corrected for thickness ratio.

A modern application of this work was provide by McCrosky, et al in Reference 19. Figure 8 of this reference shows a graph of $\tilde{C}_d$ versus $\tilde{M}$ including experimental data for four airfoils. There is also a solid line on figure 8 of Reference 19 labeled Harris correlation (a curve fit used by the present author for over 20 years). The semi-empirical curve fit (for this solid line) gives compressible airfoil drag at near zero lift coefficient for the NACA 00XX, 63A0XX, and Sikorsky SC 1095 airfoils in the similarity form of

$$\tilde{C}_d = \frac{6.4266}{1.6736^{5/2}}\left(\tilde{M}+1.6736\right)^{5/2} = 1.774\left(\tilde{M}+1.6736\right)^{5/2} \tag{A-44}$$

The constraints to Equation A-44 are three fold:

1. for $\tilde{M}$ below -1.6736, $\tilde{C}_d \equiv 0.0$

2. when $\tilde{C}_d$ gets to 4.62, stop and hold $\tilde{C}_d$ constant at 4.62 until

3. the supersonic $\tilde{C}_d$ equation of $\tilde{C}_d = \dfrac{4.762}{\sqrt{\tilde{M}}}$ is encountered.

This 1940's transonic similarity theory as outlined above gives the approximate behavior of *airfoil compressible drag at zero lift*. When applied to airfoils such as the NACA 16 series with varying thickness ratio, the compressible drag coefficient appears as shown in Figure A-15. Note that compressible drag rise for very thick airfoils that might be considered for prop-rotor inboard roots is also included on Figure A-15.[*]

There is another result given by transonic similarity theory which is quite useful. The $\Delta C_{d_{comp.}}$ will be zero when the transonic similarity drag coefficient, $\tilde{C}_d$, is zero; and $\tilde{C}_d$ will be zero when the transonic similarity Mach number, $\tilde{M}$, equals -1.6736. This fact defines a maximum airfoil thickness ratio (below which there will be no appreciable compressibility drag) for any given free stream Mach number as

$$\tilde{M} = \frac{M^2 - 1}{M^{4/3}(t/c)^{2/3}(\gamma + 1)^{2/3}} = -1.6736 \tag{A-45}$$

This result immediately gives a simple rule of thumb to avoid compressibility losses at zero lift. That is, $\Delta C_{d_{comp.}}$ will be zero (in air where $\gamma = 1.4$) as long as airfoil thickness ratio is chosen so that

$$\frac{t}{c} \le 0.192 \left(\frac{1 - M^2}{M^{4/3}} \right)^{3/2} \tag{A-46}$$

Figure J below illustrates the application of this generally conservative criteria for maximum t/c to *an unswept blade* at two forward speeds on a standard day at 25,000 feet altitude. For both 350 and 421 knots, the tip speed is 660 feet per second. The helical tip Mach number at 421 knots is 0.955 and Equation A-46 suggests that the tip airfoil thickness ratio not exceed 0.002. At this 421 knot or M = 0.70 flight speed, even the inboard blade station at r/R = 0.20 is operating at

---

[*] This is a very rough use of transonic similarity theory. For instance, the chordwise position (x/c) of the maximum thickness point influences the maximum $\tilde{C}_d$ reached. The value of $\tilde{C}_d =$ 4.62 approximately corresponds to x/c = 0.30. Other values are: for x/c = 0.25, $\tilde{C}_d = 5.02$; for x/c = 0.35, $\tilde{C}_d = 4.35$ and for x/c = 0.50, $\tilde{C}_d = 4.08$. The supersonic drag variation is also dependent on the x/c for maximum t/c being semi-empirically given as

$$\tilde{C}_d = \frac{1}{(x/c)(1 - x/c)\sqrt{\tilde{M}}}.$$
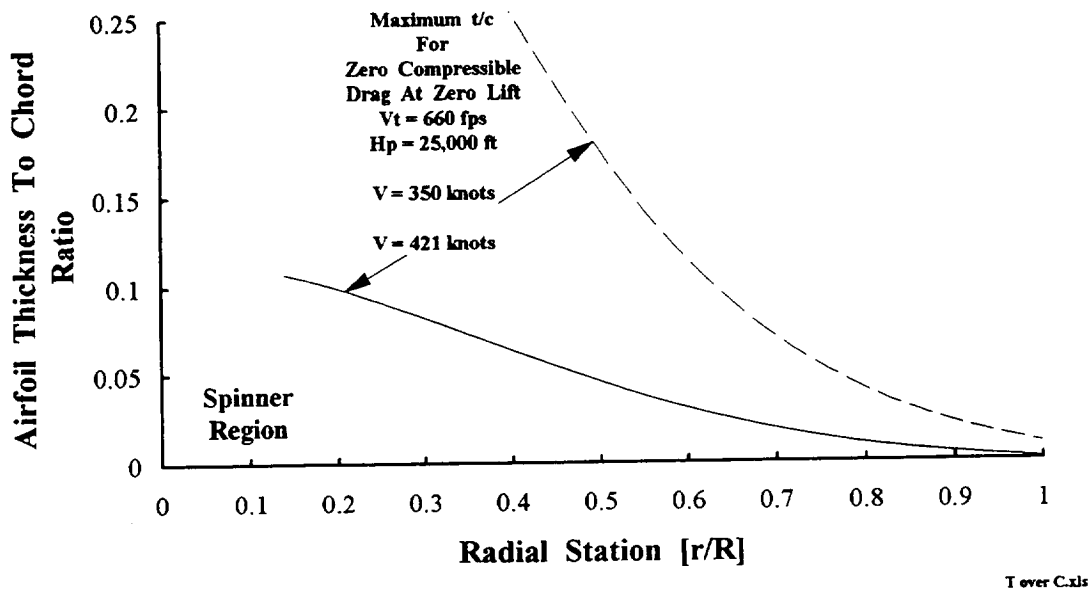
Figure J. Prop-rotor Compressibility Drag Is Avoided With Thin Airfoils.

a resultant Mach number of 0.711. The maximum t/c recommended by Equation A-46 is on the order of 0.10 for this inboard station.

The classical ways around such "structurally challenged" thin airfoils are to (1) accept some compressible drag, (2) sweep the blade leading edge by some angle, Λ and (3) never stop searching for improved airfoils. Sweep reduces the Mach number used in Equation A-46. For example, if a 30 degree sweep angle is applied to the helical Mach number of 0.955, the effective Mach number becomes $0.955 \cos 30°$ or 0.827. Equation A-46 then suggests a maximum t/c of 0.05 before compressibility losses occur.

This transonic similarity theory was used as the source of $\Delta C_{d\,comp.}$ needed by Equation A-42 to estimate the minimum, compressibility profile power increment for both PROP's 1 and 2. The calculation was carried out numerically with 100 radial stations along the blade. The value of $\Delta C_{d\,comp.}$ was obtained from Equation A-44 at each blade element station with the approximate Mach number of

$$M_x \approx \frac{\sqrt{V^2 + (x V_t)^2}}{a_s} = \frac{V}{a_s}\sqrt{1 + (x/\lambda_o)^2} = M\sqrt{1 + (x/\lambda_o)^2} \qquad (A-47)$$

The blade element chord (c) and thickness ratio (t/c) distributions (as given in Appendices C and D for PROP's 1 and 2 respectively) were used. The thickness ratio, along with the local Mach number from Equation A-47, were used to first calculate $\bar{M}$ at each radial station following Equation A-43. Then the transonic

A-25

similarity drag coefficient, $\tilde{C}_d$, was calculated from Equation A-44 subject to the three constraints. Next, with $\tilde{C}_d$ in hand, Equation A-43 was solved backwards for $\Delta C_{d\,comp.}$. Finally, the radially integrated, minimum compressible profile power increment per Equation A-42 was put in rotor coefficient form to give a $\Delta C_{Po\,comp.}$.

The results of re-estimating "Test" minimum rotor profile power coefficient including a minimum compressible profile power increment is shown in Figure A-16 for PROP 1 and Figure A-17 for PROP 2. For PROP 1, the estimate was made using twice the Blasius laminar boundary layer assumption for minimum incompressible profile power plus the incremental compressible power. That is, for PROP 1

$$C_{d\,min.} = \frac{5.312}{(Vc/\nu)^{1/2}} \quad \text{per Eq. (A-39) for PROP 1}$$

$$C_{Po\,min.} \quad \text{from Eq. (A-31b) as} \quad 2.0 \times \frac{1.328\,b}{\pi\sqrt{V_t R/\nu}}\left[\int_{x_c}^1 (c_x/R)^{1/2}(x^2+\lambda^2)^{5/4}dx\right] \quad (A\text{-}48)$$

$$\text{"Test"} \; C_{Po\,min.} \approx C_{Po\,min.} + \Delta C_{Po\,comp.}$$

For PROP 2 a fully turbulent boundary layer solution was assumed so that

$$C_{d\,min.} = \frac{0.185}{(Vc/\nu)^{1/5}} \quad \text{per Eq. (A-38) for PROP 2}$$

$$C_{Po\,min.} \quad \text{from Eq. (A-34b) as} \quad 1.25 \times \frac{0.074\,b}{\pi(V_t R/\nu)^{1/5}}\left[\int_{x_c}^1 (c_x/R)^{4/5}(x^2+\lambda^2)^{13/10}dx\right] \quad (A\text{-}49)$$

$$\text{"Test"} \; C_{Po\,min.} \approx C_{Po\,min.} + \Delta C_{Po\,comp.}$$

A comparison of Figure A-16 to Figure A-11a shows that correlation has improved for PROP 1 by including a compressible power increment. For PROP 2, the comparison of Figure A-17 to Figure A-13b shows substantially better correlation than for PROP 1. Both data sets show that this relatively simple theory captures the fundamentals of minimum compressible profile power.

The summary of both incompressible and compressible fundamentals is presented by Figure A-18. The ratio of "Test" $C_{Po\,min.}$ to theory now shows considerable improvement when compared to either Figure A-12 (PROP 1) or Figure A-14 (PROP 2). Clearly, both Reynolds and Mach number affects must be included if minimum profile power of full scale prop-rotors is to be accurately established. It appears that the small scale, PROP 1 has the more complicated boundary layer to contend with in a blade element analysis. The continued development of prop-rotor CFD solutions should offer performance analysis without having to construct large airfoil data sets from a small quantity of two-dimensional airfoil experiments.

Even with the inclusion of a minimum compressible profile power, the total "Test" C_{Po} for either PROP 1 or 2 is still not captured however. Figures A-7 and A-8 both show considerable profile power increases with increasing prop-rotor thrust. This is the next subject in this discussion of prop-rotor fundamentals.

Incremental Profile Power Due To Thrust--Part I

The magnitude of this third element (shown on the Figure A, page A-1 outline) can be a very large source of profile power. Furthermore, this power element is, perhaps, the most difficult to estimate. To understand the fundamentals, consider again Equation A-7c from page A-4 which states

$$\text{Incremental } P_o \text{ Due To Thrust} \equiv \Delta P_{o\,\text{thrust}} = b \int_{\text{root}}^{\text{tip}} V_{\text{resultant}} \, dD_{\text{lift}} \qquad \text{(A-7c)}$$

The difficulty presented by this seemingly simple equation lays in understanding the airfoil drag rise with lift. (The useful product of this airfoil lift is, of course, prop-rotor thrust.) It is relatively easy to state that

$$dD = \left(\tfrac{1}{2}\rho V_r^2\right)\!\left(c \, dr\right) C_{d\,\text{lift}} \quad \text{where} \quad C_{d\,\text{lift}} = f(C_1, RN, M, \text{and airfoil shape}) \qquad \text{(A-49)}$$

and then that profile power, accounting for all blades, will be

$$\Delta P_{o\,\text{thrust}} = b \int_{\text{root}}^{\text{tip}} V_r \left\{ \left(\tfrac{1}{2}\rho V_r^2\right)\!\left(c \, dr\right) C_{d\,\text{lift}} \right\} \qquad \text{(A-50a)}$$

or, in non-dimensional rotor coefficient form

$$\Delta C_{Po\,\text{thrust}} = \frac{b}{2\pi} \int_{x_c}^{1} \left(c_x / R\right)\!\left(x^2 + \lambda^2\right)^{3/2} C_{d\,\text{lift}} \, dx \qquad \text{(A-50b)}$$

or when blade chord is constant

$$\Delta C_{Po\,\text{thrust}} = \frac{(bc / \pi R)}{2} \int_{x_c}^{1} \left(x^2 + \lambda^2\right)^{3/2} C_{d\,\text{lift}} \, dx \qquad \text{(A-50c)}$$

Just how large this profile power element due to prop-rotor thrust is can be seen by Figures A-19 and A-20 for PROP 1 and 2 respectively. In these two figures, the total "Test" C_{Po} has been reduced by $C_{Po\,\text{min}}$ based on Reynolds number plus the transonic similarity derived $\Delta C_{Po\,\text{comp.}}$. This residual represents a first order estimate of profile power due to thrust. That is

$$\text{"Test"} \; \Delta C_{Po\,\text{thrust}} \approx \text{Total "Test"} \; C_{Po} - \text{Theory} \left(C_{Po\,\text{min}} + \Delta C_{Po\,\text{comp.}} \right) \qquad \text{(A-51)}$$

This residual, "Test" $\Delta C_{P_{o\,thrust}}$, is plotted versus rotor thrust coefficient in Figures A-19 and A-20. Understanding the trends presented by these two figures in a rotor coefficient form is not easy. This is because the power element depends on prop-rotor thrust which depends upon blade element lift and drag. As will be seen, $\Delta C_{P_{o\,thrust}}$ actually depends upon (1) total inflow ratio, (2) thrust and (3) total prop-rotor power. To lay ground work to understanding this fundamental, consider first the conversion from power and thrust to "average" or equivalent airfoil lift and drag coefficients.

"Average Airfoil" Lift and Drag Coefficients

In the Part I opening discussion of profile power due thrust, the question of airfoil drag rise due to lift has been raised. Some insight into the airfoil drag polar (i.e., C_l versus C_d) is therefore required. The lightly loaded propeller operates in many ways that can be better appreciated in the form of equivalent or average airfoil lift and drag coefficients polars rather than just total thrust and power. One good example is understanding airfoil drag due to lift in the transonic and supersonic regimes.

To gain this insight, consider integrating the elemental blade element thrust dT and power $dP = \Omega\, dQ$. Assume that each blade element airfoil is operating at a constant or average lift coefficient (i.e., $C_l = \overline{C}_L$) and corresponding drag coefficient ($C_d = \overline{C}_D$). Thus, let the blade element airloads be calculated as

$$dL = \left(\tfrac{1}{2}\rho V_r^2\right)(c\, dr)\overline{C}_L \quad \text{and} \quad dD = \left(\tfrac{1}{2}\rho V_r^2\right)(bc\, dr)\overline{C}_D \tag{A-52}$$

Now integrate from blade root to tip assuming constant lift and drag coefficients while also assuming that the blade chord is constant along the blade's span. Following the logic surrounding Equation A-9 on page A-5, the thrust from all blades becomes

$$T = b\int_{root}^{tip} dT = b\tfrac{1}{2}\rho c\left[\overline{C}_L \int_{root}^{tip} V_r^2 \cos\phi\, dr - \overline{C}_D \int_{root}^{tip} V_r^2 \sin\phi\, dr \right] \tag{A-53}$$

The power from all blades, in a similar manner, is found as

$$P = b\Omega\int_{root}^{tip} rdQ = b\Omega\tfrac{1}{2}\rho c\left[\overline{C}_L \int_{root}^{tip} rV_r^2 \sin\phi\, dr + \overline{C}_D \int_{root}^{tip} rV_r^2 \cos\phi\, dr \right] \tag{A-54}$$

The actual integration is, again, carried out more conveniently in non-dimensional form. That is, substitute

$$x = \frac{r}{R} \quad \text{so that} \quad dr = Rdx \quad \text{and} \quad root = x_c, \; tip = 1.0$$

$$V_r = \sqrt{(\Omega r)^2 + (V + v_i)^2} = V_t \sqrt{x^2 + \lambda^2}$$

$$\sin\phi = \frac{V + v_i}{V_r} = \frac{\lambda}{\sqrt{x^2 + \lambda^2}} \quad \text{and} \quad \cos\phi = \frac{\Omega r}{V_r} = \frac{x}{\sqrt{x^2 + \lambda^2}}$$

The final results, in rotor coefficient nomenclature, are

$$\frac{2C_T}{\sigma} = \overline{C}_L \, T_1 - \overline{C}_D \, T_2 \tag{A-55}$$

$$\frac{2C_P}{\sigma} = \overline{C}_L \, Q_1 + \overline{C}_D \, Q_2 \tag{A-56}$$

where T_1, T_2, Q_1 and Q_2 are associated with the several integrals and are evaluated *for a constant chord blade* as

$$T_1 = \frac{1}{3}\left[\left(1 + \lambda^2\right)^{3/2} - \left(x_c^2 + \lambda^2\right)^{3/2} \right]$$

$$T_2 = \frac{\lambda}{2}\left[\left(1 + \lambda^2\right)^{1/2} - x_c\left(x_c^2 + \lambda^2\right)^{1/2} + \lambda^2 \ln\left(\frac{1 + \left(1 + \lambda^2\right)^{1/2}}{x_c + \left(x_c^2 + \lambda^2\right)^{1/2}} \right) \right] \tag{A-57}$$

$$Q_1 = \lambda T_1$$

$$Q_2 = \frac{1}{4}\left[\left(1 + \lambda^2\right)^{3/2} - x_c\left(x_c^2 + \lambda^2\right)^{3/2} - \lambda T_2 \right]$$

These two equations (Eq. A-55 and A-56) in the two unknowns of average airfoil lift and drag coefficients are solved simultaneously to give

$$\overline{C}_L = \frac{Q_2\left(\dfrac{2C_T}{\sigma}\right) + T_2\left(\dfrac{2C_P}{\sigma}\right)}{Q_2 T_1 + Q_1 T_2} \quad \text{and} \quad \overline{C}_D = \frac{T_1\left(\dfrac{2C_P}{\sigma}\right) - Q_1\left(\dfrac{2C_T}{\sigma}\right)}{Q_2 T_1 + Q_1 T_2} \tag{A-58}$$

Equation A-58 offers an additional way of viewing prop-rotor performance. Expressing prop-rotor performance in terms of an average lift coefficient (instead of thrust) and an average drag coefficient (instead of power) is most valuable because the primary influences of inflow ratio on performance are removed. There are some cautionary shortcomings to the view however. For instance, the influence of Mach number is not removed by Equation A-58. Of course, the importance of blade element airload distribution is also lost completely. Therefore, when any given prop-rotor (with prescribed twist, planform and airfoil geometry) is operating off its design point, the equivalent lift--drag polar is distorted. This distortion is

similar to lift-drag polars of cambered versus symmetrical airfoils. Despite these short comings, both PROP 1 and PROP 2 convey unmistakable trends characteristic of two-dimensional airfoils.

PROP 1's performance behavior expressed as an average or equivalent airfoil is shown in Figure A-21a through A-21d. This data covers the wind tunnel Mach numbers of 0.60, 0.70, 0.80 and 0.90 respectively. The highest range in helical tip Mach number is noted on each figure. This high helical tip Mach number was always obtained with the lowest blade pitch angle tested. A constant solidity of 0.0721 was used for PROP 1 in Equation A-58 and the four figures for illustration purposes. (Because PROP 1 has a tapered blade, the integrals associated with T_1, T_2, Q_1 and Q_2 might be evaluated including the blade planform for a more refined analysis. However, this would be somewhat inconsistent with the broad, first order assumption that $C_1 = \overline{C}_L$ and $C_d = \overline{C}_D$.)

PROP 1's average airfoil lift-drag polars show the unmistakable character of the cambered airfoil family as implied by Figure 3d. As the forward Mach number increases from 0.60 to 0.90, the minimum drag coefficient, indicated by the vertical dashed line, increases by over a factor of 5. The trend with increasing Mach number indicates the transition from a subsonic lift-drag polar (which has a wide "drag bucket") to a supersonic polar where drag increases with lift starting almost immediately from zero lift.

Similar average airfoil lift-drag polars for PROP 2 are presented in Figure A-22a through A-22d for forward Mach numbers of 0.60, 0.70, 0.80 and 0.89. While PROP 2 results show more scatter in its polar shapes than PROP 1, the polars are clearly representative of a thin, uncambered airfoil. Note that the lift and drag scales for PROP 2 are not the same as for PROP 1. In particular, PROP 2's drag scale is about one-sixth of PROP 1's scale. Between M = 0.60 and M = 0.89, PROP 2's minimum drag coefficient only doubles which is a measure of the difference in airfoil thickness ratio between the two configurations as shown on Figure 3c. In contrast to PROP 1, PROP 2 has virtually the same shaped drag polars at all wind tunnel Mach numbers and $\beta_{.75}$ tested. This is initial evidence of a very thin, symmetrical airfoil.

There is a very important point to keep in mind while reviewing both sets of these prop-rotor, average lift-drag polars (i.e., Figures A-21 and A-22). This point is that helical Mach number is varying as lift increases as noted on the figures. This comes about because the experimenters varied RPM at constant wind tunnel Mach number in order to vary propeller inflow and thus propeller thrust. Therefore, the polars can not be viewed in the conventional sense of two-dimensional airfoil data where angle of attack is varied at constant Mach number. In effect, these average airfoil polars are indexing to slightly different Mach number lines as lift increases.

The "average" or equivalent prop-rotor lift-drag polars presented by Figures A-21a through d and A-22a through d form the basis of understanding, first, drag rise with lift and, then, profile power rise with thrust, total power and rotor inflow ratio.

Average Airfoil Drag Rise With Lift.

The average airfoil lift-drag polars illustrated by Figures A-21 and A-22 show that drag varies in a somewhat parabolic way with lift. This variation for two-dimensional, *uncambered* airfoils is frequently described in both subsonic and supersonic flow as

$$C_{d\,lift} \approx \frac{d\,C_d}{d\,C_l^2}\left(C_l^2\right) \qquad (A-59)$$

Hoerner (Reference 16, page 7-3) explains that in subsonic flow a low value of $d\,C_d/d\,C_l^2 \approx 0.01$ in Equation A-59 is characteristic of normal, *uncambered* airfoils. (These near zero, pitching moment airfoils were typically chosen for early autogyro and helicopter blades by the rotorcraft industry.) The upper limit in subsonic flow is on the order of $d\,C_d/d\,C_l^2 = 1/2\pi$. This upper boundary value occurs with a flat plate "airfoil" (i.e., zero t/c) which is unable to theoretically sustain a leading edge suction. Therefore, the drag due to lift is simply the normal force resolved into the free stream direction. Hoerner's explanation in equation form is

$$C_{d\,lift} \approx \alpha\,C_N \quad \text{and} \quad C_N \approx 2\pi\alpha \quad \text{or} \quad \alpha \approx C_N/2\pi$$

and therefore

$$C_{d\,lift} \approx \frac{C_N}{2\pi}\,C_N = \frac{1}{2\pi}C_N^2 \approx 0.159 C_N^2$$

In the supersonic flow regime, Hoerner (Reference 16, page 17-17) explains that $d\,C_d/d\,C_l^2$ becomes dependent on Mach number. The upper limit, again associated with a two-dimensional flat plate airfoil, has a drag rise with lift coefficient squared that depends on Mach number. That is

$$\frac{d\,C_d}{d\,C_l^2} = \text{constant } \sqrt{M^2-1} \approx 0.25\sqrt{M^2-1} \qquad (A-60)$$

Figure K, below, summarizes these approximate boundaries to the $d\,C_d/d\,C_l^2$ variation with Mach number. There is considerable leeway in $d\,C_d/d\,C_l^2$ values in the Mach number range from 0.8 to 1.2, This uncertainty in the critical Mach number at which the transition to supersonic behavior starts is expressed on the figure by the long, dark bar and question marks.
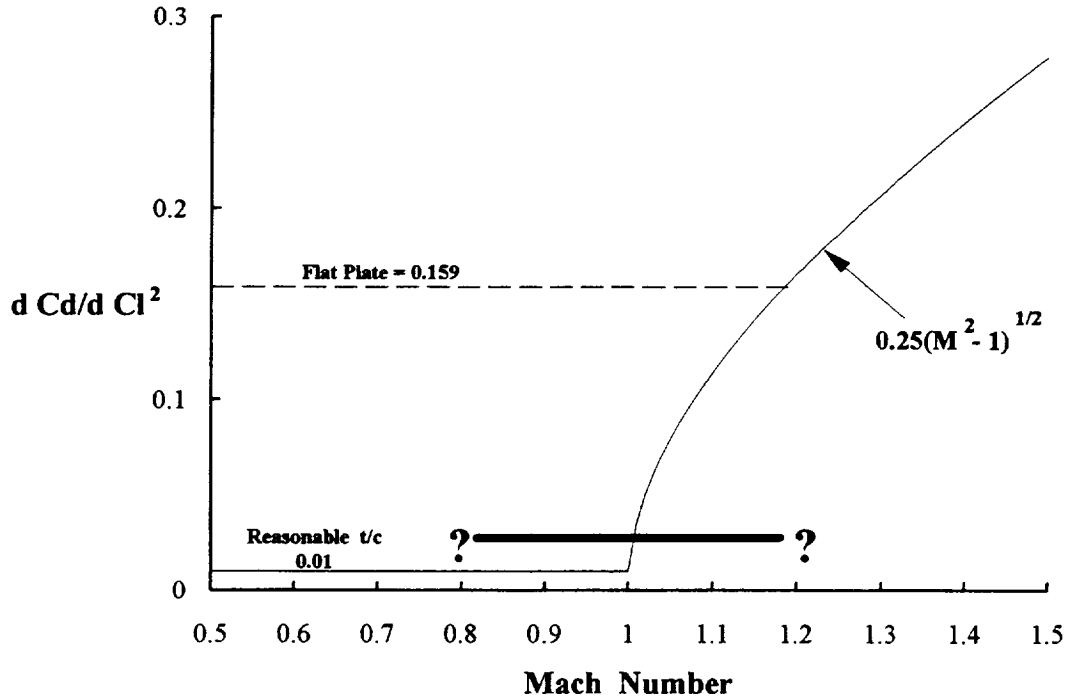
Figure K. Airfoil Drag Rise With Lift Is Bounded By Flat Plate Behavior.

Incremental Profile Power Due To Thrust--Part II

Figure K's conceptual trends of dC_d/dC_l^2 with Mach number and the first order approach from Equations A-50c, A-58 and A-59 offer a basis from which to understand the fundamentals of profile power due to thrust. That is, since

$$\Delta C_{Po\,thrust} = \frac{(bc/\pi R)}{2} \int_{x_c}^{1} \left(x^2 + \lambda^2\right)^{3/2} C_{d\,lift}\, dx \quad \text{and} \quad C_{d\,lift} \approx \frac{d\,C_d}{d\,C_l^2}\left(C_l^2\right)$$

it follows, for constant chord blades, that

$$\Delta C_{Po\,thrust} \approx \frac{(bc/\pi R)}{2} \int_{x_c}^{1} \left(x^2 + \lambda^2\right)^{3/2}\left[\frac{d\,C_d}{d\,C_l^2}\left(C_l^2\right)\right] dx \qquad (A-61)$$

The two most important keys to Equation A-61 are (1) the behavior of dC_d/dC_l^2 with Mach number and (2) the approximate magnitude of lift coefficient. Of these two keys, the magnitude of lift coefficient is, perhaps, more unfamiliar to the practicing rotary wing aerodynamics engineer. To explain this thought, consider

A-32

letting both dC_d/dC_l^2 and C_1 take on average values so that the incremental profile power due to thrust is simplified to

$$\Delta C_{P_{o\ thrust}} \approx \frac{(bc/\pi R)}{2}\left(\frac{d C_d}{d C_1^2}\right)_{ave.} \left(\overline{C}_L^2\right) \int_{x_c}^{1}\left(x^2 + \lambda^2\right)^{3/2} dx \qquad \text{(A-62a)}$$

or, with the integral recognized as $F(\lambda, x_c)$ from Equation A-25b on page A-13, simply

$$\Delta C_{P_{o\ thrust}} \approx \frac{(bc/\pi R)}{8}\left(\frac{d C_d}{d C_1^2}\right)_{ave.} \left(\overline{C}_L^2\right) F(\lambda, x_c) \qquad \text{(A-62b)}$$

Now the magnitude of the average airfoil lift coefficient was established by Equation A-58 as

$$\overline{C}_L = \frac{Q_2\left(\dfrac{2C_T}{\sigma}\right) + T_2\left(\dfrac{2C_P}{\sigma}\right)}{Q_2 T_1 + Q_1 T_2}$$

It is quite significant that the average airfoil lift coefficient depends upon prop-rotor thrust coefficient _and_ total power coefficient. The rotary wing engineer most frequently uses this average airfoil lift coefficient approximation assuming a very low total rotor inflow ratio (i.e., $\lambda \approx 0$) and even assumes that the helicopter rotor blade has small root cut out (i.e., $x_c \approx 0$) so that

$$T_1 \approx \frac{1}{3}, \quad T_2 \approx \frac{\lambda}{2}, \quad Q_1 \approx \frac{\lambda}{3}, \quad Q_2 \approx \frac{1}{4},$$

from which it follows that

$$\overline{C}_L \approx \frac{\dfrac{6C_T}{\sigma} + 12\lambda\left(\dfrac{C_P}{\sigma}\right)}{1 + 2\lambda^2} \approx \frac{6C_T}{\sigma} \quad \text{if } \lambda C_P \approx 0$$

The most common rotary wing use of $\overline{C}_L \approx 6C_T/\sigma$ is quite appropriate to helicopter hovering and very low speed flight. However, the use of this approximation for a prop-rotor in high speed flight is wholly inadequate. To emphasize this point, consider the montage of data points shown in Figure L which follows. This data collection uses PROP 2 results of average airfoil lift coefficient from Figures A-22a through A-22d which were calculated by Equation A-58. When plotted versus the rotary wing parameter of $\overline{C}_L \approx 6C_T/\sigma$, as in Figure L, the application of this approximation to high speed prop-rotors becomes clearly questionable.

For the prop-rotor, at least the first order average airfoil lift coefficient from Equation A-58 must be used before the fundamentals of profile power due
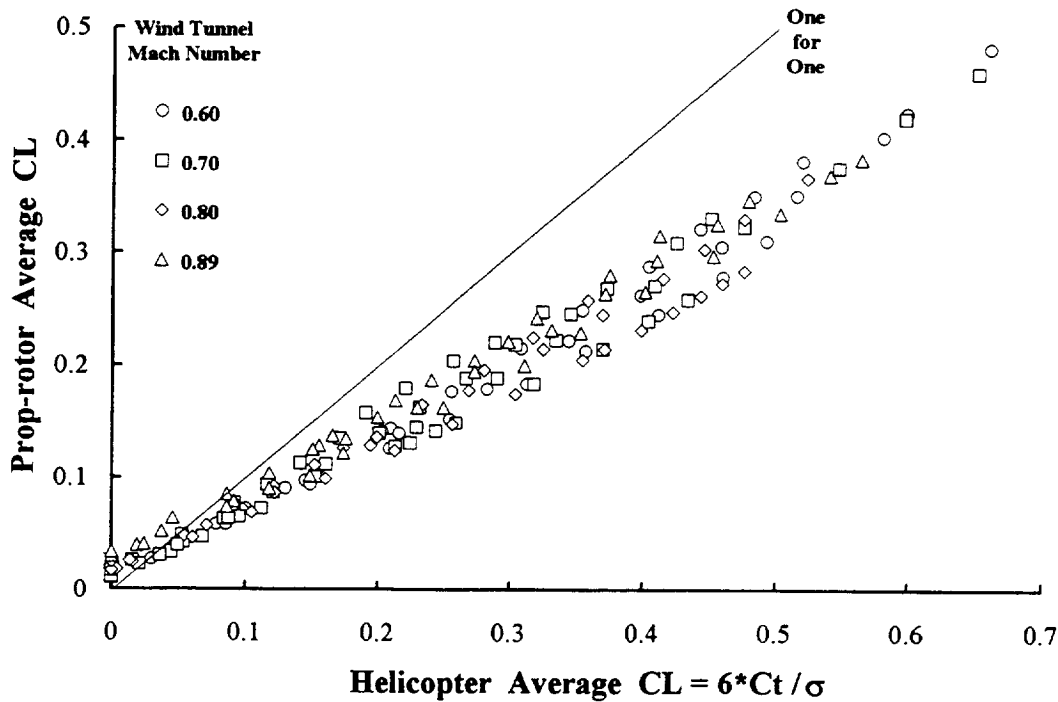
Figure L. Helicopter And Prop-rotor Average Lift Coefficients Differ. (PROP 2)

to thrust can be understood. When this substitution is made in Equation A-62b, the result for the constant chord blade is

$$\Delta C_{Po\ thrust} \approx \frac{\sigma}{8}\left(\frac{d\ C_d}{d\ C_1^2}\right)_{ave.} \left[\frac{Q_2\left(\frac{2C_T}{\sigma}\right) + T_2\left(\frac{2C_P}{\sigma}\right)}{Q_2 T_1 + Q_1 T_2}\right]^2 F(\lambda, x_c)$$

(A-63)

Because $Q_1 = \lambda T_1$ and $F(\lambda, x_c) = 4(Q_2 + \lambda T_2)$, Equation A-63 simplifies (with a little manipulation) to

$$\Delta C_{Po\ thrust} \approx \frac{8}{\sigma}\left(\frac{d\ C_d}{d\ C_1^2}\right)_{ave.} \left(\frac{Q_2^2}{F\ T_1^2}\right)\left[C_T^2 + 2(T_2/Q_2)\ C_T C_P + (T_2/Q_2)^2 C_P^2\right]$$

(A-64)

As was noted earlier, the trends in profile power due thrust shown on Figures A-19 and A-20 are rather difficult to quickly understand. Equation A-64 shows that it is the dependency on (1) total rotor inflow ratio which influences the several constants, (2) total thrust _and_ (3) _total power_ that makes $\Delta\ C_{Po\ thrust}$ complicated. The variation (with any number of parameters) of prop-rotor average airfoil drag coefficient rise with lift coefficient squared, $(d\ C_d/d\ C_1^2)_{ave.}$, is, perhaps surprisingly, much less of factor in understanding the fundamentals of profile power due to thrust.

A-34

As a first step in un-complicating this profile power element, consider regrouping Equation A-64 as follows:

$$\Delta C_{Po\,thrust} \approx \left(\frac{d\,C_d}{d\,C_l^2}\right)_{ave.} f\left(\sigma,\lambda,C_T,C_P\right) \qquad \text{(A-65a)}$$

where

$$f\left(\sigma,\lambda,C_T,C_P\right) = \frac{8}{\sigma}\left(\frac{Q_2^2}{F\,T_1^2}\right)\left[C_T^2 + 2\left(T_2/Q_2\right)C_T C_P + \left(T_2/Q_2\right)^2 C_P^2\right] \qquad \text{(A-65b)}$$

This regrouping suggests that $\Delta C_{Po\,thrust}$ can be understood in two parts. That is, when $\Delta C_{Po\,thrust}$ is plotted versus $f\left(\sigma,\lambda,C_T,C_P\right)$ then the linear range of this graph will illuminate the approximate average value of $d\,C_d/d\,C_l^2$. From Figure K on page A-32, this prop-rotor average airfoil drag coefficient rise with lift coefficient squared should have values between zero and perhaps, depending on Mach number, as high as 1/3.

All data from both PROP's 1 and 2 can be examined as Equation A-65 suggests. (This includes data well beyond the linear range associated with Equation A-65.) A significant contrast between the two prop-rotors is clearly shown by Figures A-23 and A-24. In PROP 1's case, described by Figure A-23, the average value of $d\,C_d/d\,C_l^2$ varies from a low of about 0.04 to a high of nearly 0.25. In contrast, PROP 2 shows in Figure A-24 that $d\,C_d/d\,C_l^2$ is on the order of 0.25 regardless of the test wind tunnel Mach number and $\beta_{.75}$ conditions.

A more careful data review of both propellers shows that profile power rise with prop-rotor thrust can be very dependent on critical Mach number. For example, Figure A-25 uses PROP 1 data at three wind tunnel Mach numbers to show its $d\,C_d/d\,C_l^2$ behavior. At the lowest forward Mach number tested, M = 0.175, the average drag rise with lift squared is on the order of 0.04 for the five $\beta_{.75}$ tested. The helical tip Mach number range for the M = 0.175 wind tunnel speed is 0.355 to 0.889 for the linear region. In the cruise wind tunnel Mach number range, say where M = 0.60, Figure A-25 shows that PROP 1 has reached $d\,C_d/d\,C_l^2$ of about 0.1. When tested at the maximum tunnel Mach number of M = 0.925, PROP 1 behaved more in accordance with supersonic theory with a $d\,C_d/d\,C_l^2$ of about 0.21. The helical tip Mach number varies from 1.3 up to 1.48 for this supersonic operating condition.

Note that Figure A-25 also shows, with the solid circle data symbols, the onset and growth of PROP 1's aerodynamic stall at the low wind tunnel Mach number of 0.175.

The behavior of $d\,C_d/d\,C_l^2$ with Mach number for PROP 2 differs considerably from PROP 1. This behavior difference is caused not by blade twist geometry, but because PROP 2 has very thin blades as Figure 3c shows. Figure A-26, in contrast to PROP 1's trend of Figure A-25, suggests that regardless of the wind tunnel Mach number and $\beta_{.75}$ tested, $d\,C_d/d\,C_l^2$ is bounded on the low side by $1/2\pi \approx 0.159$ for PROP 2. At the highest test Mach number of 0.96, $d\,C_d/d\,C_l^2$ has reached a supersonic value of 0.25. The interpretation of Figure A-26's results is that (1) the thin airfoils used with PROP 2 behave very much like flat plates over the majority of the blade's span and (2) the transition of $d\,C_d/d\,C_l^2$ from subsonic to supersonic values is clouded by the high, subsonic $1/2\pi$ trend of very thin airfoils.

Figure A-27 presents a summary of all $d\,C_d/d\,C_l^2$ data gleaned from both propeller tests. Take particular note that the $d\,C_d/d\,C_l^2$ values shown on Figure A-27 are graphed versus the *helical Mach number at the 0.85 radius station—not the tip helical Mach number*. This *arbitrary choice* was made so that the highest Mach number data *appears* bounded by the supersonic flat plate equation given earlier as

$$\frac{d\,C_d}{d\,C_l^2} = \text{constant}\sqrt{M^2-1} \approx 0.25\sqrt{M^2-1} \qquad (\text{see Eq. A}-60)$$

PROP 1's blade and airfoil geometry appears to follow the empirical drag rise trend that

$$\text{if } M_{0.85} \leq 0.75 \quad \text{then} \quad dC_d/d\,C_l^2 = 0.04$$
$$\text{if } M_{0.85} \geq 0.75 \quad \text{then} \quad dC_d/d\,C_l^2 = 0.04 + 0.333\big(M_{0.85} - 0.75\big) \qquad (\text{A-66})$$

On the other hand, PROP 2's thin airfoil, but high solidity, blade geometry leads to an empirical drag rise trend more on the order of

$$\text{if } M_{0.85} \leq 0.80 \quad \text{then} \quad dC_d/d\,C_l^2 = 0.159 \quad \text{or} \quad 1/2\pi$$
$$\text{if } M_{0.85} \geq 0.80 \quad \text{then} \quad dC_d/d\,C_l^2 = 0.159 + 0.333\big(M_{0.85} - 0.80\big) \qquad (\text{A-67})$$

The overall conclusion to this discussion of profile power due to thrust is summarized for both PROP's 1 and 2 with Figure A-28. The fundamental understanding and associated theory, with empirically created $d\,C_d/d\,C_l^2$ values, is correlated with "Test" $\Delta\,C_{Po\,thrust}$ defined by Equation A-51 from page A-27. The base experimental trend is captured to within ± 25 per cent. This inaccuracy would, of course, be substantially reduced using a more detailed blade element analysis.

Estimating Thrust Coefficient
Variation With $\beta_{.75}$ And Inflow Ratio

Understanding prop-rotor performance would be incomplete without some fundamental understanding of why thrust varies with inflow ratio (at fixed $\beta_{.75}$) as shown in Figures 4a for PROP 1 or Figure 5a for PROP 2. This understanding comes by using what was learned from the two earlier paragraphs of

a. converting power from torque $\times \Omega$ to force $\times$ velocity, page A-5

and

b. "average airfoil" lift and drag coefficients, page A-28.

The traditional starting point to understanding thrust begins with Equation A-9 which states that

$$dT = dL\cos\phi - dD\sin\phi \qquad (A-9)$$

from which it follows that

$$T = b\int_{root}^{tip} dT = b\int_{root}^{tip} dL\cos\phi\, dr - b\int_{root}^{tip} dD\sin\phi\, dr = T_{Lift} - T_{Drag} \qquad (A-68)$$

The prop-rotor thrust is therefore made up of two components. The first component, T_{Lift}, is the positive contribution obtained from the blade element airfoil lift. The negative contribution, T_{Drag}, is incurred because of blade element airfoil drag. The understanding of each contribution separately is very helpful.

Prop-rotor Thrust Due
To Airfoil Lift

The integration of the blade element lift contribution required by Equation A-68 can be accomplished–for a lightly loaded propeller or typical prop-rotor–in some detail without excessive assumptions. For example, in the lift portion of the dT integral, let

$$dL = \left(\tfrac{1}{2}\rho V_r^2\right)(c\,dr)C_{l(r)} \quad \text{and} \quad C_{l(r)} = a_{ave}\sin\alpha_{(r)} \quad \text{and} \quad \alpha_{(r)} = \beta_{(r)} - \phi_{(r)} \qquad (A-69)$$

Substitution of these lift oriented relationships from Equation A-69 into Equation A-68 leads to

$$T_{Lift} = b\int_{root}^{tip} dL\cos\phi\, dr = \tfrac{1}{2}\rho\, b\, c\, a_{ave.}\int_{root}^{tip} V_r^2\cos\phi\sin\alpha\, dr \qquad (A-70)$$

A-37

When the substitution of blade element angle of attack is made and the trigonometric expansion is completed, then T_{Lift} becomes

$$T_{Lift} = \tfrac{1}{2}\rho\, b\, c\, a_{ave.} \int_{root}^{tip} \left(\sin\beta\; V_r^2 \cos^2\phi - \cos\beta\; V_r^2 \cos\phi\sin\phi\right) dr \qquad (A-71)$$

Now, from Figure C on page A-7 and the non-dimensional velocity vector statements made previously, it is clear that

$$V_r^2 \cos^2\phi \equiv (\Omega r)^2 = V_t^2 \left(x^2\right) \quad \text{where } x = r/R$$
$$V_r^2 \cos\phi\sin\phi \equiv (\Omega r)(V + v_i) = V_t^2 \left(x\lambda\right) \qquad (A-72)$$

Therefore, with no small angle assumptions*, the lift contribution to thrust assuming a constant chord becomes

$$T_{Lift} = \tfrac{1}{2}\rho\, b\, c\, a_{ave.} RV_t^2 \int_{x_c}^{1} \left(x^2 \sin\beta_{(x)} - x\lambda\cos\beta_{(x)}\right) dx \qquad (A-73)$$

The blade pitch angle of a prop-rotor designed for high speed can be defined in terms of total rotor inflow. That is, the manufactured twist distribution with a preset reference $\beta_{.75}$ would resemble

$$\beta_{(x)} = \arc\tan\left(\frac{\lambda_{design}}{x}\right) \qquad (A-74)$$

Propellers have, of course, carefully designed twist distributions based on rather complete blade element analysis. These analyses account for local induced velocity and its influence on induced angle of attack. These analyses also account for airfoil camber. However, as Figure M below shows, even PROP 2's manufactured twist distribution with a reference $\beta_{.75} = 44.57$ degrees (based on a design J of 2.2 stated in Reference 3 or design λ_o of $2.2/\pi \approx 0.70$) closely follows Equation A-74.

The blade angle distribution, when referenced to the 0.75 radius station takes the general form

$$\beta_{(x)} = \beta_{.75} + f_{(x)} \qquad (A-75)$$

where $f_{(x)}$ is defined to be zero at the 0.75 radius station. (In essence, a constant value of design $\beta_{.75}$ is subtracted from the design or manufactured twist. For PROP 2 shown in Figure M, this design $\beta_{.75}$ reduction would be 44.57 degrees.)

---

* This theoretical approach to avoiding small angles was used by Castles and New in their July 1952 NACA TN 2656 report entitled, A Blade-Element Analysis for Lifting Rotors That Is Applicable for Large Inflow and Blade Angles and Any Reasonable Blade Geometry. The approach begins by assuming that $C_l = a\sin\alpha$ not $C_l = a\alpha$.
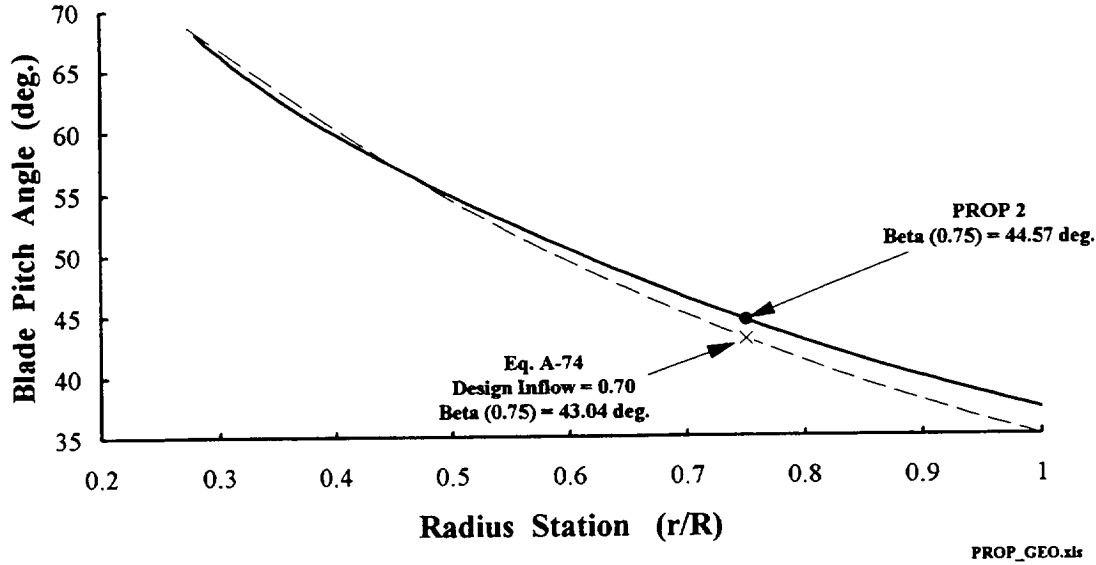
Figure M. Efficient Prop-rotors Use A Twist Distribution Approximated By

$$\beta_{(x)} = arc\ tan\left(\lambda_{design}/x\right)$$

The lift contribution to prop-rotor thrust proposed by Equation A-73 is integrated quite easily by using the general blade pitch angle distribution given by Equation A-75. The $\sin \beta_{(x)}$ and $\cos \beta_{(x)}$ terms are trigonometrically expanded and the result becomes

$$T_L = \tfrac{1}{2}\rho\, b\, c\, a_{ave}\, RV_t^2\left\{\sin\beta_{.75}\int_{x_c}^{1} x^2 \cos f_{(x)}dx + \cos\beta_{.75}\int_{x_c}^{1} x^2 \sin f_{(x)}dx\right.$$

$$\left.-\lambda\cos\beta_{.75}\int_{x_c}^{1} x\cos f_{(x)}dx + \lambda\sin\beta_{.75}\int_{x_c}^{1} x\sin f_{(x)}dx\right\} \quad (A-76)$$

In the practical cases which PROP 1 or PROP 2 offer, the four integrals required by Equation A-76 are evaluated numerically and assigned values of K_1, K_2, K_3, and K_4 respectively. Then a rotor thrust coefficient form is adopted. These steps lead to

$$C_{T_{Lift}} = \frac{(bc/\pi R)a_{ave}}{2}\left\{\sin\beta_{.75} K_1 + \cos\beta_{.75} K_2 - \lambda\cos\beta_{.75} K_3 + \lambda\sin\beta_{.75} K_4\right\} \quad (A-77)$$

Despite the blade pitch angle differences between PROP's 1 and 2 as shown on Figure 3a, the thrust constants are virtually identical as the table below conveys.

Thrust Constants	PROP 1	PROP 2
K_1	0.3237734	0.3241992
K_2	0.0028786	0.0021724
K_3	0.4568261	0.4577549
K_4	0.0231465	0.0206352

For a generic, approximate twist such as suggested by Equation A-74, the blade angle distribution referenced to $\beta_{.75}$ becomes simply

$$\beta_{(x)} = \beta_{.75} + \left[\arc\tan\left(\frac{\lambda_{design}}{x} \right) - \arc\tan\left(\frac{\lambda_{design}}{0.75} \right) \right]$$ (A-78)

where $f_{(x)}$ has been defined by the difference in the two arc tangent parameters which assures that $f_{(x)} = 0$ at $x = 0.75$.

The prop-rotor thrust constants required by Equation A-76 (i.e., K_1, K_2, K_3 and K_4) are easily evaluated using the generic blade pitch angle distribution of Equation A-78. (The $\sin\beta_{(x)}$ and $\cos\beta_{(x)}$ terms are trigonometrically expanded and the sine and cosine of an arc tangent have simple trigonometric identities so that K_1 through K_4 are easily obtained in closed form.) The very handy result is that

$$K_1 = D\left[A + B\left(2\lambda_{des}^2 - x_c^2 - 2x_c\lambda_{des} \right) - 2C\lambda_{des}^4 \right]$$

$$K_2 = \frac{D\,\lambda_{des}}{6}\left[A\left(16\lambda_{des}^2 + 1 \right) - B\left(16\lambda_{des}^2 - 8x_c^2 + 9x_c \right) - 9C\lambda_{des}^2 \right]$$ (A-79a)

$$K_3 = \frac{D}{2}\left[A\left(3 + 8\lambda_{des}^2 \right) - B\left(3x_c + 8\lambda_{des}^2 \right) - 3C\lambda_{des}^2 \right]$$

$$K_4 = D\,\lambda_{des}\left[A + B\left(2x_c - 3 \right) + 2C\lambda_{des}^2 \right]$$

where

$$A = \sqrt{1 + \lambda_{des}^2} \quad B = \sqrt{x_c^2 + \lambda_{des}^2} \quad C = \ln\left(\frac{1 + A}{x_c + B} \right) \quad D = \frac{1}{\sqrt{9 + 16\lambda_{des}^2}}$$ (A-79b)

These four thrust constants depart only slightly from nominal values for prop-rotors designed for high speed cruise. For example, PROP 2 was designed for a propeller advance ratio of $J = 2.2$ which gives a λ_{design} of $2.2/\pi \approx 0.70$. PROP 2's root cutout, x_c, is slightly over 0.27. The table below shows that, to the first approximation, just knowing a prop-rotor's design rotor inflow ratio is quite sufficient knowledge to obtain the thrust due to lift constants at a very early stage in the design process.

Thrust Constants	PROP 2 Numerical	PROP 2 $\lambda_{design} = 0.70$
K_1	0.3241992	0.3236812
K_2	0.0021724	0.0025341
K_3	0.4577549	0.4566499
K_4	0.0206352	0.0229874

The preceding discussion of thrust obtained from blade element airfoil lift can be summarized using PROP 2 experimental data as an example. PROP 2's thrust due to lift is sensitive to both rotor inflow ratio, λ_o and $\beta_{.75}$. Equation A-77 (with the above K_1 through K_4 numerical values) becomes, for PROP 2

$$C_{T_{Lift}} = \frac{(bc/\pi R)a_{ave.}}{2}\{0.3242\sin\beta_{.75} + 0.00217\cos\beta_{.75}$$
$$-\lambda(0.4577\cos\beta_{.75} - 0.02064\sin\beta_{.75})\} \qquad (A\text{-}80)$$

For a fixed $\beta_{.75}$, this fundamental expression says that thrust due to airfoil lift varies linearly with total rotor inflow ratio, $\lambda = \lambda_o + \lambda_i$. When $C_{T_{Lift}}$ is plotted versus just rotor inflow ratio due to forward speed (i.e., λ_o), there is a slight theoretical non-linearity introduced. This non-linearity comes from the induced velocity inflow ratio, λ_i, given by Equation A-11 on page A-8.

PROP 2's thrust due to lift approximation can be further quantified because its solidity is 0.2292. The average lift curve slope of the average airfoil, $a_{ave.}$, remains open to more discussion; however, for the moment, assume that this key airfoil aerodynamic parameter is a practical, 5.73 per radian as opposed to 2π per radian obtained with classical theory. Equation A-80 with $bc/\pi R = 0.2292$ and an $a_{ave.}$ of 5.73 is compared to PROP 2 measurements at a wind tunnel Mach number of 0.70 in Figure N below. The primary fundamentals of how $C_{T_{Lift}}$ varies with rotor inflow and $\beta_{.75}$ are captured by this simple analysis.
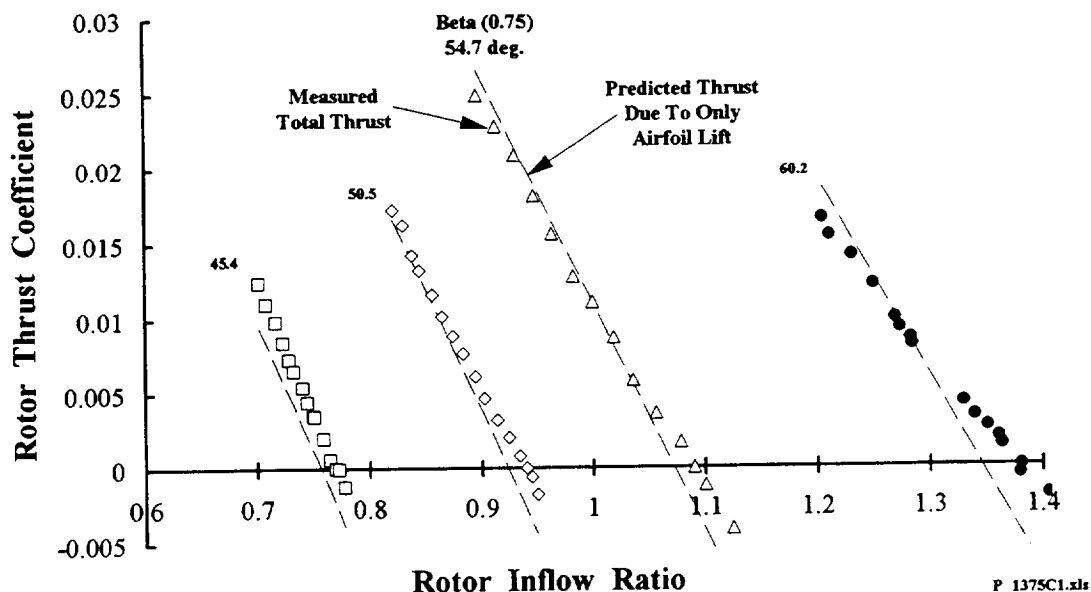
Figure N. Theoretical Thrust Due Only To Airfoil Lift Comes Close To PROP 2 Test Data At Wind Tunnel M = 0.70. ($a_{ave.}$ = 5.73 per rad.)

A-41

Prop-rotor Thrust Due
To Airfoil Drag

The Figure N comparison of predicted prop-rotor thrust (but including only the contribution due to airfoil lift) to some of PROP 2's test data is very informative. However, the comparison does not include the negative thrust created by blade element airfoil drag. To examine the airfoil drag influence, a simpler approach than that taken for the lift contribution is quite adequate. This approach assumes an average airfoil drag coefficient following Equation A-58 on page A-29 will be sufficient.

To begin with then, assume for the drag portion of the dT integral that

$$dD = \left(\tfrac{1}{2}\rho V_r^2\right)(c\,dr)C_{d(r)} \quad \text{and assume} \quad C_{d(r)} = \overline{C}_D \tag{A-81}$$

Substitution of these drag oriented relationships from Equation A-81 into Equation A-68 leads to

$$T_{Drag} = b\int_{root}^{tip} dD\sin\phi\,dr = \tfrac{1}{2}\rho b c\,\overline{C}_D \int_{root}^{tip} V_r^2\sin\phi\;dr \tag{A-82}$$

The integral here was found earlier as T_2 and is evaluated by Equation A-57 on page A-29. The rotor thrust coefficient form of Equation A-82 can therefore be written directly as

$$C_{T_{Drag}} = \frac{(bc/\pi R)\overline{C}_D\,T_2}{2} \tag{A-83}$$

where, again, the constant T_2 and average airfoil drag coefficient for a constant chord blade, $\overline{C}_D$, are

$$T_2 = \frac{\lambda}{2}\left[\left(1+\lambda^2\right)^{1/2} - x_c\left(x_c^2+\lambda^2\right)^{1/2} + \lambda^2\ln\left(\frac{1+\left(1+\lambda^2\right)^{1/2}}{x_c+\left(x_c^2+\lambda^2\right)^{1/2}}\right)\right] \tag{A-57}$$

$$\overline{C}_D = \frac{T_1\left(\dfrac{2C_P}{\sigma}\right) - Q_1\left(\dfrac{2C_T}{\sigma}\right)}{Q_2 T_1 + Q_1 T_2} \tag{A-58}$$

Note that when the average airfoil drag coefficient is introduced, the thrust due to airfoil drag, $C_{T_{Drag}}$, then depends on total thrust and power. This is a relatively minor mathematics impediment.

The comparison of theory, including both lift and drag contributions to prop-rotor thrust, to PROP 2 test results is updated in Figure O.

A-42

Rotor Thrust Coefficient

0.03

0.025

0.02

0.015

0.01

0.005

0

-0.005

Beta (0.75)
54.7 deg.

Predicted
Total Thrust

Predicted Thrust
Due To Only
Airfoil Lift

60.2

50.5

45.4

0.6   0.7   0.8   0.9   1   1.1   1.2   1.3   1.4

Rotor Inflow Ratio

P_1375C1.xls
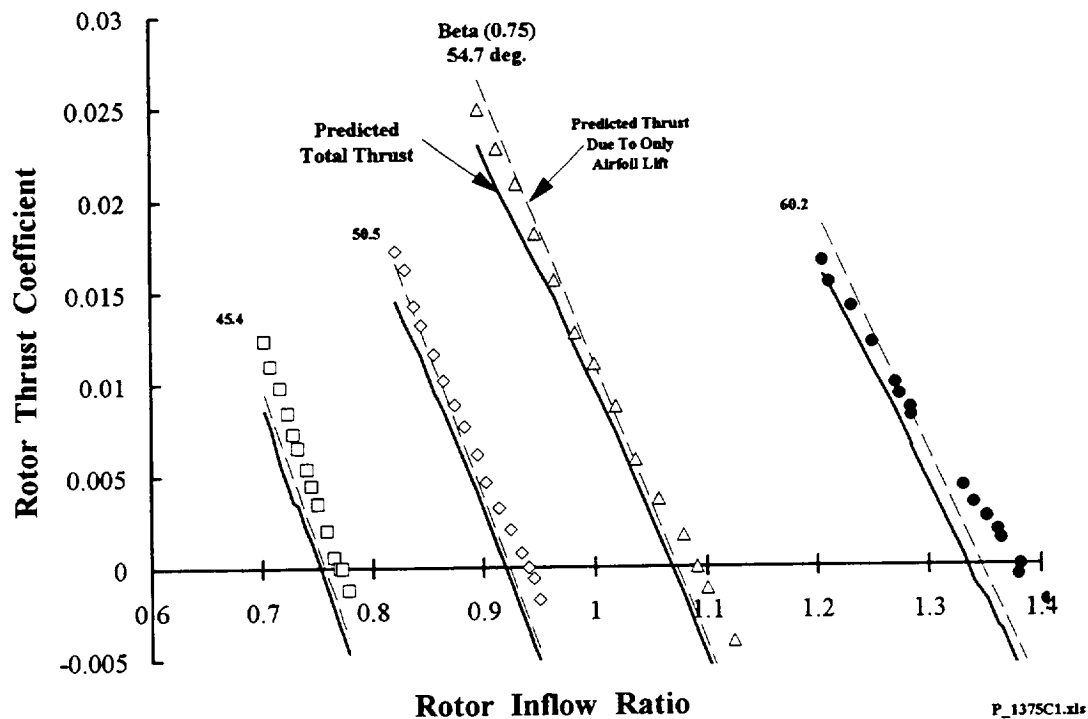
Figure O. Predicted Total Thrust With $a_{ave.} = 5.73$ /rad. Misses Inflow Where Thrust Is Zero. Theory Slope Is Also Wrong. (PROP 2 At M = 0.70)

Reconciling Theory versus Test Differences

Including the negative thrust due to airfoil drag does not significantly improve prediction of PROP 2's (or PROP 1's) total thrust experimental results as Figure O suggests. Differences between theory and test as illustrated, for example, by Figure O have been with both rotorcraft and fixed wing industries since their birth. In the case of helicopter rotors and airplane propellers, predicting C_T variations with λ_o and $\beta_{.75}$ more accurately than what Figure O shows has rarely been achieved. Figure 6 on page 25 in the primary section of this report shows that current computational fluid dynamic methods should not be expected to fair any better in this regard.

The larger discrepancies between prop-rotor aerodynamic theory and test arise because of three reasons--at least. First, experience has shown that experimental blade angle is rarely accurate to better than ±1/4 degree. Second, aerodynamic theories emphasize performance and most often do not include blade elastic deflection, particularly in torsion. Third, airfoil lift versus angle of attack is very non-linear in the transonic to supersonic Mach number region. Not accounting for these three details results in theory versus test agreement on the order of Figure O or Figure 6.

A-43

In both Figure O and Figure 6, the theoretical prop-rotor thrust (using the experimental $\beta_{.75}$) is not zero at the experimental rotor inflow ratio for zero measured thrust. This initial theory versus test difference is then compounded because the slope of C_T with rotor inflow ratio, λ_o, (at supposedly fixed $\beta_{.75}$) is also not in agreement. The difference between test and theory at or near zero thrust is most frequently reconciled by adjusting the $\beta_{.75}$ used in the theory by a small amount and restarting the computation. In the CFD comparison of Figure 6, assuming a $\Delta \beta_{.75}$ of -3/4 degree would be representative of what is required to "make the answer come out right." Of course, had torsional deflection been accounted for, this $\Delta \beta_{.75}$ might easily be unnecessary—or a +3/4 might be required! The unattractive comparison between theory and test shown with Figure O can be somewhat "repaired" using a $\Delta \beta_{.75}$ of about +0.5 to +0.7 as Figure P below illustrates.

The difference in C_T slope with λ_o is brought to the foreground in Figure P. The theoretical slope, however, has been computed using an average airfoil lift curve slope, $a_{ave.}$, of 5.73 per radian for each test point. In view of the helical tip Mach number range noted on Figure P, assuming that $a_{ave.}$ is constant is hardly correct. A commonly used adjustment to airfoil lift curve slope to account for compressibility was offered by Prandlt as

$$\frac{dC_l}{d\alpha} \equiv a = \frac{a_{2-d}}{\sqrt{1-M^2}} \approx \frac{5.73}{\sqrt{1-M^2}}$$
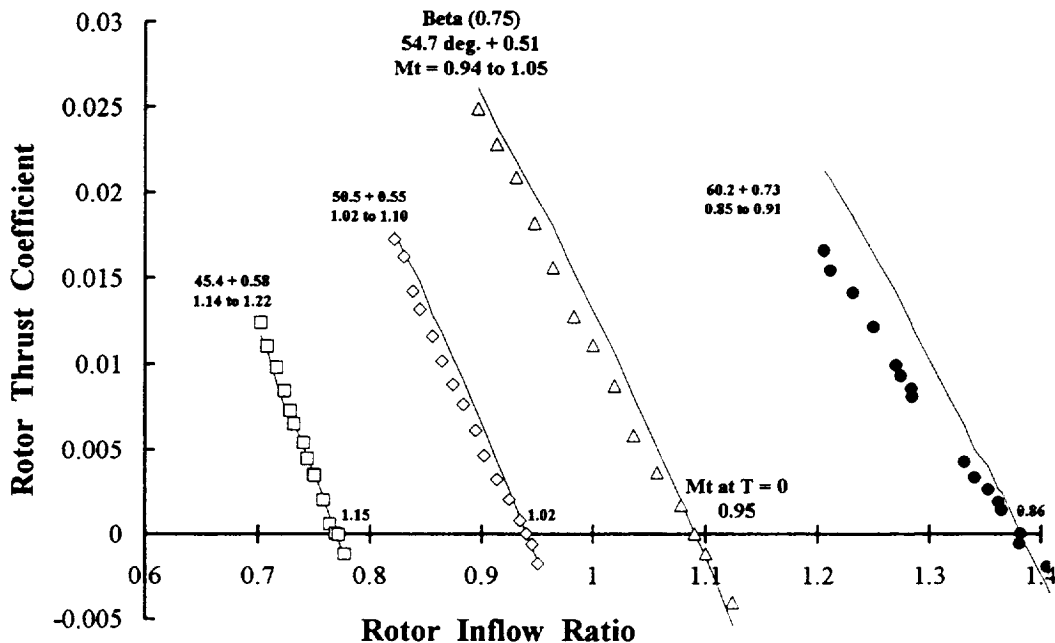
Figure P. Predicted Crossing Inflow Ratio Where Total Thrust Is Zero Can Be Empirical Fixed By Adding A $\Delta \beta_{.75}$ of +0.5. (PROP 2, M = 0.7)

This subsonic adjustment to airfoil lift curve slope is not, however, suitable to the transonic or supersonic helical tip Mach number ranges that prop-rotors encounter. In the supersonic region, Hoerner (Reference 16, page 17-17) notes that a flat plate airfoil theoretically behaves in accordance with

$$\frac{dC_l}{d\alpha} \equiv a = \frac{4}{\sqrt{M^2 - 1}}$$

Both PROP 1 and 2 testing was conducted in the helical Mach number region (see Figures A-9 and A-10) where airfoil lift curve slope is the most ill defined as Figure Q suggests.
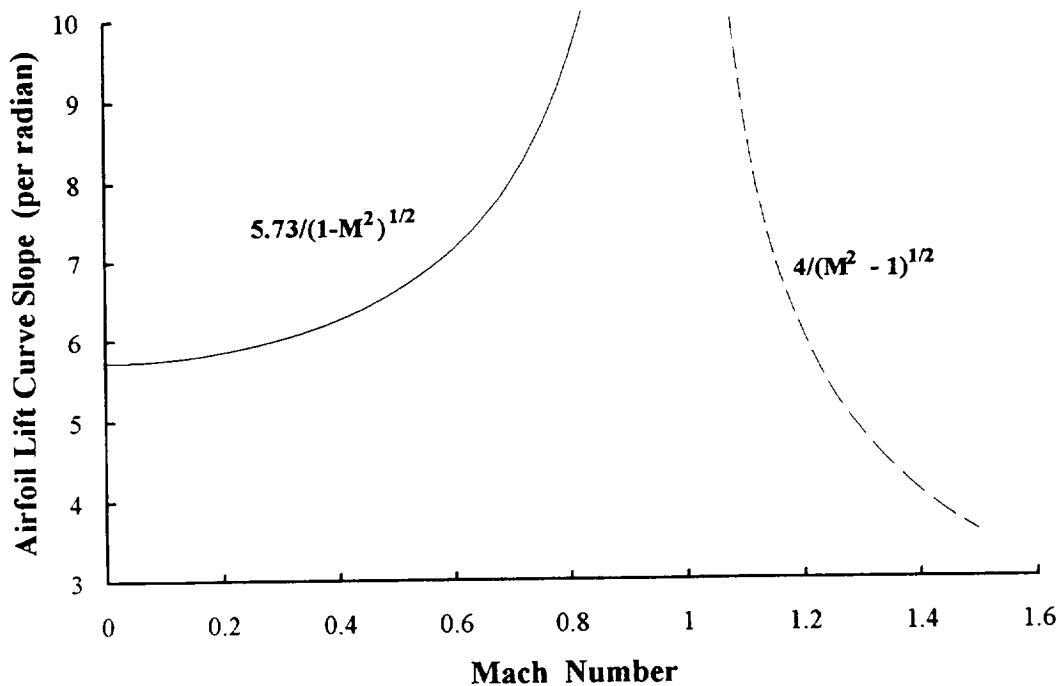
Figure Q. Prop-rotor Airfoils Operate Where Airfoil Lift Curve Slope Is Most Poorly Defined.

Some indication of how the average airfoil lift curve slope, $a_{ave.}$, varies with helical Mach number can be obtained from PROP 1 and 2 test data. By adjusting $\Delta \beta_{.75}$ and $a_{ave.}$, the total predicted rotor thrust (i.e., the sum of Equations A-77 and A-83) can be "curve fit" to each test sweep of data. The very informative results of this effort are shown on Figures A-29 and A-30. The different behavior between PROP 1 and PROP 2 is clearly evident and both data sets may well contain considerable elastic deformation as well as aerodynamic non-linearity. Very thorough computational fluid dynamic (including aeroelasticity) calculations should be able to predict both PROP's 1 and 2 thrust. This would be a prerequisite to prediction of prop-rotor performance.

Performance Fundamentals Summary

The preceding prop-rotor performance fundamentals can be summarized in a few pages accompanied by several key equations. The basis of understanding prop-rotor performance is the energy form of the power required to produce usable thrust. The conversion from calculating power as torque times shaft rotational speed to force times velocity yields

$$P = TV + Tv_i + P_o \tag{A-1}$$

or, in rotor coefficient form obtained by dividing through by $\rho A V_t^3$ and defining rotor inflow due to forward speed as $\lambda_o = V/V_t$

$$C_P = C_T \lambda_o + C_T \lambda_i + C_{P_o} \tag{A-10}$$

The minimum or ideal power required is simply equal to usable thrust times forward velocity or $T\,V$ or $C_T\,\lambda_o$. The minimum or ideal induced power required to add momentum to the air flowing through a prop-rotor producing usable thrust is $T\,v_i$ or $C_T\,\lambda_i$. The ideal induced velocity, given without derivation, is

$$v_i = \sqrt{\left(\frac{V}{2}\right)^2 + \frac{T}{2\rho A}} - \frac{V}{2} \quad \text{where } v_i \approx \frac{T}{2\rho A V} \text{ for high speed} \tag{A-2}$$

or, in rotor coefficient form obtained by dividing through by V_t

$$\lambda_i = \frac{v_i}{V_t} = \frac{1}{2}\sqrt{\lambda_o^2 + 2\,C_T} - \frac{1}{2}\lambda_o \quad \text{where } \lambda_i \approx \frac{C_T}{2\lambda_o} \text{ for high speed} \tag{A-11}$$

The profile power required, P_o, accounts for the product of airfoil drag and local resultant velocity of each airfoil element along the blade. The sum along the blade (or integral from the blade root to tip) of each blade element's drag times local resultant velocity leads to the profile power of one blade. The sum of each blade's profile power gives the prop-rotor's total profile power. Stated as an equation, profile power in its general form is

$$P_o = b \int_{root}^{tip} V_{resultant} \; dD \tag{A-6}$$

This most significant power loss is evaluated assuming

$$dD = \left(\tfrac{1}{2}\rho V_r^2\right)(c\,dr)C_d \tag{A-21}$$

and using the non-dimensional parameters

$$x = \frac{r}{R}, \quad dr = R\,dx, \quad root = x_c, \quad tip = 1.0 \quad \text{and} \quad V_r = \sqrt{(\Omega r)^2 + (V + v_i)^2} = V_t \sqrt{x^2 + \lambda^2}$$

A-46

The profile power in general rotor coefficient form is

$$C_{Po} = \frac{b}{2\pi}\left[\int_{x_c}^{1}(c_x/R)(x^2+\lambda^2)^{3/2}C_d dx\right] \qquad (A-24)$$

Three elements of profile power, defined by Figure A on page A-1, are:

1. airfoil minimum incompressible drag arising primarily from skin friction,

2. minimum compressible drag due to pressure or wave drag, and

3. incremental airfoil drag due to lift.

The first element studied was minimum incompressible profile power. This power lose arises primarily from airfoil skin friction drag. A contrast between laminar and turbulent boundary layer assumptions was developed. Profile power was calculated with both boundary layer assumptions and a comparison to both PROP 1 and 2 test data was made. The conclusion was drawn that advanced prop-rotors would more likely have a turbulent boundary layer. In that event, practical engineering recommends that the minimum airfoil drag coefficient be given as

$$C_{d\,min.} \approx 1.25 \times \frac{0.148}{(Vc/v)^{1/5}} = \frac{0.185}{(Vc/v)^{1/5}} \quad \text{for full scale prop-rotors} \qquad (A-38)$$

With this level of minimum incompressible airfoil drag, the corresponding minimum profile power is calculated for the variable chord configuration as

$$C_{Po\,min.} = 1.25 \times \frac{0.074\,b}{\pi(V_t R/v)^{1/5}}\left[\int_{x_c}^{1}(c_x/R)^{4/5}(x^2+\lambda^2)^{13/10}dx\right] \qquad (A-49)$$

Note that in this non-dimensional form provided by Equation A-49, the Reynolds number is now based on prop-rotor radius. This basis for Reynolds number is somewhat unusual. However, it is meaningful because the chord distribution is scaled by radius and the integral is performed on a planform configuration. The factor of 1.25 is semi-empirical based on study of and correlation (see Figure A-13b) with PROP 2. A more conservative, 1.50 factor would not be unreasonable.

If the full scale prop-rotor has a constant chord, the integral required by Equation A-49 can be evaluated in closed form. The minimum incompressible profile power coefficient reverts to Reynolds number based on chord and becomes

$$C_{Po\,min.} = 1.25 \times 0.074 \frac{(bc/\pi R)}{(V_t c/v)^{1/5}}\left[\frac{5}{18}T(\lambda, x_c)\right] \qquad (A-34c)$$

where the integral, defined as $T(\lambda, x_c)$, is closely approximated by

A-47

$$T(\lambda, x_c) = \left[(1+\lambda^2)^{13/10} - x_c(x_c^2 + \lambda^2)^{13/10}\right] + \frac{9}{5}\lambda^2\left[(1+\lambda^2)^{3/10} - x_c(x_c^2 + \lambda^2)^{3/10}\right]$$

$$+ \frac{18}{25}\lambda^4\left\{\ln\left[\frac{1+(1+\lambda^2)^{3/10}}{x_c + (x_c^2 + \lambda^2)^{3/10}}\right]\right\} \quad \text{for } \lambda \text{ less than } 1.3 \tag{A-35}$$

The second element studied was minimum compressible profile power. This power loss arises primarily from airfoil pressure drag. This pressure drag is very dependent on airfoil thickness ratio, t/c, and occurs when the local blade element resultant velocity exceeds a critical Mach number. Transonic similarity laws were used to show that, at zero airfoil lift, compressibility losses will not be incurred in practice if the thickness ratio remains below

$$\text{Max.} \ \frac{t}{c} \leq 0.192\left(\frac{1-M^2}{M^{4/3}}\right)^{3/2} \tag{A-46}$$

This result is applied to the prop-rotor by approximating the local blade element Mach number as

$$M_x \approx \frac{\sqrt{V^2 + (xV_t)^2}}{a_s} = \frac{V}{a_s}\sqrt{1 + (x/\lambda_o)^2} = M\sqrt{1 + (x/\lambda_o)^2} \tag{A-47}$$

If a prop-rotor blade is swept in portions of its radius, this local Mach number will be reduced by the cosine of the local sweep angle.

When this conservative thickness ratio criteria is not met, the minimum compressible profile power is found most directly by numerical integration following a few simple steps. These steps are:

A. Define the chord and thickness ratio distributions along the blade

B. Calculate the local blade element Mach number

C. Obtain the transonic similarity Mach number parameter, $\tilde{M}$, at each radius station from

$$\tilde{M} = \frac{M^2 - 1}{M^{4/3}(t/c)^{2/3}(\gamma + 1)^{2/3}} \tag{A-43}$$

D. If $\tilde{M}$ is more negative than -1.6736, the airfoil drag due to compressibility is zero. If $\tilde{M}$ is more positive than -1.6736, calculate the transonic similarity drag coefficient, $\tilde{C}_d$, as

$$\tilde{C}_d = 1.774\left(\tilde{M} + 1.6736\right)^{5/2} \tag{A-44}$$

A-48

E. When $\tilde{C}_d$ gets to 4.62, stop and hold $\tilde{C}_d$ constant at 4.62 until the supersonic $\tilde{C}_d$ equation of $\tilde{C}_d = 4.762/\sqrt{\tilde{M}}$ is encountered. Then follow the supersonic $\tilde{C}_d$ equation.

F. Given $\tilde{C}_d$ at each radius station, calculate the conventionally defined airfoil drag coefficient from

$$\Delta C_{d\ comp.} = \frac{(t/c)^{5/3}}{M^{2/3}(\gamma+1)^{1/3}} \tilde{C}_d \tag{A-43}$$

G. The minimum profile power due to compressibility is then found by

$$\Delta C_{Po\ comp.} = \frac{b}{2\pi}\left[\int_{x_c}^{1}(c_x/R)(x^2+\lambda^2)^{3/2}\Delta C_{d\ comp.}\,dx\right] \tag{A-24}$$

The preceding relatively rudimentary way to estimate minimum profile power due to compressibility was completed for both PROP's 1 and 2. The results, conveyed by Figures A-31 and A-32, indicate that this simple method is optimistic by about 25 to 50 percent. Therefore, a more conservative approach would be to increase the transonic similarity drag coefficient of Equation A-44 to

$$\tilde{C}_d = 1.3\left\{1.774(\tilde{M}+1.6736)^{5/2}\right\} \tag{A-59}$$

and then follow steps A through G.

The third element studied was profile power due to prop-rotor thrust. This element was found to depend not only on thrust but also total power and rotor inflow ratio. Furthermore, this element is clearly shown to depend on the increase in airfoil drag with airfoil lift coefficient. The approximation was made that

$$C_{d\ lift} \approx \frac{d\,C_d}{d\,C_l^2}\left(C_l^2\right) \tag{A-59}$$

Using an average airfoil and power weighted solidity as representative of the complete blade, the profile power due to thrust was reduced to

$$\Delta C_{Po\ thrust} \approx \left(\frac{d\,C_d}{d\,C_l^2}\right)_{ave.} f(\sigma,\lambda,C_T,C_P) \tag{A-65a}$$

where

$$f(\sigma,\lambda,C_T,C_P) = \frac{8}{\sigma}\left(\frac{Q_2^2}{F\,T_1^2}\right)\left[C_T^2 + 2(T_2/Q_2)\,C_T C_P + (T_2/Q_2)^2 C_P^2\right] \tag{A-65b}$$

A-49

The constants, T_1, T_2, Q_1, Q_2 and F depend on total rotor inflow. For a constant chord blade these constants are

$$T_1 = \frac{1}{3}\left[(1+\lambda^2)^{3/2} - (x_c^2 + \lambda^2)^{3/2}\right]$$

$$T_2 = \frac{\lambda}{2}\left[(1+\lambda^2)^{1/2} - x_c(x_c^2 + \lambda^2)^{1/2} + \lambda^2 \ln\left(\frac{1+(1+\lambda^2)^{1/2}}{x_c + (x_c^2 + \lambda^2)^{1/2}}\right)\right]$$

$$Q_1 = \lambda T_1 \tag{A-57}$$

$$Q_2 = \frac{1}{4}\left\{\left[(1+\lambda^2)^{3/2} - x_c(x_c^2 + \lambda^2)^{3/2}\right] - \lambda T_2\right\}$$

$$F = 4(Q_2 + \lambda T_2)$$

Considerable difference was found between PROP 1 and PROP 2 in the behavior of the average airfoil $\left(\dfrac{d C_d}{d C_l^2}\right)_{ave.}$ This difference, summarized by Figure A-27, led to the interpretation that PROP 1's blade and airfoil geometry appears to follow the empirical drag rise trend that

$$
\begin{aligned}
&\text{if } M_{0.85} \leq 0.75 \quad \text{then} \quad dC_d/dC_l^2 = 0.04 \\
&\text{if } M_{0.85} \geq 0.75 \quad \text{then} \quad dC_d/dC_l^2 = 0.04 + 0.333(M_{0.85} - 0.75)
\end{aligned}
\tag{A-66}
$$

On the other hand, PROP 2's thin airfoil, but high solidity blade geometry appeared to have an empirical drag rise trend more on the order of

$$
\begin{aligned}
&\text{if } M_{0.85} \leq 0.80 \quad \text{then} \quad dC_d/dC_l^2 = 0.159 \quad \text{or} \quad 1/2\pi \\
&\text{if } M_{0.85} \geq 0.80 \quad \text{then} \quad dC_d/dC_l^2 = 0.159 + 0.333(M_{0.85} - 0.80)
\end{aligned}
\tag{A-67}
$$

The dependence of prop-rotor thrust on 3/4 radius blade angle, $\beta_{.75}$, and inflow ratio and an average airfoil lift curve slope, $a_{ave.}$, followed the discussion of power required to produce usable thrust. The blade angle distribution, when referenced to the 0.75 radius station takes the general form

$$\beta_{(x)} = \beta_{.75} + f_{(x)} \tag{A-75}$$

where $f_{(x)}$ is defined to be zero at the 0.75 radius station. The thrust due to airfoil lift assuming an average chord is given as

$$C_{T_{Lift}} = \frac{(bc/\pi R)a_{ave.}}{2}\left\{\sin\beta_{.75}\, K_1 + \cos\beta_{.75}\, K_2 - \lambda\cos\beta_{.75}\, K_3 + \lambda\sin\beta_{.75}\, K_4\right\} \tag{A-77}$$

where the thrust constants K_1, K_2, K_3, and K_4 had an integral form (see Equation A-76 on page A-39) but could be closely approximated knowing only a design speed and tip speed (i.e., a λ_{design} = design V/V_t) and assuming a generic, approximate twist of

$$\beta_{(x)} = \beta_{.75} + \left[\arctan\left(\frac{\lambda_{design}}{x}\right) - \arctan\left(\frac{\lambda_{design}}{0.75}\right) \right] \tag{A-78}$$

The thrust constants K_1, K_2, K_3, and K_4 with this generic blade pitch angle distribution are

$$K_1 = D\left[A + B\left(2\lambda_{des.}^2 - x_c^2 - 2x_c\lambda_{des.}\right) - 2C\lambda_{des.}^4\right]$$

$$K_2 = \frac{D\,\lambda_{des.}}{6}\left[A\left(16\lambda_{des.}^2 + 1\right) - B\left(16\lambda_{des.}^2 - 8x_c^2 + 9x_c\right) - 9C\lambda_{des.}^2\right]$$

$$K_3 = \frac{D}{2}\left[A\left(3 + 8\lambda_{des.}^2\right) - B\left(3x_c + 8\lambda_{des.}^2\right) - 3C\lambda_{des.}^2\right] \tag{A-79a}$$

$$K_4 = D\,\lambda_{des.}\left[A + B\left(2x_c - 3\right) + 2C\lambda_{des.}^2\right]$$

where

$$A = \sqrt{1 + \lambda_{des.}^2} \quad B = \sqrt{x_c^2 + \lambda_{des.}^2} \quad C = \ln\left(\frac{1+A}{x_c + B}\right) \quad D = \frac{1}{\sqrt{9 + 16\lambda_{des.}^2}} \tag{A-79b}$$

Considerable difference between PROP's 1 and 2 average airfoil lift curve slope was found. This contrast is shown in Figure A-29. Furthermore, some adjustment to the experimental $\beta_{.75}$ value was necessary as shown in Figure A-30.

A negative thrust contribution due to airfoil drag was approximated as

$$C_{T_{Drag}} = \frac{(bc/\pi R)\overline{C}_D\,T_2}{2} \tag{A-83}$$

where the average airfoil drag coefficient for a constant chord blade, $\overline{C}_D$, became

$$\overline{C}_D = \frac{T_1\left(\frac{2C_P}{\sigma}\right) - Q_1\left(\frac{2C_T}{\sigma}\right)}{Q_2 T_1 + Q_1 T_2} \tag{A-58}$$

These summary semi-empirical equations were developed from two prop-rotor experiments. It is, therefore, reasonable to expect that prediction of total power required to produce usable thrust should be in agreement with the originating experimental data–at least in the linear range. Figures A-33 and A-34

A-51

show that in these two example, theory and test correlate well enough given some insight into a few empirical factors.

This seven page summary contains enough fundamentals to conceptually examine advanced prop-rotor designs. Application of these fundamentals leads to several interesting conclusions about the possible future directions advanced civil tiltrotor aircraft might take to assure a competitive place in the commercial field of transportation.
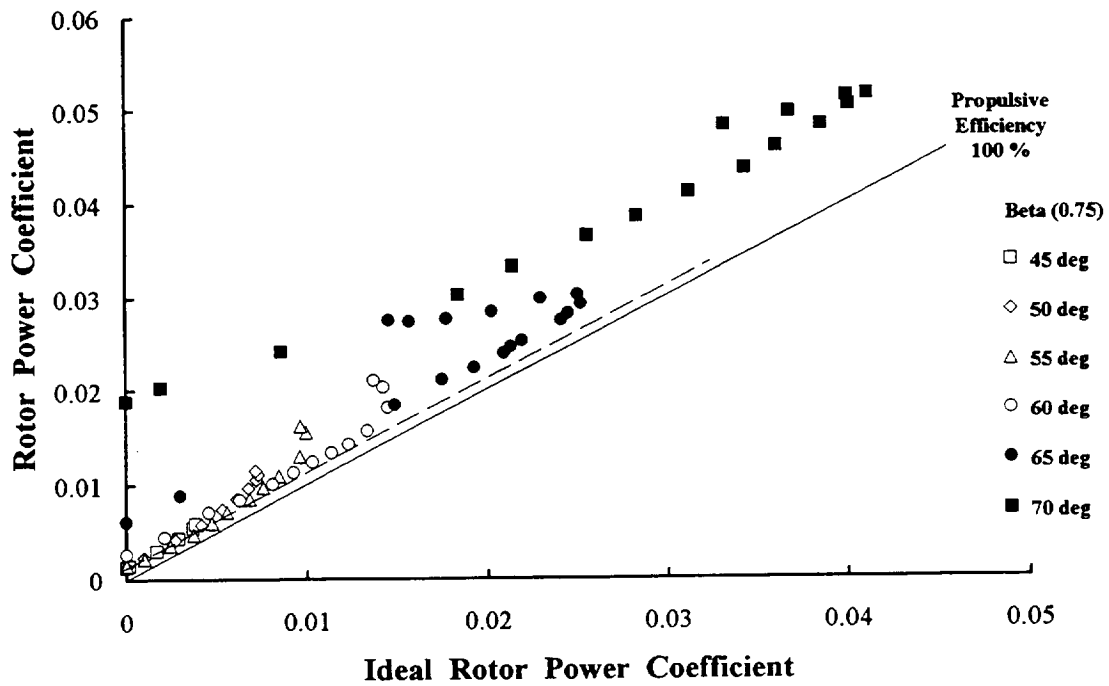
P_1949A.xls

Figure A-1. PROP 1 Data at Wind Tunnel Mach Number of 0.70.
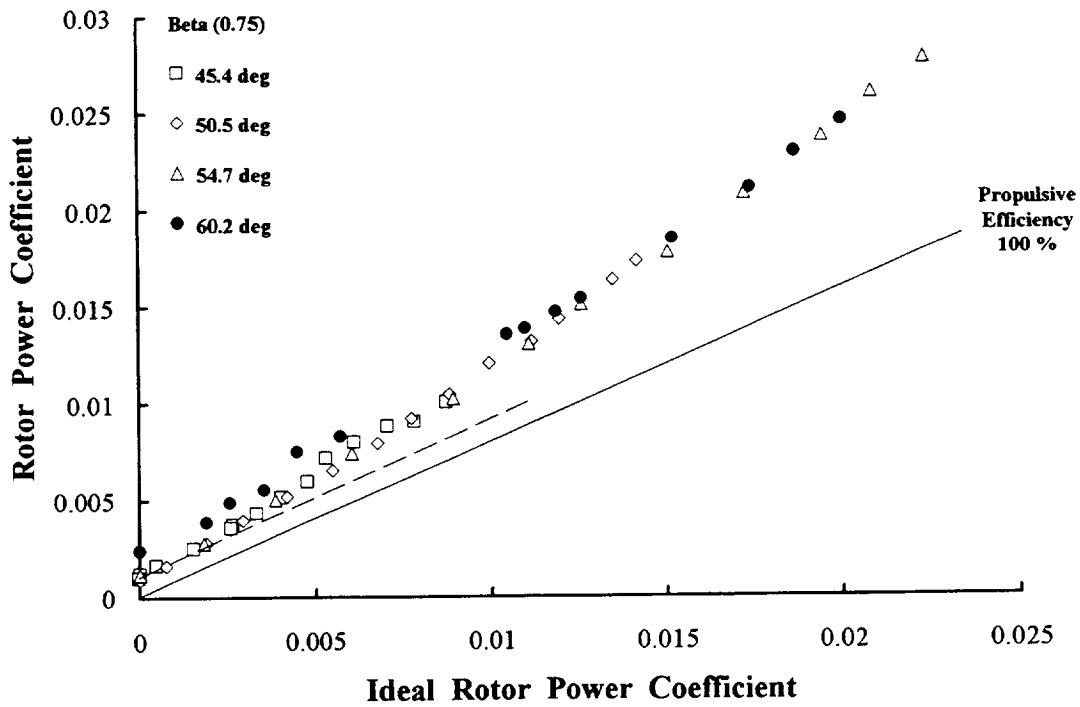
P_1375A.xls

Figure A-2. PROP 2 Data at Wind Tunnel Mach Number of 0.70.
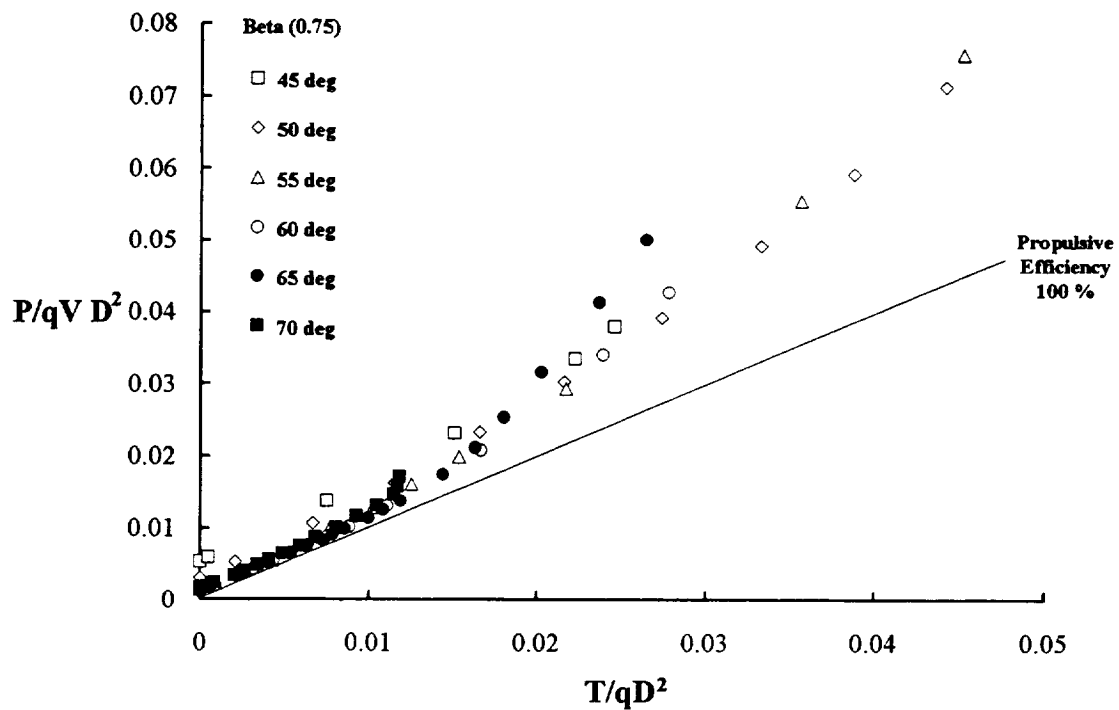
P_1949A.xls

Figure A-3. PROP 1 Data at Wind Tunnel Mach Number of 0.70.
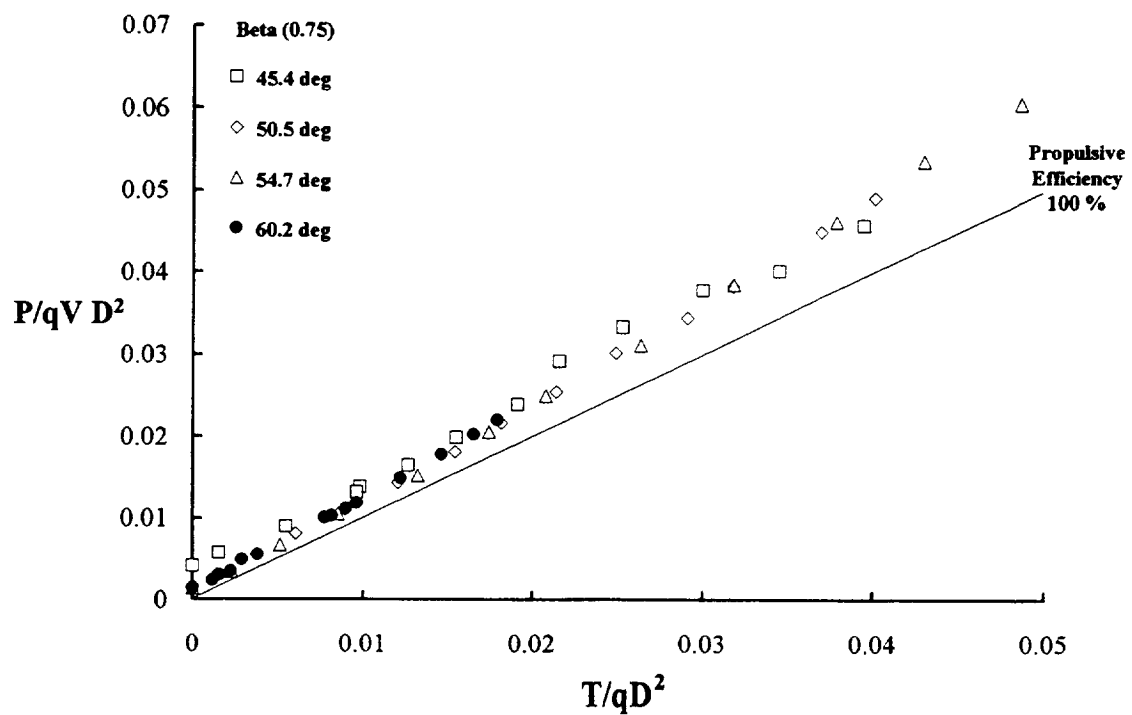
P_1375A.xls

Figure A-4. PROP 2 Data at Wind Tunnel Mach Number of 0.70.
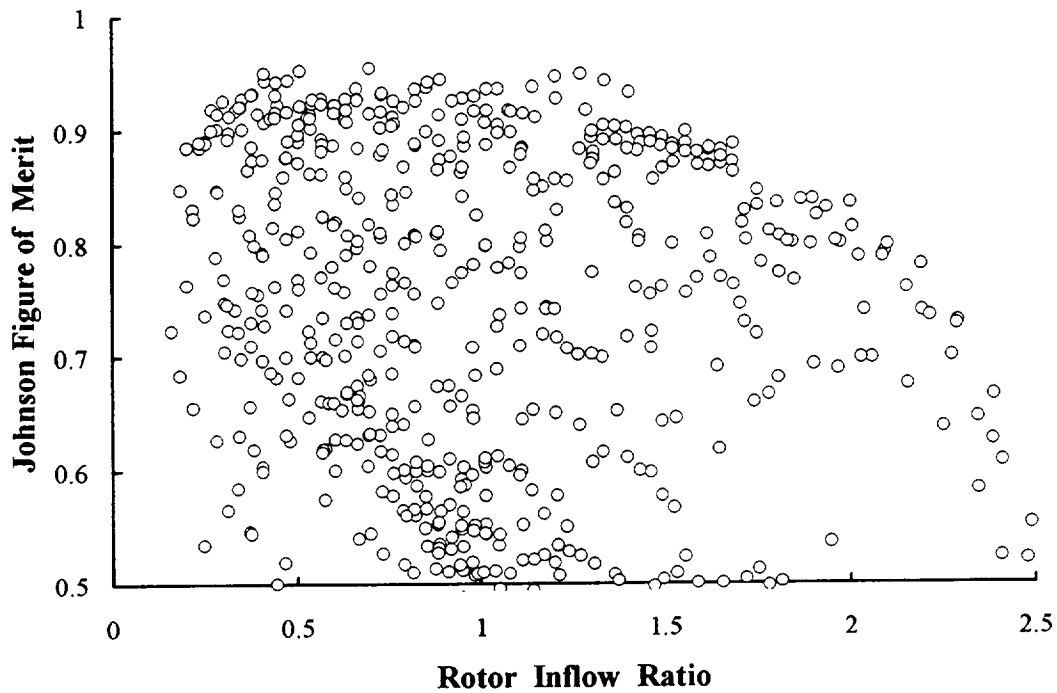
P_1949A.xls

Figure A-5. All PROP 1 Data Expressed In Johnson Figure Of Merit.
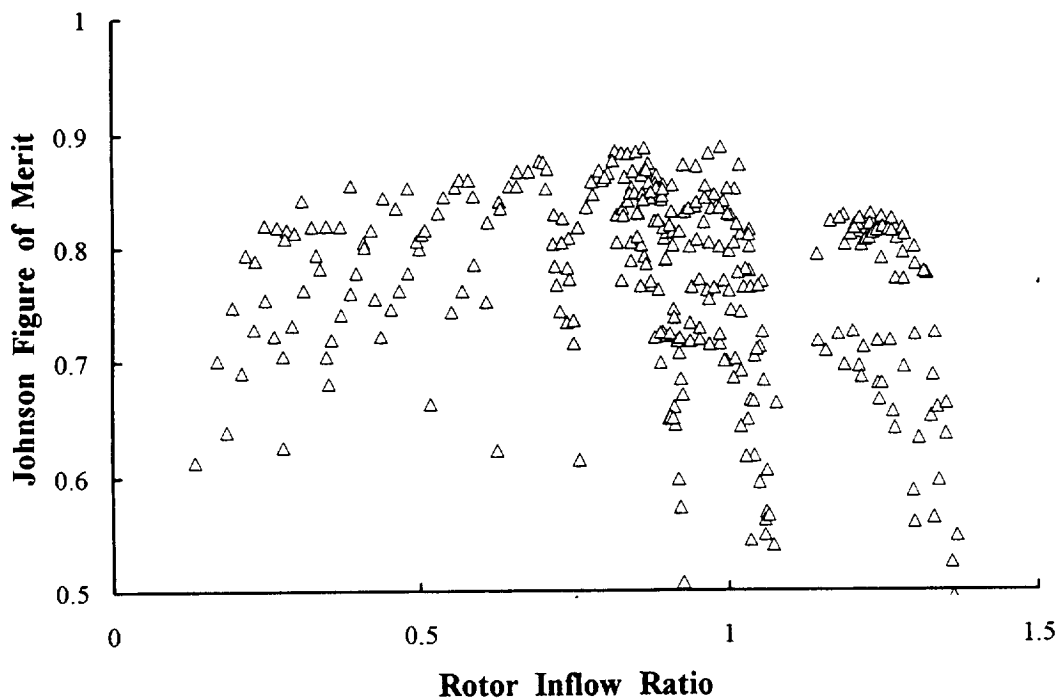
P_1375A.xls

Figure A-6. All PROP 2 Data Expressed In Johnson Figure Of Merit.

A-55
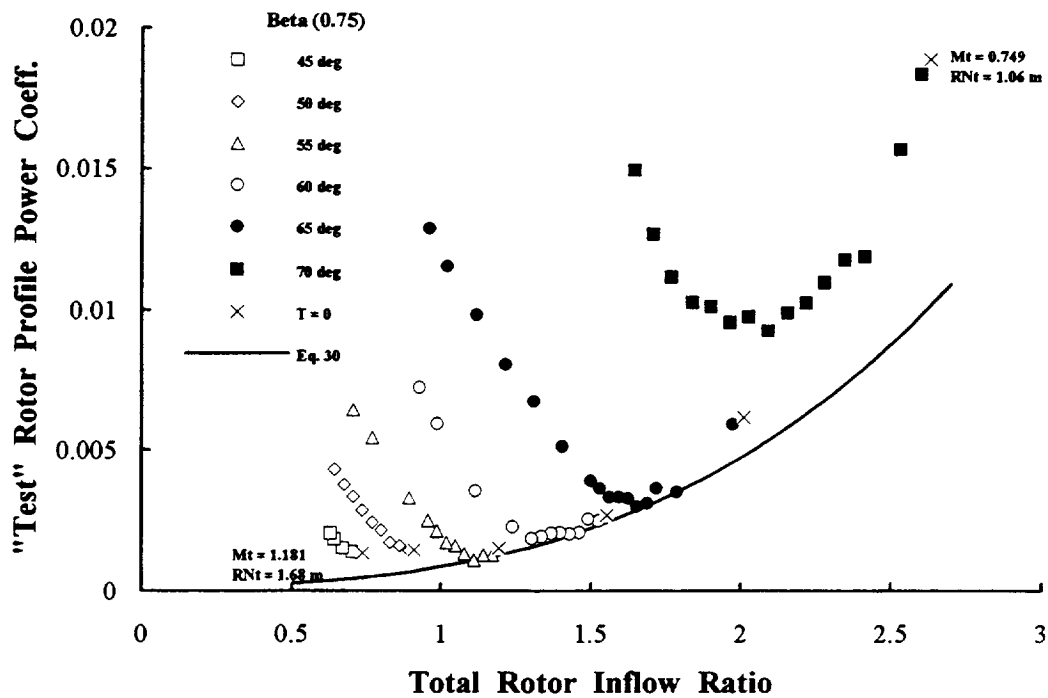
Figure A-7. PROP 1 Profile Power at Wind Tunnel Mach Number of 0.70.
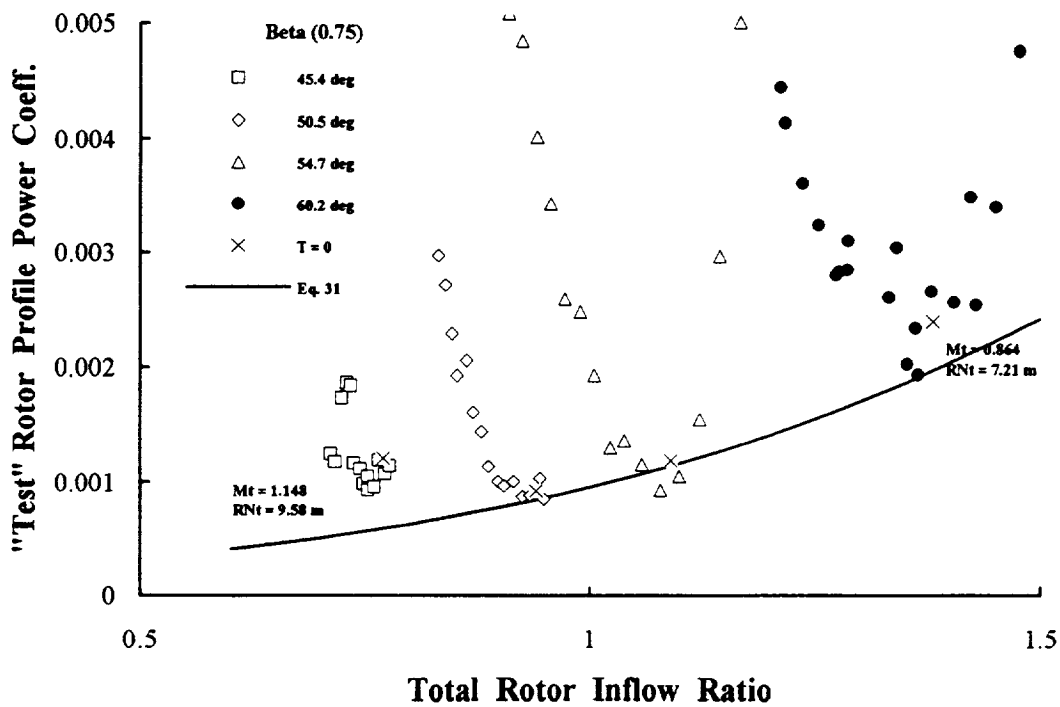
Figure A-8. PROP 2 Profile Power at Wind Tunnel Mach Number of 0.70.
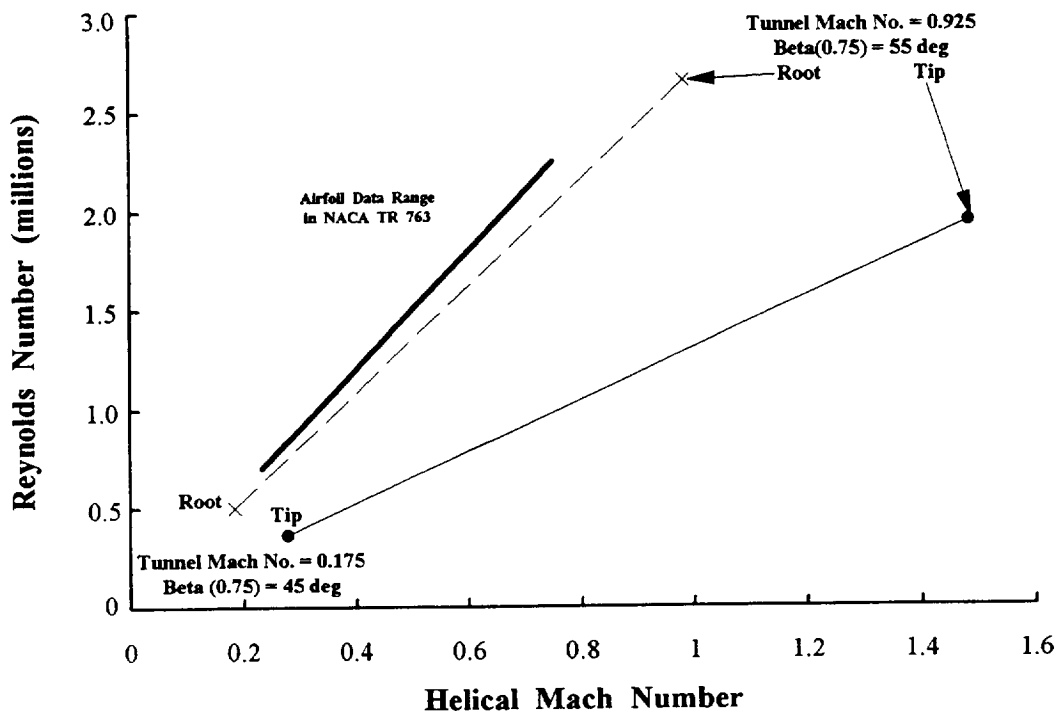
Figure A-9. PROP 1 Reynolds And Mach Number Range.
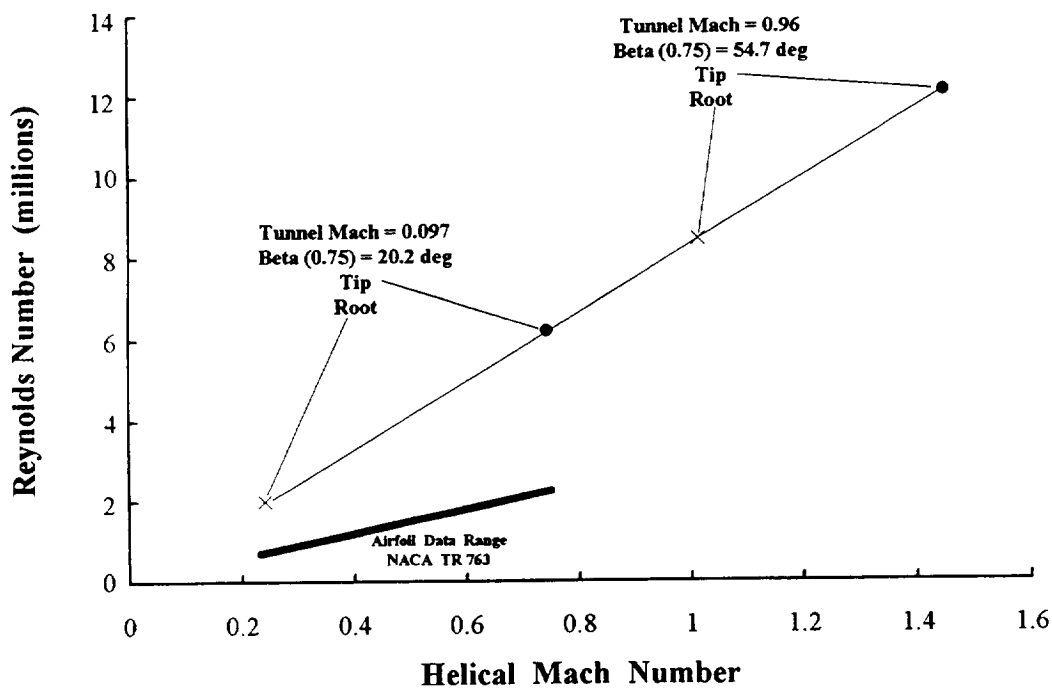
Figure A-10. PROP 2 Reynolds And Mach Number Range.
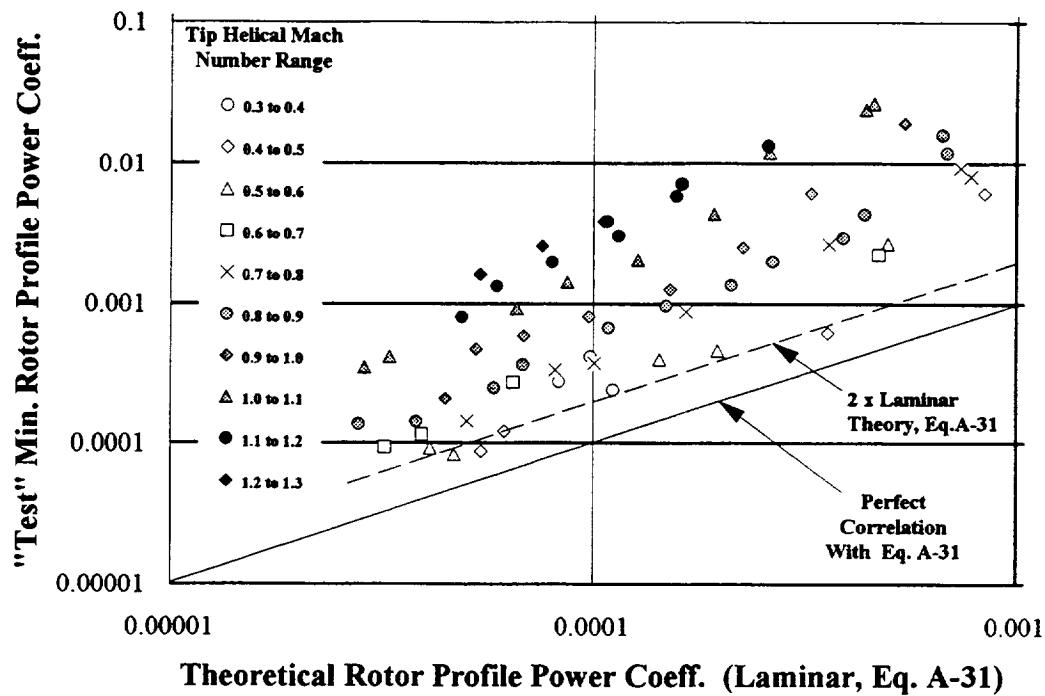
Figure A-11a. PROP 1 Compared To Laminar Theory.
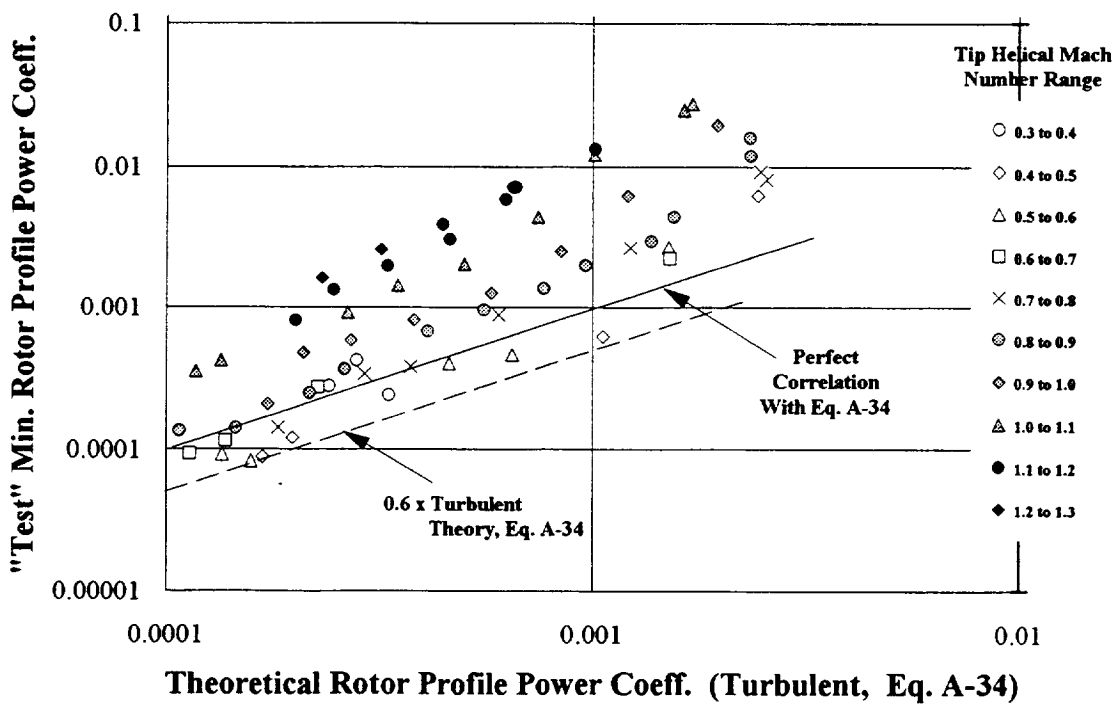
Figure A-11b. PROP 1 Compared To Turbulent Theory.

A-58
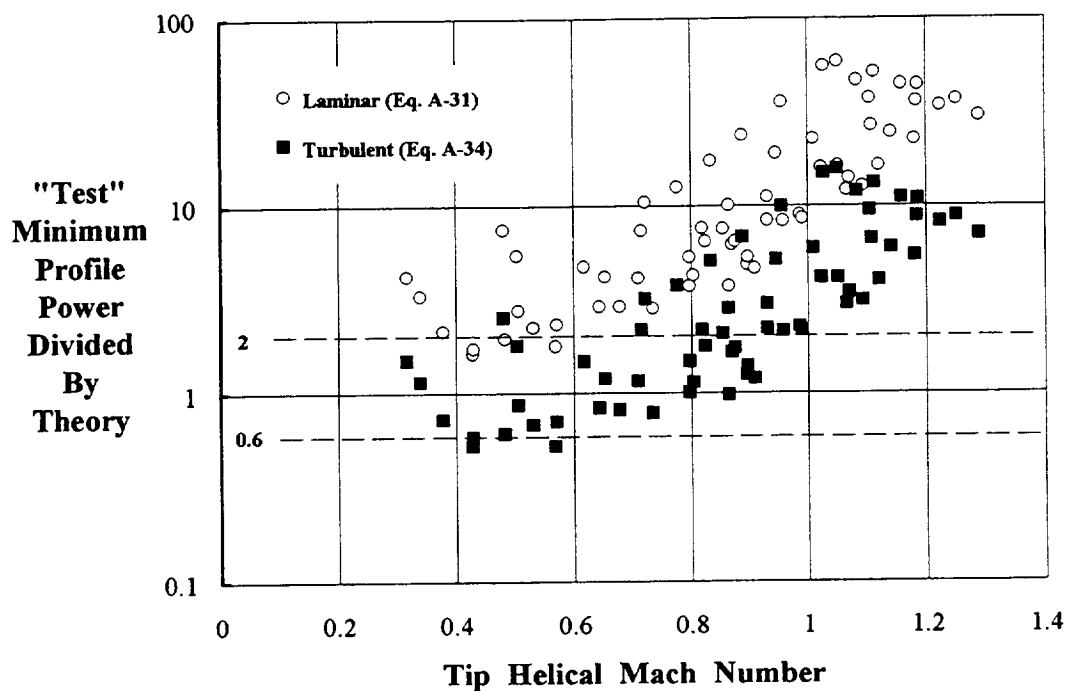
Figure A-12. PROP 1 Correlation Of Min. Profile Power.
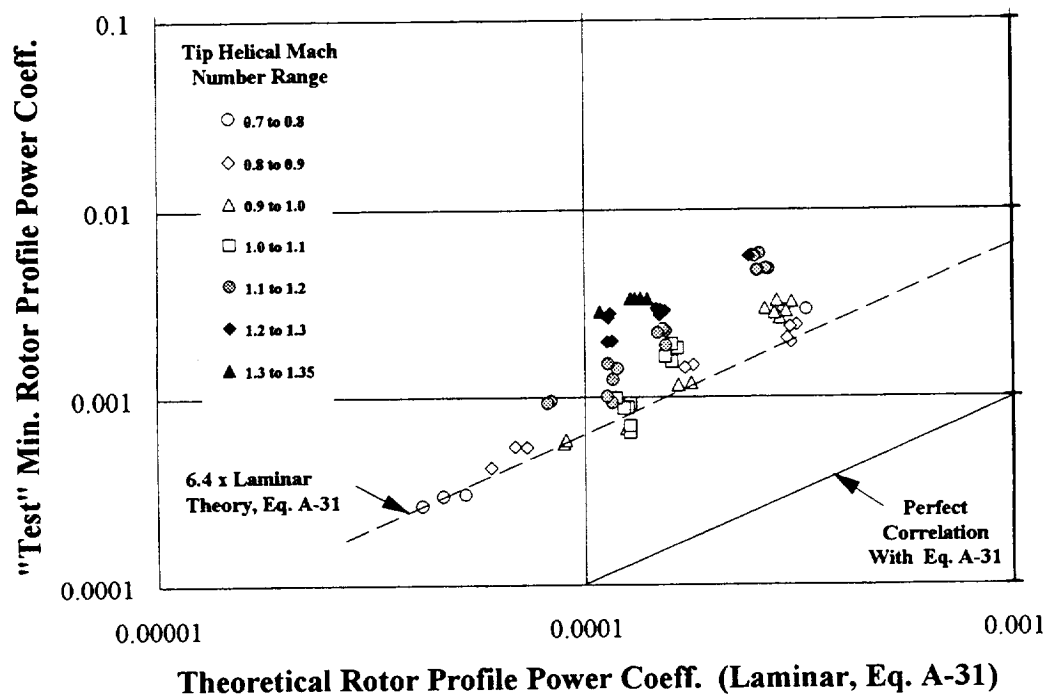
Figure A-13a. PROP 2 Compared To Laminar Theory.
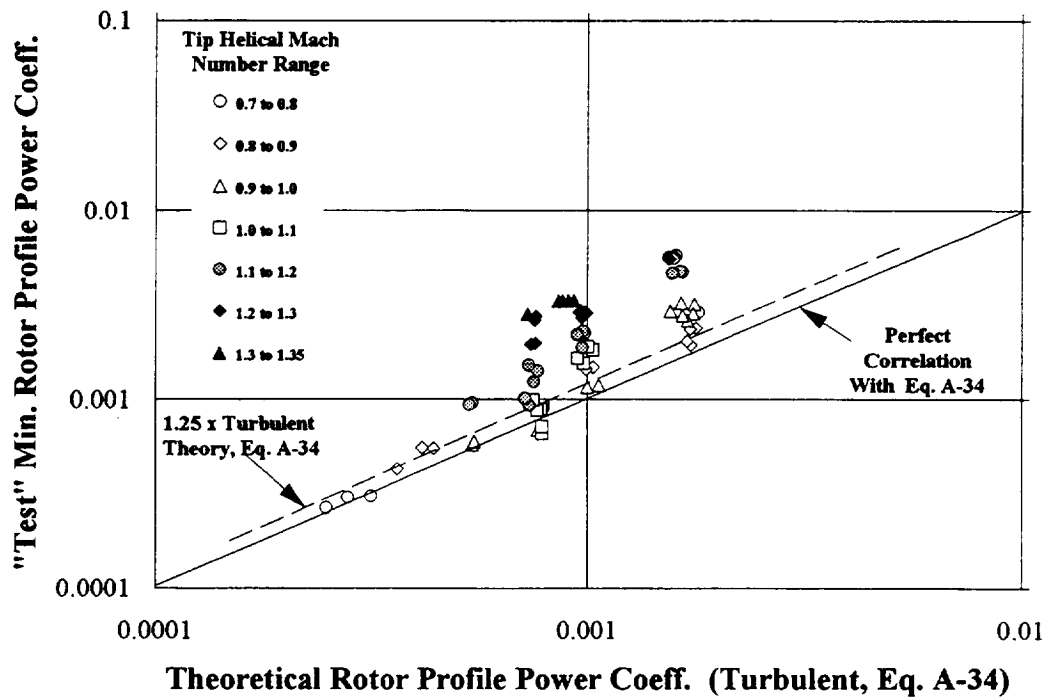
Figure A-13b. PROP 2 Compared To Turbulent Theory.
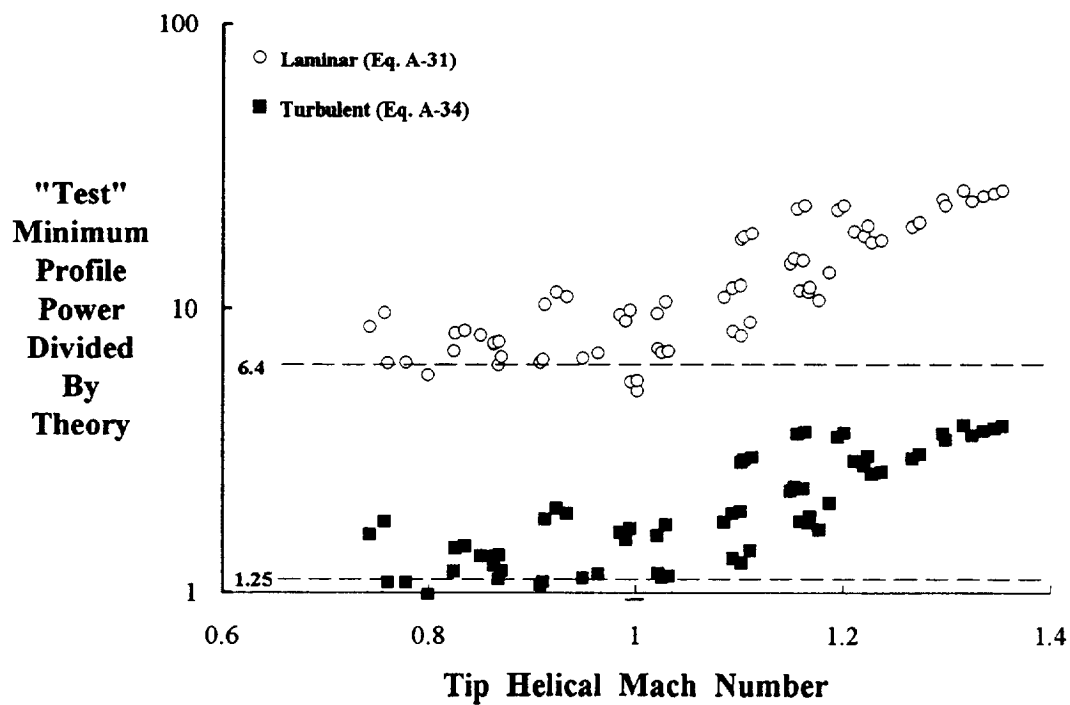
Figure A-14. PROP 2 Correlation Of Min. Profile Power.

A-60
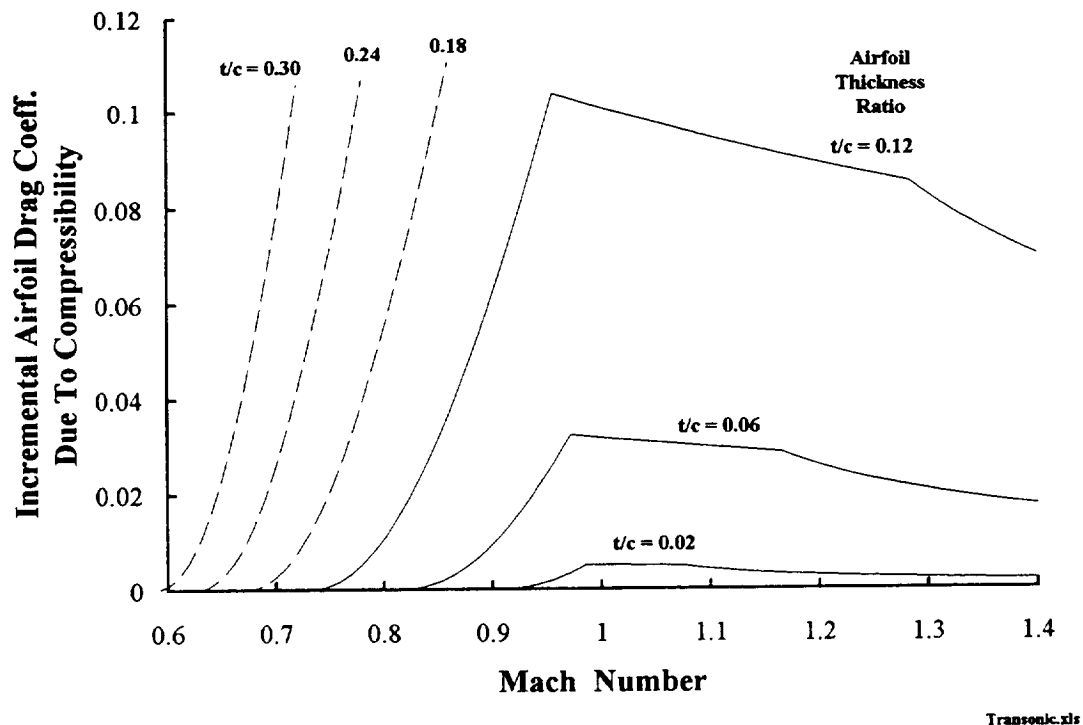
Figure A-15. Application Of Transonic Similarity Theory.
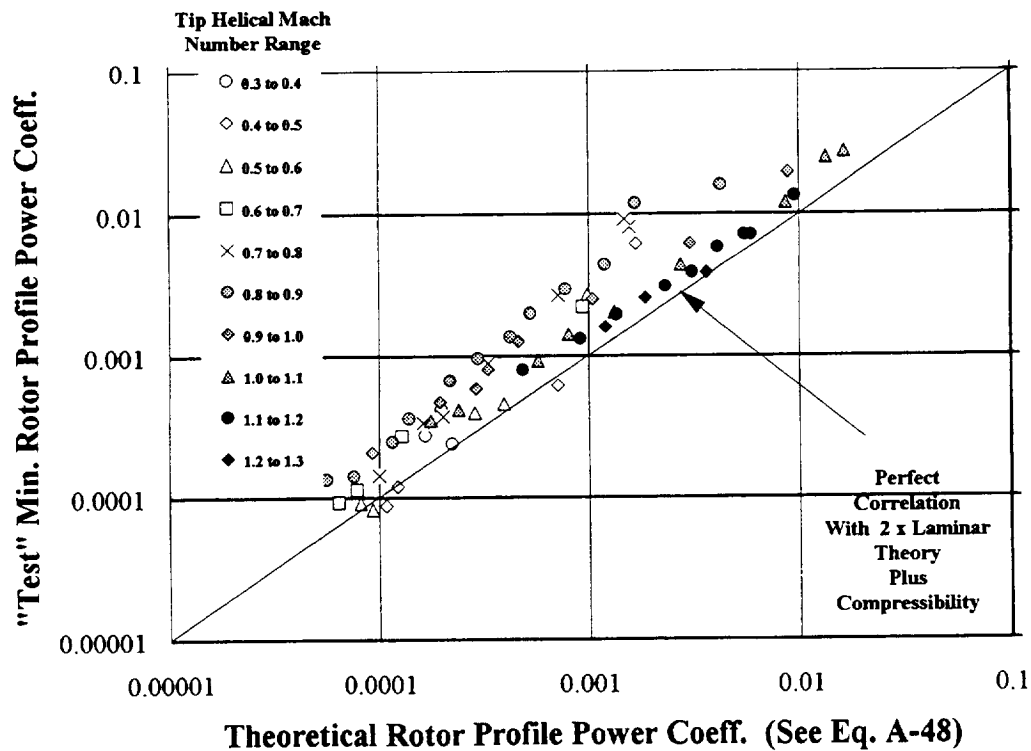
Figure A-16. PROP 1 Correlation Of Min. Profile Power.
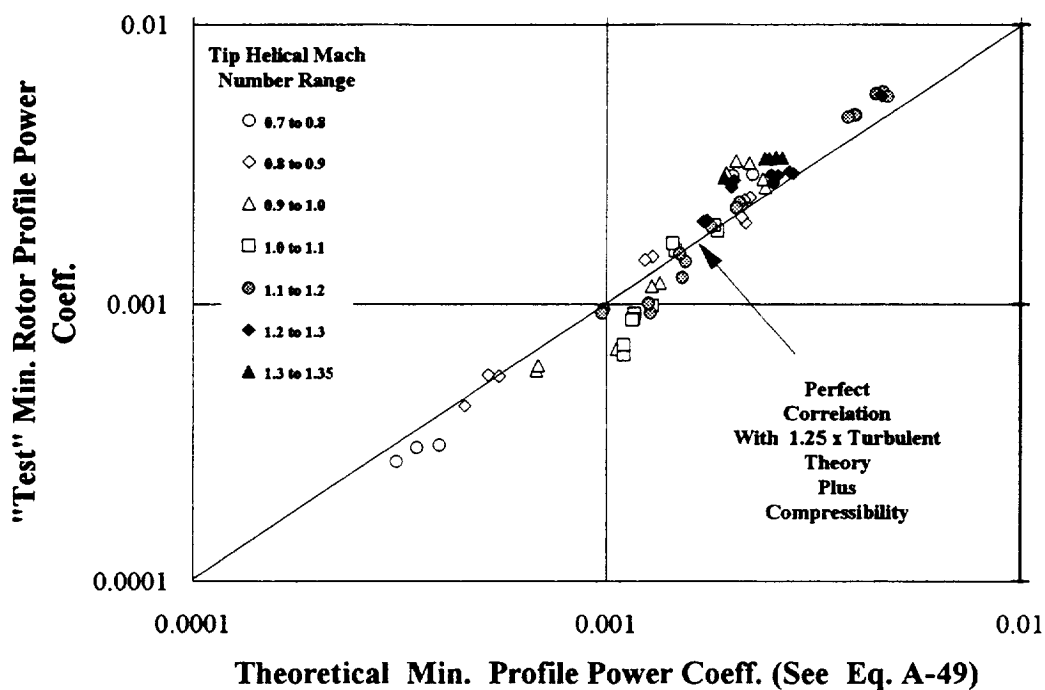
Figure A-17. PROP 2 Correlation Of Min. Profile Power.
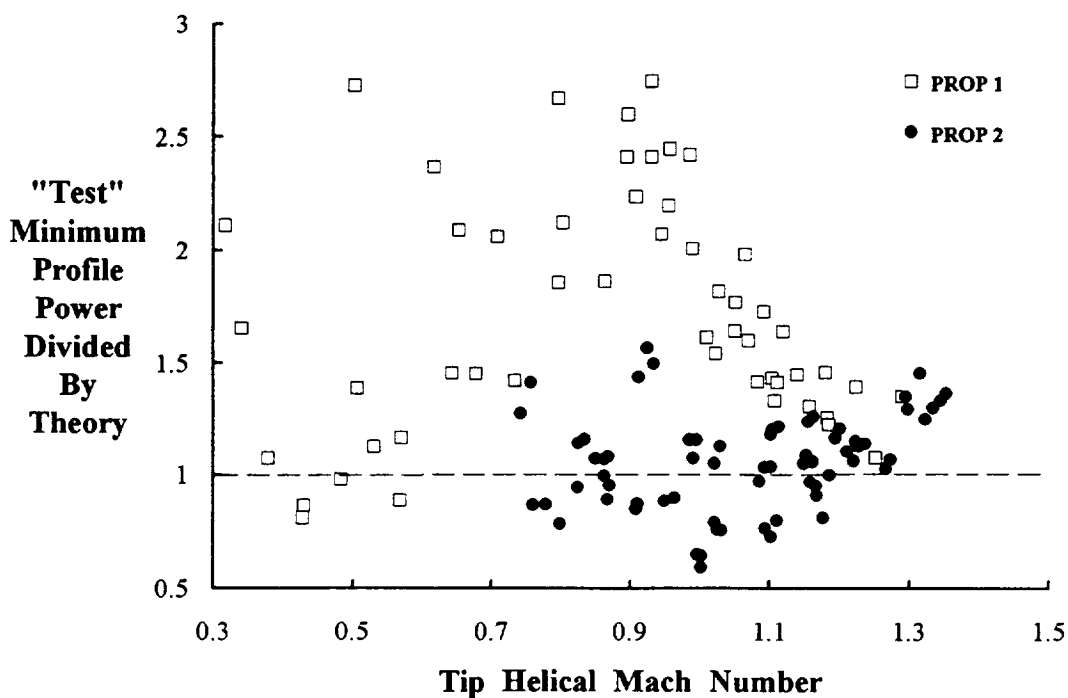
Figure A-18. PROP's 1 and 2 Correlation Of Min. Profile Power.

A-62
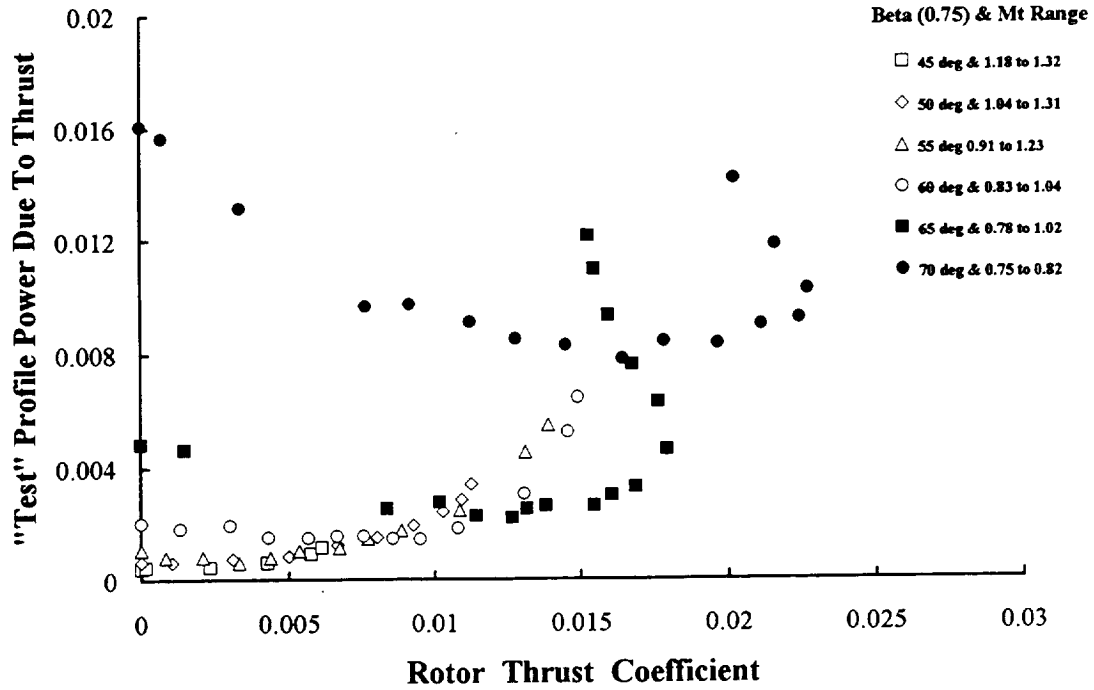
Figure A-19. PROP 1 Profile Power Increase With Thrust.
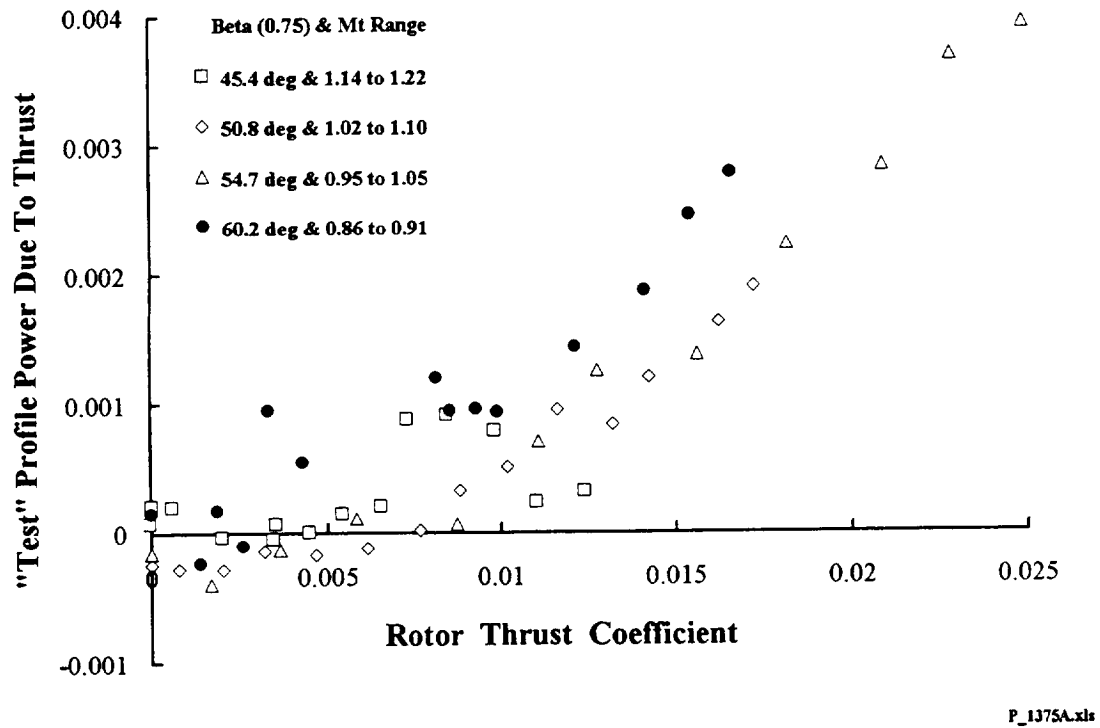
Figure A-20. PROP 2 Profile Power Increase With Thrust.

A-63
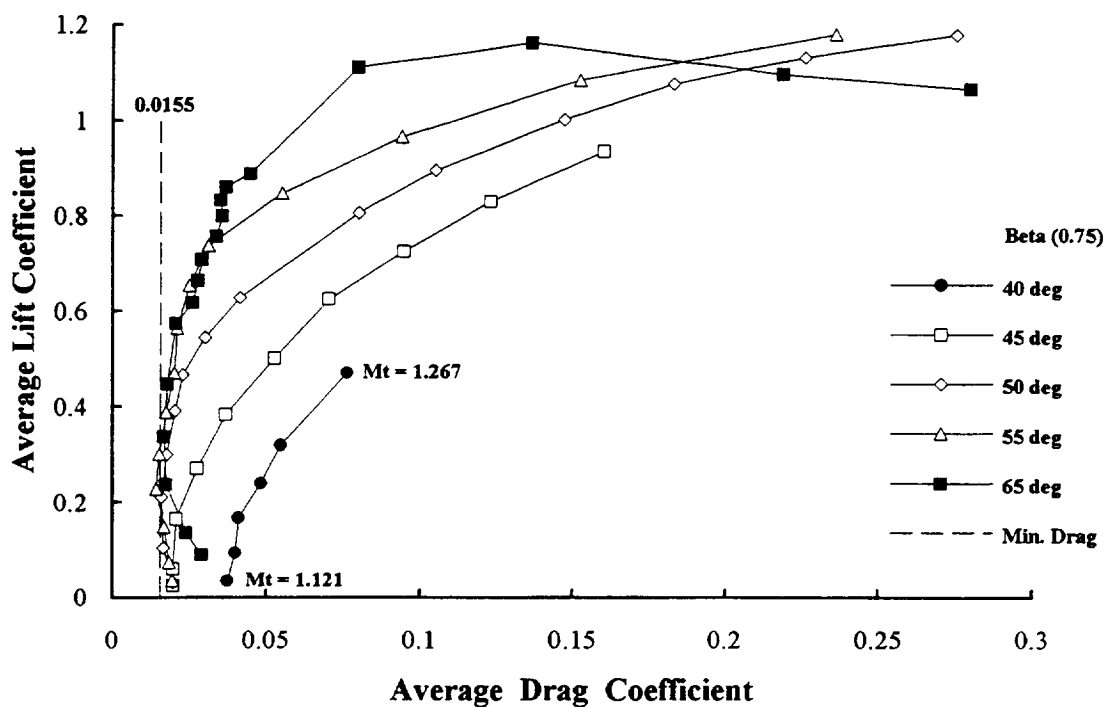
Figure A-21a. PROP 1 Average Airfoil Behavior at M=0.60
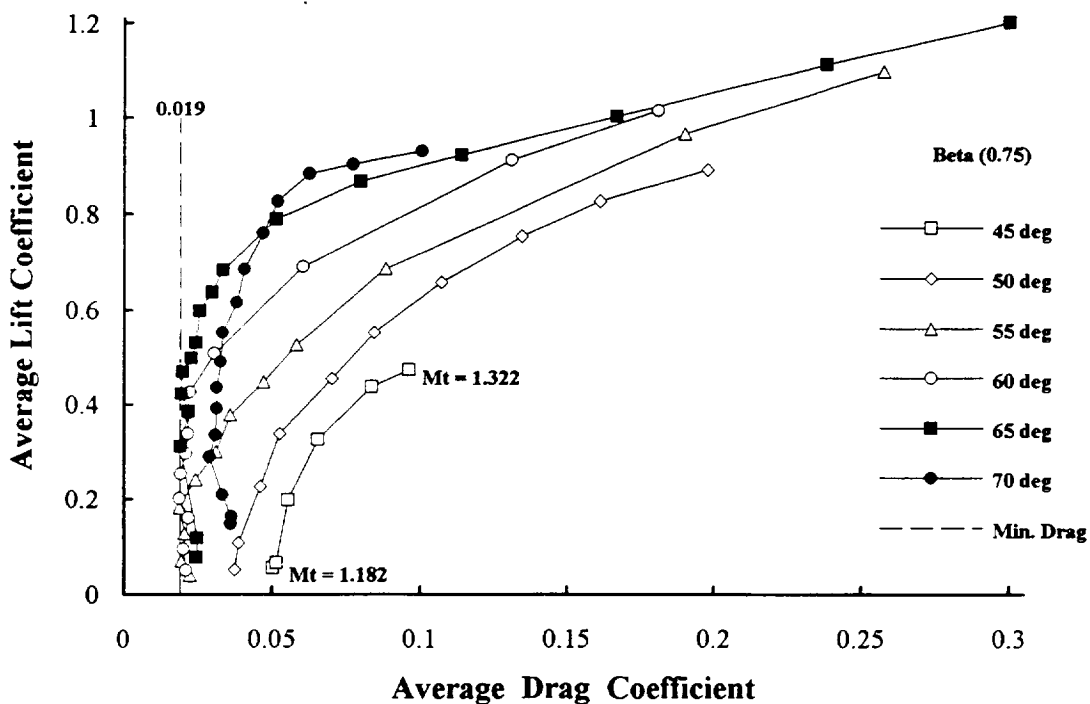
Figure A-21b. PROP 1 Average Airfoil Behavior at M=0.70
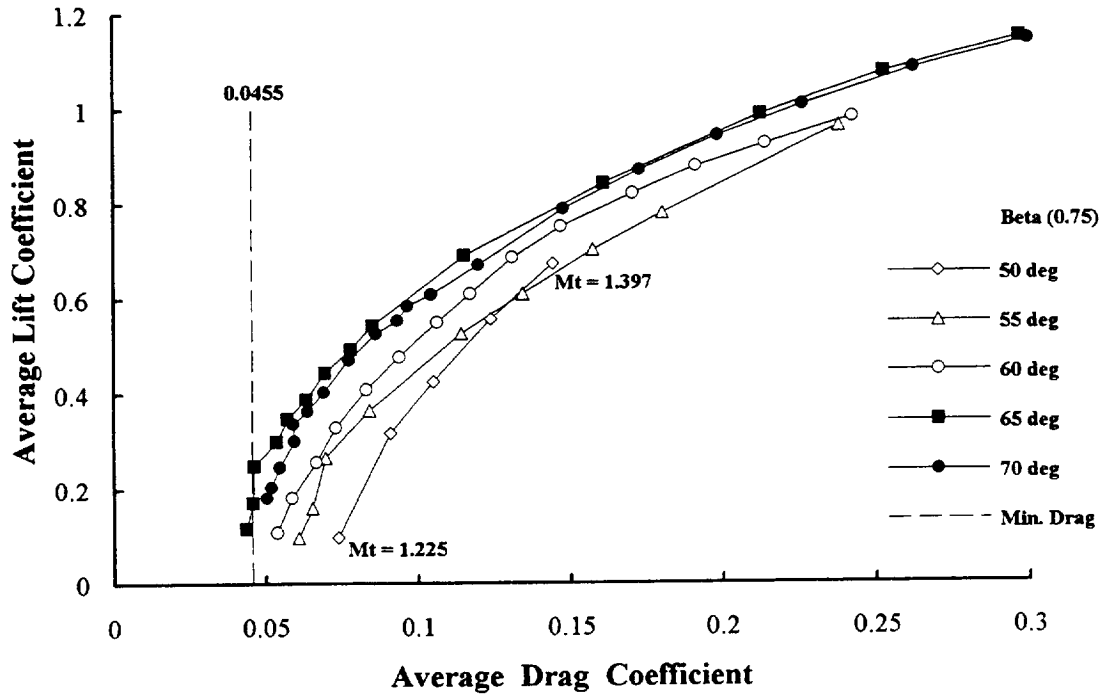
Figure A-21c. PROP 1 Average Airfoil Behavior at M=0.80
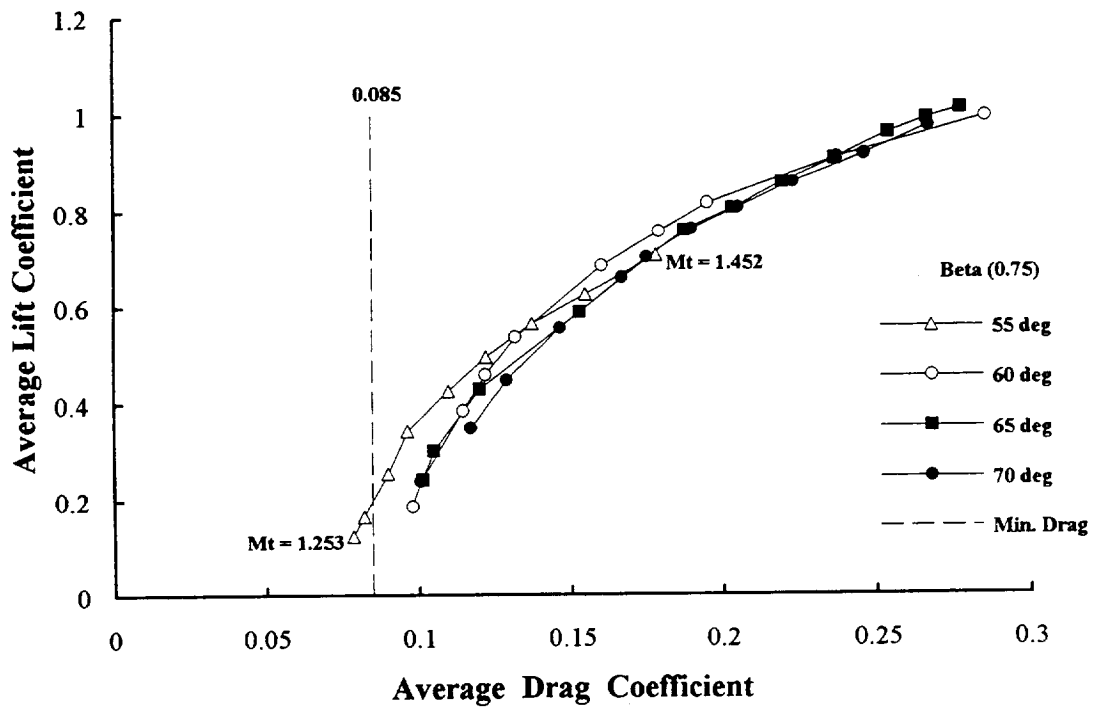
Figure A-21d. PROP 1 Average Airfoil Behavior at M=0.90
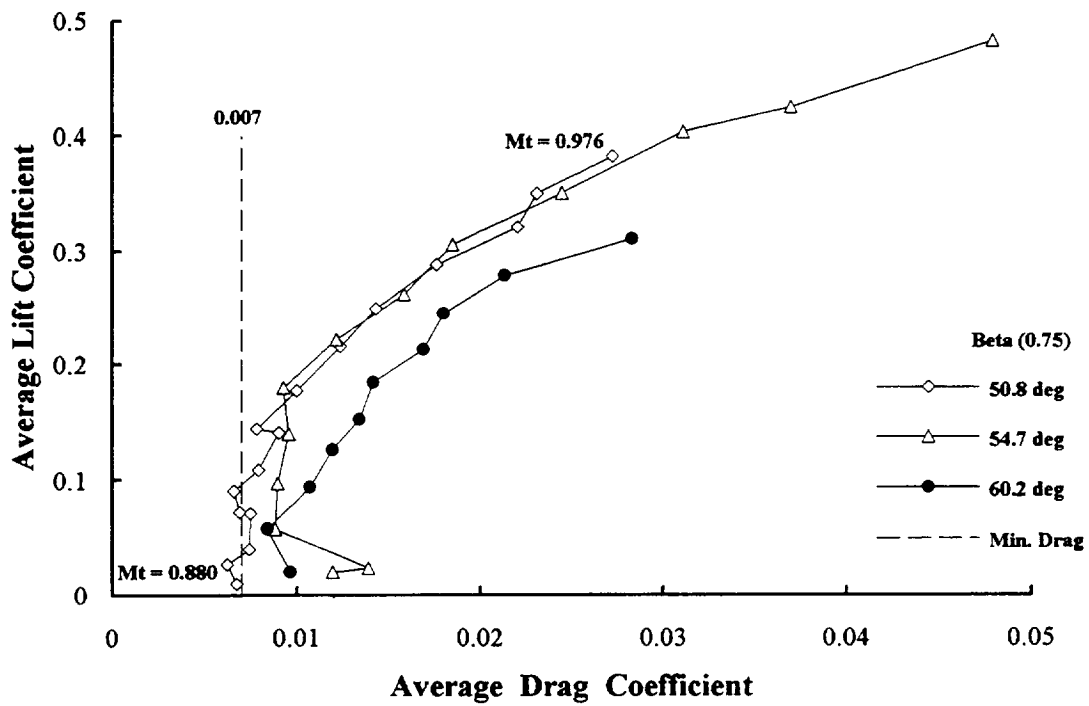
Figure A-22a. PROP 2 Average Airfoil Behavior at M=0.60
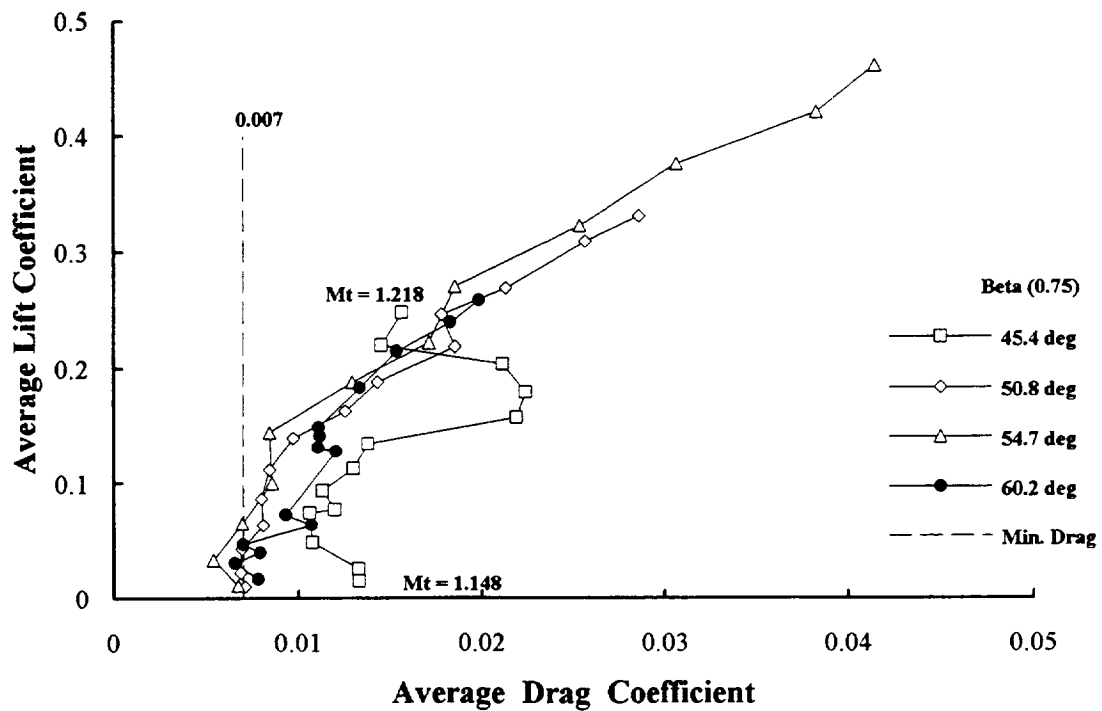
Figure A-22b. PROP 2 Average Airfoil Behavior at M=0.70

A-66
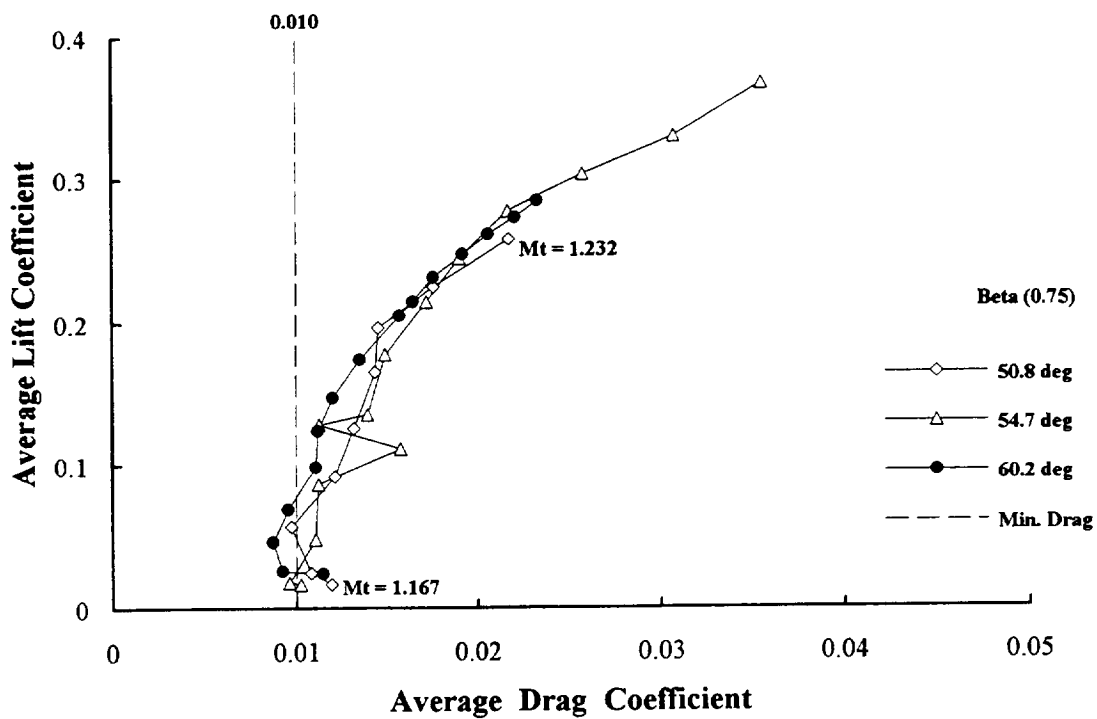
Figure A-22c. PROP 2 Average Airfoil Behavior at M=0.80
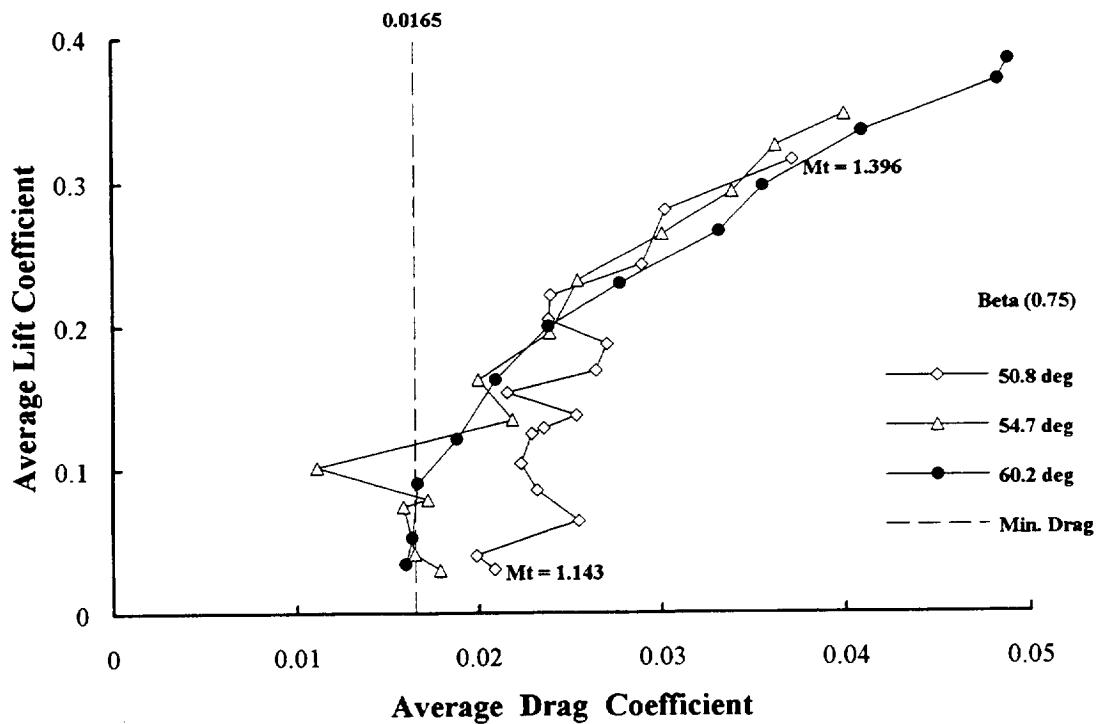
Figure A-22d. PROP 2 Average Airfoil Behavior at M=0.89

A-67
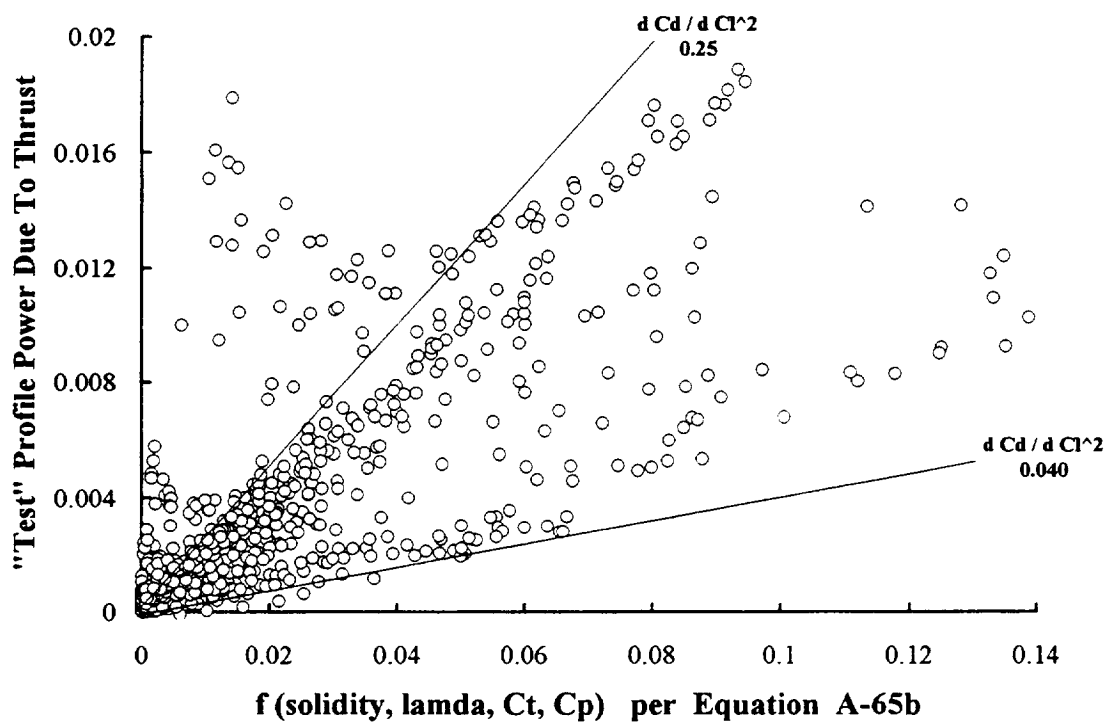
Figure A-23. PROP 1 Average Airfoil dC_d/dC_l^2.
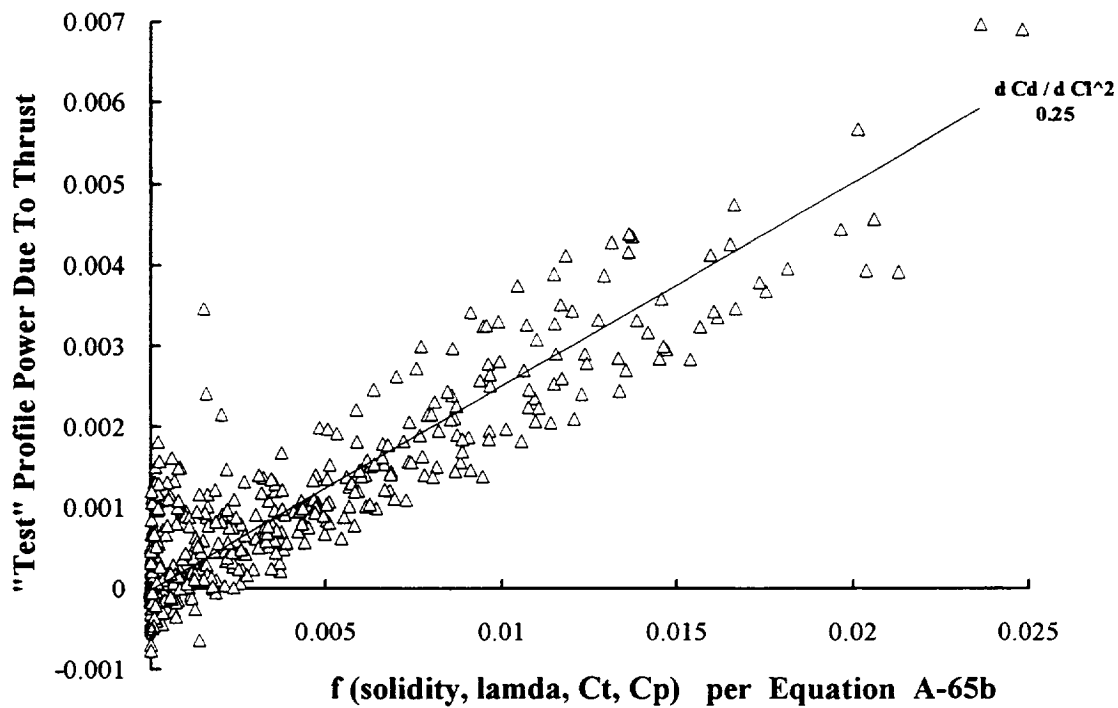
Figure A-24. PROP 2 Average Airfoil dC_d/dC_l^2.
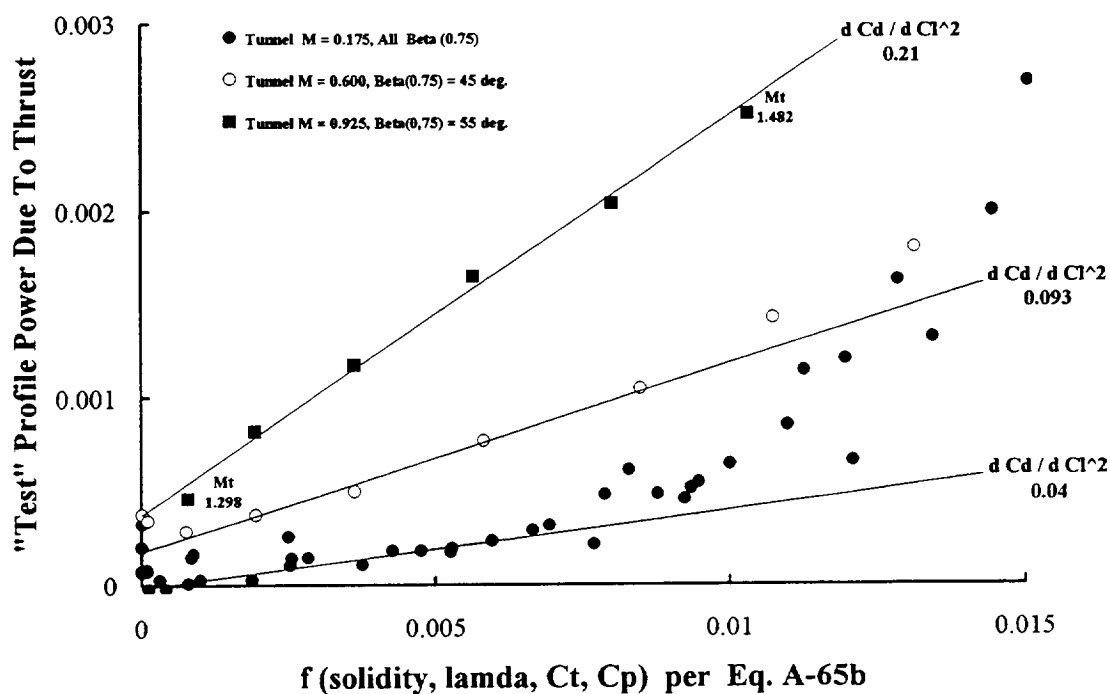
Figure A-25. PROP 1 Average Airfoil dC_d/dC_l^2.
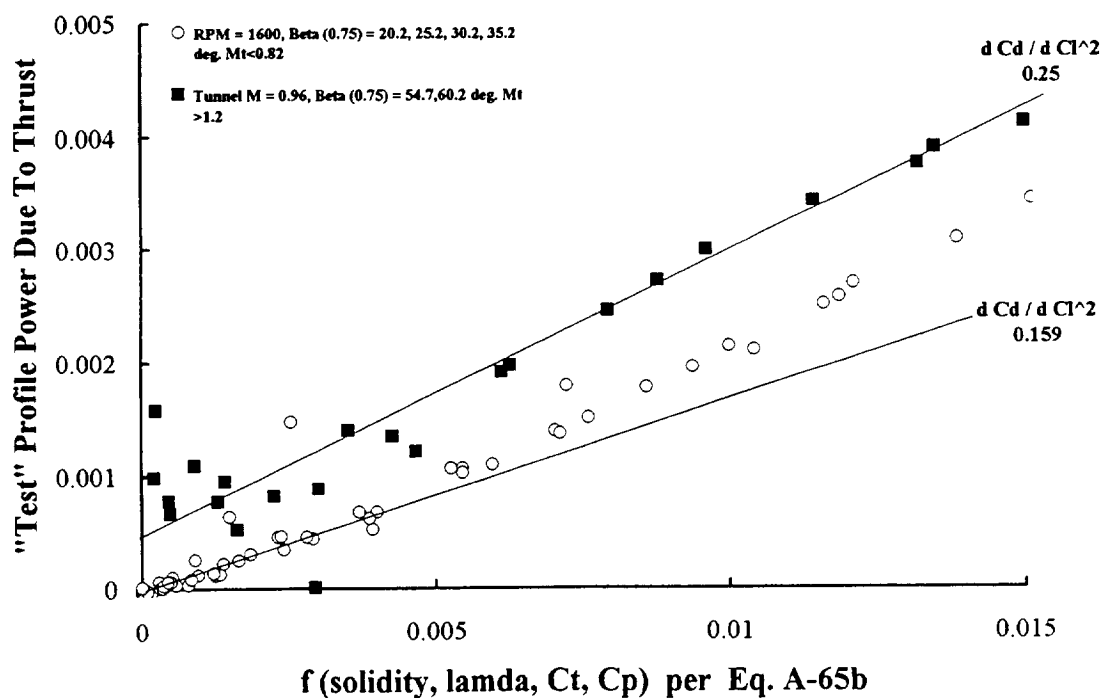
Figure A-26. PROP 2 Average Airfoil dC_d/dC_l^2.
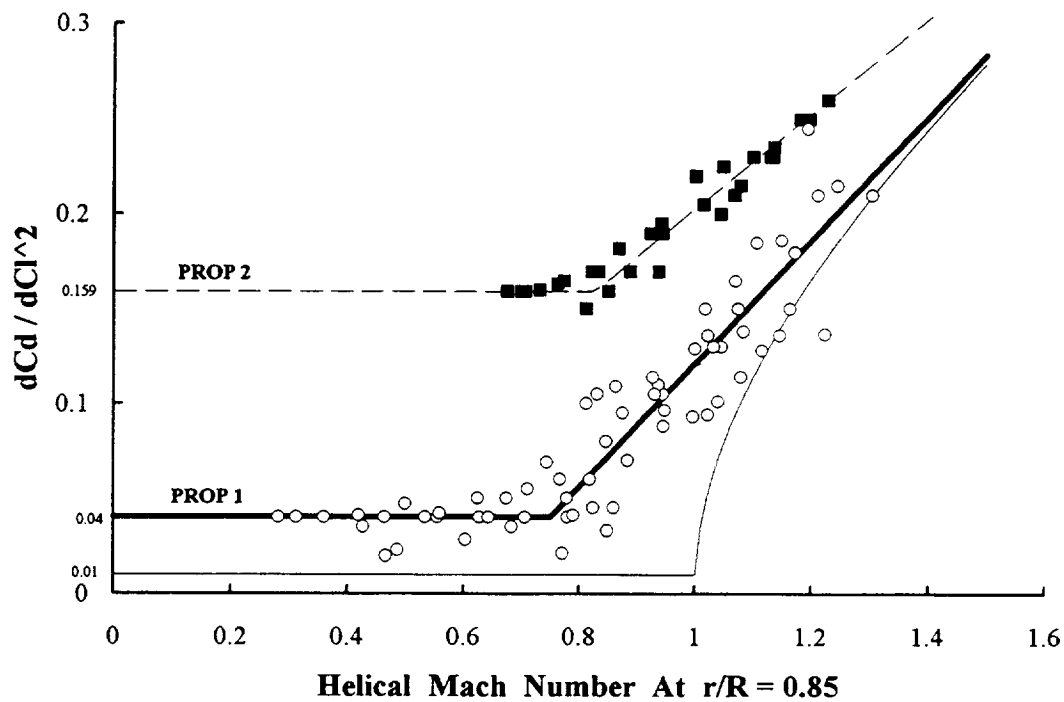
Figure A-27. PROP's 1 & 2 Average Airfoil dC_d/dC_l^2.
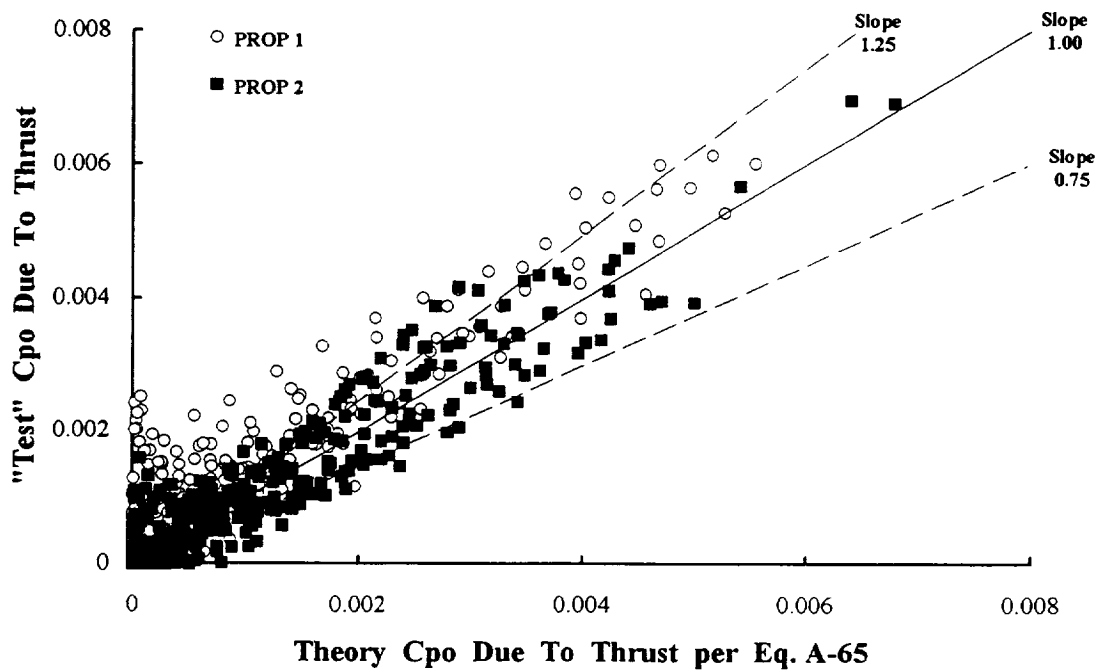
Figure A-28. PROP's 1 & 2 Correlation Of Profile Power Rise With Thrust.
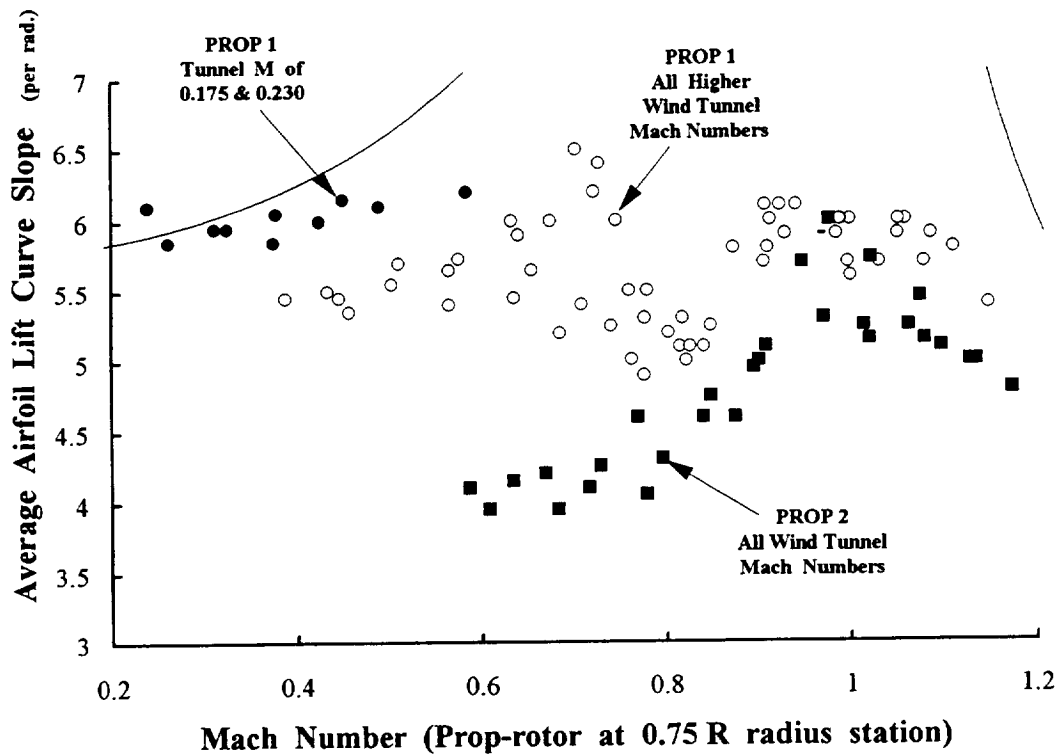
Figure A-29. PROP's 1 &2 Average Airfoil Lift Curve Slope.
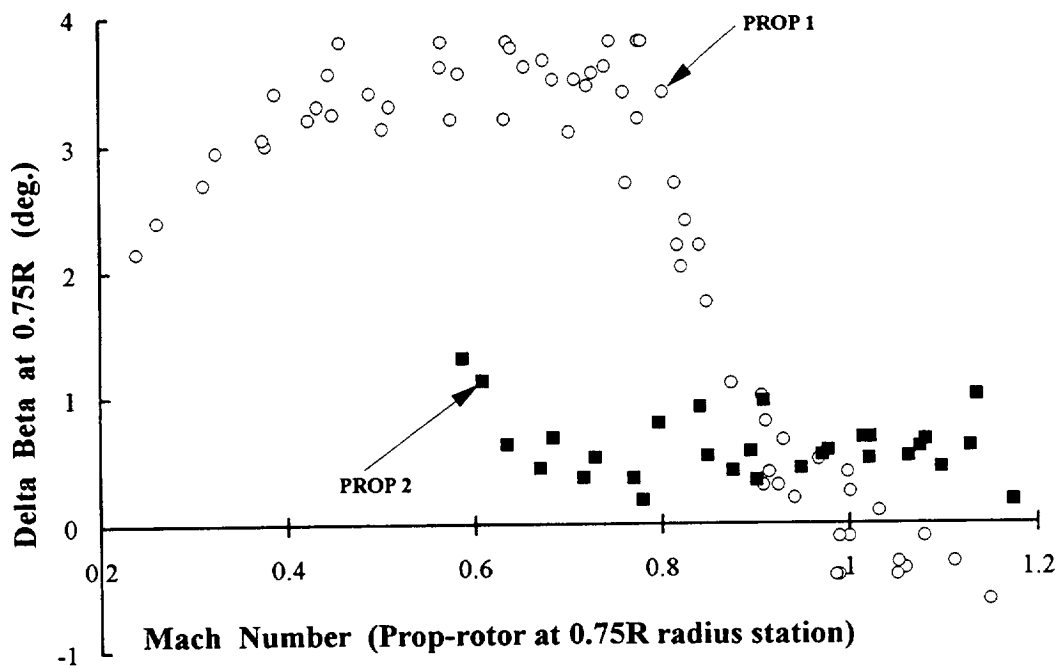
Figure A-30. PROP's 1 &2 Apparent Blade Angle Shift.
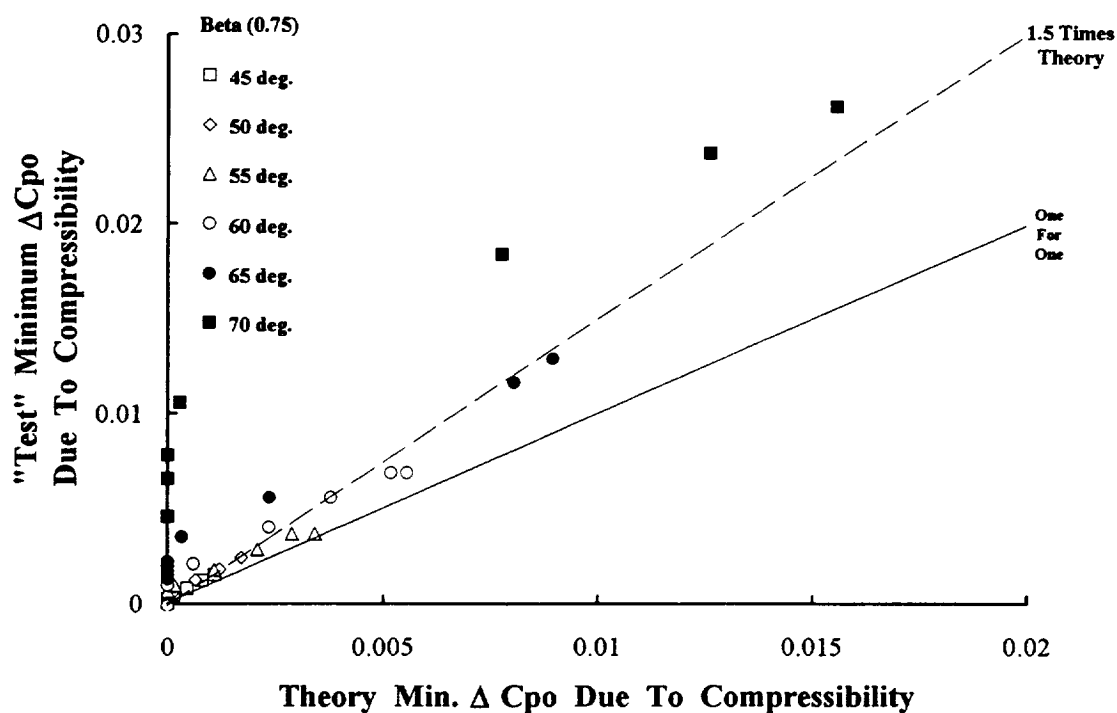
Figure A-31. PROP 1 Correlation Of Min. Compressibility Profile Power.
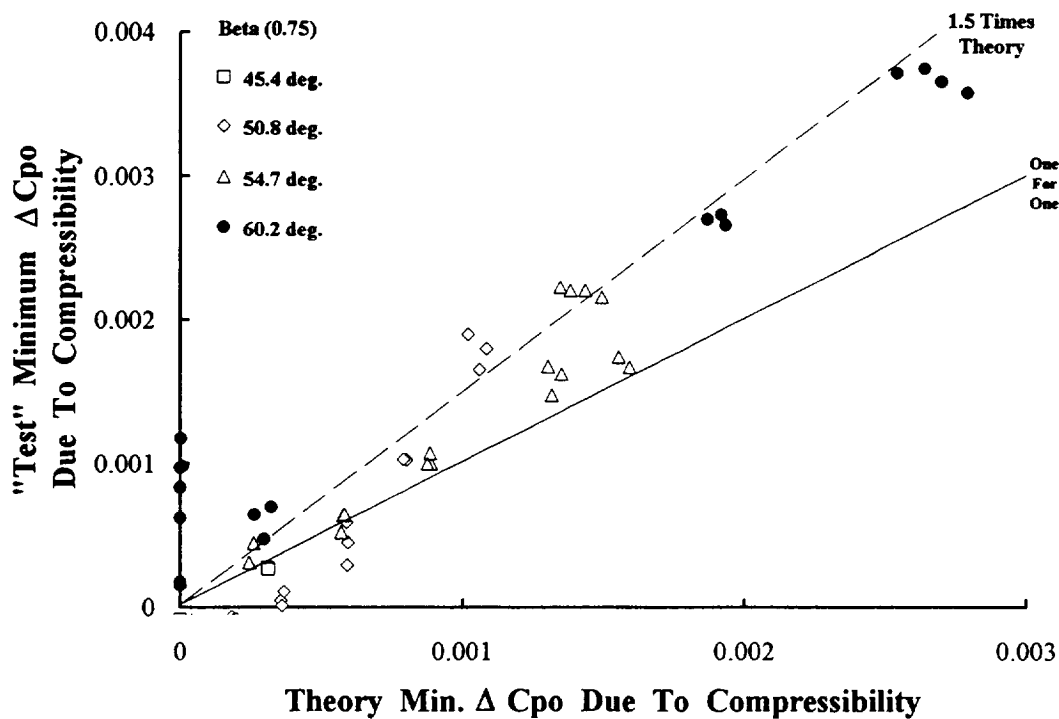
Figure A-32. PROP 2 Correlation Of Min. Compressibility Profile Power.

A-72
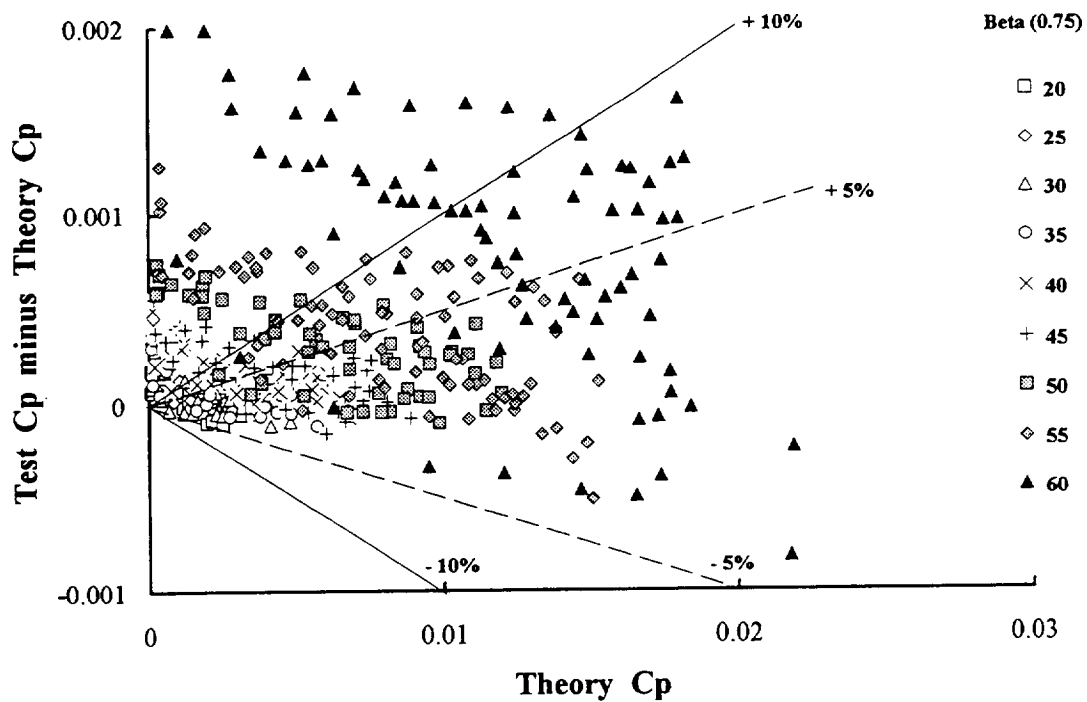
Figure A-33. PROP 1 Total Power Correlation With Theory.
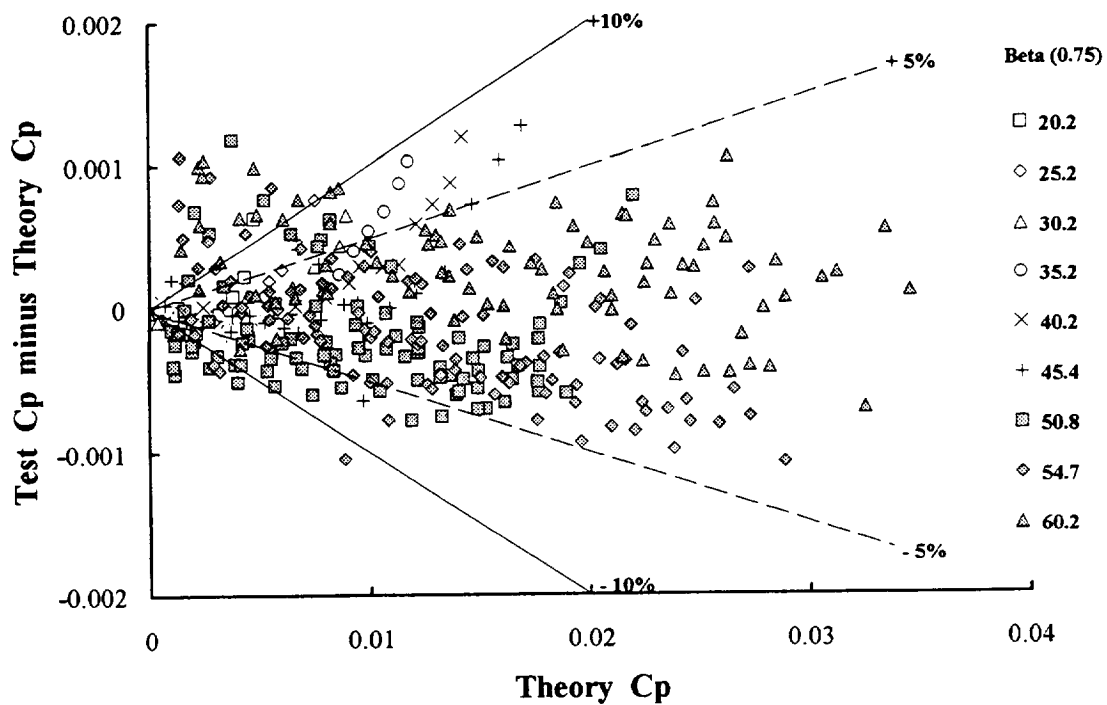
Figure A-34 PROP 2 Total Power Correlation With Theory.

This page intentionally left blank

APPENDIX B

PROP_GEO.XLS

PROP 1 is the Two Bladed Model-Scale Supersonic Propeller

Tested By Delano & Carmel. Originally In RM L9G06a (Sept. 15, 1949)
See also and later in NACA TR 999 (19xx) and 1012 (1951)
Data read from graphs by Frank Harris in Aug. 1995.
Propeller is NACA 4-(5)(08)-03 made from Duralumin
NACA 16 series Cambered Airfoils Of Varying Thickness
Variable Chord, 2-Blades, 4.00 ft. Dia., Norm. Solidity =0.07

r/R	c/R	t/c	Beta (deg)	Design CI	Beta Ref. to x = 0.75
0.271	0.18929	0.13368	67.8165	0.21228	25.1723
0.28	0.1881	0.1323	67.22	0.2210	24.57
0.29	0.1867	0.1309	66.55	0.2307	23.91
0.30	0.1854	0.1294	65.90	0.2405	23.25
0.31	0.1841	0.1280	65.25	0.2504	22.60
0.32	0.1827	0.1265	64.61	0.2602	21.96
0.33	0.1814	0.1251	63.97	0.2701	21.32
0.34	0.1800	0.1237	63.34	0.2800	20.69
0.35	0.1787	0.1223	62.71	0.2899	20.07
0.36	0.1774	0.1209	62.09	0.2997	19.45
0.37	0.1760	0.1195	61.48	0.3094	18.83
0.38	0.1747	0.1181	60.87	0.3190	18.23
0.39	0.1733	0.1167	60.27	0.3284	17.63
0.40	0.1720	0.1154	59.67	0.3378	17.03
0.41	0.1707	0.1140	59.09	0.3470	16.44
0.42	0.1693	0.1127	58.50	0.3559	15.86
0.43	0.1680	0.1114	57.92	0.3647	15.28
0.44	0.1666	0.1100	57.35	0.3733	14.71
0.45	0.1653	0.1087	56.79	0.3817	14.14
0.46	0.1640	0.1074	56.23	0.3898	13.59
0.47	0.1626	0.1062	55.68	0.3977	13.03
0.48	0.1613	0.1049	55.13	0.4052	12.49
0.49	0.1599	0.1036	54.59	0.4126	11.94
0.50	0.1586	0.1024	54.05	0.4196	11.41
0.51	0.1573	0.1011	53.52	0.4264	10.88
0.52	0.1559	0.0999	53.00	0.4329	10.36
0.53	0.1546	0.0987	52.49	0.4390	9.84
0.54	0.1532	0.0975	51.97	0.4449	9.33
0.55	0.1519	0.0963	51.47	0.4505	8.83
0.56	0.1506	0.0951	50.97	0.4558	8.33
0.57	0.1492	0.0939	50.48	0.4608	7.83
0.58	0.1479	0.0927	49.99	0.4655	7.35
0.59	0.1465	0.0916	49.51	0.4699	6.87
0.60	0.1452	0.0904	49.04	0.4740	6.39
0.61	0.1439	0.0893	48.57	0.4778	5.92

r/R	c/R	t/c	Beta (deg)	Design CI	Beta Ref. to x = 0.75
0.62	0.1425	0.0882	48.11	0.4813	5.46
0.63	0.1412	0.0871	47.65	0.4846	5.01
0.64	0.1398	0.0860	47.20	0.4876	4.56
0.65	0.1385	0.0849	46.76	0.4903	4.11
0.66	0.1372	0.0838	46.32	0.4927	3.67
0.67	0.1358	0.0827	45.88	0.4948	3.24
0.68	0.1345	0.0817	45.46	0.4967	2.81
0.69	0.1331	0.0806	45.04	0.4983	2.39
0.70	0.1318	0.0796	44.62	0.4996	1.98
0.71	0.1305	0.0785	44.22	0.5006	1.57
0.72	0.1291	0.0775	43.81	0.5013	1.17
0.73	0.1278	0.0765	43.42	0.5018	0.77
0.74	0.1264	0.0755	43.03	0.5018	0.38
0.75	0.1251	0.0745	42.64	0.5015	0.00
0.76	0.1238	0.0736	42.27	0.5009	-0.38
0.77	0.1224	0.0726	41.89	0.4998	-0.75
0.78	0.1211	0.0716	41.53	0.4984	-1.12
0.79	0.1197	0.0707	41.17	0.4964	-1.48
0.80	0.1184	0.0698	40.82	0.4939	-1.83
0.81	0.1171	0.0688	40.47	0.4908	-2.18
0.82	0.1157	0.0679	40.13	0.4871	-2.52
0.83	0.1144	0.0670	39.79	0.4828	-2.85
0.84	0.1130	0.0661	39.46	0.4776	-3.18
0.85	0.1117	0.0652	39.14	0.4716	-3.51
0.86	0.1104	0.0636	38.82	0.4646	-3.82
0.87	0.1090	0.0625	38.51	0.4566	-4.14
0.88	0.1077	0.0613	38.20	0.4474	-4.44
0.89	0.1063	0.0598	37.90	0.4370	-4.74
0.90	0.1050	0.0581	37.61	0.4251	-5.03
0.91	0.1037	0.0563	37.32	0.4117	-5.32
0.92	0.1023	0.0542	37.04	0.3966	-5.60
0.93	0.1006	0.0519	36.77	0.3795	-5.88
0.94	0.0993	0.0494	36.50	0.3604	-6.15
0.95	0.0966	0.0467	36.23	0.3390	-6.41
0.96	0.0922	0.0438	35.98	0.3151	-6.67
0.97	0.0862	0.0407	35.73	0.2885	-6.92
0.975	0.0820	0.0385	35.60	0.2741	-7.04
0.98	0.0775	0.0350	35.48	0.2589	-7.16
0.985	0.0690	0.0291	35.36	0.2370	-7.28
0.99	0.0543	0.0211	35.24	0.2000	-7.40
0.995	0.0305	0.0114	35.12	0.1298	-7.52
1.00	0.0000	0.0000	35.01	0.0000	-7.64

Two Bladed Model-Scale Supersonic Propeller Tested By Delano & Carmel. Originally In RM L9G06a (Sept.1949)

Data read from graphs by Frank Harris in Aug. 1995. Caution because data entry has not been proof read only once.

Propeller is NACA 4-(5)(08)-03. Made of Duralumin. NACA 16 series Cambered Airfoils Of Varying Thickness

Variable Chord, 2-Blades, 4.00 ft. Dia., Nom. Solidity =0.0721

| Experimental Data Read From Graphs | | | | | | | Reference | | Reduced Experimental Data | | | | |
| Data | Data | Data | Data | Data | Rotor Inflow Ratio | Helical | S.L. Forward | Speeds Std. Tip | Rotor Thrust | Rotor Power | George Schairer Coefficients | | Rotor Ct over |
Beta 0.75 R [deg]	Tunnel Mach No.	Propeller Advance Ratio	Prop Thrust Coeff. Cth	Prop Power Coeff. Cph	J/pi Lamda	Mach Number	Speed [knots]	Speed [ft/sec]	Coeff. Ct Rotor	Coeff. Cp Rotor	T/qD^2	P/qVD^2	Sigma
20	0.175	0.995	0.0000	0.0035	0.317	0.580	116	616	0.000000	0.0001437	0.0000	0.0071	0.0000
20	0.175	0.947	0.0090	0.0122	0.301	0.606	116	648	0.001166	0.0005022	0.0202	0.0288	0.0162
20	0.175	0.841	0.0296	0.0278	0.268	0.677	116	730	0.003823	0.00114	0.0838	0.0937	0.0530
20	0.175	0.735	0.0497	0.0436	0.234	0.768	116	835	0.006417	0.00179	0.1842	0.2196	0.0890
20	0.175	0.631	0.0683	0.0535	0.201	0.889	116	972	0.008809	0.00220	0.3431	0.4261	0.1222
20	0.175	0.576	0.0766	0.0588	0.183	0.970	116	1065	0.009888	0.00242	0.4619	0.6154	0.1372
20	0.175	0.497	0.0849	0.0691	0.158	1.121	116	1235	0.010952	0.00284	0.6885	1.1287	0.1519
25	0.175	1.230	0.0000	0.0041	0.392	0.480	116	499	0.000000	0.00017	0.0000	0.0044	0.0000
25	0.175	1.201	0.0054	0.0106	0.382	0.490	116	511	0.000701	0.00043	0.0075	0.0122	0.0097
25	0.175	1.150	0.0157	0.0210	0.366	0.509	116	533	0.002023	0.00086	0.0237	0.0276	0.0281
25	0.175	1.099	0.0257	0.0309	0.350	0.530	116	558	0.003320	0.00127	0.0426	0.0466	0.0461
25	0.175	0.988	0.0463	0.0524	0.314	0.584	116	621	0.005968	0.00215	0.0948	0.1087	0.0828
25	0.175	0.884	0.0603	0.0620	0.281	0.646	116	694	0.007782	0.00255	0.1543	0.1794	0.1079
25	0.175	0.780	0.0718	0.0673	0.248	0.727	116	787	0.009268	0.00276	0.2364	0.2840	0.1286
25	0.175	0.678	0.0871	0.0788	0.216	0.829	116	905	0.011233	0.00324	0.3787	0.5054	0.1558
25	0.175	0.571	0.1004	0.0979	0.182	0.979	116	1075	0.012955	0.00402	0.6169	1.0541	0.1797
30	0.175	1.510	0.0000	0.0046	0.481	0.404	116	406	0.000000	0.00019	0.0000	0.0027	0.0000
30	0.175	1.457	0.0095	0.0162	0.464	0.416	116	421	0.001229	0.00067	0.0090	0.0105	0.0171
30	0.175	1.407	0.0180	0.0277	0.448	0.428	116	436	0.002328	0.00114	0.0182	0.0199	0.0323
30	0.175	1.298	0.0388	0.0542	0.413	0.458	116	473	0.005004	0.00222	0.0461	0.0496	0.0694
30	0.175	1.195	0.0554	0.0727	0.380	0.492	116	513	0.007144	0.00299	0.0776	0.0852	0.0991
30	0.175	1.089	0.0660	0.0807	0.347	0.534	116	563	0.008508	0.00331	0.1112	0.1249	0.1180
30	0.175	0.883	0.0889	0.0989	0.281	0.647	116	695	0.011465	0.00406	0.2280	0.2873	0.1590
30	0.175	0.779	0.0959	0.1108	0.248	0.727	116	787	0.012365	0.00455	0.3155	0.4680	0.1715
30	0.175	0.676	0.1020	0.1185	0.215	0.832	116	908	0.013159	0.00487	0.4469	0.7683	0.1825
40	0.175	2.135	0.0000	0.0100	0.680	0.311	116	287	0.000000	0.00041	0.0000	0.0021	0.0000
40	0.175	2.100	0.0064	0.0204	0.669	0.315	116	292	0.000828	0.00084	0.0029	0.0044	0.0115
40	0.175	1.995	0.0229	0.0540	0.635	0.326	116	307	0.002952	0.00222	0.0115	0.0136	0.0410
40	0.175	1.886	0.0417	0.0859	0.600	0.340	116	325	0.005376	0.00353	0.0234	0.0256	0.0746
40	0.175	1.785	0.0580	0.1129	0.568	0.354	116	344	0.007482	0.00464	0.0364	0.0397	0.1038
40	0.175	1.684	0.0705	0.1319	0.536	0.370	116	364	0.009094	0.00542	0.0497	0.0552	0.1261
40	0.175	1.584	0.0753	0.1366	0.504	0.389	116	387	0.009719	0.00561	0.0601	0.0688	0.1348
40	0.175	1.494	0.0830	0.1425	0.476	0.407	116	410	0.010710	0.00585	0.0744	0.0854	0.1486
40	0.175	1.388	0.0897	0.1515	0.442	0.433	116	442	0.011576	0.00622	0.0931	0.1132	0.1606
40	0.175	1.277	0.0988	0.1652	0.407	0.465	116	480	0.012743	0.00678	0.1211	0.1585	0.1768
40	0.175	1.177	0.1008	0.1747	0.375	0.499	116	521	0.013004	0.00717	0.1454	0.2140	0.1804
40	0.175	1.076	0.1015	0.1823	0.343	0.540	116	570	0.013091	0.00748	0.1753	0.2925	0.1816
40	0.175	0.975	0.1020	0.1873	0.310	0.590	116	629	0.013164	0.00769	0.2147	0.4040	0.1826
45	0.175	1.781	0.0908	0.1846	0.567	0.355	116	344	0.011716	0.00758	0.0573	0.0653	0.1625
45	0.175	1.581	0.1022	0.2040	0.503	0.389	116	388	0.013179	0.00838	0.0818	0.1033	0.1828
45	0.175	1.397	0.1014	0.2146	0.445	0.431	116	439	0.013086	0.00881	0.1040	0.1575	0.1815
45	0.175	1.275	0.0986	0.2160	0.406	0.465	116	481	0.012723	0.00887	0.1214	0.2086	0.1765
45	0.175	1.170	0.0984	0.2198	0.372	0.501	116	524	0.012695	0.00903	0.1438	0.2746	0.1761
45	0.175	0.976	0.1061	0.2404	0.311	0.590	116	628	0.013682	0.00987	0.2226	0.5168	0.1898

Beta 0.75 R [deg]	Tunnel Mach No.	Propeller Advance Ratio	Prop Thrust Coeff. Cth	Prop Power Coeff. Cph	Inflow Ratio J/pi Lamda	Helical Mach Number	S.L. Forward Speed [knots]	Std. Tip Speed [ft/sec]	Rotor Thrust Coeff. Ct Rotor	Rotor Power Coeff. Cp Rotor	George Schairer Coefficients T/qD^2	P/qVD^2	Rotor Ct over Sigma
20	0.230	1.008	0.0000	0.0060	0.321	0.753	152	800	0.000000	0.0002464	0.0000	0.0117	0.0000
20	0.230	0.999	0.0014	0.0072	0.318	0.759	152	807	0.000184	0.00029	0.0029	0.0143	0.0026
20	0.230	0.946	0.0127	0.0158	0.301	0.798	152	852	0.001641	0.00065	0.0284	0.0373	0.0228
20	0.230	0.888	0.0234	0.0250	0.283	0.845	152	907	0.003015	0.00103	0.0592	0.0712	0.0418
20	0.230	0.836	0.0344	0.0330	0.266	0.894	152	964	0.004442	0.00135	0.0985	0.1127	0.0616
20	0.230	0.784	0.0451	0.0416	0.250	0.950	152	1028	0.005817	0.00171	0.1467	0.1724	0.0807
20	0.230	0.733	0.0523	0.0456	0.233	1.012	152	1100	0.006744	0.00187	0.1946	0.2316	0.0936
20	0.230	0.682	0.0563	0.0501	0.217	1.084	152	1181	0.007269	0.00206	0.2420	0.3150	0.1008
20	0.230	0.630	0.0645	0.0583	0.200	1.170	152	1280	0.008322	0.00239	0.3254	0.4666	0.1154
25	0.230	1.255	0.0000	0.0040	0.399	0.620	152	642	0.000000	0.00016	0.0000	0.0040	0.0000
25	0.230	1.204	0.0091	0.0138	0.383	0.643	152	670	0.001180	0.00057	0.0126	0.0159	0.0164
25	0.230	1.204	0.0091	0.0138	0.383	0.643	152	670	0.001180	0.00057	0.0126	0.0159	0.0164
25	0.230	1.101	0.0281	0.0348	0.350	0.696	152	732	0.003622	0.00143	0.0463	0.0522	0.0502
25	0.230	1.046	0.0379	0.0441	0.333	0.728	152	771	0.004885	0.00181	0.0692	0.0770	0.0678
25	0.230	0.994	0.0492	0.0553	0.316	0.763	152	811	0.006346	0.00227	0.0996	0.1126	0.0880
25	0.230	0.941	0.0582	0.0615	0.299	0.802	152	857	0.007506	0.00253	0.1315	0.1478	0.1041
25	0.230	0.887	0.0662	0.0675	0.282	0.846	152	909	0.008536	0.00277	0.1682	0.1933	0.1184
30	0.230	1.521	0.0000	0.0048	0.484	0.528	152	530	0.000000	0.00020	0.0000	0.0027	0.0000
30	0.230	1.498	0.0043	0.0097	0.477	0.534	152	538	0.000553	0.00040	0.0038	0.0058	0.0077
30	0.230	1.395	0.0233	0.0347	0.444	0.567	152	578	0.003000	0.00142	0.0239	0.0256	0.0416
30	0.230	1.290	0.0429	0.0592	0.411	0.606	152	625	0.005535	0.00243	0.0516	0.0552	0.0768
30	0.230	1.184	0.0605	0.0790	0.377	0.652	152	681	0.007803	0.00324	0.0863	0.0952	0.1082
30	0.230	1.081	0.0705	0.0859	0.344	0.707	152	745	0.009094	0.00353	0.1206	0.1358	0.1261
30	0.230	0.976	0.0844	0.0973	0.311	0.775	152	826	0.010891	0.00399	0.1774	0.2094	0.1511
30	0.230	0.871	0.0987	0.1174	0.277	0.861	152	926	0.012727	0.00482	0.2601	0.3552	0.1765
35	0.230	1.830	0.0000	0.0060	0.583	0.457	152	441	0.000000	0.00025	0.0000	0.0020	0.0000
35	0.230	1.811	0.0034	0.0107	0.576	0.461	152	445	0.000437	0.00044	0.0021	0.0036	0.0061
35	0.230	1.701	0.0207	0.0384	0.542	0.483	152	474	0.002675	0.00158	0.0143	0.0156	0.0371
35	0.230	1.598	0.0382	0.0648	0.509	0.507	152	504	0.004933	0.00266	0.0300	0.0318	0.0684
35	0.230	1.497	0.0562	0.0905	0.476	0.535	152	539	0.007244	0.00372	0.0501	0.0539	0.1005
35	0.230	1.391	0.0684	0.1044	0.443	0.568	152	580	0.008823	0.00429	0.0707	0.0776	0.1224
35	0.230	1.290	0.0761	0.1113	0.411	0.606	152	625	0.009813	0.00457	0.0915	0.1037	0.1361
35	0.230	1.187	0.0875	0.1234	0.378	0.651	152	679	0.011284	0.00507	0.1241	0.1475	0.1565
35	0.230	1.081	0.0988	0.1361	0.344	0.707	152	746	0.012751	0.00559	0.1693	0.2157	0.1769
35	0.230	0.980	0.1014	0.1461	0.312	0.772	152	822	0.013086	0.00600	0.2112	0.3104	0.1815
35	0.230	0.877	0.1037	0.1567	0.279	0.855	152	919	0.013378	0.00643	0.2696	0.4642	0.1856
35	0.230	0.771	0.1055	0.1676	0.246	0.965	152	1045	0.013606	0.00688	0.3546	0.7307	0.1887
45	0.230	2.589	0.0000	0.0142	0.824	0.362	152	311	0.000000	0.00058	0.0000	0.0016	0.0000
45	0.230	2.500	0.0138	0.0450	0.796	0.369	152	322	0.001774	0.00185	0.0044	0.0058	0.0246
45	0.230	2.404	0.0300	0.0783	0.765	0.378	152	335	0.003875	0.00321	0.0104	0.0113	0.0537
45	0.230	2.300	0.0450	0.1117	0.732	0.389	152	350	0.005802	0.00459	0.0170	0.0184	0.0805
45	0.230	2.199	0.0613	0.1424	0.700	0.401	152	367	0.007905	0.00585	0.0253	0.0268	0.1096
45	0.230	2.090	0.0710	0.1616	0.665	0.415	152	386	0.009158	0.00664	0.0325	0.0354	0.1270
45	0.230	1.988	0.0790	0.1716	0.633	0.430	152	405	0.010197	0.00704	0.0400	0.0437	0.1414
45	0.230	1.786	0.0926	0.1896	0.569	0.465	152	451	0.011945	0.00779	0.0580	0.0666	0.1657
45	0.230	1.683	0.1002	0.1999	0.536	0.487	152	479	0.012926	0.00821	0.0708	0.0839	0.1793
45	0.230	1.482	0.1041	0.2143	0.472	0.539	152	544	0.013431	0.00880	0.0948	0.1318	0.1863
45	0.230	1.277	0.1025	0.2269	0.407	0.611	152	631	0.013227	0.00932	0.1257	0.2178	0.1835
45	0.230	1.176	0.1030	0.2324	0.374	0.656	152	685	0.013285	0.00954	0.1489	0.2857	0.1843

Beta 0.75 R [deg]	Tunnel Mach No.	Propeller Advance Ratio	Prop Thrust Coeff. Cth	Prop Power Coeff. Cph	Inflow Ratio J / pi Lamda	Helical Mach Number	S.L. Forward Speed [knots]	Std. Tip Speed [ft/sec]	Rotor Thrust Coeff. Ct Rotor	Rotor Power Coeff. Cp Rotor	George Schairer Coefficients T/qD^2	P/qVD^2	Rotor Ct over Sigma
25	0.350	1.215	0.0000	0.0100	0.387	0.970	231	1010	0.000000	0.0004106	0.0000	0.0112	0.0000
25	0.350	1.203	0.0023	0.0122	0.383	0.979	231	1020	0.000294	0.00050	0.0032	0.0140	0.0041
25	0.350	1.093	0.0179	0.0283	0.348	1.065	231	1122	0.002307	0.00116	0.0299	0.0433	0.0320
25	0.350	1.044	0.0257	0.0368	0.332	1.110	231	1175	0.003321	0.00151	0.0472	0.0646	0.0461
25	0.350	0.952	0.0405	0.0530	0.303	1.207	231	1288	0.005219	0.00218	0.0893	0.1228	0.0724
30	0.350	1.553	0.0000	0.0110	0.494	0.790	231	790	0.000000	0.00045	0.0000	0.0059	0.0000
30	0.350	1.508	0.0071	0.0172	0.480	0.809	231	813	0.000921	0.00071	0.0063	0.0100	0.0128
30	0.350	1.393	0.0266	0.0408	0.443	0.864	231	881	0.003426	0.00167	0.0274	0.0302	0.0475
30	0.350	1.345	0.0354	0.0530	0.428	0.890	231	912	0.004573	0.00218	0.0392	0.0436	0.0634
30	0.350	1.236	0.0535	0.0738	0.393	0.956	231	993	0.006899	0.00303	0.0700	0.0782	0.0957
30	0.350	1.181	0.0595	0.0815	0.376	0.994	231	1038	0.007676	0.00335	0.0852	0.0988	0.1065
30	0.350	1.077	0.0725	0.0977	0.343	1.079	231	1139	0.009355	0.00401	0.1250	0.1563	0.1298
30	0.350	0.971	0.0836	0.1146	0.309	1.186	231	1264	0.010779	0.00471	0.1774	0.2507	0.1495
35	0.350	1.855	0.0000	0.0120	0.590	0.688	231	661	0.000000	0.00049	0.0000	0.0038	0.0000
35	0.350	1.813	0.0065	0.0190	0.577	0.700	231	677	0.000835	0.00078	0.0039	0.0064	0.0116
35	0.350	1.707	0.0257	0.0475	0.543	0.733	231	719	0.003312	0.00195	0.0176	0.0191	0.0459
35	0.350	1.599	0.0418	0.0733	0.509	0.772	231	767	0.005390	0.00301	0.0327	0.0358	0.0748
35	0.350	1.489	0.0611	0.1009	0.474	0.817	231	824	0.007876	0.00414	0.0551	0.0612	0.1092
35	0.350	1.383	0.0762	0.1186	0.440	0.869	231	887	0.009832	0.00487	0.0797	0.0896	0.1364
35	0.350	1.276	0.0922	0.1392	0.406	0.930	231	962	0.011889	0.00571	0.1132	0.1340	0.1649
35	0.350	1.170	0.1012	0.1531	0.372	1.003	231	1049	0.013057	0.00629	0.1479	0.1913	0.1811
35	0.350	1.067	0.1058	0.1652	0.340	1.088	231	1149	0.013644	0.00678	0.1857	0.2718	0.1893
40	0.350	2.215	0.0000	0.0130	0.705	0.607	231	554	0.000000	0.00053	0.0000	0.0024	0.0000
40	0.350	2.106	0.0167	0.0419	0.670	0.628	231	582	0.002154	0.00172	0.0075	0.0090	0.0299
40	0.350	1.999	0.0321	0.0711	0.636	0.652	231	614	0.004139	0.00292	0.0161	0.0178	0.0574
40	0.350	1.896	0.0486	0.1009	0.604	0.677	231	647	0.006272	0.00414	0.0270	0.0296	0.0870
40	0.350	1.785	0.0637	0.1306	0.568	0.708	231	687	0.008217	0.00536	0.0400	0.0459	0.1140
40	0.350	1.665	0.0778	0.1447	0.530	0.747	231	737	0.010039	0.00594	0.0561	0.0627	0.1393
40	0.350	1.583	0.0838	0.1511	0.504	0.778	231	775	0.010807	0.00620	0.0668	0.0762	0.1499
40	0.350	1.479	0.1008	0.1749	0.471	0.822	231	829	0.012998	0.00718	0.0921	0.1081	0.1803
40	0.350	1.369	0.1128	0.1964	0.436	0.876	231	896	0.014545	0.00806	0.1204	0.1532	0.2018
40	0.350	1.270	0.1130	0.2020	0.404	0.934	231	966	0.014583	0.00829	0.1402	0.1972	0.2023
40	0.350	1.168	0.1104	0.2059	0.372	1.005	231	1051	0.014242	0.00846	0.1619	0.2587	0.1975
40	0.350	1.066	0.1116	0.2157	0.339	1.089	231	1151	0.014403	0.00886	0.1965	0.3560	0.1998
50	0.350	3.220	0.0000	0.0227	1.025	0.489	231	381	0.000000	0.00093	0.0000	0.0014	0.0000
50	0.350	3.008	0.0251	0.0853	0.957	0.506	231	408	0.003237	0.00350	0.0055	0.0063	0.0449
50	0.350	2.801	0.0455	0.1464	0.891	0.526	231	438	0.005874	0.00601	0.0116	0.0133	0.0815
50	0.350	2.694	0.0608	0.1758	0.858	0.538	231	455	0.007847	0.00722	0.0168	0.0180	0.1089
50	0.350	2.593	0.0713	0.1989	0.825	0.550	231	473	0.009195	0.00817	0.0212	0.0228	0.1275
50	0.350	2.491	0.0793	0.2164	0.793	0.563	231	492	0.010229	0.00889	0.0256	0.0280	0.1419
50	0.350	2.287	0.0928	0.2377	0.728	0.595	231	536	0.011965	0.00976	0.0355	0.0397	0.1660
50	0.350	2.086	0.0994	0.2643	0.664	0.633	231	588	0.012829	0.01085	0.0457	0.0582	0.1779
50	0.350	1.877	0.1123	0.2758	0.597	0.682	231	654	0.014489	0.01133	0.0638	0.0834	0.2010
50	0.350	1.673	0.1052	0.2782	0.532	0.745	231	733	0.013568	0.01142	0.0752	0.1189	0.1882
50	0.350	1.469	0.1119	0.3266	0.468	0.826	231	835	0.014432	0.01341	0.1037	0.2060	0.2002
50	0.350	1.265	0.1033	0.3280	0.403	0.937	231	970	0.013322	0.01347	0.1290	0.3240	0.1848
50	0.350	1.063	0.0975	0.3070	0.338	1.092	231	1154	0.012572	0.01261	0.1725	0.5113	0.1744

Beta 0.75 R [deg]	Tunnel Mach No.	Propeller Advance Ratio	Prop Thrust Coeff. Cth	Prop Power Coeff. Cph	Inflow Ratio J/pi Lamda	Helical Mach Number	S.L. Forward Speed [knots]	Std. Tip Speed [ft/sec]	Rotor Thrust Coeff. Ct Rotor	Rotor Power Coeff. Cp Rotor	George Schairer Coefficients T/qD^2	George Schairer Coefficients P/qVD^2	Rotor Ct over Sigma
60	0.350	4.920	0.0000	0.0420	1.566	0.415	231	249	0.000000	0.00172	0.0000	0.0007	0.0000
60	0.350	4.806	0.0109	0.0811	1.530	0.418	231	255	0.001404	0.00333	0.0009	0.0015	0.0195
60	0.350	4.615	0.0282	0.1523	1.469	0.423	231	266	0.003643	0.00625	0.0027	0.0031	0.0505
60	0.350	4.407	0.0472	0.2232	1.403	0.430	231	278	0.006083	0.00916	0.0049	0.0052	0.0844
60	0.350	4.202	0.0636	0.2844	1.338	0.437	231	292	0.008209	0.01168	0.0072	0.0077	0.1139
60	0.350	4.000	0.0817	0.3458	1.273	0.445	231	307	0.010542	0.01420	0.0102	0.0108	0.1462
60	0.350	3.790	0.0971	0.3904	1.206	0.455	231	324	0.012524	0.01603	0.0135	0.0143	0.1737
60	0.350	3.591	0.1072	0.4130	1.143	0.465	231	342	0.013833	0.01696	0.0166	0.0178	0.1919
60	0.350	3.384	0.1128	0.4186	1.077	0.478	231	362	0.014545	0.01719	0.0197	0.0216	0.2018
60	0.350	3.182	0.1222	0.4322	1.013	0.492	231	385	0.015770	0.01775	0.0241	0.0268	0.2187
60	0.350	2.979	0.1281	0.4463	0.948	0.509	231	412	0.016528	0.01833	0.0289	0.0337	0.2293
60	0.350	2.775	0.1302	0.4516	0.883	0.529	231	442	0.016794	0.01854	0.0338	0.0423	0.2329
60	0.350	2.583	0.1197	0.4401	0.822	0.551	231	475	0.015438	0.01807	0.0359	0.0511	0.2141
30	0.430	1.445	0.0000	0.0115	0.460	1.029	284	1043	0.000000	0.0004722	0.0000	0.0076	0.0000
30	0.430	1.396	0.0079	0.0222	0.444	1.059	284	1080	0.001023	0.00091	0.0081	0.0163	0.0142
30	0.430	1.346	0.0164	0.0324	0.428	1.092	284	1120	0.002115	0.00133	0.0181	0.0265	0.0293
30	0.430	1.293	0.0249	0.0448	0.412	1.130	284	1165	0.003217	0.00184	0.0298	0.0414	0.0446
30	0.430	1.239	0.0339	0.0563	0.394	1.172	284	1217	0.004367	0.00231	0.0441	0.0593	0.0606
30	0.430	1.191	0.0419	0.0673	0.379	1.213	284	1265	0.005410	0.00276	0.0591	0.0795	0.0750
35	0.430	1.895	0.0000	0.0100	0.603	0.833	284	795	0.000000	0.00041	0.0000	0.0029	0.0000
35	0.430	1.795	0.0073	0.0211	0.571	0.867	284	840	0.000937	0.00087	0.0045	0.0073	0.0130
35	0.430	1.690	0.0273	0.0515	0.538	0.908	284	892	0.003526	0.00212	0.0191	0.0214	0.0489
35	0.430	1.587	0.0421	0.0746	0.505	0.953	284	949	0.005431	0.00306	0.0334	0.0373	0.0753
35	0.430	1.485	0.0554	0.0953	0.473	1.006	284	1015	0.007141	0.00391	0.0502	0.0581	0.0991
35	0.430	1.385	0.0684	0.1158	0.441	1.066	284	1088	0.008823	0.00475	0.0713	0.0872	0.1224
35	0.430	1.285	0.0812	0.1360	0.409	1.136	284	1173	0.010474	0.00559	0.0984	0.1283	0.1453
35	0.430	1.180	0.0907	0.1525	0.376	1.223	284	1277	0.011702	0.00626	0.1302	0.1855	0.1623
40	0.430	2.180	0.0000	0.0155	0.694	0.754	284	691	0.000000	0.00064	0.0000	0.0030	0.0000
40	0.430	1.994	0.0335	0.0731	0.635	0.803	284	756	0.004318	0.00300	0.0168	0.0184	0.0599
40	0.430	1.890	0.0515	0.1073	0.602	0.834	284	797	0.006639	0.00440	0.0288	0.0317	0.0921
40	0.430	1.784	0.0707	0.1386	0.568	0.871	284	845	0.009122	0.00569	0.0444	0.0488	0.1265
40	0.430	1.685	0.0867	0.1636	0.536	0.910	284	894	0.011191	0.00672	0.0611	0.0684	0.1552
40	0.430	1.583	0.0951	0.1768	0.504	0.956	284	952	0.012272	0.00726	0.0759	0.0892	0.1702
40	0.430	1.481	0.1020	0.1933	0.471	1.008	284	1017	0.013161	0.00794	0.0930	0.1189	0.1826
40	0.430	1.385	0.1088	0.2047	0.441	1.066	284	1088	0.014032	0.00840	0.1135	0.1542	0.1946
40	0.430	1.277	0.1155	0.2210	0.407	1.142	284	1180	0.014901	0.00907	0.1416	0.2120	0.2067
45	0.430	2.640	0.0000	0.0140	0.840	0.668	284	571	0.000000	0.00057	0.0000	0.0015	0.0000
45	0.430	2.603	0.0058	0.0256	0.828	0.674	284	579	0.000744	0.00105	0.0017	0.0029	0.0103
45	0.430	2.399	0.0351	0.0926	0.764	0.709	284	628	0.004522	0.00380	0.0122	0.0134	0.0627
45	0.430	2.296	0.0483	0.1218	0.731	0.729	284	656	0.006232	0.00500	0.0183	0.0201	0.0864
45	0.430	2.196	0.0626	0.1515	0.699	0.751	284	686	0.008077	0.00622	0.0260	0.0286	0.1120
45	0.430	2.089	0.0777	0.1772	0.665	0.776	284	721	0.010020	0.00728	0.0356	0.0389	0.1390
45	0.430	1.781	0.1152	0.2436	0.567	0.872	284	846	0.014863	0.01000	0.0726	0.0862	0.2062
45	0.430	1.584	0.1223	0.2599	0.504	0.955	284	951	0.015781	0.01067	0.0975	0.1307	0.2189
45	0.430	1.477	0.1223	0.2674	0.470	1.010	284	1020	0.015781	0.01098	0.1121	0.1658	0.2189

Beta 0.75 R [deg]	Tunnel Mach No.	Propeller Advance Ratio	Prop Thrust Coeff. Cth	Prop Power Coeff. Cph	Inflow Ratio J / pi Lamda	Helical Mach Number	S.L. Forward Speed [knots]	Std. Tip Speed [ft/sec]	Rotor Thrust Coeff. Ct Rotor	Rotor Power Coeff. Cp Rotor	George Schairer Coefficients T/qD^2	P/qVD^2	Rotor Ct over Sigma
55	0.430	3.870	0.0000	0.0280	1.232	0.554	284	389	0.000000	0.00115	0.0000	0.0010	0.0000
55	0.430	3.811	0.0067	0.0506	1.213	0.557	284	395	0.000870	0.00208	0.0009	0.0018	0.0121
55	0.430	3.711	0.0189	0.0878	1.181	0.563	284	406	0.002444	0.00360	0.0028	0.0034	0.0339
55	0.430	3.612	0.0317	0.1258	1.150	0.570	284	417	0.004088	0.00517	0.0049	0.0053	0.0567
55	0.430	3.508	0.0432	0.1662	1.117	0.577	284	430	0.005576	0.00682	0.0070	0.0077	0.0773
55	0.430	3.405	0.0528	0.1969	1.084	0.585	284	443	0.006813	0.00808	0.0091	0.0100	0.0945
55	0.430	3.295	0.0652	0.2306	1.049	0.594	284	457	0.008416	0.00947	0.0120	0.0129	0.1167
55	0.430	3.202	0.0763	0.2623	1.019	0.602	284	471	0.009846	0.01077	0.0149	0.0160	0.1366
55	0.430	3.097	0.0852	0.2856	0.986	0.612	284	487	0.010996	0.01173	0.0178	0.0192	0.1525
55	0.430	2.997	0.0925	0.3008	0.954	0.623	284	503	0.011934	0.01235	0.0206	0.0223	0.1655
55	0.430	2.795	0.1031	0.3181	0.890	0.647	284	539	0.013297	0.01306	0.0264	0.0291	0.1844
55	0.430	2.595	0.1169	0.3458	0.826	0.675	284	581	0.015084	0.01420	0.0347	0.0396	0.2092
55	0.430	2.386	0.1288	0.3693	0.760	0.711	284	632	0.016611	0.01517	0.0452	0.0544	0.2304
55	0.430	2.189	0.1175	0.3543	0.697	0.752	284	688	0.015153	0.01455	0.0490	0.0675	0.2102
55	0.430	2.090	0.1105	0.3479	0.665	0.776	284	721	0.014254	0.01429	0.0506	0.0762	0.1977
65	0.430	6.520	0.0000	0.1150	2.075	0.477	284	231	0.000000	0.00472	0.0000	0.0008	0.0000
65	0.430	6.122	0.0210	0.2400	1.949	0.483	284	246	0.002714	0.00986	0.0011	0.0021	0.0376
65	0.430	5.798	0.0466	0.3377	1.845	0.489	284	260	0.006011	0.01387	0.0028	0.0035	0.0834
65	0.430	5.504	0.0653	0.4317	1.752	0.495	284	274	0.008419	0.01773	0.0043	0.0052	0.1168
65	0.430	5.192	0.0849	0.5076	1.653	0.503	284	290	0.010951	0.02084	0.0063	0.0073	0.1519
65	0.430	4.991	0.0982	0.5585	1.589	0.508	284	302	0.012670	0.02293	0.0079	0.0090	0.1757
65	0.430	4.785	0.1122	0.6077	1.523	0.514	284	315	0.014477	0.02495	0.0098	0.0111	0.2008
65	0.430	4.590	0.1257	0.6462	1.461	0.521	284	328	0.016215	0.02653	0.0119	0.0134	0.2249
65	0.430	4.483	0.1299	0.6527	1.427	0.525	284	336	0.016751	0.02680	0.0129	0.0145	0.2324
65	0.430	4.389	0.1343	0.6566	1.397	0.529	284	343	0.017324	0.02696	0.0139	0.0155	0.2403
65	0.430	4.287	0.1352	0.6447	1.364	0.533	284	352	0.017438	0.02647	0.0147	0.0164	0.2419
65	0.430	4.193	0.1364	0.6358	1.335	0.537	284	359	0.017593	0.02611	0.0155	0.0173	0.2440
65	0.430	4.089	0.1368	0.6293	1.301	0.542	284	369	0.017650	0.02584	0.0164	0.0184	0.2448
65	0.430	3.988	0.1396	0.6335	1.269	0.547	284	378	0.018004	0.02601	0.0175	0.0200	0.2497
65	0.430	3.785	0.1444	0.6415	1.205	0.559	284	398	0.018624	0.02634	0.0202	0.0237	0.2583
65	0.430	3.677	0.1480	0.6444	1.170	0.566	284	410	0.019092	0.02646	0.0219	0.0259	0.2648
65	0.430	3.477	0.1476	0.6492	1.107	0.580	284	433	0.019044	0.02666	0.0244	0.0309	0.2642
65	0.430	3.280	0.1352	0.6154	1.044	0.595	284	459	0.017438	0.02527	0.0251	0.0349	0.2419
65	0.430	2.978	0.1079	0.5469	0.948	0.625	284	506	0.013923	0.02246	0.0243	0.0414	0.1931
70	0.430	8.550	0.0000	0.3400	2.722	0.458	284	176	0.000000	0.01396	0.0000	0.0011	0.0000
70	0.430	8.105	0.0179	0.4578	2.580	0.461	284	186	0.002303	0.01880	0.0005	0.0017	0.0320
70	0.430	7.818	0.0402	0.5689	2.489	0.463	284	193	0.005188	0.02336	0.0013	0.0024	0.0720
70	0.430	7.506	0.0566	0.6388	2.389	0.466	284	201	0.007300	0.02623	0.0020	0.0030	0.1013
70	0.430	7.202	0.0745	0.7357	2.293	0.469	284	209	0.009614	0.03021	0.0029	0.0039	0.1333
70	0.430	6.894	0.0915	0.8095	2.194	0.473	284	219	0.011802	0.03324	0.0039	0.0049	0.1637
70	0.430	6.584	0.1037	0.8637	2.096	0.476	284	229	0.013379	0.03547	0.0048	0.0061	0.1856
70	0.430	6.290	0.1222	0.9223	2.002	0.481	284	240	0.015767	0.03787	0.0062	0.0074	0.2187
70	0.430	6.085	0.1301	0.9549	1.937	0.484	284	248	0.016780	0.03921	0.0070	0.0085	0.2328
70	0.430	5.975	0.1350	0.9644	1.902	0.486	284	252	0.017420	0.03960	0.0076	0.0090	0.2416
70	0.430	5.877	0.1379	0.9695	1.871	0.488	284	256	0.017794	0.03981	0.0080	0.0096	0.2468
70	0.430	5.673	0.1421	0.9674	1.806	0.492	284	266	0.018328	0.03972	0.0088	0.0106	0.2542
70	0.430	5.374	0.1433	0.9449	1.710	0.498	284	280	0.018492	0.03880	0.0099	0.0122	0.2565
70	0.430	5.074	0.1478	0.9321	1.615	0.506	284	297	0.019073	0.03828	0.0115	0.0143	0.2646
70	0.430	4.779	0.1520	0.9132	1.521	0.515	284	315	0.019609	0.03750	0.0133	0.0167	0.2720
70	0.430	4.464	0.1528	0.9019	1.421	0.526	284	338	0.019714	0.03703	0.0153	0.0203	0.2735
70	0.430	4.177	0.1454	0.8737	1.329	0.538	284	361	0.018757	0.03588	0.0167	0.0240	0.2602
70	0.430	3.983	0.1329	0.8314	1.268	0.548	284	378	0.017143	0.03414	0.0168	0.0263	0.2378

Beta 0.75 R [deg]	Tunnel Mach No.	Propeller Advance Ratio	Prop Thrust Coeff. Cth	Prop Power Coeff. Cph	Inflow Ratio J/pi Lamda	Helical Mach Number	S.L. Forward Speed [knots]	Std. Tip Speed [ft/sec]	Rotor Thrust Coeff. Ct Rotor	Rotor Power Coeff. Cp Rotor	George Schairer Coefficients T/qD^2	P/qVD^2	Rotor Ct over Sigma
40	0.530	2.200	0.0000	0.0145	0.700	0.924	350	844	0.000000	0.0005954	0.0000	0.0027	0.0000
40	0.530	2.109	0.0117	0.0371	0.671	0.951	350	881	0.001508	0.00152	0.0053	0.0079	0.0209
40	0.530	2.005	0.0240	0.0599	0.638	0.985	350	927	0.003101	0.00246	0.0120	0.0149	0.0430
40	0.530	1.902	0.0365	0.0854	0.605	1.023	350	977	0.004715	0.00351	0.0202	0.0248	0.0654
40	0.530	1.794	0.0493	0.1083	0.571	1.069	350	1035	0.006355	0.00445	0.0306	0.0375	0.0881
40	0.530	1.692	0.0630	0.1364	0.539	1.118	350	1098	0.008129	0.00560	0.0440	0.0563	0.1128
40	0.530	1.588	0.0744	0.1584	0.506	1.175	350	1170	0.009599	0.00651	0.0590	0.0791	0.1332
45	0.530	2.650	0.0000	0.0180	0.844	0.822	350	701	0.000000	0.00074	0.0000	0.0019	0.0000
45	0.530	2.513	0.0215	0.0641	0.800	0.849	350	739	0.002777	0.00263	0.0068	0.0081	0.0385
45	0.530	2.407	0.0372	0.0993	0.766	0.872	350	772	0.004798	0.00408	0.0128	0.0142	0.0666
45	0.530	2.305	0.0525	0.1306	0.734	0.896	350	806	0.006775	0.00536	0.0198	0.0213	0.0940
45	0.530	2.196	0.0643	0.1556	0.699	0.925	350	846	0.008291	0.00639	0.0267	0.0294	0.1150
45	0.530	2.093	0.0740	0.1769	0.666	0.956	350	887	0.009542	0.00727	0.0338	0.0386	0.1324
45	0.530	1.989	0.0842	0.1976	0.633	0.991	350	934	0.010868	0.00812	0.0426	0.0502	0.1508
45	0.530	1.887	0.0919	0.2155	0.601	1.029	350	984	0.011851	0.00885	0.0516	0.0642	0.1644
45	0.530	1.783	0.0994	0.2346	0.568	1.074	350	1042	0.012824	0.00963	0.0625	0.0828	0.1779
45	0.530	1.673	0.1074	0.2546	0.532	1.128	350	1111	0.013854	0.01045	0.0768	0.1088	0.1922
45	0.530	1.580	0.1106	0.2635	0.503	1.180	350	1176	0.014265	0.01082	0.0886	0.1336	0.1979
45	0.530	1.477	0.1102	0.2658	0.470	1.245	350	1257	0.014218	0.01092	0.1010	0.1649	0.1972
50	0.530	3.240	0.0000	0.0210	1.031	0.738	350	573	0.000000	0.00086	0.0000	0.0012	0.0000
50	0.530	3.111	0.0162	0.0611	0.990	0.753	350	597	0.002089	0.00251	0.0033	0.0041	0.0290
50	0.530	3.009	0.0283	0.0956	0.958	0.766	350	617	0.003654	0.00392	0.0063	0.0070	0.0507
50	0.530	2.909	0.0411	0.1296	0.926	0.780	350	639	0.005305	0.00532	0.0097	0.0105	0.0736
50	0.530	2.808	0.0545	0.1629	0.894	0.795	350	662	0.007032	0.00669	0.0138	0.0147	0.0975
50	0.530	2.703	0.0663	0.1913	0.860	0.813	350	687	0.008550	0.00785	0.0181	0.0194	0.1186
50	0.530	2.598	0.0798	0.2256	0.827	0.832	350	715	0.010296	0.00926	0.0237	0.0257	0.1428
50	0.530	2.388	0.1041	0.2781	0.760	0.876	350	778	0.013426	0.01142	0.0365	0.0408	0.1862
50	0.530	2.311	0.1106	0.2932	0.736	0.894	350	804	0.014265	0.01204	0.0414	0.0475	0.1979
50	0.530	1.979	0.1224	0.3265	0.630	0.994	350	938	0.015792	0.01341	0.0625	0.0842	0.2190
50	0.530	1.779	0.1205	0.3321	0.566	1.075	350	1044	0.015543	0.01364	0.0761	0.1179	0.2156
65	0.530	6.283	0.0000	0.1650	2.000	0.593	350	296	0.000000	0.00678	0.0000	0.0013	0.0000
65	0.530	6.116	0.0145	0.2220	1.947	0.596	350	304	0.001869	0.00911	0.0008	0.0019	0.0259
65	0.530	5.691	0.0505	0.3721	1.811	0.605	350	326	0.006515	0.01528	0.0031	0.0040	0.0904
65	0.530	5.291	0.0788	0.4793	1.684	0.616	350	351	0.010167	0.01968	0.0056	0.0065	0.1410
65	0.530	5.296	0.0807	0.4826	1.686	0.616	350	351	0.010412	0.01982	0.0058	0.0065	0.1444
65	0.530	5.092	0.0926	0.5354	1.621	0.623	350	365	0.011940	0.02199	0.0071	0.0081	0.1656
65	0.530	5.094	0.0936	0.5406	1.621	0.623	350	365	0.012076	0.02220	0.0072	0.0082	0.1675
65	0.530	4.897	0.1062	0.5874	1.559	0.630	350	379	0.013704	0.02412	0.0089	0.0100	0.1901
65	0.530	4.698	0.1211	0.6390	1.496	0.638	350	395	0.015621	0.02624	0.0110	0.0123	0.2167
65	0.530	4.507	0.1334	0.6798	1.435	0.646	350	412	0.017209	0.02791	0.0131	0.0149	0.2387
65	0.530	4.107	0.1419	0.6692	1.307	0.667	350	452	0.018301	0.02748	0.0168	0.0193	0.2538
65	0.530	4.104	0.1435	0.6725	1.306	0.667	350	453	0.018515	0.02762	0.0170	0.0195	0.2568
65	0.530	3.700	0.1537	0.7058	1.178	0.695	350	502	0.019829	0.02898	0.0225	0.0279	0.2750
65	0.530	3.305	0.1482	0.6713	1.052	0.731	350	562	0.019119	0.02757	0.0271	0.0372	0.2652
65	0.530	3.011	0.1092	0.5638	0.958	0.766	350	617	0.014083	0.02315	0.0241	0.0413	0.1953
40	0.600	1.991	0.0000	0.0195	0.634	1.121	397	1056	0.000000	0.0008007	0.0000	0.0049	0.0000
40	0.600	1.947	0.0071	0.0341	0.620	1.139	397	1080	0.000921	0.00140	0.0038	0.0092	0.0128
40	0.600	1.900	0.0159	0.0504	0.605	1.160	397	1107	0.002046	0.00207	0.0088	0.0147	0.0284
40	0.600	1.843	0.0239	0.0670	0.587	1.186	397	1141	0.003080	0.00275	0.0141	0.0214	0.0427
40	0.600	1.795	0.0325	0.0839	0.571	1.210	397	1172	0.004195	0.00345	0.0202	0.0290	0.0582
40	0.600	1.690	0.0477	0.1142	0.538	1.267	397	1245	0.006150	0.00469	0.0334	0.0474	0.0853

Beta 0.75 R [deg]	Tunnel Mach No.	Propeller Advance Ratio	Prop Thrust Coeff. Cth	Prop Power Coeff. Cph	Inflow Ratio J/pi Lamda	Helical Mach Number	S.L. Forward Speed [knots]	Std. Tip Speed [ft/sec]	Rotor Thrust Coeff. Ct Rotor	Rotor Power Coeff. Cp Rotor	George Schairer Coefficients T/qD^2	George Schairer Coefficients P/qVD^2	Rotor Ct over Sigma
45	0.600	2.540	0.0000	0.0150	0.809	0.954	397	828	0.000000	0.00062	0.0000	0.0018	0.0000
45	0.600	2.498	0.0051	0.0273	0.795	0.964	397	842	0.000659	0.00112	0.0016	0.0035	0.0091
45	0.600	2.394	0.0191	0.0602	0.762	0.990	397	878	0.002469	0.00247	0.0067	0.0088	0.0342
45	0.600	2.294	0.0320	0.0914	0.730	1.017	397	917	0.004128	0.00375	0.0122	0.0151	0.0573
45	0.600	2.193	0.0449	0.1211	0.698	1.048	397	959	0.005786	0.00497	0.0187	0.0230	0.0803
45	0.600	2.094	0.0571	0.1503	0.667	1.082	397	1004	0.007369	0.00617	0.0261	0.0327	0.1022
45	0.600	1.994	0.0696	0.1775	0.635	1.120	397	1055	0.008976	0.00729	0.0350	0.0448	0.1245
45	0.600	1.898	0.0781	0.1974	0.604	1.161	397	1108	0.010075	0.00811	0.0434	0.0578	0.1397
45	0.600	1.791	0.0865	0.2147	0.570	1.211	397	1174	0.011158	0.00882	0.0539	0.0747	0.1548
45	0.600	1.689	0.0940	0.2317	0.538	1.267	397	1245	0.012131	0.00952	0.0660	0.0962	0.1683
50	0.600	3.245	0.0000	0.0240	1.033	0.835	397	648	0.000000	0.00099	0.0000	0.0014	0.0000
50	0.600	3.096	0.0127	0.0577	0.985	0.855	397	679	0.001641	0.00237	0.0027	0.0039	0.0228
50	0.600	2.995	0.0292	0.1040	0.953	0.870	397	702	0.003764	0.00427	0.0065	0.0077	0.0522
50	0.600	2.897	0.0418	0.1386	0.922	0.885	397	726	0.005398	0.00569	0.0100	0.0114	0.0749
50	0.600	2.794	0.0541	0.1704	0.889	0.903	397	753	0.006979	0.00700	0.0139	0.0156	0.0968
50	0.600	2.689	0.0636	0.1914	0.856	0.923	397	782	0.008205	0.00786	0.0176	0.0197	0.1138
50	0.600	2.591	0.0722	0.2121	0.825	0.943	397	812	0.009314	0.00871	0.0215	0.0244	0.1292
50	0.600	2.488	0.0807	0.2331	0.792	0.966	397	845	0.010406	0.00957	0.0261	0.0302	0.1443
50	0.600	2.290	0.0957	0.2739	0.729	1.019	397	918	0.012351	0.01125	0.0365	0.0456	0.1713
50	0.600	2.200	0.1026	0.2930	0.700	1.046	397	956	0.013231	0.01203	0.0424	0.0550	0.1835
50	0.600	2.085	0.1089	0.3141	0.664	1.085	397	1009	0.014052	0.01290	0.0501	0.0693	0.1949
50	0.600	1.985	0.1124	0.3244	0.632	1.123	397	1059	0.014502	0.01332	0.0571	0.0829	0.2011
50	0.600	1.888	0.1131	0.3303	0.601	1.165	397	1114	0.014593	0.01356	0.0635	0.0982	0.2024
50	0.600	1.788	0.1125	0.3339	0.569	1.213	397	1176	0.014518	0.01371	0.0704	0.1169	0.2014
55	0.600	3.860	0.0000	0.0345	1.229	0.774	397	545	0.000000	0.00142	0.0000	0.0012	0.0000
55	0.600	3.805	0.0075	0.0602	1.211	0.778	397	553	0.000972	0.00247	0.0010	0.0022	0.0135
55	0.600	3.707	0.0212	0.1061	1.180	0.787	397	567	0.002741	0.00436	0.0031	0.0042	0.0380
55	0.600	3.601	0.0359	0.1510	1.146	0.796	397	584	0.004627	0.00620	0.0055	0.0065	0.0642
55	0.600	3.499	0.0474	0.1881	1.114	0.806	397	601	0.006117	0.00772	0.0077	0.0088	0.0848
55	0.600	3.399	0.0607	0.2306	1.082	0.817	397	619	0.007834	0.00947	0.0105	0.0117	0.1087
55	0.600	3.294	0.0725	0.2651	1.049	0.829	397	638	0.009347	0.01088	0.0134	0.0148	0.1297
55	0.600	3.197	0.0864	0.3026	1.018	0.841	397	658	0.011142	0.01243	0.0169	0.0185	0.1546
55	0.600	3.094	0.0981	0.3333	0.985	0.855	397	680	0.012656	0.01369	0.0205	0.0225	0.1756
55	0.600	2.992	0.1077	0.3571	0.952	0.870	397	703	0.013900	0.01467	0.0241	0.0267	0.1928
55	0.600	2.787	0.1152	0.3743	0.887	0.904	397	754	0.014856	0.01537	0.0296	0.0346	0.2061
55	0.600	2.587	0.1209	0.3914	0.824	0.944	397	813	0.015591	0.01607	0.0361	0.0452	0.2163
55	0.600	2.392	0.1240	0.4074	0.761	0.990	397	879	0.015997	0.01673	0.0433	0.0595	0.2219
55	0.600	2.192	0.1215	0.4147	0.698	1.049	397	960	0.015669	0.01703	0.0506	0.0788	0.2173
65	0.600	6.285	0.0000	0.1750	2.001	0.671	397	335	0.000000	0.00719	0.0000	0.0014	0.0000
65	0.600	6.116	0.0171	0.2396	1.947	0.675	397	344	0.002210	0.00984	0.0009	0.0021	0.0307
65	0.600	5.817	0.0484	0.3675	1.852	0.682	397	362	0.006241	0.01509	0.0029	0.0037	0.0866
65	0.600	5.507	0.0716	0.4667	1.753	0.691	397	382	0.009239	0.01916	0.0047	0.0056	0.1282
65	0.600	5.194	0.0939	0.5542	1.653	0.701	397	405	0.012111	0.02276	0.0070	0.0079	0.1680
65	0.600	4.895	0.1171	0.6401	1.558	0.713	397	430	0.015109	0.02629	0.0098	0.0109	0.2096
65	0.600	4.787	0.1219	0.6635	1.524	0.718	397	439	0.015731	0.02725	0.0106	0.0121	0.2182
65	0.600	4.684	0.1292	0.6859	1.491	0.722	397	449	0.016671	0.02817	0.0118	0.0134	0.2312
65	0.600	4.592	0.1362	0.7065	1.462	0.727	397	458	0.017570	0.02901	0.0129	0.0146	0.2437
65	0.600	4.482	0.1421	0.7253	1.427	0.733	397	469	0.018327	0.02978	0.0141	0.0161	0.2542
65	0.600	4.394	0.1479	0.7393	1.399	0.738	397	479	0.019082	0.03036	0.0153	0.0174	0.2647
65	0.600	4.299	0.1527	0.7406	1.368	0.743	397	489	0.019703	0.03041	0.0165	0.0186	0.2733
65	0.600	4.192	0.1550	0.7333	1.334	0.750	397	502	0.019998	0.03011	0.0176	0.0199	0.2774
65	0.600	4.097	0.1550	0.7305	1.304	0.756	397	513	0.019990	0.03000	0.0185	0.0212	0.2773
65	0.600	3.801	0.1765	0.8148	1.210	0.778	397	553	0.022770	0.03346	0.0244	0.0297	0.3158
65	0.600	3.486	0.1602	0.7591	1.110	0.808	397	603	0.020669	0.03117	0.0264	0.0358	0.2867
65	0.600	3.186	0.1223	0.6511	1.014	0.843	397	660	0.015781	0.02673	0.0241	0.0403	0.2189
65	0.600	2.996	0.1021	0.6000	0.954	0.869	397	702	0.013169	0.02464	0.0227	0.0446	0.1827

Beta 0.75 R [deg]	Tunnel Mach No.	Propeller Advance Ratio	Prop Thrust Coeff. Cth	Prop Power Coeff. Cph	Inflow Ratio J/pi Lamda	Helical Mach Number	S.L. Forward Speed [knots]	Std. Tip Speed [ft/sec]	Rotor Thrust Coeff. Ct Rotor	Rotor Power Coeff. Cp Rotor	George Schairer Coefficients T/qD^2	P/qVD^2	Rotor Ct over Sigma
45	0.650	2.400	0.0000	0.0225	0.764	1.071	430	949	0.000000	0.0009239	0.0000	0.0033	0.0000
45	0.650	2.308	0.0119	0.0521	0.735	1.098	430	987	0.001533	0.00214	0.0045	0.0085	0.0213
45	0.650	2.204	0.0287	0.0933	0.702	1.132	430	1033	0.003698	0.00383	0.0118	0.0174	0.0513
45	0.650	2.100	0.0426	0.1233	0.669	1.169	430	1085	0.005491	0.00506	0.0193	0.0266	0.0762
45	0.650	2.001	0.0563	0.1557	0.637	1.210	430	1139	0.007260	0.00639	0.0281	0.0389	0.1007
45	0.650	1.902	0.0683	0.1838	0.605	1.255	430	1198	0.008808	0.00755	0.0377	0.0534	0.1222
45	0.650	1.820	0.0745	0.1972	0.579	1.297	430	1252	0.009612	0.00810	0.0450	0.0655	0.1333
50	0.650	3.110	0.0000	0.0250	0.990	0.924	430	733	0.000000	0.00103	0.0000	0.0017	0.0000
50	0.650	3.104	0.0007	0.0258	0.988	0.925	430	734	0.000084	0.00106	0.0001	0.0017	0.0012
50	0.650	2.997	0.0120	0.0597	0.954	0.942	430	760	0.001549	0.00245	0.0027	0.0044	0.0215
50	0.650	2.905	0.0221	0.0841	0.925	0.957	430	784	0.002852	0.00345	0.0052	0.0069	0.0396
50	0.650	2.806	0.0320	0.1132	0.893	0.976	430	812	0.004122	0.00465	0.0081	0.0102	0.0572
50	0.650	2.600	0.0535	0.1733	0.828	1.019	430	876	0.006896	0.00712	0.0158	0.0197	0.0957
50	0.650	2.500	0.0645	0.2029	0.796	1.044	430	911	0.008327	0.00833	0.0207	0.0260	0.1155
50	0.650	2.401	0.0742	0.2321	0.764	1.071	430	949	0.009578	0.00953	0.0258	0.0335	0.1329
50	0.650	2.295	0.0838	0.2572	0.730	1.102	430	993	0.010813	0.01056	0.0318	0.0426	0.1500
50	0.650	2.092	0.0979	0.2911	0.666	1.173	430	1089	0.012624	0.01195	0.0447	0.0636	0.1751
50	0.650	1.994	0.1004	0.3047	0.635	1.213	430	1143	0.012955	0.01251	0.0505	0.0769	0.1797
50	0.650	1.897	0.1033	0.3180	0.604	1.257	430	1201	0.013326	0.01306	0.0574	0.0932	0.1848
55	0.650	3.870	0.0000	0.0400	1.232	0.837	430	589	0.000000	0.00164	0.0000	0.0014	0.0000
55	0.650	3.801	0.0097	0.0691	1.210	0.843	430	599	0.001253	0.00284	0.0013	0.0025	0.0174
55	0.650	3.701	0.0234	0.1167	1.178	0.853	430	615	0.003013	0.00479	0.0034	0.0046	0.0418
55	0.650	3.597	0.0383	0.1629	1.145	0.863	430	633	0.004941	0.00669	0.0059	0.0070	0.0685
55	0.650	3.495	0.0502	0.1995	1.113	0.874	430	652	0.006482	0.00819	0.0082	0.0093	0.0899
55	0.650	3.397	0.0592	0.2328	1.081	0.885	430	671	0.007640	0.00956	0.0103	0.0119	0.1060
55	0.650	3.294	0.0683	0.2515	1.049	0.898	430	692	0.008808	0.01033	0.0126	0.0141	0.1222
55	0.650	3.194	0.0754	0.2729	1.017	0.912	430	713	0.009731	0.01120	0.0148	0.0167	0.1350
55	0.650	2.993	0.0893	0.3101	0.953	0.942	430	761	0.011524	0.01273	0.0199	0.0231	0.1598
55	0.650	2.787	0.0998	0.3457	0.887	0.979	430	817	0.012870	0.01419	0.0257	0.0319	0.1785
55	0.650	2.584	0.1076	0.3719	0.822	1.023	430	882	0.013876	0.01527	0.0322	0.0431	0.1925
55	0.650	2.388	0.1130	0.3988	0.760	1.074	430	954	0.014578	0.01637	0.0396	0.0586	0.2022
60	0.650	4.855	0.0000	0.0750	1.545	0.774	430	469	0.000000	0.00308	0.0000	0.0013	0.0000
60	0.650	4.815	0.0050	0.0926	1.533	0.776	430	473	0.000651	0.00380	0.0004	0.0017	0.0090
60	0.650	4.803	0.0063	0.0955	1.529	0.777	430	474	0.000813	0.00392	0.0005	0.0017	0.0113
60	0.650	4.700	0.0154	0.1433	1.496	0.782	430	485	0.001980	0.00588	0.0014	0.0028	0.0275
60	0.650	4.595	0.0291	0.1892	1.463	0.787	430	496	0.003748	0.00777	0.0028	0.0039	0.0520
60	0.650	4.498	0.0423	0.2364	1.432	0.793	430	506	0.005458	0.00971	0.0042	0.0052	0.0757
60	0.650	4.291	0.0616	0.3071	1.366	0.806	430	531	0.007945	0.01261	0.0067	0.0078	0.1102
60	0.650	4.094	0.0810	0.3700	1.303	0.819	430	556	0.010450	0.01519	0.0097	0.0108	0.1450
60	0.650	4.044	0.0910	0.4025	1.287	0.823	430	563	0.011735	0.01653	0.0111	0.0122	0.1628
60	0.650	3.791	0.1242	0.5105	1.207	0.844	430	601	0.016025	0.02096	0.0173	0.0187	0.2223
60	0.650	3.488	0.1320	0.5275	1.110	0.875	430	653	0.017024	0.02166	0.0217	0.0249	0.2361
60	0.650	3.184	0.1282	0.5154	1.014	0.913	430	715	0.016533	0.02116	0.0253	0.0319	0.2293
70	0.650	8.310	0.0000	0.4400	2.645	0.695	430	274	0.000000	0.01807	0.0000	0.0015	0.0000
70	0.650	8.080	0.0152	0.5227	2.572	0.697	430	282	0.001965	0.02146	0.0005	0.0020	0.0273
70	0.650	7.787	0.0424	0.6337	2.479	0.701	430	293	0.005471	0.02602	0.0014	0.0027	0.0759
70	0.650	7.496	0.0614	0.7349	2.386	0.705	430	304	0.007919	0.03018	0.0022	0.0035	0.1098
70	0.650	7.193	0.0843	0.8349	2.290	0.709	430	317	0.010875	0.03429	0.0033	0.0045	0.1508
70	0.650	6.900	0.0976	0.9121	2.196	0.714	430	330	0.012588	0.03745	0.0041	0.0056	0.1746
70	0.650	6.606	0.1184	0.9812	2.103	0.720	430	345	0.015272	0.04029	0.0054	0.0068	0.2118
70	0.650	6.403	0.1184	1.0272	2.038	0.724	430	356	0.015272	0.04218	0.0058	0.0078	0.2118
70	0.650	6.304	0.1355	1.0518	2.007	0.726	430	361	0.017482	0.04319	0.0068	0.0084	0.2425
70	0.650	6.204	0.1372	1.0663	1.975	0.729	430	367	0.017694	0.04379	0.0071	0.0089	0.2454
70	0.650	6.005	0.1508	1.1018	1.911	0.734	430	379	0.019456	0.04524	0.0084	0.0102	0.2699
70	0.650	5.696	0.1601	1.1351	1.813	0.742	430	400	0.020650	0.04661	0.0099	0.0123	0.2864
70	0.650	5.406	0.1678	1.1346	1.721	0.752	430	421	0.021650	0.04659	0.0115	0.0144	0.3003
70	0.650	5.103	0.1748	1.1385	1.624	0.763	430	446	0.022556	0.04675	0.0134	0.0171	0.3129

Beta 0.75 R [deg]	Tunnel Mach No.	Propeller Advance Ratio	Prop Thrust Coeff. Cth	Prop Power Coeff. Cph	Inflow Ratio J/pi Lamda	Helical Mach Number	S.L. Forward Speed [knots]	Std. Tip Speed [ft/sec]	Rotor Thrust Coeff. Ct Rotor	Rotor Power Coeff. Cp Rotor	George Schairer Coefficients T/qD^2	P/qVD^2	Rotor Ct over Sigma
70	0.650	4.892	0.1777	1.1569	1.557	0.772	430	466	0.022929	0.04751	0.0149	0.0198	0.3180
70	0.650	4.600	0.1773	1.1367	1.464	0.787	430	495	0.022870	0.04668	0.0168	0.0234	0.3172
70	0.650	4.299	0.1545	1.0237	1.368	0.805	430	530	0.019931	0.04204	0.0167	0.0258	0.2765
45	0.700	2.310	0.0000	0.0325	0.735	1.182	463	1062	0.000000	0.0013346	0.0000	0.0053	0.0000
45	0.700	2.301	0.0013	0.0361	0.732	1.185	463	1066	0.000168	0.00148	0.0005	0.0059	0.0023
45	0.700	2.202	0.0182	0.0735	0.701	1.219	463	1114	0.002342	0.00302	0.0075	0.0138	0.0325
45	0.700	2.096	0.0331	0.1066	0.667	1.261	463	1171	0.004272	0.00438	0.0151	0.0231	0.0593
45	0.700	2.000	0.0445	0.1339	0.637	1.303	463	1227	0.005736	0.00550	0.0222	0.0335	0.0796
45	0.700	1.960	0.0473	0.1430	0.624	1.322	463	1252	0.006099	0.00587	0.0246	0.0380	0.0846
50	0.700	2.860	0.0000	0.0350	0.910	1.040	463	858	0.000000	0.00144	0.0000	0.0030	0.0000
50	0.700	2.801	0.0082	0.0580	0.892	1.052	463	876	0.001062	0.00238	0.0021	0.0053	0.0147
50	0.700	2.697	0.0242	0.1044	0.858	1.075	463	910	0.003125	0.00429	0.0067	0.0106	0.0433
50	0.700	2.592	0.0387	0.1422	0.825	1.100	463	946	0.004994	0.00584	0.0115	0.0163	0.0693
50	0.700	2.494	0.0515	0.1812	0.794	1.126	463	984	0.006646	0.00744	0.0166	0.0233	0.0922
50	0.700	2.395	0.0619	0.2079	0.762	1.155	463	1024	0.007987	0.00854	0.0216	0.0303	0.1108
50	0.700	2.290	0.0718	0.2352	0.729	1.189	463	1072	0.009267	0.00966	0.0274	0.0392	0.1285
50	0.700	2.188	0.0797	0.2577	0.697	1.225	463	1121	0.010277	0.01058	0.0333	0.0492	0.1426
50	0.700	2.090	0.0847	0.2706	0.665	1.264	463	1174	0.010927	0.01111	0.0388	0.0593	0.1516
50	0.700	1.989	0.0873	0.2808	0.633	1.309	463	1234	0.011264	0.01153	0.0442	0.0714	0.1562
55	0.700	3.750	0.0000	0.0370	1.194	0.913	463	654	0.000000	0.00152	0.0000	0.0014	0.0000
55	0.700	3.683	0.0065	0.0549	1.172	0.920	463	666	0.000842	0.00225	0.0010	0.0022	0.0117
55	0.700	3.587	0.0163	0.0893	1.142	0.931	463	684	0.002097	0.00367	0.0025	0.0039	0.0291
55	0.700	3.488	0.0259	0.1170	1.110	0.942	463	703	0.003343	0.00481	0.0043	0.0055	0.0464
55	0.700	3.386	0.0340	0.1472	1.078	0.955	463	725	0.004380	0.00604	0.0059	0.0076	0.0608
55	0.700	3.289	0.0413	0.1750	1.047	0.968	463	746	0.005332	0.00719	0.0076	0.0098	0.0740
55	0.700	3.187	0.0520	0.2085	1.015	0.983	463	770	0.006714	0.00856	0.0102	0.0129	0.0931
55	0.700	3.085	0.0596	0.2364	0.982	0.999	463	795	0.007692	0.00971	0.0125	0.0161	0.1067
55	0.700	2.990	0.0686	0.2665	0.952	1.015	463	821	0.008854	0.01094	0.0154	0.0199	0.1228
55	0.700	2.784	0.0842	0.3159	0.886	1.055	463	881	0.010860	0.01297	0.0217	0.0293	0.1506
55	0.700	2.388	0.1017	0.3778	0.760	1.157	463	1028	0.013117	0.01552	0.0357	0.0555	0.1819
55	0.700	2.183	0.1076	0.3944	0.695	1.227	463	1124	0.013884	0.01620	0.0452	0.0759	0.1926
60	0.700	4.880	0.0000	0.0650	1.553	0.833	463	503	0.000000	0.00267	0.0000	0.0011	0.0000
60	0.700	4.797	0.0104	0.1098	1.527	0.837	463	511	0.001347	0.00451	0.0009	0.0020	0.0187
60	0.700	4.687	0.0236	0.1721	1.492	0.843	463	523	0.003041	0.00707	0.0021	0.0033	0.0422
60	0.700	4.589	0.0334	0.2038	1.461	0.848	463	535	0.004313	0.00837	0.0032	0.0042	0.0598
60	0.700	4.490	0.0438	0.2458	1.429	0.854	463	546	0.005652	0.01009	0.0043	0.0054	0.0784
60	0.700	4.389	0.0513	0.2757	1.397	0.861	463	559	0.006621	0.01132	0.0053	0.0065	0.0918
60	0.700	4.291	0.0585	0.3009	1.366	0.868	463	572	0.007549	0.01236	0.0064	0.0076	0.1047
60	0.700	4.190	0.0662	0.3247	1.334	0.875	463	586	0.008543	0.01333	0.0075	0.0088	0.1185
60	0.700	4.082	0.0737	0.3465	1.299	0.883	463	601	0.009503	0.01423	0.0088	0.0102	0.1318
60	0.700	3.884	0.0837	0.3814	1.236	0.900	463	632	0.010801	0.01566	0.0111	0.0130	0.1498
60	0.700	3.488	0.1013	0.4412	1.110	0.942	463	703	0.013066	0.01812	0.0167	0.0208	0.1812
60	0.700	3.073	0.1129	0.4939	0.978	1.001	463	798	0.014565	0.02028	0.0239	0.0340	0.2020
60	0.700	2.885	0.1157	0.5125	0.918	1.035	463	850	0.014920	0.02105	0.0278	0.0427	0.2070

Beta 0.75 R [deg]	Tunnel Mach No.	Propeller Advance Ratio	Prop Thrust Coeff. Cth	Prop Power Coeff. Cph	Inflow Ratio J / pi Lamda	Helical Mach Number	S.L. Forward Speed [knots]	Std. Tip Speed [ft/sec]	Rotor Thrust Coeff. Ct Rotor	Rotor Power Coeff. Cp Rotor	George Schairer Coefficients T/qD^2	P/qVD^2	Rotor Ct over Sigma
65	0.700	6.320	0.0000	0.1500	2.012	0.782	463	388	0.000000	0.00616	0.0000	0.0012	0.0000
65	0.700	6.202	0.0116	0.2156	1.974	0.785	463	396	0.001495	0.00885	0.0006	0.0018	0.0207
65	0.700	5.610	0.0646	0.4483	1.786	0.802	463	437	0.008339	0.01841	0.0041	0.0051	0.1157
65	0.700	5.395	0.0789	0.5148	1.717	0.810	463	455	0.010182	0.02114	0.0054	0.0066	0.1412
65	0.700	5.300	0.0885	0.5452	1.687	0.814	463	463	0.011423	0.02239	0.0063	0.0073	0.1584
65	0.700	5.191	0.0981	0.5829	1.652	0.818	463	473	0.012659	0.02394	0.0073	0.0083	0.1756
65	0.700	5.093	0.1020	0.6000	1.621	0.822	463	482	0.013155	0.02464	0.0079	0.0091	0.1825
65	0.700	4.995	0.1070	0.6170	1.590	0.827	463	491	0.013807	0.02534	0.0086	0.0099	0.1915
65	0.700	4.896	0.1199	0.6691	1.559	0.832	463	501	0.015461	0.02748	0.0100	0.0114	0.2145
65	0.700	4.791	0.1245	0.6872	1.525	0.837	463	512	0.016063	0.02822	0.0108	0.0125	0.2228
65	0.700	4.695	0.1308	0.7116	1.495	0.842	463	523	0.016874	0.02922	0.0119	0.0137	0.2341
65	0.700	4.391	0.1389	0.7372	1.398	0.861	463	559	0.017913	0.03027	0.0144	0.0174	0.2485
65	0.700	4.093	0.1367	0.7262	1.303	0.882	463	599	0.017634	0.02982	0.0163	0.0212	0.2446
65	0.700	3.795	0.1299	0.6922	1.208	0.909	463	646	0.016754	0.02842	0.0180	0.0253	0.2324
65	0.700	3.493	0.1237	0.6741	1.112	0.942	463	702	0.015952	0.02768	0.0203	0.0316	0.2213
65	0.700	3.184	0.1201	0.6667	1.014	0.983	463	770	0.015487	0.02738	0.0237	0.0413	0.2148
65	0.700	2.993	0.1185	0.6712	0.953	1.015	463	820	0.015293	0.02756	0.0265	0.0501	0.2121
70	0.700	8.260	0.0000	0.4600	2.629	0.749	463	297	0.000000	0.01889	0.0000	0.0016	0.0000
70	0.700	8.165	0.0057	0.4941	2.599	0.750	463	300	0.000734	0.02029	0.0002	0.0018	0.0102
70	0.700	7.950	0.0263	0.5905	2.531	0.753	463	309	0.003388	0.02425	0.0008	0.0024	0.0470
70	0.700	7.576	0.0591	0.7372	2.411	0.758	463	324	0.007620	0.03027	0.0021	0.0034	0.1057
70	0.700	7.365	0.0709	0.8090	2.344	0.761	463	333	0.009142	0.03322	0.0026	0.0041	0.1268
70	0.700	7.152	0.0870	0.8908	2.276	0.765	463	343	0.011229	0.03658	0.0034	0.0049	0.1558
70	0.700	6.963	0.0990	0.9403	2.216	0.768	463	352	0.012775	0.03861	0.0041	0.0056	0.1772
70	0.700	6.767	0.1124	1.0029	2.154	0.772	463	363	0.014499	0.04118	0.0049	0.0065	0.2011
70	0.700	6.562	0.1274	1.0637	2.089	0.776	463	374	0.016434	0.04368	0.0059	0.0075	0.2280
70	0.700	6.361	0.1382	1.1189	2.025	0.781	463	386	0.017829	0.04595	0.0068	0.0087	0.2473
70	0.700	6.163	0.1524	1.1750	1.962	0.786	463	398	0.019662	0.04825	0.0080	0.0100	0.2727
70	0.700	5.956	0.1639	1.2256	1.896	0.791	463	412	0.021141	0.05033	0.0092	0.0116	0.2932
70	0.700	5.762	0.1738	1.2549	1.834	0.797	463	426	0.022425	0.05153	0.0105	0.0131	0.3111
70	0.700	5.536	0.1759	1.2494	1.762	0.805	463	443	0.022695	0.05131	0.0115	0.0147	0.3148
70	0.700	5.352	0.1675	1.2080	1.704	0.812	463	458	0.021613	0.04961	0.0117	0.0158	0.2998
70	0.700	5.155	0.1568	1.1750	1.641	0.820	463	476	0.020228	0.04825	0.0118	0.0172	0.2806
45	0.750	2.243	0.0000	0.0395	0.714	1.291	496	1172	0.000000	0.001622	0.0000	0.0070	0.0000
45	0.750	2.198	0.0074	0.0570	0.700	1.308	496	1196	0.000958	0.00234	0.0031	0.0107	0.0133
45	0.750	2.097	0.0244	0.0949	0.667	1.351	496	1254	0.003145	0.00390	0.0111	0.0206	0.0436
50	0.750	2.740	0.0000	0.0480	0.872	1.141	496	959	0.000000	0.00197	0.0000	0.0047	0.0000
50	0.750	2.677	0.0095	0.0741	0.852	1.156	496	982	0.001220	0.00304	0.0026	0.0077	0.0169
50	0.750	2.587	0.0250	0.1155	0.824	1.180	496	1016	0.003221	0.00474	0.0075	0.0133	0.0447
50	0.750	2.488	0.0388	0.1511	0.792	1.208	496	1057	0.005002	0.00621	0.0125	0.0196	0.0694
50	0.750	2.388	0.0481	0.1807	0.760	1.239	496	1101	0.006205	0.00742	0.0169	0.0265	0.0861
50	0.750	2.286	0.0568	0.2070	0.728	1.275	496	1150	0.007324	0.00850	0.0217	0.0347	0.1016
50	0.750	2.185	0.0666	0.2324	0.696	1.313	496	1203	0.008587	0.00954	0.0279	0.0445	0.1191
50	0.750	2.088	0.0756	0.2558	0.665	1.355	496	1259	0.009748	0.01050	0.0347	0.0562	0.1352
55	0.750	3.380	0.0000	0.0500	1.076	1.024	496	778	0.000000	0.00205	0.0000	0.0026	0.0000
55	0.750	3.278	0.0139	0.1009	1.043	1.039	496	802	0.001796	0.00414	0.0026	0.0057	0.0249
55	0.750	3.174	0.0292	0.1530	1.010	1.055	496	828	0.003771	0.00628	0.0058	0.0096	0.0523
55	0.750	3.076	0.0421	0.1987	0.979	1.072	496	855	0.005425	0.00816	0.0089	0.0137	0.0753
55	0.750	2.984	0.0516	0.2325	0.950	1.089	496	881	0.006663	0.00955	0.0116	0.0175	0.0924
55	0.750	2.873	0.0620	0.2655	0.915	1.111	496	915	0.008002	0.01090	0.0150	0.0224	0.1110
55	0.750	2.776	0.0697	0.2886	0.884	1.133	496	947	0.008985	0.01185	0.0181	0.0270	0.1246
55	0.750	2.584	0.0858	0.3403	0.823	1.181	496	1017	0.011064	0.01397	0.0257	0.0394	0.1535
55	0.750	2.386	0.0923	0.3625	0.759	1.240	496	1102	0.011910	0.01488	0.0324	0.0534	0.1652

Beta 0.75 R [deg]	Tunnel Mach No.	Propeller Advance Ratio	Prop Thrust Coeff. Cth	Prop Power Coeff. Cph	Inflow Ratio J / pi Lamda	Helical Mach Number	S.L. Forward Speed [knots]	Std. Tip Speed [ft/sec]	Rotor Thrust Coeff. Ct Rotor	Rotor Power Coeff. Cp Rotor	George Schairer Coefficients T/qD^2	P/qVD^2	Rotor Ct over Sigma
60	0.750	4.430	0.0000	0.0800	1.410	0.919	496	593	0.000000	0.00329	0.0000	0.0018	0.0000
60	0.750	4.377	0.0036	0.1020	1.393	0.923	496	601	0.000458	0.00419	0.0004	0.0024	0.0064
60	0.750	4.277	0.0149	0.1251	1.361	0.931	496	615	0.001916	0.00514	0.0016	0.0032	0.0266
60	0.750	4.181	0.0241	0.1635	1.331	0.938	496	629	0.003103	0.00671	0.0028	0.0045	0.0430
60	0.750	3.974	0.0411	0.2335	1.265	0.956	496	662	0.005307	0.00959	0.0052	0.0074	0.0736
60	0.750	3.882	0.0482	0.2652	1.236	0.965	496	677	0.006214	0.01089	0.0064	0.0091	0.0862
60	0.750	3.778	0.0582	0.2975	1.203	0.975	496	696	0.007511	0.01222	0.0082	0.0110	0.1042
60	0.750	3.674	0.0649	0.3329	1.169	0.987	496	716	0.008376	0.01367	0.0096	0.0134	0.1162
60	0.750	3.479	0.0797	0.3930	1.107	1.011	496	756	0.010282	0.01614	0.0132	0.0187	0.1426
60	0.750	3.275	0.0898	0.4291	1.042	1.039	496	803	0.011579	0.01762	0.0167	0.0244	0.1606
60	0.750	3.077	0.0995	0.4772	0.980	1.072	496	854	0.012834	0.01959	0.0210	0.0327	0.1780
60	0.750	2.877	0.1058	0.5027	0.916	1.110	496	914	0.013648	0.02064	0.0256	0.0422	0.1893
60	0.750	2.679	0.1095	0.5133	0.853	1.156	496	981	0.014131	0.02108	0.0305	0.0534	0.1960
65	0.750	6.150	0.0000	0.1500	1.958	0.842	496	427	0.000000	0.00616	0.0000	0.0013	0.0000
65	0.750	5.898	0.0188	0.2409	1.877	0.850	496	446	0.002423	0.00989	0.0011	0.0023	0.0336
65	0.750	5.597	0.0415	0.3491	1.782	0.860	496	470	0.005356	0.01434	0.0027	0.0040	0.0743
65	0.750	5.493	0.0497	0.3799	1.748	0.864	496	479	0.006408	0.01560	0.0033	0.0046	0.0889
65	0.750	5.392	0.0550	0.4073	1.716	0.868	496	488	0.007097	0.01672	0.0038	0.0052	0.0984
65	0.750	5.298	0.0620	0.4315	1.686	0.872	496	496	0.007997	0.01772	0.0044	0.0058	0.1109
65	0.750	5.191	0.0669	0.4521	1.652	0.877	496	506	0.008627	0.01857	0.0050	0.0065	0.1197
65	0.750	4.987	0.0756	0.4915	1.587	0.886	496	527	0.009754	0.02018	0.0061	0.0079	0.1353
65	0.750	4.685	0.0879	0.5431	1.491	0.903	496	561	0.011344	0.02230	0.0080	0.0106	0.1573
65	0.750	4.390	0.0951	0.5846	1.397	0.922	496	599	0.012269	0.02400	0.0099	0.0138	0.1702
65	0.750	4.091	0.1074	0.6289	1.302	0.946	496	643	0.013857	0.02582	0.0128	0.0184	0.1922
65	0.750	3.784	0.1119	0.6544	1.205	0.975	496	695	0.014438	0.02687	0.0156	0.0242	0.2003
65	0.750	3.490	0.1176	0.6883	1.111	1.009	496	753	0.015169	0.02826	0.0193	0.0324	0.2104
65	0.750	3.182	0.1179	0.6940	1.013	1.054	496	826	0.015203	0.02850	0.0233	0.0431	0.2109
65	0.750	2.987	0.1167	0.6867	0.951	1.089	496	880	0.015060	0.02820	0.0262	0.0516	0.2089
70	0.750	8.200	0.0000	0.5100	2.610	0.803	496	321	0.000000	0.02094	0.0000	0.0018	0.0000
70	0.750	8.076	0.0087	0.5180	2.571	0.805	496	326	0.001118	0.02127	0.0003	0.0020	0.0155
70	0.750	7.873	0.0262	0.6195	2.506	0.808	496	334	0.003374	0.02544	0.0008	0.0025	0.0468
70	0.750	7.666	0.0391	0.6768	2.440	0.811	496	343	0.005045	0.02779	0.0013	0.0030	0.0700
70	0.750	7.567	0.0500	0.7230	2.409	0.812	496	347	0.006450	0.02969	0.0017	0.0033	0.0895
70	0.750	7.371	0.0618	0.7816	2.346	0.815	496	357	0.007971	0.03210	0.0023	0.0039	0.1106
70	0.750	7.076	0.0776	0.8619	2.252	0.821	496	371	0.010007	0.03539	0.0031	0.0049	0.1388
70	0.750	6.774	0.0911	0.9156	2.156	0.827	496	388	0.011756	0.03760	0.0040	0.0059	0.1631
70	0.750	6.469	0.1035	0.9615	2.059	0.834	496	406	0.013353	0.03948	0.0049	0.0071	0.1852
70	0.750	6.378	0.1059	0.9693	2.030	0.836	496	412	0.013656	0.03980	0.0052	0.0075	0.1894
70	0.750	6.179	0.1103	0.9920	1.967	0.841	496	425	0.014228	0.04074	0.0058	0.0084	0.1974
70	0.750	5.981	0.1151	0.9967	1.904	0.847	496	440	0.014849	0.04093	0.0064	0.0093	0.2060
70	0.750	5.677	0.1207	1.0092	1.807	0.857	496	463	0.015573	0.04144	0.0075	0.0110	0.2160
70	0.750	5.472	0.1205	1.0027	1.742	0.865	496	480	0.015540	0.04117	0.0080	0.0122	0.2156
70	0.750	5.172	0.1184	0.9928	1.646	0.878	496	508	0.015269	0.04077	0.0089	0.0144	0.2118
50	0.800	2.710	0.0000	0.0630	0.863	1.225	529	1035	0.000000	0.002587	0.0000	0.0063	0.0000
50	0.800	2.493	0.0288	0.1391	0.793	1.287	529	1125	0.003717	0.00571	0.0093	0.0180	0.0516
50	0.800	2.391	0.0413	0.1715	0.761	1.321	529	1173	0.005322	0.00704	0.0144	0.0251	0.0738
50	0.800	2.291	0.0559	0.2089	0.729	1.358	529	1224	0.007207	0.00858	0.0213	0.0347	0.1000
50	0.800	2.195	0.0679	0.2378	0.699	1.397	529	1277	0.008760	0.00977	0.0282	0.0450	0.1215

PROP_1.XLS

Beta 0.75 R [deg]	Tunnel Mach No.	Propeller Advance Ratio	Prop Thrust Coeff. Cth	Prop Power Coeff. Cph	Inflow Ratio J / pi Lamda	Helical Mach Number	S.L. Forward Speed [knots]	Std. Tip Speed [ft/sec]	Rotor Thrust Coeff. Ct Rotor	Rotor Power Coeff. Cp Rotor	George Schairer Coefficients T/qD^2	P/qVD^2	Rotor Ct over Sigma
55	0.800	3.275	0.0000	0.0750	1.042	1.109	529	856	0.000000	0.00308	0.0000	0.0043	0.0000
55	0.800	3.189	0.0093	0.1061	1.015	1.123	529	879	0.001197	0.00436	0.0018	0.0065	0.0166
55	0.800	3.091	0.0255	0.1557	0.984	1.141	529	907	0.003293	0.00639	0.0053	0.0105	0.0457
55	0.800	2.994	0.0375	0.1995	0.953	1.160	529	937	0.004837	0.00819	0.0084	0.0149	0.0671
55	0.800	2.788	0.0551	0.2574	0.888	1.205	529	1006	0.007105	0.01057	0.0142	0.0238	0.0986
55	0.800	2.694	0.0632	0.2852	0.858	1.229	529	1041	0.008149	0.01171	0.0174	0.0292	0.1130
55	0.800	2.596	0.0718	0.3130	0.826	1.256	529	1080	0.009262	0.01285	0.0213	0.0358	0.1285
55	0.800	2.505	0.0784	0.3331	0.797	1.283	529	1119	0.010111	0.01368	0.0250	0.0424	0.1402
55	0.800	2.298	0.0932	0.3722	0.731	1.355	529	1220	0.012021	0.01528	0.0353	0.0614	0.1667
60	0.800	4.075	0.0000	0.1075	1.297	1.010	529	688	0.000000	0.00441	0.0000	0.0032	0.0000
60	0.800	3.967	0.0126	0.1604	1.263	1.021	529	707	0.001629	0.00659	0.0016	0.0051	0.0226
60	0.800	3.868	0.0240	0.2118	1.231	1.031	529	725	0.003098	0.00870	0.0032	0.0073	0.0430
60	0.800	3.771	0.0351	0.2559	1.200	1.041	529	744	0.004533	0.01051	0.0049	0.0095	0.0629
60	0.800	3.677	0.0461	0.3026	1.170	1.052	529	763	0.005950	0.01242	0.0068	0.0122	0.0825
60	0.800	3.575	0.0547	0.3364	1.138	1.065	529	784	0.007054	0.01381	0.0086	0.0147	0.0978
60	0.800	3.473	0.0632	0.3699	1.106	1.079	529	807	0.008159	0.01519	0.0105	0.0177	0.1132
60	0.800	3.377	0.0700	0.3929	1.075	1.093	529	830	0.009033	0.01613	0.0123	0.0204	0.1253
60	0.800	3.279	0.0784	0.4221	1.044	1.108	529	855	0.010120	0.01733	0.0146	0.0239	0.1404
60	0.800	3.178	0.0845	0.4420	1.011	1.125	529	882	0.010900	0.01815	0.0167	0.0275	0.1512
60	0.800	3.070	0.0893	0.4624	0.977	1.145	529	913	0.011520	0.01899	0.0189	0.0320	0.1598
60	0.800	2.974	0.0928	0.4745	0.947	1.164	529	943	0.011978	0.01948	0.0210	0.0361	0.1661
60	0.800	2.880	0.0946	0.4813	0.917	1.184	529	974	0.012199	0.01976	0.0228	0.0403	0.1692
60	0.800	2.779	0.0969	0.4908	0.885	1.207	529	1009	0.012496	0.02015	0.0251	0.0457	0.1733
65	0.800	5.330	0.0000	0.1700	1.697	0.929	529	526	0.000000	0.00698	0.0000	0.0022	0.0000
65	0.800	5.182	0.0125	0.2307	1.649	0.936	529	541	0.001608	0.00947	0.0009	0.0033	0.0223
65	0.800	4.989	0.0305	0.3039	1.588	0.945	529	562	0.003928	0.01248	0.0024	0.0049	0.0545
65	0.800	4.885	0.0377	0.3520	1.555	0.951	529	574	0.004867	0.01445	0.0032	0.0060	0.0675
65	0.800	4.792	0.0464	0.3929	1.525	0.957	529	585	0.005985	0.01613	0.0040	0.0071	0.0830
65	0.800	4.687	0.0521	0.4236	1.492	0.963	529	598	0.006720	0.01739	0.0047	0.0082	0.0932
65	0.800	4.591	0.0604	0.4648	1.462	0.969	529	611	0.007796	0.01909	0.0057	0.0096	0.1081
65	0.800	4.497	0.0664	0.4989	1.431	0.976	529	624	0.008566	0.02049	0.0066	0.0110	0.1188
65	0.800	4.389	0.0732	0.5275	1.397	0.984	529	639	0.009447	0.02166	0.0076	0.0125	0.1310
65	0.800	4.094	0.0886	0.6000	1.303	1.008	529	685	0.011435	0.02464	0.0106	0.0175	0.1586
65	0.800	3.794	0.0992	0.6545	1.208	1.039	529	739	0.012799	0.02688	0.0138	0.0240	0.1775
65	0.800	3.499	0.1072	0.6832	1.114	1.075	529	801	0.013831	0.02805	0.0175	0.0319	0.1919
65	0.800	3.290	0.1106	0.6853	1.047	1.106	529	852	0.014272	0.02814	0.0204	0.0385	0.1980
65	0.800	3.114	0.1108	0.6822	0.991	1.136	529	900	0.014289	0.02801	0.0228	0.0452	0.1982
70	0.800	7.200	0.0000	0.4400	2.292	0.873	529	389	0.000000	0.01807	0.0000	0.0024	0.0000
70	0.800	7.084	0.0065	0.4788	2.255	0.875	529	396	0.000837	0.01966	0.0003	0.0027	0.0116
70	0.800	6.880	0.0177	0.5427	2.190	0.879	529	408	0.002285	0.02229	0.0007	0.0033	0.0317
70	0.800	6.687	0.0301	0.6242	2.129	0.884	529	419	0.003877	0.02563	0.0013	0.0042	0.0538
70	0.800	6.496	0.0414	0.6585	2.068	0.889	529	432	0.005341	0.02704	0.0020	0.0048	0.0741
70	0.800	6.372	0.0449	0.6853	2.028	0.892	529	440	0.005790	0.02814	0.0022	0.0053	0.0803
70	0.800	6.192	0.0517	0.7223	1.971	0.897	529	453	0.006671	0.02966	0.0027	0.0061	0.0925
70	0.800	5.892	0.0634	0.7685	1.875	0.907	529	476	0.008185	0.03156	0.0037	0.0075	0.1135
70	0.800	5.705	0.0712	0.8105	1.816	0.913	529	492	0.009184	0.03328	0.0044	0.0087	0.1274
70	0.800	5.597	0.0734	0.8257	1.782	0.917	529	501	0.009463	0.03391	0.0047	0.0094	0.1313
70	0.800	5.509	0.0787	0.8470	1.754	0.921	529	509	0.010157	0.03478	0.0052	0.0101	0.1409
70	0.800	5.401	0.0795	0.8533	1.719	0.925	529	519	0.010260	0.03504	0.0055	0.0108	0.1423
70	0.800	5.198	0.0847	0.8814	1.655	0.935	529	539	0.010928	0.03619	0.0063	0.0126	0.1516
70	0.800	4.811	0.0961	0.9102	1.531	0.955	529	583	0.012401	0.03738	0.0083	0.0164	0.1720
70	0.800	4.617	0.1011	0.9407	1.470	0.968	529	607	0.013043	0.03863	0.0095	0.0191	0.1809
70	0.800	4.410	0.1045	0.9477	1.404	0.982	529	636	0.013476	0.03892	0.0107	0.0221	0.1869
70	0.800	4.217	0.1060	0.9459	1.342	0.998	529	665	0.013679	0.03884	0.0119	0.0252	0.1897
70	0.800	4.020	0.1076	0.9494	1.280	1.015	529	698	0.013882	0.03898	0.0133	0.0292	0.1926
70	0.800	3.822	0.1063	0.9315	1.216	1.036	529	734	0.013713	0.03825	0.0146	0.0334	0.1902

Beta 0.75 R [deg]	Tunnel Mach No.	Propeller Advance Ratio	Prop Thrust Coeff. Cth	Prop Power Coeff. Cph	Inflow Ratio J/pi Lamda	Helical Mach Number	S.L. Forward Speed [knots]	Std. Tip Speed [ft/sec]	Rotor Thrust Coeff. Ct Rotor	Rotor Power Coeff. Cp Rotor	George Schairer Coefficients T/qD^2	P/qVD^2	Rotor Ct over Sigma
55	0.850	3.235	0.0000	0.0950	1.030	1.185	562	921	0.000000	0.0039011	0.0000	0.0056	0.0000
55	0.850	3.108	0.0149	0.1457	0.989	1.209	562	959	0.001926	0.00598	0.0031	0.0097	0.0267
55	0.850	3.006	0.0274	0.1793	0.957	1.230	562	991	0.003534	0.00736	0.0061	0.0132	0.0490
55	0.850	2.802	0.0514	0.2563	0.892	1.277	562	1063	0.006632	0.01052	0.0131	0.0233	0.0920
55	0.850	2.692	0.0635	0.2845	0.857	1.306	562	1107	0.008189	0.01168	0.0175	0.0292	0.1136
55	0.850	2.593	0.0746	0.3207	0.825	1.335	562	1149	0.009629	0.01317	0.0222	0.0368	0.1336
55	0.850	2.492	0.0819	0.3426	0.793	1.368	562	1195	0.010571	0.01407	0.0264	0.0443	0.1466
55	0.850	2.397	0.0874	0.3536	0.763	1.401	562	1243	0.011269	0.01452	0.0304	0.0513	0.1563
60	0.850	3.960	0.0000	0.1450	1.261	1.085	562	752	0.000000	0.00595	0.0000	0.0047	0.0000
60	0.850	3.786	0.0208	0.2223	1.205	1.105	562	787	0.002685	0.00913	0.0029	0.0082	0.0372
60	0.850	3.697	0.0312	0.2630	1.177	1.115	562	806	0.004031	0.01080	0.0046	0.0104	0.0559
60	0.850	3.586	0.0414	0.3012	1.141	1.130	562	831	0.005336	0.01237	0.0064	0.0131	0.0740
60	0.850	3.493	0.0487	0.3274	1.112	1.143	562	853	0.006287	0.01344	0.0080	0.0154	0.0872
60	0.850	3.298	0.0622	0.3787	1.050	1.174	562	903	0.008028	0.01555	0.0114	0.0211	0.1114
60	0.850	3.185	0.0706	0.4083	1.014	1.194	562	935	0.009106	0.01676	0.0139	0.0253	0.1263
60	0.850	3.090	0.0763	0.4293	0.983	1.212	562	964	0.009839	0.01763	0.0160	0.0291	0.1365
60	0.850	2.984	0.0820	0.4483	0.950	1.234	562	998	0.010579	0.01841	0.0184	0.0338	0.1467
60	0.850	2.894	0.0857	0.4609	0.921	1.254	562	1029	0.011059	0.01892	0.0205	0.0380	0.1534
60	0.850	2.790	0.0908	0.4765	0.888	1.280	562	1068	0.011715	0.01957	0.0233	0.0439	0.1625
60	0.850	2.688	0.0966	0.4905	0.856	1.307	562	1108	0.012464	0.02014	0.0267	0.0505	0.1729
65	0.850	4.950	0.0000	0.2450	1.576	1.007	562	602	0.000000	0.01006	0.0000	0.0040	0.0000
65	0.850	4.814	0.0143	0.3102	1.532	1.015	562	619	0.001840	0.01274	0.0012	0.0056	0.0255
65	0.850	4.613	0.0351	0.3951	1.468	1.028	562	646	0.004525	0.01622	0.0033	0.0080	0.0628
65	0.850	4.506	0.0439	0.4394	1.434	1.036	562	661	0.005664	0.01804	0.0043	0.0096	0.0786
65	0.850	4.410	0.0521	0.4752	1.404	1.044	562	676	0.006726	0.01951	0.0054	0.0111	0.0933
65	0.850	4.310	0.0586	0.5032	1.372	1.052	562	691	0.007554	0.02067	0.0063	0.0126	0.1048
65	0.850	4.103	0.0711	0.5650	1.306	1.071	562	726	0.009168	0.02320	0.0084	0.0164	0.1272
65	0.850	3.992	0.0759	0.5785	1.271	1.082	562	746	0.009789	0.02375	0.0095	0.0182	0.1358
65	0.850	3.895	0.0806	0.5956	1.240	1.092	562	765	0.010400	0.02446	0.0106	0.0202	0.1443
65	0.850	3.877	0.0849	0.6000	1.234	1.094	562	768	0.010951	0.02464	0.0113	0.0206	0.1519
65	0.850	3.796	0.0861	0.6135	1.208	1.103	562	785	0.011102	0.02519	0.0119	0.0224	0.1540
65	0.850	3.680	0.0896	0.6296	1.171	1.118	562	810	0.011554	0.02585	0.0132	0.0253	0.1603
65	0.850	3.592	0.0910	0.6296	1.143	1.129	562	830	0.011745	0.02585	0.0141	0.0272	0.1629
65	0.850	3.297	0.0982	0.6576	1.049	1.174	562	904	0.012674	0.02700	0.0181	0.0367	0.1758
65	0.850	3.155	0.1000	0.6630	1.004	1.200	562	944	0.012900	0.02723	0.0201	0.0422	0.1789
70	0.850	6.250	0.0000	0.4800	1.989	0.951	562	477	0.000000	0.01971	0.0000	0.0039	0.0000
70	0.850	6.093	0.0135	0.5567	1.939	0.956	562	489	0.001739	0.02286	0.0007	0.0049	0.0241
70	0.850	5.781	0.0361	0.6854	1.840	0.967	562	515	0.004660	0.02814	0.0022	0.0071	0.0646
70	0.850	5.475	0.0530	0.7756	1.743	0.980	562	544	0.006843	0.03185	0.0035	0.0095	0.0949
70	0.850	5.333	0.0607	0.8130	1.698	0.987	562	559	0.007830	0.03338	0.0043	0.0107	0.1086
70	0.850	5.176	0.0685	0.8545	1.647	0.994	562	576	0.008834	0.03509	0.0051	0.0123	0.1225
70	0.850	5.036	0.0732	0.8752	1.603	1.002	562	592	0.009445	0.03594	0.0058	0.0137	0.1310
70	0.850	4.880	0.0809	0.9100	1.553	1.011	562	611	0.010441	0.03737	0.0068	0.0157	0.1448
70	0.850	4.569	0.0893	0.9424	1.454	1.032	562	652	0.011520	0.03870	0.0086	0.0198	0.1598
70	0.850	4.276	0.0934	0.9546	1.361	1.055	562	697	0.012047	0.03920	0.0102	0.0244	0.1671
70	0.850	3.972	0.0980	0.9414	1.264	1.084	562	750	0.012641	0.03866	0.0124	0.0300	0.1753
55	0.900	3.245	0.0000	0.0950	1.033	1.253	595	972	0.000000	0.0039011	0.0000	0.0056	0.0000
55	0.900	3.193	0.0062	0.1158	1.016	1.263	595	988	0.000793	0.00475	0.0012	0.0071	0.0110
55	0.900	3.089	0.0190	0.1572	0.983	1.284	595	1021	0.002447	0.00646	0.0040	0.0107	0.0339
55	0.900	2.987	0.0315	0.1931	0.951	1.306	595	1056	0.004059	0.00793	0.0071	0.0145	0.0563
55	0.900	2.888	0.0412	0.2251	0.919	1.330	595	1092	0.005321	0.00924	0.0099	0.0187	0.0738
55	0.900	2.785	0.0489	0.2467	0.886	1.357	595	1133	0.006314	0.01013	0.0126	0.0228	0.0876
55	0.900	2.683	0.0561	0.2667	0.854	1.386	595	1176	0.007233	0.01095	0.0156	0.0276	0.1003
55	0.900	2.581	0.0612	0.2808	0.822	1.418	595	1222	0.007901	0.01153	0.0184	0.0327	0.1096
55	0.900	2.482	0.0682	0.3018	0.790	1.452	595	1271	0.008796	0.01239	0.0221	0.0395	0.1220

Beta 0.75 R [deg]	Tunnel Mach No.	Propeller Advance Ratio	Prop Thrust Coeff. Cth	Prop Power Coeff. Cph	Inflow Ratio J / pi Lamda	Helical Mach Number	S.L. Forward Speed [knots]	Std. Tip Speed [ft/sec]	Rotor Thrust Coeff. Ct Rotor	Rotor Power Coeff. Cp Rotor	George Schairer Coefficients T/qD^2	P/qVD^2	Rotor Ct over Sigma
60	0.900	3.880	0.0000	0.1750	1.235	1.158	595	813	0.000000	0.00719	0.0000	0.0060	0.0000
60	0.900	3.795	0.0095	0.2075	1.208	1.168	595	831	0.001227	0.00852	0.0013	0.0076	0.0170
60	0.900	3.587	0.0322	0.2876	1.142	1.196	595	879	0.004151	0.01181	0.0050	0.0125	0.0576
60	0.900	3.488	0.0431	0.3234	1.110	1.211	595	904	0.005563	0.01328	0.0071	0.0152	0.0772
60	0.900	3.387	0.0536	0.3573	1.078	1.228	595	931	0.006908	0.01467	0.0093	0.0184	0.0958
60	0.900	3.178	0.0703	0.4114	1.012	1.265	595	993	0.009063	0.01689	0.0139	0.0256	0.1257
60	0.900	3.081	0.0769	0.4347	0.981	1.285	595	1024	0.009914	0.01785	0.0162	0.0297	0.1375
60	0.900	2.978	0.0824	0.4476	0.948	1.308	595	1059	0.010633	0.01838	0.0186	0.0339	0.1475
60	0.900	2.787	0.0873	0.4605	0.887	1.356	595	1132	0.011268	0.01891	0.0225	0.0425	0.1563
60	0.900	2.568	0.0901	0.4571	0.817	1.422	595	1228	0.011619	0.01877	0.0273	0.0540	0.1612
65	0.900	4.850	0.0000	0.3100	1.544	1.072	595	650	0.000000	0.01273	0.0000	0.0054	0.0000
65	0.900	4.688	0.0129	0.3560	1.492	1.083	595	673	0.001663	0.01462	0.0012	0.0069	0.0231
65	0.900	4.402	0.0346	0.4424	1.401	1.106	595	717	0.004459	0.01817	0.0036	0.0104	0.0619
65	0.900	4.098	0.0541	0.5340	1.304	1.134	595	770	0.006980	0.02193	0.0064	0.0155	0.0968
65	0.900	3.771	0.0748	0.5998	1.200	1.171	595	836	0.009644	0.02463	0.0105	0.0224	0.1338
65	0.900	3.676	0.0783	0.6132	1.170	1.184	595	858	0.010095	0.02518	0.0116	0.0247	0.1400
65	0.900	3.572	0.0828	0.6260	1.137	1.199	595	883	0.010679	0.02570	0.0130	0.0275	0.1481
65	0.900	3.470	0.0865	0.6352	1.105	1.214	595	909	0.011164	0.02609	0.0144	0.0304	0.1549
65	0.900	3.366	0.0909	0.6430	1.071	1.231	595	937	0.011730	0.02640	0.0160	0.0337	0.1627
65	0.900	3.297	0.0924	0.6435	1.049	1.243	595	957	0.011915	0.02642	0.0170	0.0359	0.1653
65	0.900	3.246	0.0930	0.6433	1.033	1.253	595	972	0.011998	0.02642	0.0177	0.0376	0.1664
70	0.900	6.000	0.0000	0.6230	1.910	1.016	595	526	0.000000	0.02558	0.0000	0.0058	0.0000
70	0.900	5.699	0.0214	0.7199	1.814	1.028	595	554	0.002757	0.02956	0.0013	0.0078	0.0382
70	0.900	5.405	0.0395	0.8066	1.720	1.041	595	584	0.005102	0.03312	0.0027	0.0102	0.0708
70	0.900	5.092	0.0548	0.8599	1.621	1.057	595	619	0.007072	0.03531	0.0042	0.0130	0.0981
70	0.900	4.963	0.0613	0.8755	1.580	1.065	595	636	0.007907	0.03595	0.0050	0.0143	0.1097
70	0.900	4.800	0.0681	0.8969	1.528	1.076	595	657	0.008783	0.03683	0.0059	0.0162	0.1218
70	0.900	4.657	0.0718	0.9060	1.482	1.086	595	677	0.009259	0.03720	0.0066	0.0179	0.1284
70	0.900	4.506	0.0756	0.9146	1.434	1.097	595	700	0.009752	0.03756	0.0074	0.0200	0.1353
70	0.900	4.340	0.0788	0.9205	1.382	1.111	595	727	0.010170	0.03780	0.0084	0.0225	0.1411
70	0.900	4.190	0.0831	0.9257	1.334	1.125	595	753	0.010721	0.03801	0.0095	0.0252	0.1487
55	0.925	3.190	0.0000	0.0970	1.015	1.298	611	1016	0.000000	0.0039832	0.0000	0.0060	0.0000
55	0.925	3.088	0.0113	0.1340	0.983	1.320	611	1050	0.001461	0.00550	0.0024	0.0091	0.0203
55	0.925	2.987	0.0232	0.1708	0.951	1.342	611	1085	0.002996	0.00702	0.0052	0.0128	0.0416
55	0.925	2.885	0.0337	0.2045	0.918	1.368	611	1124	0.004348	0.00840	0.0081	0.0170	0.0603
55	0.925	2.780	0.0444	0.2348	0.885	1.396	611	1166	0.005732	0.00964	0.0115	0.0219	0.0795
55	0.925	2.674	0.0531	0.2600	0.851	1.427	611	1212	0.006855	0.01067	0.0149	0.0272	0.0951
55	0.925	2.509	0.0653	0.2943	0.799	1.482	611	1292	0.008426	0.01208	0.0207	0.0372	0.1169
60	0.925	3.910	0.0000	0.1750	1.245	1.187	611	829	0.000000	0.00719	0.0000	0.0059	0.0000
60	0.925	3.775	0.0152	0.2256	1.201	1.203	611	859	0.001955	0.00926	0.0021	0.0084	0.0271
60	0.925	3.667	0.0276	0.2623	1.167	1.218	611	884	0.003558	0.01077	0.0041	0.0106	0.0494
60	0.925	3.571	0.0376	0.2975	1.137	1.232	611	908	0.004851	0.01222	0.0059	0.0131	0.0673
60	0.925	3.470	0.0443	0.3235	1.104	1.248	611	934	0.005715	0.01328	0.0074	0.0155	0.0793
60	0.925	3.262	0.0567	0.3627	1.038	1.284	611	994	0.007317	0.01490	0.0107	0.0209	0.1015
60	0.925	3.164	0.0606	0.3771	1.007	1.304	611	1025	0.007822	0.01548	0.0121	0.0238	0.1085
60	0.925	3.068	0.0659	0.3910	0.977	1.324	611	1057	0.008500	0.01605	0.0140	0.0271	0.1179
60	0.925	2.968	0.0702	0.4048	0.945	1.347	611	1092	0.009055	0.01662	0.0159	0.0310	0.1256
60	0.925	2.868	0.0736	0.4158	0.913	1.372	611	1131	0.009499	0.01707	0.0179	0.0353	0.1318
60	0.925	2.760	0.0786	0.4251	0.879	1.401	611	1175	0.010146	0.01746	0.0206	0.0404	0.1407
60	0.925	2.565	0.0831	0.4431	0.816	1.463	611	1264	0.010717	0.01820	0.0253	0.0525	0.1487

Beta 0.75 R [deg]	Tunnel Mach No.	Propeller Advance Ratio	Prop Thrust Coeff. Cth	Prop Power Coeff. Cph	Inflow Ratio J / pi Lamda	Helical Mach Number	S.L. Forward Speed [knots]	Std. Tip Speed [ft/sec]	Rotor Thrust Coeff. Ct Rotor	Rotor Power Coeff. Cp Rotor	George Schairer Coefficients		Rotor Ct over Sigma
											T/qD^2	P/qVD^2	
65	0.925	4.770	0.0000	0.3300	1.518	1.108	611	680	0.000000	0.01355	0.0000	0.0061	0.0000
65	0.925	4.703	0.0053	0.3510	1.497	1.112	611	689	0.000679	0.01441	0.0005	0.0067	0.0094
65	0.925	4.394	0.0318	0.4502	1.399	1.137	611	738	0.004103	0.01849	0.0033	0.0106	0.0569
65	0.925	4.092	0.0535	0.5247	1.303	1.166	611	792	0.006908	0.02154	0.0064	0.0153	0.0958
65	0.925	3.790	0.0707	0.5849	1.206	1.202	611	856	0.009118	0.02402	0.0098	0.0215	0.1265
65	0.925	3.685	0.0759	0.5909	1.173	1.216	611	880	0.009788	0.02426	0.0112	0.0236	0.1358
65	0.925	3.583	0.0805	0.6114	1.140	1.230	611	905	0.010382	0.02511	0.0125	0.0266	0.1440
65	0.925	3.480	0.0835	0.6218	1.108	1.246	611	932	0.010777	0.02553	0.0138	0.0295	0.1495
65	0.925	3.372	0.0870	0.6192	1.073	1.264	611	962	0.011227	0.02543	0.0153	0.0323	0.1557
65	0.925	3.283	0.0862	0.6195	1.045	1.280	611	987	0.011120	0.02544	0.0160	0.0350	0.1542
65	0.925	3.172	0.0872	0.6140	1.010	1.302	611	1022	0.011245	0.02521	0.0173	0.0385	0.1560
70	0.925	5.830	0.0000	0.6600	1.856	1.051	611	556	0.000000	0.02710	0.0000	0.0067	0.0000
70	0.925	5.817	0.0009	0.6644	1.852	1.051	611	557	0.000116	0.02728	0.0001	0.0068	0.0016
70	0.925	5.617	0.0151	0.7212	1.788	1.060	611	577	0.001942	0.02962	0.0010	0.0081	0.0269
70	0.925	5.401	0.0282	0.7757	1.719	1.070	611	600	0.003634	0.03185	0.0019	0.0098	0.0504
70	0.925	5.202	0.0381	0.8188	1.656	1.081	611	623	0.004915	0.03362	0.0028	0.0116	0.0682
70	0.925	5.004	0.0489	0.8531	1.593	1.092	611	648	0.006305	0.03503	0.0039	0.0136	0.0875
70	0.925	4.808	0.0580	0.8834	1.530	1.105	611	674	0.007477	0.03628	0.0050	0.0159	0.1037
70	0.925	4.606	0.0659	0.8993	1.466	1.120	611	704	0.008498	0.03693	0.0062	0.0184	0.1179
70	0.925	4.197	0.0756	0.9061	1.336	1.155	611	772	0.009755	0.03721	0.0086	0.0245	0.1353
70	0.925	4.003	0.0787	0.8975	1.274	1.176	611	810	0.010156	0.03685	0.0098	0.0280	0.1409

This page intentionally left blank

APPENDIX C

PROP 2 is the Three Bladed Full-Scale Supersonic Propeller

Tested By Evans & Liner. NACA TR 1375 (1958)

Originally In RM L53F01 (July 30, 1953)

Data read from graphs by Frank Harris in Aug. 1995.

Propeller is Curtiss-Wright Corp. Design No. 109622

NACA 16 series Symmetrical Airfoils Of Varying Thickness

Const. Chord, 3-Blades, 9.75 ft. Dia., Nom. Solidity =0.22918,

r/R	c/R	t/c	Beta (deg)	Design Cl	Beta Ref. to x = 0.75
0.2735	0.24	0.06	68.7116	0	24.141
0.28	0.2400	0.0565	68.08	0.00	23.51
0.29	0.2400	0.0535	67.17	0.00	22.60
0.30	0.2400	0.0515	66.32	0.00	21.75
0.31	0.2400	0.0496	65.51	0.00	20.94
0.32	0.2400	0.0484	64.76	0.00	20.19
0.33	0.2400	0.0471	64.04	0.00	19.47
0.34	0.2400	0.0459	63.36	0.00	18.79
0.35	0.2400	0.0447	62.71	0.00	18.14
0.36	0.2400	0.0436	62.09	0.00	17.51
0.37	0.2400	0.0426	61.49	0.00	16.91
0.38	0.2400	0.0418	60.91	0.00	16.33
0.39	0.2400	0.0411	60.34	0.00	15.77
0.40	0.2400	0.0404	59.79	0.00	15.22
0.41	0.2400	0.0397	59.26	0.00	14.69
0.42	0.2400	0.0390	58.73	0.00	14.16
0.43	0.2400	0.0384	58.21	0.00	13.64
0.44	0.2400	0.0377	57.70	0.00	13.13
0.45	0.2400	0.0371	57.21	0.00	12.63
0.46	0.2400	0.0365	56.71	0.00	12.14
0.47	0.2400	0.0359	56.23	0.00	11.66
0.48	0.2400	0.0353	55.76	0.00	11.19
0.49	0.2400	0.0348	55.30	0.00	10.73
0.50	0.2400	0.0343	54.85	0.00	10.28
0.51	0.2400	0.0338	54.39	0.00	9.82
0.52	0.2400	0.0334	53.95	0.00	9.38
0.53	0.2400	0.0330	53.51	0.00	8.94
0.54	0.2400	0.0326	53.06	0.00	8.49
0.55	0.2400	0.0321	52.62	0.00	8.05
0.56	0.2400	0.0317	52.18	0.00	7.61
0.57	0.2400	0.0313	51.75	0.00	7.18
0.58	0.2400	0.0309	51.31	0.00	6.74
0.59	0.2400	0.0305	50.88	0.00	6.31
0.60	0.2400	0.0302	50.45	0.00	5.88
0.61	0.2400	0.0298	50.03	0.00	5.46

r/R	c/R	t/c	Beta (deg)	Design Cl	Beta Ref. to x = 0.75
0.62	0.2400	0.0294	49.61	0.00	5.04
0.63	0.2400	0.0290	49.19	0.00	4.62
0.64	0.2400	0.0287	48.78	0.00	4.21
0.65	0.2400	0.0283	48.37	0.00	3.80
0.66	0.2400	0.0280	47.97	0.00	3.40
0.67	0.2400	0.0276	47.57	0.00	3.00
0.68	0.2400	0.0273	47.18	0.00	2.60
0.69	0.2400	0.0270	46.79	0.00	2.22
0.70	0.2400	0.0266	46.40	0.00	1.83
0.71	0.2400	0.0263	46.03	0.00	1.46
0.72	0.2400	0.0260	45.65	0.00	1.08
0.73	0.2400	0.0257	45.29	0.00	0.72
0.74	0.2400	0.0254	44.93	0.00	0.36
0.75	0.2400	0.0251	44.57	0.00	0.00
0.76	0.2400	0.0248	44.22	0.00	-0.35
0.77	0.2400	0.0245	43.88	0.00	-0.69
0.78	0.2400	0.0242	43.54	0.00	-1.03
0.79	0.2400	0.0240	43.20	0.00	-1.37
0.80	0.2400	0.0237	42.88	0.00	-1.69
0.81	0.2400	0.0235	42.55	0.00	-2.02
0.82	0.2400	0.0232	42.24	0.00	-2.33
0.83	0.2400	0.0230	41.92	0.00	-2.65
0.84	0.2400	0.0227	41.62	0.00	-2.95
0.85	0.2400	0.0225	41.31	0.00	-3.26
0.86	0.2400	0.0223	41.02	0.00	-3.55
0.87	0.2400	0.0221	40.72	0.00	-3.85
0.88	0.2400	0.0219	40.44	0.00	-4.13
0.89	0.2400	0.0217	40.15	0.00	-4.42
0.90	0.2400	0.0215	39.87	0.00	-4.70
0.91	0.2400	0.0213	39.59	0.00	-4.98
0.92	0.2400	0.0211	39.32	0.00	-5.25
0.93	0.2400	0.0210	39.05	0.00	-5.52
0.94	0.2400	0.0208	38.78	0.00	-5.79
0.95	0.2400	0.0206	38.52	0.00	-6.05
0.96	0.2400	0.0205	38.25	0.00	-6.32
0.97	0.2400	0.0204	37.99	0.00	-6.58
0.975	0.2400	0.0203	37.86	0.00	-6.71
0.98	0.2400	0.0202	37.73	0.00	-6.84
0.985	0.2400	0.0202	37.60	0.00	-6.97
0.99	0.2400	0.0201	37.47	0.00	-7.10
0.995	0.2400	0.0201	37.34	0.00	-7.23
1.00	0.2400	0.0200	37.21	0.00	-7.36

Three Bladed Full-Scale Supersonic Propeller Tested By Evans & Liner. NACA TR 1375 (1958)													
Originally In RM L53F01 (July 30, 1953)													
Data read from graphs by Frank Harris in Aug. 1995. Caution because data entry has not been proof read only once.													
Propeller is Curtiss-Wright Corp. Design No. 109622													
Solid 6415 Steel, NACA 16 series Symmetrical Airfoils Of Varying Thickness													
Constant Chord, 3-Blades, 9.75 ft. Dia., Nom. Solidity =0.229183													

Experimental Data Read From Graphs							Reference	Speeds	Reduced Experimental Data				
Data	Data	Data	Data	Data	Rotor		S.L.	Std.	Rotor	Rotor			Rotor
			Prop	Prop	Inflow		Forward	Tip	Thrust	Power	George Schairer		Ct
Beta	Tunnel	Propeller	Thrust	Power	Ratio	Helical	Speed	Speed	Coeff.	Coeff.	Coefficients		over
0.75 R	Mach	Advance	Coeff.	Coeff.	J / pi	Mach			Ct Rotor	Cp Rotor	T/qD^2	P/qVD^2	Sigma
[deg]	No.	Ratio	Cth	Cph	Lamda	Number	[knots]	[ft/sec]					
20.2	0.097	0.416	0.1396	0.1301	0.132	0.737	64	817	0.018005	0.005342	1.6127	3.6126	0.0786
20.2	0.123	0.530	0.1194	0.1102	0.169	0.741	82	817	0.015401	0.004524	0.8504	1.4812	0.0672
20.2	0.141	0.608	0.1001	0.0935	0.194	0.744	94	817	0.012908	0.003840	0.5412	0.8317	0.0563
20.2	0.157	0.676	0.0809	0.0759	0.215	0.747	104	817	0.010440	0.003118	0.3540	0.4913	0.0456
20.2	0.169	0.726	0.0612	0.0602	0.231	0.750	112	817	0.007890	0.002471	0.2318	0.3139	0.0344
20.2	0.180	0.774	0.0460	0.0455	0.246	0.752	119	817	0.005939	0.001867	0.1537	0.1960	0.0259
20.2	0.191	0.823	0.0274	0.0320	0.262	0.755	127	817	0.003540	0.001315	0.0810	0.1149	0.0154
20.2	0.202	0.868	0.0125	0.0175	0.276	0.758	134	817	0.001611	0.000718	0.0331	0.0534	0.0070
20.2	0.211	0.906	0.0000	0.0071	0.288	0.760	139	817	0.000000	0.000292	0.0000	0.0191	0.0000
20.2	0.214	0.919	-0.0044	0.0034	0.293	0.761	141	817	-0.000570	0.000138	-0.0105	0.0086	-0.0025
20.2	0.226	0.972	-0.0220	-0.0142	0.310	0.765	150	817	-0.002843	-0.000584	-0.0466	-0.0309	-0.0124
20.2	0.235	1.011	-0.0398	-0.0288	0.322	0.768	156	817	-0.005128	-0.001181	-0.0778	-0.0557	-0.0224
20.2	0.251	1.078	-0.0536	-0.0449	0.343	0.772	166	817	-0.006908	-0.001843	-0.0921	-0.0716	-0.0301
20.2	0.254	1.091	-0.0697	-0.0589	0.347	0.773	168	817	-0.008997	-0.002418	-0.1173	-0.0908	-0.0393
25.2	0.134	0.577	0.1767	0.2018	0.184	0.743	89	817	0.022794	0.008287	1.0617	2.1020	0.0995
25.2	0.153	0.657	0.1559	0.1769	0.209	0.746	101	817	0.020107	0.007264	0.7220	1.2469	0.0877
25.2	0.167	0.718	0.1353	0.1527	0.228	0.749	110	817	0.017455	0.006270	0.5256	0.8266	0.0762
25.2	0.181	0.776	0.1191	0.1364	0.247	0.753	119	817	0.015366	0.005600	0.3954	0.5832	0.0670
25.2	0.195	0.840	0.1017	0.1133	0.267	0.756	129	817	0.013125	0.004650	0.2882	0.3818	0.0573
25.2	0.206	0.887	0.0872	0.1011	0.282	0.759	136	817	0.011254	0.004150	0.2218	0.2897	0.0491
25.2	0.204	0.879	0.0855	0.0990	0.280	0.759	135	817	0.011025	0.004065	0.2212	0.2915	0.0481
25.2	0.215	0.926	0.0692	0.0826	0.295	0.762	142	817	0.008925	0.003391	0.1613	0.2080	0.0389
25.2	0.225	0.966	0.0573	0.0683	0.308	0.764	149	817	0.007397	0.002803	0.1229	0.1513	0.0323
25.2	0.236	1.016	0.0387	0.0491	0.323	0.768	156	817	0.004987	0.002015	0.0750	0.0937	0.0218
25.2	0.246	1.060	0.0277	0.0381	0.337	0.771	163	817	0.003575	0.001566	0.0494	0.0641	0.0156
25.2	0.257	1.104	0.0125	0.0204	0.351	0.774	170	817	0.001611	0.000837	0.0205	0.0303	0.0070
25.2	0.264	1.134	0.0022	0.0098	0.361	0.777	174	817	0.000280	0.000403	0.0034	0.0135	0.0012
25.2	0.265	1.138	0.0000	0.0080	0.362	0.777	175	817	0.000000	0.000329	0.0000	0.0109	0.0000
25.2	0.273	1.175	-0.0144	-0.0085	0.374	0.780	181	817	-0.001855	-0.000349	-0.0208	-0.0105	-0.0081
25.2	0.284	1.222	-0.0325	-0.0302	0.389	0.784	188	817	-0.004186	-0.001240	-0.0434	-0.0331	-0.0183
25.2	0.294	1.264	-0.0520	-0.0492	0.402	0.788	194	817	-0.006712	-0.002020	-0.0651	-0.0487	-0.0293
25.2	0.304	1.309	-0.0679	-0.0619	0.417	0.791	201	817	-0.008756	-0.002542	-0.0792	-0.0552	-0.0382
25.2	0.316	1.357	-0.0907	-0.0739	0.432	0.796	209	817	-0.011696	-0.003035	-0.0984	-0.0591	-0.0510
30.2	0.202	0.868	0.1685	0.2337	0.276	0.758	134	817	0.021736	0.009597	0.4470	0.7140	0.0948
30.2	0.213	0.915	0.1599	0.2215	0.291	0.761	141	817	0.020624	0.009097	0.3823	0.5793	0.0900
30.2	0.227	0.974	0.1369	0.1896	0.310	0.765	150	817	0.017661	0.007787	0.2883	0.4098	0.0771
30.2	0.242	1.040	0.1162	0.1619	0.331	0.770	160	817	0.014987	0.006646	0.2148	0.2878	0.0654
30.2	0.254	1.091	0.0996	0.1392	0.347	0.773	168	817	0.012852	0.005718	0.1675	0.2147	0.0561
30.2	0.270	1.163	0.0751	0.1102	0.370	0.779	179	817	0.009682	0.004524	0.1110	0.1401	0.0422
30.2	0.283	1.218	0.0573	0.0835	0.388	0.784	187	817	0.007387	0.003428	0.0772	0.0924	0.0322
30.2	0.298	1.283	0.0339	0.0548	0.408	0.789	197	817	0.004377	0.002251	0.0412	0.0519	0.0191
30.2	0.312	1.342	0.0131	0.0234	0.427	0.795	207	817	0.001691	0.000961	0.0146	0.0194	0.0074
30.2	0.320	1.377	0.0000	0.0075	0.438	0.798	212	817	0.000000	0.000308	0.0000	0.0058	0.0000
30.2	0.327	1.407	-0.0115	-0.0082	0.448	0.801	216	817	-0.001477	-0.000335	-0.0116	-0.0059	-0.0064
30.2	0.341	1.465	-0.0328	-0.0370	0.466	0.806	225	817	-0.004233	-0.001519	-0.0306	-0.0236	-0.0185
30.2	0.355	1.525	-0.0489	-0.0614	0.485	0.812	235	817	-0.006311	-0.002520	-0.0421	-0.0346	-0.0275

Beta 0.75 R [deg]	Tunnel Mach No.	Propeller Advance Ratio	Prop Thrust Coeff. Cth	Prop Power Coeff. Cph	Inflow Ratio J / pi Lamda	Helical Mach Number	S.L. Forward Speed [knots]	Std. Tip Speed [ft/sec]	Rotor Thrust Coeff. Ct Rotor	Rotor Power Coeff. Cp Rotor	George Schairer Coefficients T/qD^2	P/qVD^2	Rotor Ct over Sigma
35.2	0.254	1.092	0.1847	0.3122	0.348	0.773	168	817	0.023827	0.012821	0.3098	0.4796	0.1040
35.2	0.260	1.118	0.1772	0.2984	0.356	0.775	172	817	0.022861	0.012255	0.2835	0.4271	0.0998
35.2	0.271	1.165	0.1643	0.2768	0.371	0.779	179	817	0.021197	0.011364	0.2422	0.3502	0.0925
35.2	0.283	1.216	0.1509	0.2559	0.387	0.783	187	817	0.019463	0.010510	0.2041	0.2847	0.0849
35.2	0.289	1.244	0.1403	0.2364	0.396	0.786	191	817	0.018098	0.009708	0.1815	0.2459	0.0790
35.2	0.299	1.285	0.1282	0.2154	0.409	0.789	198	817	0.016536	0.008846	0.1553	0.2031	0.0722
35.2	0.307	1.322	0.1174	0.1980	0.421	0.793	203	817	0.015147	0.008132	0.1343	0.1713	0.0661
35.2	0.322	1.385	0.0949	0.1604	0.441	0.798	213	817	0.012243	0.006587	0.0989	0.1207	0.0534
35.2	0.337	1.449	0.0734	0.1301	0.461	0.805	223	817	0.009465	0.005342	0.0699	0.0855	0.0413
35.2	0.352	1.512	0.0526	0.0946	0.481	0.811	233	817	0.006788	0.003885	0.0460	0.0547	0.0296
35.2	0.365	1.571	0.0306	0.0607	0.500	0.817	242	817	0.003953	0.002493	0.0248	0.0313	0.0172
35.2	0.378	1.627	0.0126	0.0310	0.518	0.823	250	817	0.001623	0.001271	0.0095	0.0144	0.0071
35.2	0.386	1.659	0.0000	0.0114	0.528	0.826	255	817	0.000000	0.000468	0.0000	0.0050	0.0000
35.2	0.391	1.681	-0.0075	-0.0020	0.535	0.829	259	817	-0.000973	-0.000083	-0.0053	-0.0009	-0.0042
35.2	0.406	1.744	-0.0310	-0.0379	0.555	0.836	268	817	-0.004003	-0.001555	-0.0204	-0.0143	-0.0175
35.2	0.421	1.810	-0.0599	-0.0714	0.576	0.843	278	817	-0.007724	-0.002933	-0.0366	-0.0241	-0.0337
40.2	0.319	1.372	0.1867	0.3761	0.437	0.797	211	817	0.024091	0.015443	0.1983	0.2910	0.1051
40.2	0.331	1.422	0.1772	0.3554	0.453	0.802	219	817	0.022861	0.014596	0.1752	0.2471	0.0998
40.2	0.341	1.465	0.1650	0.3318	0.466	0.806	225	817	0.021290	0.013625	0.1538	0.2111	0.0929
40.2	0.351	1.510	0.1535	0.3102	0.481	0.811	232	817	0.019808	0.012740	0.1347	0.1802	0.0864
40.2	0.362	1.557	0.1417	0.2837	0.496	0.815	240	817	0.018281	0.011650	0.1169	0.1503	0.0798
40.2	0.368	1.583	0.1314	0.2644	0.504	0.818	244	817	0.016950	0.010856	0.1049	0.1333	0.0740
40.2	0.372	1.600	0.1187	0.2395	0.509	0.820	246	817	0.015309	0.009833	0.0927	0.1170	0.0668
40.2	0.387	1.665	0.1096	0.2249	0.530	0.827	256	817	0.014136	0.009236	0.0791	0.0975	0.0617
40.2	0.394	1.695	0.0959	0.1962	0.540	0.830	261	817	0.012369	0.008058	0.0668	0.0806	0.0540
40.2	0.408	1.753	0.0773	0.1611	0.558	0.837	270	817	0.009970	0.006615	0.0503	0.0598	0.0435
40.2	0.413	1.778	0.0666	0.1394	0.566	0.839	273	817	0.008592	0.005724	0.0422	0.0496	0.0375
40.2	0.424	1.822	0.0524	0.1122	0.580	0.845	280	817	0.006765	0.004606	0.0316	0.0371	0.0295
40.2	0.429	1.844	0.0399	0.0876	0.587	0.847	284	817	0.005146	0.003598	0.0235	0.0279	0.0225
40.2	0.444	1.911	0.0233	0.0593	0.608	0.855	294	817	0.003001	0.002435	0.0127	0.0170	0.0131
40.2	0.456	1.961	0.0112	0.0354	0.624	0.861	302	817	0.001450	0.001455	0.0058	0.0094	0.0063
40.2	0.462	1.988	0.0000	0.0150	0.633	0.865	306	817	0.000000	0.000616	0.0000	0.0038	0.0000
40.2	0.465	1.998	-0.0033	0.0060	0.636	0.866	307	817	-0.000421	0.000248	-0.0016	0.0015	-0.0018
40.2	0.477	2.051	-0.0220	-0.0262	0.653	0.872	316	817	-0.002843	-0.001077	-0.0105	-0.0061	-0.0124
40.2	0.484	2.081	-0.0280	-0.0393	0.662	0.876	320	817	-0.003612	-0.001615	-0.0129	-0.0087	-0.0158
40.2	0.493	2.119	-0.0495	-0.0614	0.674	0.881	326	817	-0.006391	-0.002520	-0.0221	-0.0129	-0.0279
40.2	0.499	2.148	-0.0610	-0.0786	0.684	0.885	330	817	-0.007871	-0.003227	-0.0265	-0.0159	-0.0343
45.4	0.403	1.734	0.1834	0.4433	0.552	0.834	267	817	0.023655	0.018203	0.1220	0.1702	0.1032
45.4	0.416	1.790	0.1702	0.4128	0.570	0.841	275	817	0.021957	0.016951	0.1062	0.1440	0.0958
45.4	0.430	1.848	0.1551	0.3752	0.588	0.848	284	817	0.020014	0.015406	0.0909	0.1189	0.0873
45.4	0.445	1.915	0.1401	0.3341	0.610	0.856	295	817	0.018075	0.013719	0.0764	0.0951	0.0789
45.4	0.460	1.977	0.1245	0.2984	0.629	0.863	304	817	0.016055	0.012255	0.0637	0.0773	0.0701
45.4	0.461	1.980	0.1234	0.2984	0.630	0.864	305	817	0.015918	0.012255	0.0629	0.0769	0.0695
45.4	0.471	2.027	0.1102	0.2658	0.645	0.869	312	817	0.014219	0.010915	0.0537	0.0639	0.0620
45.4	0.481	2.069	0.0986	0.2384	0.659	0.875	318	817	0.012714	0.009788	0.0460	0.0538	0.0555
45.4	0.481	2.066	0.0945	0.2316	0.658	0.874	318	817	0.012186	0.009508	0.0442	0.0525	0.0532
45.4	0.495	2.128	0.0758	0.1878	0.677	0.882	327	817	0.009775	0.007713	0.0335	0.0390	0.0427
45.4	0.508	2.183	0.0638	0.1604	0.695	0.890	336	817	0.008236	0.006587	0.0268	0.0308	0.0359
45.4	0.516	2.217	0.0518	0.1357	0.706	0.894	341	817	0.006685	0.005571	0.0211	0.0249	0.0292
45.4	0.525	2.257	0.0398	0.1089	0.719	0.900	347	817	0.005136	0.004474	0.0156	0.0189	0.0224
45.4	0.535	2.301	0.0288	0.0804	0.732	0.906	354	817	0.003712	0.003303	0.0109	0.0132	0.0162
45.4	0.540	2.322	0.0173	0.0548	0.739	0.909	357	817	0.002232	0.002251	0.0064	0.0088	0.0097
45.4	0.550	2.364	0.0063	0.0302	0.752	0.914	364	817	0.000808	0.001242	0.0022	0.0046	0.0035
45.4	0.555	2.385	0.0000	0.0180	0.759	0.917	367	817	0.000000	0.000739	0.0000	0.0027	0.0000
45.4	0.560	2.407	-0.0041	0.0039	0.766	0.920	370	817	-0.000525	0.000160	-0.0014	0.0006	-0.0023
45.4	0.565	2.430	-0.0162	-0.0220	0.773	0.924	374	817	-0.002085	-0.000901	-0.0055	-0.0031	-0.0091

Beta 0.75 R [deg]	Tunnel Mach No.	Propeller Advance Ratio	Prop Thrust Coeff. Cth	Prop Power Coeff. Cph	Inflow Ratio J / pi Lamda	Helical Mach Number	S.L. Forward Speed [knots]	Std. Tip Speed [ft/sec]	Rotor Thrust Coeff. Ct Rotor	Rotor Power Coeff. Cp Rotor	George Schairer Coefficients T/qD^2	P/qVD^2	Rotor Ct over Sigma
50.8	0.526	2.262	0.1879	0.5550	0.720	0.900	348	817	0.024242	0.022789	0.0734	0.0959	0.1058
50.8	0.543	2.334	0.1731	0.5102	0.743	0.910	359	817	0.022336	0.020949	0.0636	0.0802	0.0975
50.8	0.553	2.379	0.1636	0.4845	0.757	0.916	366	817	0.021105	0.019896	0.0578	0.0720	0.0921
50.8	0.563	2.422	0.1548	0.4564	0.771	0.923	373	817	0.019969	0.018741	0.0528	0.0643	0.0871
50.8	0.571	2.453	0.1459	0.4291	0.781	0.927	377	817	0.018822	0.017621	0.0485	0.0581	0.0821
50.8	0.582	2.504	0.1341	0.3960	0.797	0.934	385	817	0.017305	0.016260	0.0428	0.0505	0.0755
50.8	0.589	2.533	0.1228	0.3635	0.806	0.938	390	817	0.015836	0.014927	0.0383	0.0448	0.0691
50.8	0.597	2.569	0.1142	0.3354	0.818	0.944	395	817	0.014734	0.013772	0.0346	0.0396	0.0643
50.8	0.609	2.618	0.0965	0.2956	0.833	0.951	403	817	0.012449	0.012137	0.0282	0.0329	0.0543
50.8	0.619	2.661	0.0867	0.2681	0.847	0.957	409	817	0.011186	0.011010	0.0245	0.0285	0.0488
50.8	0.629	2.706	0.0754	0.2377	0.861	0.964	416	817	0.009727	0.009760	0.0206	0.0240	0.0424
50.8	0.637	2.738	0.0629	0.1980	0.871	0.969	421	817	0.008111	0.008132	0.0168	0.0193	0.0354
50.8	0.647	2.780	0.0477	0.1543	0.885	0.976	428	817	0.006157	0.006335	0.0123	0.0144	0.0269
50.8	0.655	2.818	0.0361	0.1191	0.897	0.981	434	817	0.004655	0.004892	0.0091	0.0106	0.0203
50.8	0.665	2.860	0.0247	0.0851	0.910	0.988	440	817	0.003185	0.003494	0.0060	0.0073	0.0139
50.8	0.674	2.896	0.0139	0.0571	0.922	0.994	446	817	0.001796	0.002345	0.0033	0.0047	0.0078
50.8	0.683	2.938	0.0005	0.0173	0.935	1.000	452	817	0.000062	0.000712	0.0001	0.0014	0.0003
50.8	0.683	2.939	0.0000	0.0173	0.935	1.000	452	817	0.000000	0.000710	0.0000	0.0014	0.0000
50.8	0.692	2.975	-0.0136	-0.0244	0.947	1.006	458	817	-0.001753	-0.001004	-0.0031	-0.0019	-0.0076
50.8	0.701	3.015	-0.0266	-0.0567	0.960	1.013	464	817	-0.003429	-0.002330	-0.0058	-0.0041	-0.0150
50.8	0.712	3.062	-0.0413	-0.0911	0.975	1.020	471	817	-0.005323	-0.003743	-0.0088	-0.0064	-0.0232
50.8	0.600	2.447	0.1540	0.4462	0.779	0.976	397	859	0.019868	0.018322	0.0514	0.0609	0.0867
50.8	0.600	2.487	0.1432	0.4162	0.791	0.967	397	846	0.018474	0.017090	0.0463	0.0541	0.0806
50.8	0.600	2.516	0.1313	0.3880	0.801	0.960	397	836	0.016933	0.015934	0.0415	0.0487	0.0739
50.8	0.600	2.556	0.1197	0.3533	0.813	0.951	397	823	0.015446	0.014506	0.0367	0.0423	0.0674
50.8	0.600	2.600	0.1049	0.3121	0.828	0.941	397	809	0.013538	0.012815	0.0310	0.0355	0.0591
50.8	0.600	2.635	0.0913	0.2749	0.839	0.934	397	798	0.011777	0.011286	0.0263	0.0300	0.0514
50.8	0.600	2.678	0.0757	0.2307	0.852	0.925	397	785	0.009759	0.009474	0.0211	0.0240	0.0426
50.8	0.600	2.720	0.0620	0.1910	0.866	0.917	397	773	0.007997	0.007845	0.0168	0.0190	0.0349
50.8	0.600	2.729	0.0600	0.1895	0.869	0.915	397	771	0.007740	0.007782	0.0161	0.0187	0.0338
50.8	0.600	2.775	0.0461	0.1511	0.883	0.906	397	758	0.005951	0.006205	0.0120	0.0141	0.0260
50.8	0.600	2.805	0.0385	0.1275	0.893	0.901	397	750	0.004971	0.005235	0.0098	0.0116	0.0217
50.8	0.600	2.820	0.0298	0.1045	0.898	0.898	397	746	0.003850	0.004290	0.0075	0.0093	0.0168
50.8	0.600	2.826	0.0289	0.1039	0.900	0.897	397	744	0.003731	0.004266	0.0072	0.0092	0.0163
50.8	0.600	2.872	0.0141	0.0630	0.914	0.889	397	732	0.001823	0.002588	0.0034	0.0053	0.0080
50.8	0.600	2.898	0.0088	0.0446	0.923	0.885	397	726	0.001135	0.001830	0.0021	0.0037	0.0050
50.8	0.600	2.930	0.0000	0.0210	0.933	0.880	397	718	0.000000	0.000862	0.0000	0.0017	0.0000
50.8	0.600	2.977	-0.0119	-0.0136	0.948	0.872	397	706	-0.001534	-0.000558	-0.0027	-0.0010	-0.0067
50.8	0.600	3.008	-0.0218	-0.0420	0.958	0.868	397	699	-0.002808	-0.001726	-0.0048	-0.0031	-0.0123
50.8	0.600	3.121	-0.0570	-0.1271	0.993	0.851	397	674	-0.007355	-0.005218	-0.0117	-0.0084	-0.0321
54.7	0.600	2.703	0.1956	0.6704	0.860	0.920	397	778	0.025235	0.027530	0.0535	0.0679	0.1101
54.7	0.600	2.773	0.1772	0.6054	0.883	0.907	397	758	0.022859	0.024859	0.0461	0.0568	0.0997
54.7	0.600	2.808	0.1719	0.5815	0.894	0.900	397	749	0.022180	0.023878	0.0436	0.0525	0.0968
54.7	0.600	2.863	0.1527	0.5170	0.911	0.891	397	735	0.019694	0.021231	0.0373	0.0441	0.0859
54.7	0.600	2.916	0.1360	0.4589	0.928	0.882	397	721	0.017538	0.018844	0.0320	0.0370	0.0765
54.7	0.600	2.984	0.1178	0.4069	0.950	0.871	397	705	0.015200	0.016707	0.0265	0.0306	0.0663
54.7	0.600	3.046	0.1019	0.3542	0.970	0.862	397	690	0.013143	0.014544	0.0220	0.0251	0.0573
54.7	0.600	3.108	0.0837	0.2946	0.989	0.853	397	677	0.010797	0.012097	0.0173	0.0196	0.0471
54.7	0.600	3.179	0.0640	0.2398	1.012	0.844	397	661	0.008254	0.009845	0.0127	0.0149	0.0360
54.7	0.600	3.255	0.0430	0.1753	1.036	0.834	397	646	0.005549	0.007199	0.0081	0.0102	0.0242
54.7	0.600	3.324	0.0232	0.1129	1.058	0.826	397	633	0.002989	0.004638	0.0042	0.0062	0.0130
54.7	0.600	3.407	0.0002	0.0600	1.084	0.816	397	617	0.000027	0.002463	0.0000	0.0030	0.0001
54.7	0.600	3.408	0.0000	0.0510	1.085	0.816	397	617	0.000000	0.002094	0.0000	0.0026	0.0000
54.7	0.600	3.515	-0.0292	-0.0354	1.119	0.805	397	598	-0.003764	-0.001453	-0.0047	-0.0016	-0.0164
54.7	0.600	3.597	-0.0512	-0.1146	1.145	0.797	397	585	-0.006606	-0.004708	-0.0079	-0.0049	-0.0288
54.7	0.600	3.685	-0.0761	-0.1822	1.173	0.788	397	571	-0.009819	-0.007481	-0.0112	-0.0073	-0.0428

Beta 0.75 R [deg]	Tunnel Mach No.	Propeller Advance Ratio	Prop Thrust Coeff. Cth	Prop Power Coeff. Cph	Inflow Ratio J / pi Lamda	Helical Mach Number	S.L. Forward Speed [knots]	Std. Tip Speed [ft/sec]	Rotor Thrust Coeff. Ct Rotor	Rotor Power Coeff. Cp Rotor	George Schairer Coefficients T/qD^2	P/qVD^2	Rotor Ct over Sigma
60.2	0.600	3.597	0.1460	0.6665	1.145	0.797	397	585	0.018831	0.027368	0.0226	0.0287	0.0822
60.2	0.600	3.664	0.1362	0.6102	1.166	0.790	397	574	0.017565	0.025058	0.0203	0.0248	0.0766
60.2	0.600	3.729	0.1218	0.5515	1.187	0.785	397	564	0.015713	0.022647	0.0175	0.0213	0.0686
60.2	0.600	3.804	0.1057	0.4967	1.211	0.778	397	553	0.013631	0.020396	0.0146	0.0180	0.0595
60.2	0.600	3.874	0.0926	0.4413	1.233	0.773	397	543	0.011951	0.018123	0.0123	0.0152	0.0521
60.2	0.600	3.921	0.0753	0.3751	1.248	0.769	397	536	0.009714	0.015401	0.0098	0.0124	0.0424
60.2	0.600	3.996	0.0617	0.3203	1.272	0.763	397	526	0.007961	0.013152	0.0077	0.0100	0.0347
60.2	0.600	4.093	0.0442	0.2506	1.303	0.756	397	514	0.005701	0.010292	0.0053	0.0073	0.0249
60.2	0.600	4.170	0.0254	0.1627	1.327	0.751	397	504	0.003275	0.006681	0.0029	0.0045	0.0143
60.2	0.600	4.305	0.0000	0.0700	1.370	0.743	397	488	0.000000	0.002874	0.0000	0.0018	0.0000
60.2	0.600	4.272	-0.0018	0.0904	1.360	0.745	397	492	-0.000231	0.003711	-0.0002	0.0023	-0.0010
60.2	0.600	4.357	-0.0101	0.0330	1.387	0.740	397	483	-0.001304	0.001357	-0.0011	0.0008	-0.0057
60.2	0.600	4.445	-0.0261	-0.0459	1.415	0.735	397	473	-0.003370	-0.001884	-0.0026	-0.0010	-0.0147
45.4	0.7	2.205	0.0961	0.2451	0.702	1.218	463	1113	0.012395	0.0100636	0.0395	0.0457	0.0541
45.4	0.700	2.224	0.0854	0.2207	0.708	1.211	463	1103	0.011015	0.009062	0.0345	0.0401	0.0481
45.4	0.700	2.251	0.0761	0.2152	0.717	1.202	463	1090	0.009811	0.008837	0.0300	0.0377	0.0428
45.4	0.700	2.272	0.0654	0.1952	0.723	1.195	463	1080	0.008434	0.008017	0.0253	0.0333	0.0368
45.4	0.700	2.288	0.0565	0.1749	0.728	1.189	463	1072	0.007282	0.007182	0.0216	0.0292	0.0318
45.4	0.700	2.299	0.0506	0.1454	0.732	1.185	463	1067	0.006524	0.005972	0.0191	0.0239	0.0285
45.4	0.700	2.326	0.0419	0.1251	0.740	1.176	463	1055	0.005401	0.005138	0.0155	0.0199	0.0236
45.4	0.700	2.338	0.0346	0.1051	0.744	1.172	463	1049	0.004458	0.004314	0.0126	0.0164	0.0195
45.4	0.700	2.355	0.0273	0.0900	0.750	1.167	463	1042	0.003518	0.003697	0.0098	0.0138	0.0154
45.4	0.700	2.356	0.0268	0.0859	0.750	1.167	463	1041	0.003453	0.003529	0.0096	0.0131	0.0151
45.4	0.700	2.382	0.0156	0.0604	0.758	1.159	463	1030	0.002007	0.002481	0.0055	0.0089	0.0088
45.4	0.700	2.401	0.0045	0.0399	0.764	1.153	463	1022	0.000581	0.001638	0.0016	0.0058	0.0025
45.4	0.700	2.417	0.0000	0.0295	0.769	1.148	463	1015	0.000000	0.001211	0.0000	0.0042	0.0000
45.4	0.700	2.425	-0.0005	0.0250	0.772	1.146	463	1012	-0.000065	0.001025	-0.0002	0.0035	-0.0003
45.4	0.700	2.442	-0.0095	0.0047	0.777	1.141	463	1005	-0.001227	0.000194	-0.0032	0.0006	-0.0054
50.8	0.700	2.580	0.1336	0.4215	0.821	1.103	463	951	0.017240	0.017308	0.0401	0.0491	0.0752
50.8	0.700	2.608	0.1259	0.3980	0.830	1.096	463	941	0.016237	0.016343	0.0370	0.0449	0.0708
50.8	0.700	2.634	0.1103	0.3492	0.838	1.090	463	931	0.014233	0.014339	0.0318	0.0382	0.0621
50.8	0.700	2.653	0.1024	0.3212	0.845	1.085	463	925	0.013210	0.013189	0.0291	0.0344	0.0576
50.8	0.700	2.689	0.0901	0.2942	0.856	1.076	463	912	0.011621	0.012081	0.0249	0.0302	0.0507
50.8	0.700	2.716	0.0789	0.2551	0.864	1.070	463	903	0.010182	0.010477	0.0214	0.0255	0.0444
50.8	0.700	2.747	0.0685	0.2245	0.875	1.063	463	893	0.008838	0.009218	0.0182	0.0217	0.0386
50.8	0.700	2.775	0.0594	0.1934	0.883	1.057	463	884	0.007666	0.007943	0.0154	0.0181	0.0334
50.8	0.700	2.810	0.0476	0.1588	0.894	1.050	463	873	0.006141	0.006522	0.0121	0.0143	0.0268
50.8	0.700	2.834	0.0360	0.1260	0.902	1.045	463	866	0.004648	0.005175	0.0090	0.0111	0.0203
50.8	0.700	2.870	0.0250	0.0963	0.914	1.038	463	855	0.003219	0.003952	0.0061	0.0081	0.0140
50.8	0.700	2.903	0.0159	0.0674	0.924	1.031	463	845	0.002047	0.002769	0.0038	0.0055	0.0089
50.8	0.700	2.934	0.0061	0.0395	0.934	1.026	463	836	0.000788	0.001620	0.0014	0.0031	0.0034
50.8	0.700	2.953	0.0000	0.0225	0.940	1.022	463	831	0.000000	0.000924	0.0000	0.0017	0.0000
50.8	0.700	2.968	-0.0046	0.0115	0.945	1.019	463	827	-0.000597	0.000471	-0.0011	0.0009	-0.0026
50.8	0.700	2.985	-0.0138	-0.0204	0.950	1.016	463	822	-0.001782	-0.000839	-0.0031	-0.0015	-0.0078
54.7	0.7	2.816	0.1931	0.6758	0.896	1.049	463	871	0.024907	0.0277522	0.0487	0.0605	0.1087
54.7	0.700	2.869	0.1770	0.6327	0.913	1.038	463	855	0.022834	0.025982	0.0430	0.0536	0.0996
54.7	0.700	2.924	0.1621	0.5773	0.931	1.028	463	839	0.020908	0.023704	0.0379	0.0462	0.0912
54.7	0.700	2.976	0.1410	0.5071	0.947	1.018	463	824	0.018187	0.020824	0.0318	0.0385	0.0794
54.7	0.700	3.029	0.1210	0.4326	0.964	1.009	463	810	0.015613	0.017763	0.0264	0.0311	0.0681
54.7	0.700	3.088	0.0991	0.3683	0.983	0.999	463	794	0.012783	0.015122	0.0208	0.0250	0.0558
54.7	0.700	3.141	0.0860	0.3186	1.000	0.990	463	781	0.011091	0.013083	0.0174	0.0206	0.0484
54.7	0.700	3.201	0.0678	0.2498	1.019	0.981	463	766	0.008743	0.010257	0.0132	0.0152	0.0381
54.7	0.700	3.255	0.0452	0.1810	1.036	0.973	463	754	0.005832	0.007432	0.0085	0.0105	0.0254
54.7	0.700	3.320	0.0284	0.1225	1.057	0.964	463	739	0.003657	0.005028	0.0051	0.0067	0.0160
54.7	0.700	3.388	0.0131	0.0670	1.078	0.955	463	724	0.001691	0.002753	0.0023	0.0034	0.0074
54.7	0.700	3.426	0.0000	0.0290	1.090	0.950	463	716	0.000000	0.001191	0.0000	0.0014	0.0000
54.7	0.700	3.456	-0.0091	-0.0058	1.100	0.946	463	710	-0.001174	-0.000237	-0.0015	-0.0003	-0.0051

Beta 0.75 R [deg]	Tunnel Mach No.	Propeller Advance Ratio	Prop Thrust Coeff. Cth	Prop Power Coeff. Cph	Inflow Ratio J/pi Lamda	Helical Mach Number	S.L. Forward Speed [knots]	Std. Tip Speed [ft/sec]	Rotor Thrust Coeff. Ct Rotor	Rotor Power Coeff. Cp Rotor	George Schairer Coefficients T/qD^2	P/qVD^2	Rotor Ct over Sigma
54.7	0.700	3.532	-0.0315	-0.0732	1.124	0.937	463	695	-0.004061	-0.003007	-0.0050	-0.0033	-0.0177
54.7	0.700	3.607	-0.0550	-0.1256	1.148	0.928	463	680	-0.007090	-0.005156	-0.0084	-0.0054	-0.0309
54.7	0.700	3.684	-0.0801	-0.1721	1.173	0.920	463	666	-0.010331	-0.007068	-0.0118	-0.0069	-0.0451
60.2	0.700	3.787	0.1285	0.5977	1.206	0.909	463	648	0.016580	0.024543	0.0179	0.0220	0.0723
60.2	0.700	3.805	0.1195	0.5578	1.211	0.908	463	645	0.015416	0.022904	0.0165	0.0202	0.0673
60.2	0.700	3.869	0.1095	0.5134	1.231	0.902	463	634	0.014125	0.021081	0.0146	0.0177	0.0616
60.2	0.700	3.927	0.0941	0.4499	1.250	0.896	463	625	0.012145	0.018475	0.0122	0.0149	0.0530
60.2	0.700	3.990	0.0767	0.3749	1.270	0.891	463	615	0.009895	0.015396	0.0096	0.0118	0.0432
60.2	0.700	4.002	0.0721	0.3581	1.274	0.890	463	613	0.009297	0.014704	0.0090	0.0112	0.0406
60.2	0.700	4.033	0.0663	0.3372	1.284	0.887	463	608	0.008551	0.013847	0.0082	0.0103	0.0373
60.2	0.700	4.035	0.0631	0.3305	1.284	0.887	463	608	0.008134	0.013573	0.0077	0.0101	0.0355
60.2	0.700	4.181	0.0332	0.2023	1.331	0.876	463	587	0.004286	0.008308	0.0038	0.0055	0.0187
60.2	0.700	4.209	0.0259	0.1832	1.340	0.873	463	583	0.003346	0.007524	0.0029	0.0049	0.0146
60.2	0.700	4.247	0.0203	0.1353	1.352	0.871	463	578	0.002612	0.005557	0.0022	0.0035	0.0114
60.2	0.700	4.277	0.0146	0.1194	1.362	0.869	463	574	0.001887	0.004901	0.0016	0.0031	0.0082
60.2	0.700	4.286	0.0108	0.0932	1.364	0.868	463	572	0.001387	0.003826	0.0012	0.0024	0.0061
60.2	0.700	4.340	0.0000	0.0580	1.381	0.864	463	565	0.000000	0.002382	0.0000	0.0014	0.0000
60.2	0.700	4.336	-0.0044	0.0454	1.380	0.864	463	566	-0.000568	0.001864	-0.0005	0.0011	-0.0025
60.2	0.700	4.415	-0.0152	-0.0051	1.405	0.859	463	556	-0.001965	-0.000210	-0.0016	-0.0001	-0.0086
60.2	0.700	4.476	-0.0313	-0.0552	1.425	0.855	463	548	-0.004037	-0.002267	-0.0031	-0.0012	-0.0176
60.2	0.700	4.496	-0.0349	-0.0951	1.431	0.854	463	546	-0.004502	-0.003905	-0.0035	-0.0021	-0.0196
60.2	0.700	4.568	-0.0545	-0.1657	1.454	0.850	463	537	-0.007027	-0.006805	-0.0052	-0.0035	-0.0307
60.2	0.700	4.653	-0.0769	-0.2412	1.481	0.845	463	527	-0.009919	-0.009905	-0.0071	-0.0048	-0.0433
50.8	0.740	2.580	0.1309	0.4252	0.821	1.166	489	1005	0.016888	0.017459	0.0393	0.0495	0.0737
50.8	0.740	2.610	0.1220	0.3890	0.831	1.158	489	994	0.015737	0.015972	0.0358	0.0437	0.0687
50.8	0.740	2.644	0.1127	0.3549	0.842	1.149	489	981	0.014542	0.014575	0.0322	0.0384	0.0634
50.8	0.740	2.670	0.1024	0.3252	0.850	1.143	489	971	0.013215	0.013354	0.0287	0.0342	0.0577
50.8	0.740	2.708	0.0886	0.2851	0.862	1.133	489	958	0.011423	0.011708	0.0242	0.0287	0.0498
50.8	0.740	2.741	0.0748	0.2408	0.873	1.126	489	946	0.009655	0.009887	0.0199	0.0234	0.0421
50.8	0.740	2.779	0.0608	0.1991	0.885	1.117	489	933	0.007841	0.008174	0.0157	0.0185	0.0342
50.8	0.740	2.812	0.0499	0.1654	0.895	1.110	489	922	0.006440	0.006794	0.0126	0.0149	0.0281
50.8	0.740	2.850	0.0359	0.1251	0.907	1.101	489	910	0.004626	0.005138	0.0088	0.0108	0.0202
50.8	0.740	2.885	0.0211	0.0848	0.918	1.094	489	899	0.002716	0.003483	0.0051	0.0071	0.0118
50.8	0.740	2.925	0.0051	0.0409	0.931	1.086	489	887	0.000658	0.001681	0.0012	0.0033	0.0029
50.8	0.740	2.937	0.0000	0.0280	0.935	1.084	489	883	0.000000	0.001150	0.0000	0.0022	0.0000
50.8	0.740	2.962	-0.0109	0.0006	0.943	1.079	489	876	-0.001400	0.000025	-0.0025	0.0000	-0.0061
50.8	0.740	2.994	-0.0180	-0.0150	0.953	1.073	489	866	-0.002327	-0.000617	-0.0040	-0.0011	-0.0102
50.8	0.740	3.023	-0.0333	-0.0311	0.962	1.067	489	858	-0.004296	-0.001277	-0.0073	-0.0023	-0.0187
50.8	0.740	3.056	-0.0410	-0.0651	0.973	1.061	489	849	-0.005285	-0.002673	-0.0088	-0.0046	-0.0231
54.7	0.740	2.864	0.1783	0.6458	0.912	1.098	489	905	0.023001	0.026517	0.0435	0.0550	0.1004
54.7	0.740	2.899	0.1691	0.6101	0.923	1.091	489	895	0.021810	0.025054	0.0402	0.0501	0.0952
54.7	0.740	2.944	0.1556	0.5551	0.937	1.082	489	881	0.020072	0.022793	0.0359	0.0435	0.0876
54.7	0.740	2.983	0.1435	0.5151	0.950	1.075	489	869	0.018512	0.021152	0.0322	0.0388	0.0808
54.7	0.740	3.025	0.1257	0.4547	0.963	1.067	489	857	0.016217	0.018671	0.0275	0.0329	0.0708
54.7	0.740	3.076	0.1054	0.3852	0.979	1.058	489	843	0.013591	0.015817	0.0223	0.0265	0.0593
54.7	0.740	3.122	0.0883	0.3299	0.994	1.050	489	831	0.011395	0.013545	0.0181	0.0217	0.0497
54.7	0.740	3.161	0.0743	0.2847	1.006	1.043	489	821	0.009581	0.011693	0.0149	0.0180	0.0418
54.7	0.740	3.208	0.0591	0.2345	1.021	1.036	489	809	0.007626	0.009630	0.0115	0.0142	0.0333
54.7	0.740	3.256	0.0431	0.1803	1.036	1.028	489	797	0.005554	0.007404	0.0081	0.0105	0.0242
54.7	0.740	3.307	0.0280	0.1302	1.053	1.021	489	784	0.003611	0.005347	0.0051	0.0072	0.0158
54.7	0.740	3.359	0.0105	0.0797	1.069	1.013	489	772	0.001356	0.003273	0.0019	0.0042	0.0059
54.7	0.740	3.388	0.0000	0.0490	1.078	1.009	489	766	0.000000	0.002012	0.0000	0.0025	0.0000
54.7	0.740	3.415	-0.0078	0.0221	1.087	1.005	489	759	-0.001008	0.000909	-0.0013	0.0011	-0.0044
54.7	0.740	3.461	-0.0101	0.0150	1.102	0.999	489	749	-0.001297	0.000616	-0.0017	0.0007	-0.0057
54.7	0.740	3.457	-0.0141	-0.0030	1.100	1.000	489	750	-0.001815	-0.000123	-0.0024	-0.0001	-0.0079
54.7	0.740	3.497	-0.0296	-0.0495	1.113	0.995	489	742	-0.003818	-0.002032	-0.0048	-0.0023	-0.0167
54.7	0.740	3.540	-0.0515	-0.1050	1.127	0.989	489	733	-0.006647	-0.004311	-0.0082	-0.0047	-0.0290

Beta 0.75 R [deg]	Tunnel Mach No.	Propeller Advance Ratio	Prop Thrust Coeff. Cth	Prop Power Coeff. Cph	Inflow Ratio J/pi Lamda	Helical Mach Number	S.L. Forward Speed [knots]	Std. Tip Speed [ft/sec]	Rotor Thrust Coeff. Ct Rotor	Rotor Power Coeff. Cp Rotor	George Schairer Coefficients T/qD^2	P/qVD^2	Rotor Ct over Sigma
60.2	0.740	3.711	0.1710	0.7751	1.181	0.970	489	699	0.022056	0.031827	0.0248	0.0303	0.0962
60.2	0.740	3.738	0.1598	0.7504	1.190	0.967	489	694	0.020619	0.030816	0.0229	0.0287	0.0900
60.2	0.740	3.766	0.1509	0.7055	1.199	0.964	489	689	0.019468	0.028971	0.0213	0.0264	0.0849
60.2	0.740	3.788	0.1455	0.6795	1.206	0.961	489	685	0.018768	0.027902	0.0203	0.0250	0.0819
60.2	0.740	3.812	0.1401	0.6510	1.213	0.959	489	680	0.018075	0.026735	0.0193	0.0235	0.0789
60.2	0.740	3.821	0.1358	0.6510	1.216	0.958	489	679	0.017514	0.026735	0.0186	0.0233	0.0764
60.2	0.740	3.863	0.1223	0.5792	1.230	0.954	489	671	0.015781	0.023783	0.0164	0.0201	0.0689
60.2	0.740	3.923	0.1072	0.5112	1.249	0.948	489	661	0.013835	0.020993	0.0139	0.0169	0.0604
60.2	0.740	3.975	0.0932	0.4511	1.265	0.943	489	653	0.012029	0.018524	0.0118	0.0144	0.0525
60.2	0.740	4.030	0.0793	0.3925	1.283	0.938	489	644	0.010230	0.016119	0.0098	0.0120	0.0446
60.2	0.740	4.095	0.0631	0.3303	1.304	0.933	489	633	0.008144	0.013562	0.0075	0.0096	0.0355
60.2	0.740	4.154	0.0541	0.2903	1.322	0.928	489	624	0.006984	0.011919	0.0063	0.0081	0.0305
60.2	0.740	4.205	0.0361	0.2304	1.338	0.924	489	617	0.004651	0.009461	0.0041	0.0062	0.0203
60.2	0.740	4.348	0.0010	0.0819	1.384	0.913	489	597	0.000129	0.003361	0.0001	0.0020	0.0006
60.2	0.740	4.353	0.0000	0.0790	1.385	0.913	489	596	0.000000	0.003244	0.0000	0.0019	0.0000
50.8	0.800	2.682	0.1060	0.3456	0.854	1.232	529	1046	0.013680	0.014193	0.0295	0.0358	0.0597
50.8	0.800	2.713	0.0939	0.3051	0.863	1.224	529	1034	0.012117	0.012529	0.0255	0.0306	0.0529
50.8	0.800	2.753	0.0830	0.2710	0.876	1.214	529	1019	0.010709	0.011130	0.0219	0.0260	0.0467
50.8	0.800	2.790	0.0690	0.2350	0.888	1.205	529	1005	0.008898	0.009648	0.0177	0.0216	0.0388
50.8	0.800	2.831	0.0514	0.1850	0.901	1.195	529	991	0.006632	0.007598	0.0128	0.0163	0.0289
50.8	0.800	2.871	0.0359	0.1401	0.914	1.186	529	977	0.004636	0.005755	0.0087	0.0118	0.0202
50.8	0.800	2.913	0.0210	0.0914	0.927	1.177	529	963	0.002709	0.003753	0.0049	0.0074	0.0118
50.8	0.800	2.950	0.0045	0.0476	0.939	1.169	529	950	0.000581	0.001956	0.0010	0.0037	0.0025
50.8	0.800	2.959	0.0000	0.0380	0.942	1.167	529	948	0.000000	0.001560	0.0000	0.0029	0.0000
50.8	0.800	3.011	-0.0220	-0.0200	0.958	1.156	529	931	-0.002837	-0.000820	-0.0049	-0.0015	-0.0124
54.7	0.800	2.952	0.1550	0.5782	0.940	1.168	529	950	0.019995	0.023741	0.0356	0.0449	0.0872
54.7	0.800	2.986	0.1410	0.5270	0.950	1.161	529	939	0.018187	0.021642	0.0316	0.0396	0.0794
54.7	0.800	3.023	0.1321	0.4903	0.962	1.154	529	928	0.017042	0.020135	0.0289	0.0355	0.0744
54.7	0.800	3.061	0.1229	0.4545	0.974	1.146	529	916	0.015856	0.018664	0.0262	0.0317	0.0692
54.7	0.800	3.101	0.1094	0.4091	0.987	1.139	529	904	0.014109	0.016800	0.0227	0.0274	0.0616
54.7	0.800	3.144	0.0962	0.3670	1.001	1.131	529	892	0.012410	0.015072	0.0195	0.0236	0.0542
54.7	0.800	3.187	0.0795	0.3106	1.014	1.123	529	880	0.010259	0.012752	0.0157	0.0192	0.0448
54.7	0.800	3.234	0.0590	0.2450	1.029	1.115	529	867	0.007606	0.010061	0.0113	0.0145	0.0332
54.7	0.800	3.250	0.0575	0.2313	1.035	1.113	529	863	0.007418	0.009498	0.0109	0.0135	0.0324
54.7	0.800	3.276	0.0450	0.2100	1.043	1.108	529	856	0.005807	0.008623	0.0084	0.0119	0.0253
54.7	0.800	3.319	0.0361	0.1653	1.057	1.101	529	845	0.004652	0.006788	0.0065	0.0090	0.0203
54.7	0.800	3.370	0.0160	0.1000	1.073	1.094	529	832	0.002064	0.004106	0.0028	0.0052	0.0090
54.7	0.800	3.418	0.0011	0.0450	1.088	1.087	529	820	0.000142	0.001849	0.0002	0.0023	0.0006
54.7	0.800	3.419	0.0000	0.0440	1.088	1.086	529	820	0.000000	0.001807	0.0000	0.0022	0.0000
54.7	0.800	3.461	-0.0189	-0.0100	1.102	1.080	529	810	-0.002438	-0.000411	-0.0032	-0.0005	-0.0106
54.7	0.800	3.515	-0.0340	-0.0591	1.119	1.073	529	798	-0.004391	-0.002425	-0.0055	-0.0027	-0.0192
60.2	0.800	3.841	0.1410	0.6762	1.223	1.033	529	730	0.018188	0.027766	0.0191	0.0239	0.0794
60.2	0.800	3.860	0.1361	0.6542	1.229	1.031	529	726	0.017558	0.026862	0.0183	0.0227	0.0766
60.2	0.800	3.879	0.1313	0.6308	1.235	1.029	529	723	0.016939	0.025905	0.0175	0.0216	0.0739
60.2	0.800	3.900	0.1250	0.6019	1.241	1.027	529	719	0.016126	0.024716	0.0164	0.0203	0.0704
60.2	0.800	3.928	0.1180	0.5697	1.250	1.024	529	714	0.015223	0.023395	0.0153	0.0188	0.0664
60.2	0.800	3.959	0.1098	0.5356	1.260	1.021	529	708	0.014165	0.021995	0.0140	0.0173	0.0618
60.2	0.800	3.975	0.1050	0.5147	1.265	1.020	529	705	0.013546	0.021136	0.0133	0.0164	0.0591
60.2	0.800	4.040	0.0900	0.4500	1.286	1.013	529	694	0.011611	0.018479	0.0110	0.0136	0.0507
60.2	0.800	4.092	0.0758	0.3891	1.302	1.009	529	685	0.009781	0.015977	0.0091	0.0114	0.0427
60.2	0.800	4.140	0.0629	0.3353	1.318	1.004	529	677	0.008111	0.013768	0.0073	0.0094	0.0354
60.2	0.800	4.195	0.0474	0.2750	1.335	1.000	529	668	0.006115	0.011293	0.0054	0.0075	0.0267
60.2	0.800	4.250	0.0310	0.1995	1.353	0.995	529	660	0.004005	0.008191	0.0034	0.0052	0.0175
60.2	0.800	4.300	0.0178	0.1400	1.369	0.991	529	652	0.002301	0.005749	0.0019	0.0035	0.0100
60.2	0.800	4.362	0.0040	0.0866	1.388	0.986	529	643	0.000516	0.003554	0.0004	0.0021	0.0023
60.2	0.800	4.362	0.0000	0.0860	1.388	0.986	529	643	0.000000	0.003531	0.0000	0.0021	0.0000

Beta 0.75 R [deg]	Tunnel Mach No.	Propeller Advance Ratio	Prop Thrust Coeff. Cth	Prop Power Coeff. Cph	Inflow Ratio J/pi Lamda	Helical Mach Number	S.L. Forward Speed [knots]	Std. Tip Speed [ft/sec]	Rotor Thrust Coeff. Ct Rotor	Rotor Power Coeff. Cp Rotor	George Schairer Coefficients T/qD^2	P/qVD^2	Rotor Ct over Sigma
50.8	0.840	2.652	0.1050	0.3495	0.844	1.302	555	1110	0.013546	0.014352	0.0299	0.0375	0.0591
50.8	0.840	2.681	0.0981	0.3280	0.853	1.294	555	1098	0.012661	0.013469	0.0273	0.0340	0.0552
50.8	0.840	2.718	0.0839	0.2900	0.865	1.284	555	1083	0.010829	0.011909	0.0227	0.0289	0.0473
50.8	0.840	2.756	0.0722	0.2610	0.877	1.274	555	1068	0.009308	0.010718	0.0190	0.0249	0.0406
50.8	0.840	2.791	0.0612	0.2250	0.888	1.265	555	1055	0.007891	0.009239	0.0157	0.0207	0.0344
50.8	0.840	2.829	0.0470	0.1850	0.900	1.255	555	1041	0.006067	0.007597	0.0118	0.0163	0.0265
50.8	0.840	2.868	0.0321	0.1400	0.913	1.246	555	1027	0.004145	0.005749	0.0078	0.0119	0.0181
50.8	0.840	2.905	0.0132	0.0858	0.925	1.237	555	1013	0.001700	0.003525	0.0031	0.0070	0.0074
50.8	0.840	2.944	0.0000	0.0480	0.937	1.228	555	1000	0.000000	0.001971	0.0000	0.0038	0.0000
50.8	0.840	2.947	-0.0010	0.0451	0.938	1.228	555	999	-0.000124	0.001854	-0.0002	0.0035	-0.0005
50.8	0.840	2.990	-0.0177	-0.0005	0.952	1.218	555	985	-0.002280	-0.000021	-0.0040	0.0000	-0.0099
54.7	0.840	3.050	0.1108	0.4236	0.971	1.206	555	965	0.014289	0.017393	0.0238	0.0299	0.0623
54.7	0.840	3.100	0.0970	0.3780	0.987	1.196	555	950	0.012514	0.015522	0.0202	0.0254	0.0546
54.7	0.840	3.150	0.0825	0.3280	1.003	1.186	555	935	0.010643	0.013469	0.0166	0.0210	0.0464
54.7	0.840	3.175	0.0752	0.2986	1.011	1.182	555	927	0.009701	0.012260	0.0149	0.0187	0.0423
54.7	0.840	3.195	0.0705	0.2910	1.017	1.178	555	921	0.009095	0.011951	0.0138	0.0178	0.0397
54.7	0.840	3.225	0.0610	0.2580	1.027	1.173	555	913	0.007863	0.010594	0.0117	0.0154	0.0343
54.7	0.840	3.262	0.0500	0.2139	1.038	1.166	555	903	0.006450	0.008783	0.0094	0.0123	0.0281
54.7	0.840	3.290	0.0394	0.1830	1.047	1.161	555	895	0.005083	0.007515	0.0073	0.0103	0.0222
54.7	0.840	3.335	0.0230	0.1350	1.062	1.154	555	883	0.002967	0.005544	0.0041	0.0073	0.0129
54.7	0.840	3.340	0.0255	0.1410	1.063	1.153	555	881	0.003290	0.005790	0.0046	0.0076	0.0144
54.7	0.840	3.361	0.0142	0.1020	1.070	1.150	555	876	0.001832	0.004189	0.0025	0.0054	0.0080
54.7	0.840	3.405	0.0000	0.0603	1.084	1.143	555	865	0.000000	0.002476	0.0000	0.0031	0.0000
54.7	0.840	3.410	-0.0015	0.0546	1.085	1.142	555	863	-0.000194	0.002244	-0.0003	0.0028	-0.0008
54.7	0.840	3.415	-0.0018	0.0580	1.087	1.141	555	862	-0.000232	0.002382	-0.0003	0.0029	-0.0010
54.7	0.840	3.430	-0.0103	0.0259	1.092	1.139	555	858	-0.001322	0.001062	-0.0017	0.0013	-0.0058
54.7	0.840	3.475	-0.0275	-0.0140	1.106	1.132	555	847	-0.003548	-0.000575	-0.0046	-0.0007	-0.0155
50.8	0.890	2.600	0.1220	0.4160	0.828	1.396	588	1200	0.015739	0.017083	0.0361	0.0473	0.0687
50.8	0.890	2.650	0.1110	0.3770	0.844	1.380	588	1177	0.014320	0.015481	0.0316	0.0405	0.0625
50.8	0.890	2.700	0.0948	0.3370	0.859	1.365	588	1155	0.012230	0.013839	0.0260	0.0342	0.0534
50.8	0.890	2.730	0.0885	0.3100	0.869	1.357	588	1143	0.011417	0.012730	0.0237	0.0305	0.0498
50.8	0.890	2.750	0.0809	0.2910	0.875	1.351	588	1134	0.010437	0.011950	0.0214	0.0280	0.0455
50.8	0.890	2.770	0.0711	0.2750	0.882	1.346	588	1126	0.009172	0.011293	0.0185	0.0259	0.0400
50.8	0.890	2.800	0.0630	0.2539	0.891	1.338	588	1114	0.008127	0.010426	0.0161	0.0231	0.0355
50.8	0.890	2.815	0.0590	0.2300	0.896	1.334	588	1108	0.007611	0.009445	0.0149	0.0206	0.0332
50.8	0.890	2.840	0.0490	0.2150	0.904	1.327	588	1098	0.006321	0.008829	0.0122	0.0188	0.0276
50.8	0.890	2.851	0.0460	0.2021	0.908	1.324	588	1094	0.005934	0.008300	0.0113	0.0174	0.0259
50.8	0.890	2.861	0.0446	0.1970	0.911	1.322	588	1090	0.005754	0.008089	0.0109	0.0168	0.0251
50.8	0.890	2.890	0.0350	0.1698	0.920	1.315	588	1079	0.004515	0.006971	0.0084	0.0141	0.0197
50.8	0.890	2.910	0.0254	0.1460	0.926	1.310	588	1072	0.003277	0.005995	0.0060	0.0118	0.0143
50.8	0.890	2.940	0.0135	0.1200	0.936	1.303	588	1061	0.001738	0.004928	0.0031	0.0094	0.0076
50.8	0.890	2.956	0.0055	0.0795	0.941	1.299	588	1055	0.000707	0.003263	0.0013	0.0062	0.0031
50.8	0.890	2.968	0.0000	0.0670	0.945	1.296	588	1051	0.000000	0.002751	0.0000	0.0051	0.0000
50.8	0.890	2.995	-0.0105	0.0300	0.953	1.290	588	1042	-0.001355	0.001232	-0.0023	0.0022	-0.0059
50.8	0.890	3.025	-0.0254	0.0000	0.963	1.283	588	1031	-0.003278	0.000000	-0.0056	0.0000	-0.0143
54.7	0.890	2.960	0.1420	0.5550	0.942	1.298	588	1054	0.018319	0.022790	0.0324	0.0428	0.0799
54.7	0.890	3.000	0.1350	0.5300	0.955	1.289	588	1040	0.017416	0.021764	0.0300	0.0393	0.0760
54.7	0.890	3.040	0.1215	0.4885	0.968	1.280	588	1026	0.015674	0.020061	0.0263	0.0348	0.0684
54.7	0.890	3.075	0.1100	0.4459	0.979	1.272	588	1014	0.014191	0.018309	0.0233	0.0307	0.0619
54.7	0.890	3.125	0.0980	0.4000	0.995	1.262	588	998	0.012643	0.016426	0.0201	0.0262	0.0552
54.7	0.890	3.160	0.0809	0.3450	1.006	1.255	588	987	0.010437	0.014167	0.0162	0.0219	0.0455
54.7	0.890	3.210	0.0680	0.2950	1.022	1.245	588	972	0.008772	0.012114	0.0132	0.0178	0.0383
54.7	0.890	3.255	0.0520	0.2550	1.036	1.237	588	958	0.006708	0.010471	0.0098	0.0148	0.0293
54.7	0.890	3.300	0.0440	0.1900	1.050	1.229	588	945	0.005676	0.007802	0.0081	0.0106	0.0248
54.7	0.890	3.330	0.0270	0.1600	1.060	1.224	588	937	0.003483	0.006570	0.0049	0.0087	0.0152
54.7	0.890	3.350	0.0255	0.1510	1.066	1.220	588	931	0.003290	0.006201	0.0045	0.0080	0.0144
54.7	0.890	3.400	0.0071	0.0940	1.082	1.212	588	917	0.000917	0.003862	0.0012	0.0048	0.0040

Beta 0.75 R [deg]	Tunnel Mach No.	Propeller Advance Ratio	Prop Thrust Coeff. Cth	Prop Power Coeff. Cph	Inflow Ratio J / pi Lamda	Helical Mach Number	S.L. Forward Speed [knots]	Std. Tip Speed [ft/sec]	Rotor Thrust Coeff. Ct Rotor	Rotor Power Coeff. Cp Rotor	George Schairer Coefficients T/qD^2	P/qVD^2	Rotor Ct over Sigma
54.7	0.890	3.415	0.0000	0.0765	1.087	1.209	588	913	0.000000	0.003141	0.0000	0.0038	0.0000
54.7	0.890	3.450	-0.0120	0.0400	1.098	1.204	588	904	-0.001548	0.001643	-0.0020	0.0019	-0.0068
60.2	0.890	3.600	0.1670	0.8450	1.146	1.181	588	866	0.021544	0.034699	0.0258	0.0362	0.0940
60.2	0.890	3.640	0.1601	0.8290	1.159	1.176	588	857	0.020654	0.034042	0.0242	0.0344	0.0901
60.2	0.890	3.700	0.1490	0.7675	1.178	1.168	588	843	0.019222	0.031517	0.0218	0.0303	0.0839
60.2	0.890	3.775	0.1341	0.7020	1.202	1.158	588	826	0.017298	0.028827	0.0188	0.0261	0.0755
60.2	0.890	3.830	0.1189	0.6430	1.219	1.151	588	814	0.015338	0.026404	0.0162	0.0229	0.0669
60.2	0.890	3.900	0.1045	0.5710	1.241	1.143	588	800	0.013486	0.023448	0.0137	0.0193	0.0588
60.2	0.890	3.965	0.0920	0.5100	1.262	1.136	588	787	0.011870	0.020943	0.0117	0.0164	0.0518
60.2	0.890	4.035	0.0738	0.4300	1.284	1.128	588	773	0.009518	0.017657	0.0091	0.0131	0.0415
60.2	0.890	4.110	0.0515	0.3350	1.308	1.120	588	759	0.006644	0.013756	0.0061	0.0097	0.0290
60.2	0.890	4.185	0.0350	0.2600	1.332	1.113	588	745	0.004515	0.010677	0.0040	0.0071	0.0197
60.2	0.890	4.265	0.0110	0.1630	1.358	1.105	588	731	0.001419	0.006693	0.0012	0.0042	0.0062
60.2	0.890	4.290	0.0000	0.1150	1.366	1.103	588	727	0.000000	0.004722	0.0000	0.0029	0.0000
60.2	0.890	4.340	-0.0180	0.0500	1.381	1.099	588	719	-0.002322	0.002053	-0.0019	0.0012	-0.0101
60.2	0.890	4.410	-0.0400	-0.0420	1.404	1.093	588	707	-0.005160	-0.001725	-0.0041	-0.0010	-0.0225
54.7	0.930	2.950	0.1215	0.4930	0.939	1.359	615	1105	0.015668	0.020245	0.0279	0.0384	0.0684
54.7	0.930	3.000	0.1115	0.4625	0.955	1.347	615	1087	0.014384	0.018992	0.0248	0.0343	0.0628
54.7	0.930	3.050	0.1050	0.4275	0.971	1.335	615	1069	0.013546	0.017555	0.0226	0.0301	0.0591
54.7	0.930	3.100	0.0890	0.3880	0.987	1.324	615	1051	0.011482	0.015933	0.0185	0.0260	0.0501
54.7	0.930	3.135	0.0789	0.3550	0.998	1.317	615	1040	0.010177	0.014578	0.0161	0.0230	0.0444
54.7	0.930	3.180	0.0673	0.3060	1.012	1.307	615	1025	0.008676	0.012566	0.0133	0.0190	0.0379
54.7	0.930	3.210	0.0624	0.2910	1.022	1.301	615	1015	0.008054	0.011950	0.0121	0.0176	0.0351
54.7	0.930	3.240	0.0489	0.2450	1.031	1.295	615	1006	0.006314	0.010061	0.0093	0.0144	0.0275
54.7	0.930	3.270	0.0466	0.2300	1.041	1.290	615	997	0.006012	0.009445	0.0087	0.0132	0.0262
54.7	0.930	3.275	0.0386	0.2050	1.042	1.289	615	995	0.004980	0.008418	0.0072	0.0117	0.0217
54.7	0.930	3.300	0.0351	0.1950	1.050	1.284	615	988	0.004523	0.008007	0.0064	0.0109	0.0197
54.7	0.930	3.330	0.0280	0.1700	1.060	1.279	615	979	0.003612	0.006981	0.0051	0.0092	0.0158
54.7	0.930	3.360	0.0176	0.1310	1.070	1.273	615	970	0.002272	0.005379	0.0031	0.0069	0.0099
54.7	0.930	3.395	0.0030	0.0810	1.081	1.267	615	960	0.000391	0.003326	0.0005	0.0041	0.0017
54.7	0.930	3.416	0.0000	0.0610	1.087	1.263	615	954	0.000000	0.002505	0.0000	0.0031	0.0000
54.7	0.930	3.420	-0.0011	0.0550	1.089	1.263	615	953	-0.000142	0.002259	-0.0002	0.0027	-0.0006
54.7	0.930	3.460	-0.0115	0.0150	1.101	1.256	615	942	-0.001484	0.000616	-0.0019	0.0007	-0.0065
54.7	0.930	3.490	-0.0170	-0.0050	1.111	1.251	615	934	-0.002193	-0.000205	-0.0028	-0.0002	-0.0096
54.7	0.930	3.520	-0.0311	-0.0400	1.120	1.247	615	926	-0.004010	-0.001643	-0.0050	-0.0018	-0.0175
60.2	0.930	3.805	0.1165	0.6410	1.211	1.206	615	857	0.015029	0.026322	0.0161	0.0233	0.0656
60.2	0.930	3.900	0.0938	0.5400	1.241	1.194	615	836	0.012101	0.022175	0.0123	0.0182	0.0528
60.2	0.930	3.920	0.0940	0.5440	1.248	1.192	615	832	0.012127	0.022339	0.0122	0.0181	0.0529
60.2	0.930	3.975	0.0771	0.4690	1.265	1.185	615	820	0.009946	0.019259	0.0098	0.0149	0.0434
60.2	0.930	4.080	0.0503	0.3500	1.299	1.174	615	799	0.006489	0.014372	0.0060	0.0103	0.0283
60.2	0.930	4.175	0.0200	0.2210	1.329	1.164	615	781	0.002580	0.009075	0.0023	0.0061	0.0113
60.2	0.930	4.245	0.0000	0.1400	1.351	1.157	615	768	0.000000	0.005749	0.0000	0.0037	0.0000
60.2	0.930	4.290	-0.0115	0.0950	1.366	1.153	615	760	-0.001484	0.003901	-0.0012	0.0024	-0.0065
60.2	0.930	4.390	-0.0489	-0.0610	1.397	1.144	615	742	-0.006308	-0.002505	-0.0051	-0.0014	-0.0275

Beta 0.75 R [deg]	Tunnel Mach No.	Propeller Advance Ratio	Prop Thrust Coeff. Cth	Prop Power Coeff. Cph	Inflow Ratio J / pi Lamda	Helical Mach Number	S.L. Forward Speed [knots]	Std. Tip Speed [ft/sec]	Rotor Thrust Coeff. Ct Rotor	Rotor Power Coeff. Cp Rotor	George Schairer Coefficients T/qD^2	P/qVD^2	Rotor Ct over Sigma
54.7	0.960	2.800	0.1355	0.5290	0.891	1.443	635	1202	0.017480	0.021723	0.0346	0.0482	0.0763
54.7	0.960	2.850	0.1260	0.5010	0.907	1.429	635	1181	0.016255	0.020573	0.0310	0.0433	0.0709
54.7	0.960	2.900	0.1159	0.4710	0.923	1.415	635	1160	0.014952	0.019341	0.0276	0.0386	0.0652
54.7	0.960	2.950	0.1052	0.4360	0.939	1.402	635	1141	0.013571	0.017904	0.0242	0.0340	0.0592
54.7	0.960	3.000	0.0950	0.3990	0.955	1.390	635	1122	0.012256	0.016385	0.0211	0.0296	0.0535
54.7	0.960	3.050	0.0834	0.3580	0.971	1.378	635	1103	0.010759	0.014701	0.0179	0.0252	0.0469
54.7	0.960	3.100	0.0720	0.3100	0.987	1.367	635	1085	0.009288	0.012730	0.0150	0.0208	0.0405
54.7	0.960	3.125	0.0669	0.3000	0.995	1.361	635	1077	0.008631	0.012319	0.0137	0.0197	0.0377
54.7	0.960	3.151	0.0590	0.2450	1.003	1.356	635	1068	0.007611	0.010061	0.0119	0.0157	0.0332
54.7	0.960	3.170	0.0549	0.2550	1.009	1.352	635	1061	0.007082	0.010471	0.0109	0.0160	0.0309
54.7	0.960	3.205	0.0450	0.2250	1.020	1.344	635	1050	0.005805	0.009239	0.0088	0.0137	0.0253
54.7	0.960	3.231	0.0370	0.1940	1.028	1.339	635	1041	0.004773	0.007966	0.0071	0.0115	0.0208
54.7	0.960	3.255	0.0297	0.1780	1.036	1.334	635	1034	0.003831	0.007309	0.0056	0.0103	0.0167
54.7	0.960	3.285	0.0200	0.1560	1.046	1.328	635	1024	0.002580	0.006406	0.0037	0.0088	0.0113
54.7	0.960	3.310	0.0115	0.1190	1.054	1.324	635	1017	0.001484	0.004887	0.0021	0.0066	0.0065
54.7	0.960	3.340	0.0000	0.0900	1.063	1.318	635	1008	0.000000	0.003696	0.0000	0.0048	0.0000
54.7	0.960	3.345	-0.0020	0.0980	1.065	1.317	635	1006	-0.000258	0.004024	-0.0004	0.0052	-0.0011
54.7	0.960	3.370	-0.0100	0.0500	1.073	1.312	635	998	-0.001290	0.002053	-0.0018	0.0026	-0.0056
54.7	0.960	3.395	-0.0215	0.0250	1.081	1.308	635	991	-0.002774	0.001027	-0.0037	0.0013	-0.0121
60.2	0.960	3.730	0.1160	0.6250	1.187	1.255	635	902	0.014965	0.025665	0.0167	0.0241	0.0653
60.2	0.960	3.815	0.1056	0.5900	1.214	1.244	635	882	0.013620	0.024228	0.0145	0.0213	0.0594
60.2	0.960	3.905	0.0822	0.4840	1.243	1.232	635	862	0.010604	0.019875	0.0108	0.0163	0.0463
60.2	0.960	3.985	0.0658	0.4100	1.268	1.222	635	844	0.008489	0.016836	0.0083	0.0130	0.0370
60.2	0.960	4.085	0.0438	0.3200	1.300	1.211	635	824	0.005650	0.013140	0.0052	0.0094	0.0247
60.2	0.960	4.175	0.0190	0.2150	1.329	1.201	635	806	0.002451	0.008829	0.0022	0.0059	0.0107
60.2	0.960	4.230	0.0000	0.1350	1.346	1.196	635	795	0.000000	0.005544	0.0000	0.0036	0.0000
60.2	0.960	4.275	-0.0151	0.0710	1.361	1.191	635	787	-0.001948	0.002916	-0.0017	0.0018	-0.0085
60.2	0.960	4.375	-0.0475	-0.0570	1.393	1.182	635	769	-0.006128	-0.002341	-0.0050	-0.0014	-0.0267

13. ABSTRACT (Maximum 200 words)

Two 1940s "supersonic" propeller experiments conducted by NACA have provided an immensely valuable data bank with which to study prop-rotor behavior at transonic and supersonic helical tip Mach numbers. Very accurate "blades alone" data were obtained by using nearly an infinite hub. Tabulated data were recreated from the many thrust and power figures and are included in two Appendices to this report. This data set is exceptionally well suited to reevaluating classical blade element theories as well as evolving computational fluid dynamic (CFD) analyses. A limited comparison of one propeller's experimental results to a modern rotorcraft CFD code is made. This code, referred to as TURNS, gives very encouraging results.

Detailed analysis of the performance data from both propellers is provided in Appendix A. This appendix quantifies the minimum power required to produce usable prop-rotor thrust. The dependence of minimum profile power on Reynolds number is quantified. First order compressibility power losses are quantified as well and a first approximation to design airfoil thickness ratio to avoid compressibility losses is provided. Appendix A's results are applied to study high speed civil tiltrotor cruise performance. Predicted tiltrotor performance is compared to two turboprop commercial transports. The comparison shows that there is no fundamental aerodynamic reason why the rotorcraft industry could not develop civil tiltrotor aircraft which have competitive cruise performance with today's regional, turboprop airlines. Recommendations for future study that will insure efficient prop-rotor performance to well beyond 400 knots are given.

14. SUBJECT TERMS Propellers, Rotorcraft, Tiltrotor performance			15. NUMBER OF PAGES 152
			16. PRICE CODE A08

17. SECURITY CLASSIFICATION OF REPORT Unclassified	18. SECURITY CLASSIFICATION OF THIS PAGE Unclassified	19. SECURITY CLASSIFICATION OF ABSTRACT	20. LIMITATION OF ABSTRACT